No. 105
CAS/CHEM-20-87

VIRGINIA TECH
CENTER FOR ADHESION SCIENCE

FINAL REPORT

SURFACE CHARACTERIZATION IN COMPOSITE AND TITANIUM BONDING: CARBON FIBER SURFACE TREATMENTS FOR IMPROVED ADHESION TO THERMOPLASTIC POLYMERS

BY

T. A. DeVILBISS AND J. P. WIGHTMAN

VIRGINIA POLYTECHNIC INSTITUTE
AND STATE UNIVERSITY

216 NORRIS HALL
BLACKSBURG, VIRGINIA 24061

Telephone: (703) 961-6824
TLX: EZLINK 9103331861
VPI-BKS

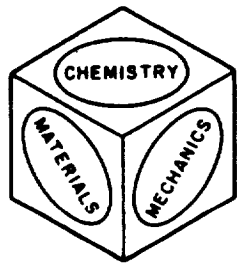

FINAL REPORT

SURFACE CHARACTERIZATION IN COMPOSITE AND TITANIUM BONDING: CARBON FIBER SURFACE TREATMENTS FOR IMPROVED ADHESION TO THERMOPLASTIC POLYMERS

BY

T. A. DeVILBISS AND J. P. WIGHTMAN

PREPARED FOR

NATIONAL AERONAUTICS AND SPACE ADMINISTRATION

NASA - Langley Research Center

Materials Division

Hampton, VA 23655

D. J. Progar

Grant #NAG-1-343

from

Chemistry Department

Virginia Polytechnic Institute and State University

Blacksburg, VA 14061

September, 1987*

*This report covers the period January 1, 1987 to July 31, 1987

SURFACE CHARACTERIZATION IN COMPOSITE AND TITANIUM BONDING: CARBON FIBER SURFACE TREATMENTS FOR IMPROVED ADHESION TO THERMOPLASTIC POLYMERS

ABSTRACT

The effect of anodization in NaOH, H_2SO_4, and amine salts on the surface chemistry of carbon fibers was examined by x-ray photoelectron spectroscopy (XPS). The surfaces of carbon fibers after anodization in NaOH and H_2SO_4 were examined by scanning transmission electron microscopy (STEM), angular dependent XPS, ultraviolet (UV) absorption spectroscopy of the anodization bath, secondary ion mass spectrometry, and polar/dispersive surface energy analysis. Hercules AS-4, Dexter Hysol XAS, and Union Carbide T-300 fibers were examined by STEM, angular dependent XPS, and breaking strength measurement before and after commercial surface treatment. The fibers from the three companies were anodized to create similar surface chemistry on each fiber. XPS was used to compare the surface chemistry after anodization. Adhesion of carbon fibers to polysulfone, polycarbonate, and polyetherimide was studied using the fiber critical length test.

Oxygen and nitrogen were added to the fiber surfaces by anodization in amine salts. Analysis of the plasmon peak in the carbon 1s signal indicated that H_2SO_4 anodization affected the morphological structure of the carbon fiber surface. UV

absorption spectra of the anodization bath, SIMS, and angular dependent XPS indicate that NaOH anodization removes amorphous carbon from the fiber. The oxygen and nitrogen content on the fiber surfaces were affected by commercial surface treatment. The Union Carbide fiber had much lower oxygen content after laboratory anodization than the Hercules or Dexter Hysol fibers. The breaking strength of all three fibers was increased by anodization. Laboratory anodization resulted in better fiber/matrix adhesion than the commercial surface treatment for the Hercules and Dexter Hysol fibers. Fiber/matrix adhesion was better for the commercially treated Union Carbide fiber than for the laboratory treated fiber. The work of adhesion of carbon fibers to thermoplastic resins was calculated using the geometric mean relationship. A correlation was observed between the dispersive component of the work of adhesion and the interfacial adhesion.

TABLE OF CONTENTS

ABSTRACT ii
LIST OF TABLES viii
LIST OF FIGURES x

1) INTRODUCTION 1

2) LITERATURE REVIEW 4

2.1 ADHESION PRINCIPLES 4
2.1.1 Theories of Adhesion 4
2.1.2 Forces of Attraction Across an Interface . 5

2.2 CARBON FIBER SYNTHESIS AND PHYSICAL PROPERTIES 7
2.2.1 Thermal Treatments for PAN Based Carbon Fiber Synthesis 8
2.2.2 Carbon Fiber Structure 11
2.2.3 Tensile Breaking Strength and Modulus of Carbon Fibers 18
2.2.4 Carbon Fiber Surface Treatment 20
2.2.5 Carbon Fiber Sizing 21

2.3 SURFACE ENERGY MEASUREMENT 22
2.3.1 Contact Angle Measurement 22
2.3.2 Contact Angle Measurement on Small Diameter Fibers 27
2.3.3 Inverse Gas Chromatography for Measurement of Solid/Vapor Interaction 28
2.3.4 Calorimetric Measurement of Solid/Liquid Interaction 29

2.4 DETECTION OF FUNCTIONAL GROUPS AND MOLECULAR STRUCTURE OF CARBON AND POLYMER SURFACES . . 30
2.4.1 Titrimetric Methods for Carbon Fiber Surface Functionality Determination . . 30
2.4.2 X-ray Photoelectron Spectroscopy (XPS) of Carbon Fiber Surfaces 32
2.4.2.1 Angular Dependent Depth Profiling . . 34
2.4.2.2 Peak Shape Analysis 35
2.4.2.2.1 Carbon 1s Peak Shape Analysis. . . 38
2.4.2.2.2 Oxygen 1s Peak Shape Analysis. . . 39
2.4.2.2.3 Nitrogen 1s Peak Shape Analysis. . 39
2.4.2.3 Derivatization. 40
2.4.3 Secondary Ion Mass Spectrometry 40
2.4.4 Models for Fiber Breaking Strength as a Function of Length. 42

2.5 TESTS OF ADHESION OF CARBON FIBER TO POLYMERIC MATRICES 44
2.5.1 Single Fiber Adhesion Tests. 44
2.5.1.1 Fiber Pull Out. 44
2.5.1.2 Fiber Critical Length Experiment. . . 45
2.5.2 Photoelastic Stress Transfer Observation in the Fiber Critical Length Experiment 50

2.6 SURFACE PROPERTIES OF CARBON FIBERS. 50
2.6.1 Studies of Carbon Fiber Adhesion to Polymeric Matrices. 53
2.6.2 Effect of Surface Treatment on Carbon Fiber Surface Properties. 57

3) METHODS AND MATERIALS. 59

3.1 APPROACH 59

3.2 MATERIALS. 61
3.2.1 Carbon Fibers. 61
3.2.2 Thermoplastic Resins 61

3.3 CARBON FIBER SURFACE ANALYSIS. 65
3.3.1 X-Ray Photoelectron Spectroscopy. . . . 65
3.3.2 Elemental Labelling of Functional Groups. 66
3.3.3 Scanning Transmission Electron Microscopy. 69
3.3.4 Surface Energy Analysis 70
3.3.5 Breaking Strength Measurement 73

3.4 ADHESION OF THERMOPLASTIC RESINS TO CARBON FIBERS 73
3.4.1 Fiber Critical Length Experiment. . . . 75
3.4.2 Photoelastic Stress Transfer Observation 76

3.5 CARBON FIBER SURFACE TREATMENT 78
3.5.1 Anodization Apparatus 78
3.5.2 Anodization in Various Electrolyte Solutions 81
3.5.3 Anodization at Different Electolyte Solution Concentrations 81
3.5.4 Anodization as a Function of Time . . . 83
3.5.5 Anodization of Fibers from Various Producers 83

4) RESULTS AND DISCUSSION 86

4.1 ANALYSIS OF EFFECT OF SURFACE TREATMENT ON SURFACE CHEMISTRY OF CARBON FIBERS 86
4.1.1 Analysis of X-ray Photoelectron Spectroscopy Data 86
4.1.2 XPS Analysis of the Effect of Anodization of Carbon Fibers in Various Electrolyte Solutions on Surface Functionality. . . 89
4.1.3 Derivatization. 98

4.2 EFFECT OF ANODIZATION IN SULFURIC ACID AND SODIUM HYDROXIDE ON THE PHYSICAL PROPERTIES OF CARBON FIBERS. 103
4.2.1 Scanning Transmission Electron Microscopy. 103
4.2.2 Depth Profiling of Sulfuric Acid and Sodium Hydroxide Anodized Fibers Using Angular Dependent XPS 105
4.2.3 Ultraviolet Absorption Spectra of Anodization Bath. 110
4.2.4 Fast Atom Bombardment Mass Spectra. . . 112
4.2.5 Surface Energy Analysis of Treated Fibers. 117
4.2.6 Breaking Strength as a Function of Anodization Time. 121
4.2.7 Summary of Effect of Anodization on Surface Properties of Carbon Fibers . . 123

4.3 SURFACE ANALYSIS OF COMMERCIAL CARBON FIBERS 124
4.3.1 Scanning Transmission Electron Microscopy. 124
4.3.2 X-ray Photoelectron Spectrocopy 127

4.4 SURFACE ANALYSIS OF FIBERS FROM VARIOUS MANUFACTURERS WITH THE SAME SURFACE TREATMENT. 138
4.4.1 Scanning Transmission Electron Microscopy. 138
4.4.2 X-Ray Photoelectron Spectroscopy. . . . 142
4.4.3 Surface Energy Analysis 145
4.4.4 Breaking Strengths. 152
4.4.5 Summary of Effects of Surface Treatment on the Surface Properties of Commercially Available Fibers 159

4.5 ADHESION TO THERMOPLASTIC MATRICES 160
4.5.1 Effect of Annealing Temperature on Adhesion. 159
4.5.2 Adhesion to Surface Treated Fibers. . . 167
4.5.3 Photoelastic Stress Transfer Observation 171
4.5.4 Work of Adhesion. 178

5) SUMMARY 183

6) REFERENCES 187

APPENDICES 198
I) DERIVATIZATION REACTIONS. 198
II) ESTIMATION OF WEIBULL DISTRIBUTION PARAMETERS. 199
III) CURVE FIT XPS RESULTS 206
IV) SURFACE ENERGY ANALYSIS 210
V) BREAKING STRENGTHS. 214
VI) FIBER FRAGMENT LENGTHS AS A FUNCTION OF ANNEALING TEMPERATURE 218
VII) FIBER FRAGMENT LENGTHS AFTER SURFACE TREATMENT 222
VIII) COMPUTER PROGRAM FOR SURFACE ENERGY ANALYSIS. 226
IX) COMPUTER PROGRAM FOR BREAKING STRENGTH ANALYSIS. 230
X) COMPUTER PROGRAM FOR FIBER FRAGMENT LENGTH ANALYSIS. 238

LIST OF TABLES

3.1	Carbon fibers used for adhesion studies	62
3.2	Thermoplastic resins used for adhesion studies.	63
3.3	Sensitivity factors, kinetic energies, and photoionization cross sections (74), used for quantitative analysis of XPS data..	67
3.4	Liquids used for surface energy determination and their surface energy components	72
3.5	Anodization conditions in various electrolyte solutions	80
3.6	Anodization conditions for ultraviolet-visible absorption spectroscopy of anodization bath . .	82
3.7	Anodization conditions of AU-4 fibers as a function of time.	84
3.8	Anodization conditions for treatment of various commercial fibers	85
4.1	Atomic percentages (%), binding energies (BE) of elements, oxygen (O/C), and nitrogen to carbon (N/C) ratios detected by XPS on the surface of carbon fibers after anodization..	90
4.2	Summary of results obtained by curve fitting XPS carbon 1s peaks of Hercules A fibers anodized in various electrolytes.	94
4.3	Percentage of elements detected on the surface of Hercules AS-4 Fibers after derivatization reactions..	101
4.4	Percentage of elements detected by XPS after derivatization on the surface of Hercules AS-4 fibers boiled in nitric acid for 3 hours. . . .	102
4.5	Atomic percentages (%), binding energy (BE) of elements, oxygen to carbon (O/C), and nitrogen to carbon (N/C) ratios detected by XPS at 90°, 30, and 10° take off angles on the surface of Hercules AU-4 fibers anodized in 0.5 M NaOH and 0.5 M H_2SO_4 at 6V for 2 minutes..	107
4.6	Summary of results obtained by curve fitting XPS carbon 1s photopeaks obtained at 90, 30, and 10° take-off angles of Hercules AU-4 fibers anodized in 0.5 M NaOH and 0.5 M H_2SO_4 at 6 V for 2 minutes..	109
4.7	Summary of organic mass fragments ejected from fiber surfaces during fast atom bombardmant . .	116
4.8	Surface energies of Hercules AU-4 fibers anodized in 0.5 M NaOH and 0.5 M H_2SO_4 at 6 V for 2 minutes	119

LIST OF TABLES (cont.)

4.9	Breaking strengths of carbon fibers after anodization in 0.5M H_2SO_4 and 0.5M NaOH at 6 volts for various lengths of time.	122
4.10	Atomic percentages (%), binding energies (BE) of elements, oxygen to carbon (O/C), and nitrogen to carbon (N/C) ratios detected by XPS on the surface of carbon fibers as received.	129
4.11	Summary of results obtained by curve fitting XPS carbon 1s peaks of fibers before and after commercial surface treatment.	133
4.12	Atomic percentages (%), binding energies (BE) of elements, oxygen to carbon (O/C), and nitrogen (N/C) ratios detected on the surface of carbon fibers after laboratory surface treatment. . . .	143
4.13	Summary of results obtained by curve fitting XPS carbon 1s photopeaks of fibers before and after laboratory surface treatment.	145
4.14	Surface energies of carbon fibers before and after surface treatment.	148
4.15	Breaking strengths at different lengths of commercial carbon fibers as received.	153
4.16	Breaking strengths at different lengths of carbon fibers after laboratory surface treatment	154
4.17	Slope and intercept of logarithm breaking strength versus logarithm length for carbon fibers before and after laboratory surface treatment.	158
4.18	Fiber critical lengths (FCL) of Hercules AS-4 and Dexter Hysol XAS fibers embedded in polysulfone (PS), polycarbonate (PC), and polyetherimide (PEI) and annealed at various temperatures for 8 hours.	163
4.19	Fiber critical lengths (FCL) of surface treated fibers embedded in polysulfone (PS), polycarbonate (PC), and polyetherimide (PEI).	169
4.20	Interfacial stress transfer coefficients (ISTC) for fibers embedded in polysulfone (PS), polycarbonate (PC), and polyetherimide (PEI). .	170
4.21	Modes of failure of fiber/matrix interface as observed under crossed polarizers in the fiber critical length experiment.	177
4.22	Work of adhesion for surface treated fibers in polysulfone.	179
4.23	Work of adhesion for surface treated fibers in polycarbonate.	180

LIST OF FIGURES

2.1 Presently accepted mechanism for cyclization and oxidation of polyacrylonitrile (ref. 30). . . 9
2.2 Proposed mechanism for carbonization of cyclized PAN fiber into aromatic carbon sheets (ref. 29) 10
2.3 Schematic of a) perfect graphite sheets and b) imperfect carbon sheets which are more indicative of the structure in carbon fibers (ref. 32) 12
2.4 Structural models of graphite and carbon structure a) perfect graphite crystal, b) turbostratic model (ref. 33) 14
2.5 Proposed structure of PAN based carbon fibers showing layers undulating in and out of crystalline regions (ref. 34) 15
2.6 Proposed structure for carbon fiber morphology showing higher order at the fiber surface. Outer layers have basal planes oriented normal to the fiber surface (ref. 36). 16
2.7 Sketches of TEM images of carbon fiber surface after carbonization at a) 1000° C, b) 1500° C, c) 2500° C. The crystalline order increases with carbonization temperature. (ref. 38) . . . 17
2.8 Dependence of PAN based carbon fiber tensile strength (σ_B) and modulus (E) on carbonization temperature (ref. 28) 19
2.9 Diagram of contact angle experiment (ref. 51) . 24
2.10 Predicted oxygen functional groups on carbon surfaces a) carboxyl group, b) phenolic hydroxyl, c) quinone, d) lactone, e) fluorescein-like lactone, f) carboxylic acid anhydride, g) cylclic peroxide (ref. 66). 31
2.11 Schematic diagram of x-ray photoelectron spectroscopy experiment (ref. 72) 33
2.12 Schematic diagram for angular dependent depth profiling using XPS (ref. 51) 36
2.13 Diagram of fiber critical length experiment (ref. 90) 46
2.14 Theoretical stress distibution at the tip of a broken fiber in the fiber critical length experiment (ref. 92). 51
2.15 Diagram of possible failure modes in the fiber critical length experiment a) matrix cracking, b) frictional stress transfer, c) shear stress transfer (ref. 95). 52

LIST OF FIGURES (cont.)

2.16 Effect of surface acidic groups on the interlaminar shear strength (i.l.s.s.) of carbon fiber composites. (ref. 97) 54

2.17 Effect of surface oxygen content on interfacial shear strength measured on single fiber. AU and HMU indicate no commercial surface treatment. AS and HMS indicate commercial surface treatment. Temperatures indicate heat treatment for removal of oxygen. (ref. 100) 55

3.1 Chemical structure of thermoplastic resins used for adhesion studies. a) polysulfone, b) polycarbonate, c) polyetherimide. 64

3.2 Schematic diagram of derivatization scheme and reagents. 68

3.3 Schematic diagram of apparatus used for wetting force measurement. 71

3.4 Schematic diagram of fiber critical length experiment using an aluminum substrate. 74

3.5 Schematic diagram of anodization apparatus. . . 79

4.1 Curve fit XPS photopeaks obtained on Hercules AU-4 fibers anodized in various electrolytes. a) untreated fiber, b) commercially treated fiber, c) anodized in NH_4HCO_3, d) anodized in $(NH_4)_2SO_4$, e) commercially treated fiber (AS-4) boiled in HNO_3, f) anodized in H_2SO_4, g) anodized in NaOH, h) anodized in H_2O Anodization conditions are listed in Table 3.5. . . 92

4.2 STEM photomicrographs of Hercules AU-4 fibers anodized in a) 0.05 M NaOH, b) 0.5 M NaOH, c) 0.05 M H_2SO_4, and d) 0.5 M H_2SO_4 at 4V for 30 minutes (12,500X). 104

4.3 Oxygen to carbon ratios as detected by XPS versus sine of the take-off angle for Hercules fibers anodized in (▲) 0.5 M NaOH, and (●) 0.5 M H_2SO_4. 108

4.4 Ultraviolet absoption spectra of a) NaOH and b) H_2SO_4 anodization baths after anodization of Hercules AU-4 fibers at 4V. 111

4.5 Positive fast atom bombardment mass spectra of Hercules AU-4 fibers anodized in 0.5 M H_2SO_4 at 6V for 2 minutes. a) 0 - 100 atomic mass units (AMU) b) 100 -200 AMU. 114

LIST OF FIGURES (cont.)

4.6	Positive fast atom bombardment mass spectra of Hercules AU-4 fibers anodized in 0.5 M NaOH at 6V for 2 minutes. a) 0 - 100 atomic mass units (AMU) b) 100 -200 AMU.	115
4.7	Negative fast atom bombardment mass spectra of Hercules AU-4 fibers anodized in a) 0.5 M H_2SO_4 and b) 0.5 M NaOH at 6V for 2 minutes..	118
4.8	Linear regression plot for determination of polar and dispersive components of surface energy of Hercules AU-4 fibers anodized in ( ) H_2SO_4 and ( ) NaOH	120
4.9	STEM photomicrographs of untreated commercial fibers as received. (12,500X).	125
4.10	STEM photomicrographs of commercially treated fibers as received. (12,500X).	126
4.11	STEM photomicrographs of Dexter Hysol XA fibers a) before and b) after commercial surface treatment. (50,000X).	128
4.12	Curve fit XPS photopeaks for untreated commercial fibers as received	131
4.13	Curve fit XPS photopeaks for commercially treated fibers as received.	132
4.14	Oxygen to carbon ratios as detected by XPS versus sine of the take-off angle (θ) for commercial fibers before and after commercial surface treatment	135
4.15	Nitrogen to carbon ratios as detected by XPS versus sine of the take-off angle (θ) for commercial fibers before and after commercial surface treatment	137
4.16	STEM photomicrographs of Hercules A fibers before and after surface treatment (12,500X). .	139
4.17	STEM photomicrographs of Dexter Hysol XA fibers before and after surface treatment (12,500X). .	140
4.18	STEM photomicrographs of Union Carbide T-300 fibers before and after surface treatment (12,500X)..	141
4.19	Curve fit XPS photopeaks for commercial fibers anodized in H_2SO_4.	146
4.20	Curve fit XPS photopeaks for commercial fibers anodized in NaOH.	147
4.21	Plot of polar component of surface energy verses oxygen to carbon ratio for carbon fibers before and after surface treatment (●) Hercules, (▲) Dexter Hysol, (■) Union Carbide fibers. .	151

LIST OF FIGURES (cont.)

4.22 Breaking strength of Hercules A fibers at three gauge lengths before and after surface treatment 155

4.23 Breaking strength of Dexter Hysol XA fibers at three gauge lengths before and after surface treatment 156

4.24 Breaking strength of Union Carbide T-300 fibers at three gauge lengths before and after surface treatment 157

4.25 Cumulative frequency plots of fragment lengths in fiber critical length test of Hercules AS-4 fibers in polysulfone a) 70° C, b) 170° C, c) 210° C, and d) 265° C annealing temperature. 162

4.26 Interfacial shear stress transfer coefficient across fiber/polysulfone interface as a function of annealing temperature (○) Hercules AS-4, (●) Dexter Hysol XAS 164

4.27 Interfacial shear stress transfer coefficient across fiber/polycarbonate interface as a function of annealing temperature (□) Hercules AS-4, (■) Dexter Hysol XAS 165

4.28 Interfacial shear stress transfer coefficient across fiber/polyetherimide interface as a function of annealing temperature (△) Hercules AS-4, (▲) Dexter Hysol XAS. 166

4.29 Cumulative frequency plots of fragment lengths in fiber critical length test of surface treated Hercules AU-4 fibers in polysulfone a) untreated fiber, b) H_2SO_4 anodized fiber, c) NaOH anodized fiber, and d) commercially treated fiber. . . . 167

4.30 Optical photomicrographs of fiber break obtained from a single fiber embedded in a thermoplastic and pull in tension for untreated fibers. . . . 173

4.31 Optical photomicrographs of fiber break obtained from a single fiber embedded in a thermoplastic and pulled in tension for commercially treated fibers. 174

4.32 Optical photomicrographs of fiber break obtained from a single fiber embedded in a thermoplastic and pulled in tension for H_2SO_4 treated fibers. 175

4.33 Optical photomicrographs of fiber break obtained from a single fiber embedded in a thermoplastic and pull in tension for NaOH treated fibers.. . 176

LIST OF FIGURES (cont.)

4.34 Work of adhesion due to a) dispersion forces, b) polar forces, and c) total surface energy versus interfacial stress transfer coefficient for 1) Hercules A fibers, 2) Dexter Hysol XA fibers, and 3) Union Carbide T-300 fibers polysulfone polycarbonate. 182

1) INTRODUCTION

Carbon fibers produced from polyacrylonitrile (PAN) precursor are finding increased usage in fiber reinforced plastics (1). Despite their present relatively high cost, carbon fibers are finding uses where weight savings are more important than cost consideration. As new applications for carbon fiber composites are being found, new demands on the composite mechanical performance are occurring. These demands are resulting in a wider choice of carbon fiber and polymeric matrix mechanical properties.

The first generation of composites using carbon fibers was made with thermosetting resins such as epoxies (2). It is now becoming apparent that these composites are too brittle for many current design applications (3-5). Recent trends in composite development are towards composites that can withstand impact loads and still function properly. These demands in composite performance are being met by improving the toughness of the matrix resin.

Methods used to increase matrix toughness have included; modifying existing epoxy formulations by adding a second phase (such as rubber or a thermoplastic resin) that can absorb energy (3-7), use of thermoplastic resins (8-11), or depositing a ductile material on the fiber surface (12-14).

Although the newer materials being used as matrix materials have increased toughness it is difficult to predict the mechanical properties of a composite based on the properties of the individual components alone (11,15). The main reason for this is that the interaction of the fiber with the matrix also has an important effect on the mechanical properties of composites (15-17). This interaction between fiber and matrix includes adhesion and wetting as well as the effect that the fiber has on the morphological characteristic of the polymer.

Adhesion between fiber and matrix can be altered by surface treating the fiber (16,17). Previous surface treatments of carbon fibers have been developed for epoxy systems. The optimum surface treatment for epoxy systems may be inadequate for newer resin systems. It may also be possible that by tailoring the interface between fiber and matrix the mechanical properties of the composite can be controlled. In order to tailor the interface, it is necessary to be able to understand the nature of carbon fiber surfaces and their reactions when surface treated.

The objective of the present research is to advance the present state of knowledge in the understanding of carbon fiber surfaces and their adhesion to thermoplastic matrices. The effect of surface treatment by anodization on the carbon fiber surface chemical and physical properties was explored.

The surface properties of several commercially available fibers were examined. Some of the important parameters such as carbon fiber surface chemistry and surface structure were related to fiber matrix adhesion.

2) LITERATURE REVIEW

2.1 ADHESION PRINCIPLES

Adhesion commonly refers to the potential for stress transfer across an interface between two materials (18). In a fiber reinforced composite adhesion will result in stress transfer between fiber and matrix. The matrix thus acts to transfer stress between adjacent fibers. The adhesion between fiber and matrix will affect shear stress transfer in a composite. In addition, stress will be transferred from the ends of broken fibers to adjacent fibers through the interface and the matrix.

2.1.1 Theories of Adhesion

To form an adhesive bond between two materials, it is necessary that they come into close molecular contact with each other. One of the materials must be capable of flowing, wetting the other material, and solidifying (18-20).

The mechanisms that cause two materials to adhere to one another are not well understood. For bonding of a polymeric material to a solid surface, two mechanisms for stress transfer across the interface are possible namely, mechanical interlocking and electronic attraction.

The mechanical interlocking theory assumes that

adhesion is due to irregularities on the surface into which the liquid material can penetrate. Upon solidification, the now solid material is held in place by the geometry of the adsorbed layer. Mechanical interlocking is thus enhanced by increasing the surface roughness or porosity of the solid material.

The electronic attraction theory assumes adhesion to be caused by the electronic attraction between the atoms in the two materials being bonded. These forces of attraction will result from interaction of specific functional groups on the two surfaces as well as from non-localized electronic interaction due to the molecular structure of the materials being bonded.

In order for either of these mechanisms to be valid, it is first necessary that the polymer used as the adhesive form close contact with the solid. Huntsberger (19,20) has shown that the adhesive bond strength of polymethyl-methacrylate to aluminum adherands was dependent on the temperature at which the bond was formed. This result was thought to be caused by inadequate molecular contact between adhesive and adherand at lower temperatures.

2.1.2 Forces of Attraction Across an Interface

The basic electronic forces which hold "homogeneous" materials together (21,22) include ionic bonding, dipolar

interactions, covalent bonding, dispersion forces, metallic bonding, and hydrogen bonding. Ionic bonding results from the electrostatic attraction between oppositely charged ions. Dipolar bonding results from interaction of permanent dipoles within the material. Covalent bonding results from the actual formation of chemical bonds within the material. Dispersion force bonding results from attraction between local electron density fluctuations in the material caused by electron mobility. Metallic bonding results from attraction of metal ions to a sea of electrons. Hydrogen bonding is similar to ionic bonding and results from sharing of an adjacent hydrogen atom by two other atoms.

When two dissimilar materials are brought into contact, as is the case in an adhesive bond, the resulting electronic attraction can be caused by any combination of the interactions listed above. The attractive forces across the interface have been classified into two broad categories namely, dispersion and polar. These forces have been discussed by Atkins (23) and Wake (24). The polar component results from electric dipoles associated with specific atom pairs or functional groups on the material surface. The dispersion component results from loosely bound electrons such as those in the conduction band of metals or simply from electrons in the atoms or molecules in the material.

If the possibility of interdiffusion between the two

materials does not exist, then the interaction can be simplified. The attraction across an interface can thus result from dispersion-dispersion interaction or dipole-dipole interactions. In addition, dipolar groups in one material can induce dipoles and thus create a dipole-induced dipole attractive force.

In order to predict and understand adhesion between two materials, it is first necessary to understand the chemical and physical structure of the materials being bonded. Carbon fiber synthesis and physical properties are discussed in the next section.

2.2 CARBON FIBER SYNTHESIS AND PHYSICAL PROPERTIES

Most of the presently available carbon fibers are synthesized from polyacrylonitrile (PAN) starting material. Although several other precursors do exist such as rayon and pitch (25), PAN precursor fibers have the best mechanical properties for structural applications.

The technology of carbon fiber synthesis is protected very strongly by carbon fiber producers. However, the basic chemistry of carbon fiber synthesis is known. A brief review is included here.

2.2.1 Thermal Treatments for PAN Based Carbon Fiber Synthesis

The processes involved in the synthesis of carbon fibers from PAN have been outlined by Diefendorf and co-workers (26,27). These processes include spinning of the PAN into fiber form, oxidation of the fiber at 200-300° C and carbonization of the fiber at 1000-2500° C in an inert atmosphere, surface treatment, and sizing. The strength, modulus, and structure of the fiber can be controlled by stretching the fiber during the process as well as by changing the heating rates, extent of oxidation, and the final carbonization temperature.

The chemical changes occurring during carbon fiber formation from PAN have been reviewed by Watt (28) and by Goodhew, et al. (29). Coleman and co-workers (30,31) have proposed the chemical changes that occur during oxidation of PAN at 200° C. These chemical changes are outlined in Figure 2.1. The first step is cyclization within the polymer backbone to form a ladder structure. This ladder structure stabilizes the polymer for heating to higher temperatures. The polymer is stretched during cyclization to maintain alignment of the polymer molecules in the fiber direction. The ladder structure is then oxidized.

The chemical changes occurring during carbonization of the fiber are shown in Figure 2.2. Although the fiber is

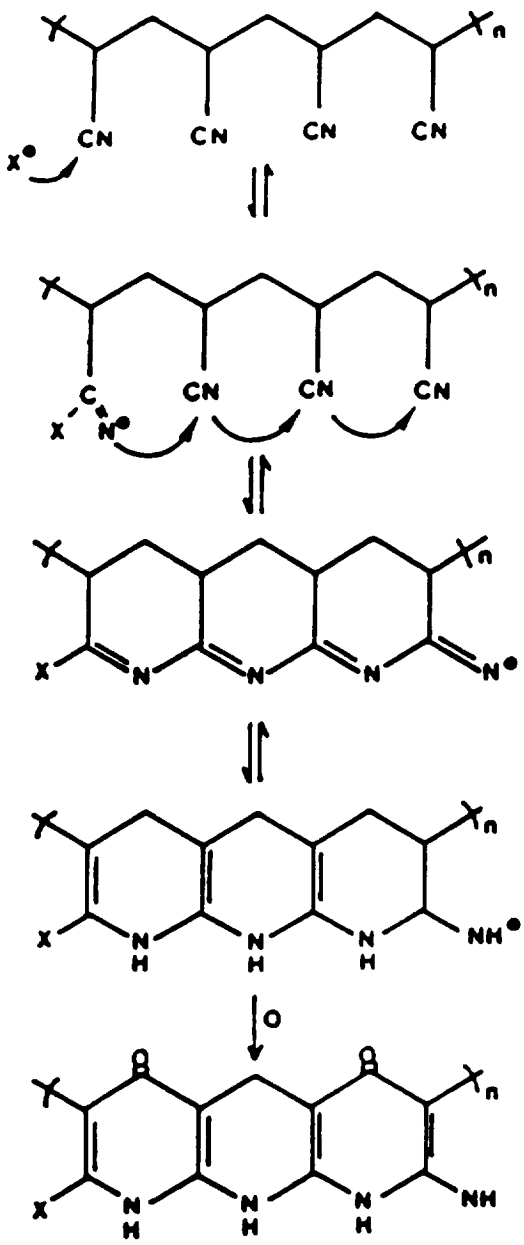

Figure 2.1 Presently accepted mechanism for cyclization and oxidation of polyacrylonitrile (ref. 30)

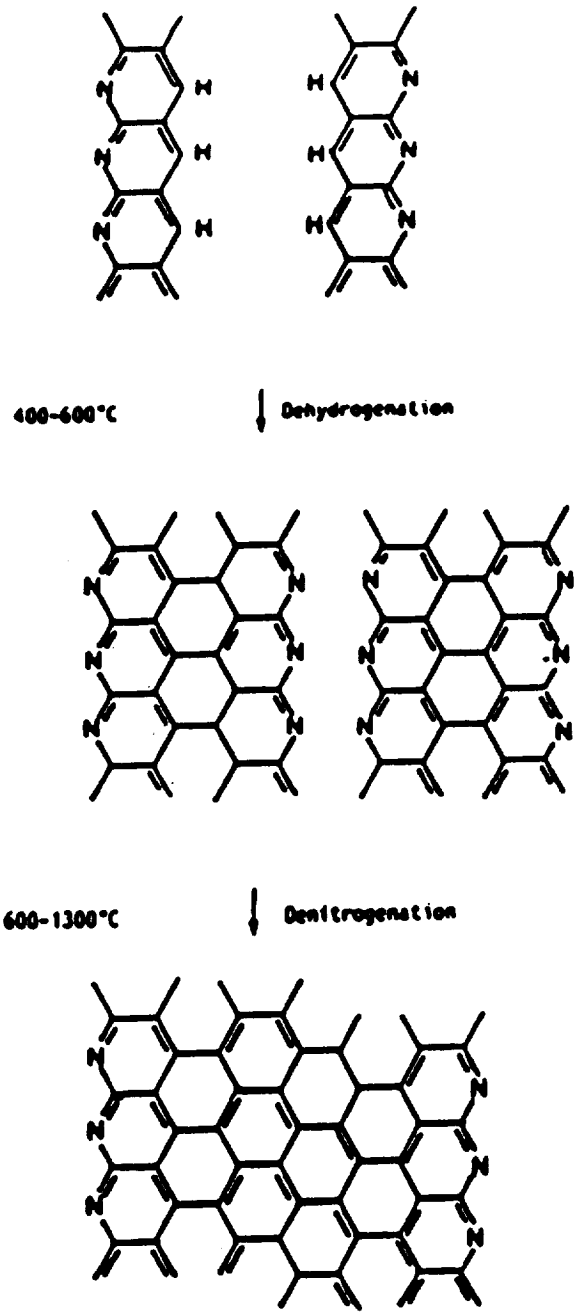

Figure 2.2 Proposed mechanism for carbonization of cyclized PAN fiber into aromatic carbon sheets (ref. 29)

carbonized between 1000 and 2500° C, reactions begin to occur at much lower temperatures as the fibers are being heated to the carbonization temperature. At 400 - 600° C, the cyclized molecules begin to link together resulting in loss of hydrogen and probably oxygen. This is followed by nitrogen loss and further linking at 600 - 1300° C to form graphitic sheets.

2.2.2 Carbon Fiber Structure

After carbonization the carbon is in a sheet form as shown in Figure 2.3a. The carbon is in an sp^2 hybrid state. There is an unbonded electron in an orbital perpendicular to the graphite plane. The unbonded electron coupled with unbonded electrons from adjacent carbon atoms will cause the formation of a conduction band of electrons between the carbon layers. The structure shown in Figure 2.3a is an idealized model for the molecular structure of graphitic carbon (32). The carbon in a carbon fiber will contain some discontinuities (32). Figure 2.3b shows an imperfect graphite sheet which is probably more representative of the structure of carbon fibers. The carbon fiber is made up of many sheets which will coalesce to form aggregates similar in structure to the graphite unit cell. Since the carbon sheet is imperfect, the ideal graphite structure shown in Figure 2.4a cannot be formed. Instead a disordered crystal

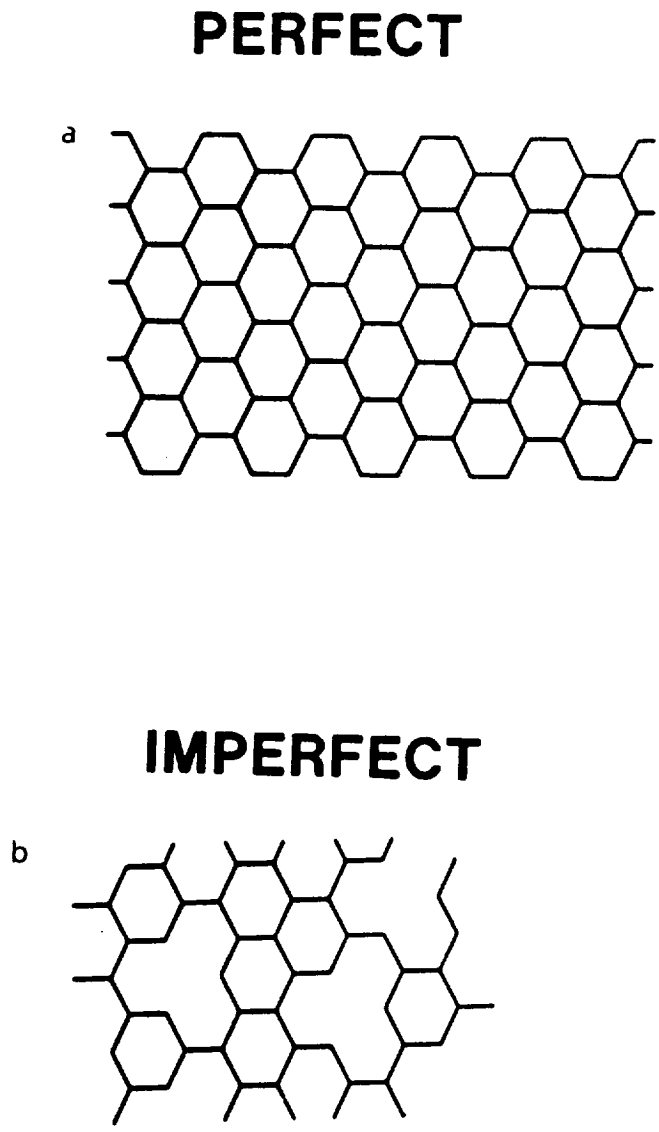

Figure 2.3 Schematic diagram of a) perfect graphite sheets and b) imperfect sheets which are more indicative of the structure in carbon fibers (ref. 32)

structure, the turbostratic structure, is formed as shown in Figure 2.4b (33). These turbostratic crystals can form aggregates several hundred angstroms in size. The layers of carbon twist and undulate along the length of the fiber as shown in Figure 2.5 (34). Between the ordered areas there are areas of amorphous carbon (35).

The structure from the core to the surface of the fiber varies also. A model for the PAN based carbon fiber structure proposed by Diefendorf and reported by Drzal (36) is shown in Figure 2.6. In this model, the carbon layers are highly oriented at the fiber surface. The carbon layers in the core are less ordered. At the fiber surface, graphitic basal planes are oriented perpendicular to the outer fiber surface. In the fiber core, the graphitic basal planes are oriented radially from the center of the fiber outward. This model for carbon fiber morphology is referred to as an onion skin structure.

The degree of order of the fiber surface was shown by Bennet (37,38) to depend on the carbonization temperature. Figure 2.7 shows sketches of longitudinal sections of carbon fibers examined by Bennet with the transmission electron microscope (TEM). The structural order of the fiber surface increases with increasing carbonization temperature. Fibers formed at higher temperatures are thus difficult to adhere to with polymeric resins.

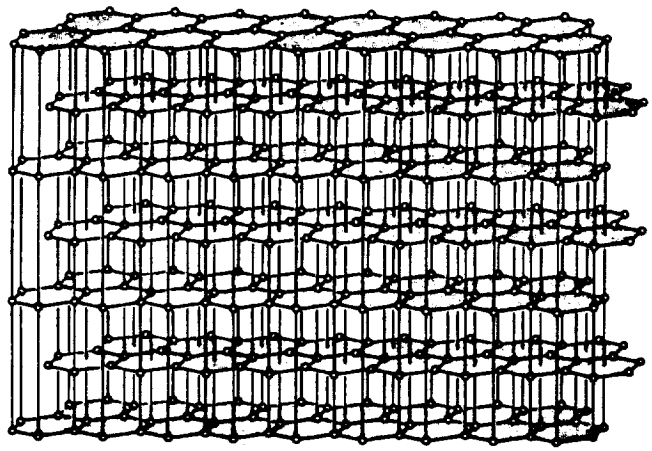

(a)

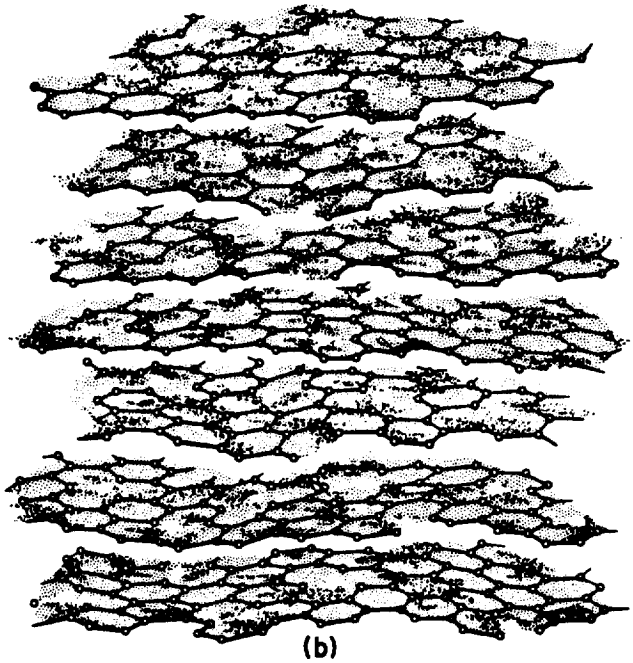

(b)

Figure 2.4 Structural models of graphite and carbon structure a) perfect graphite crystal, b) turbostratic model (ref. 33)

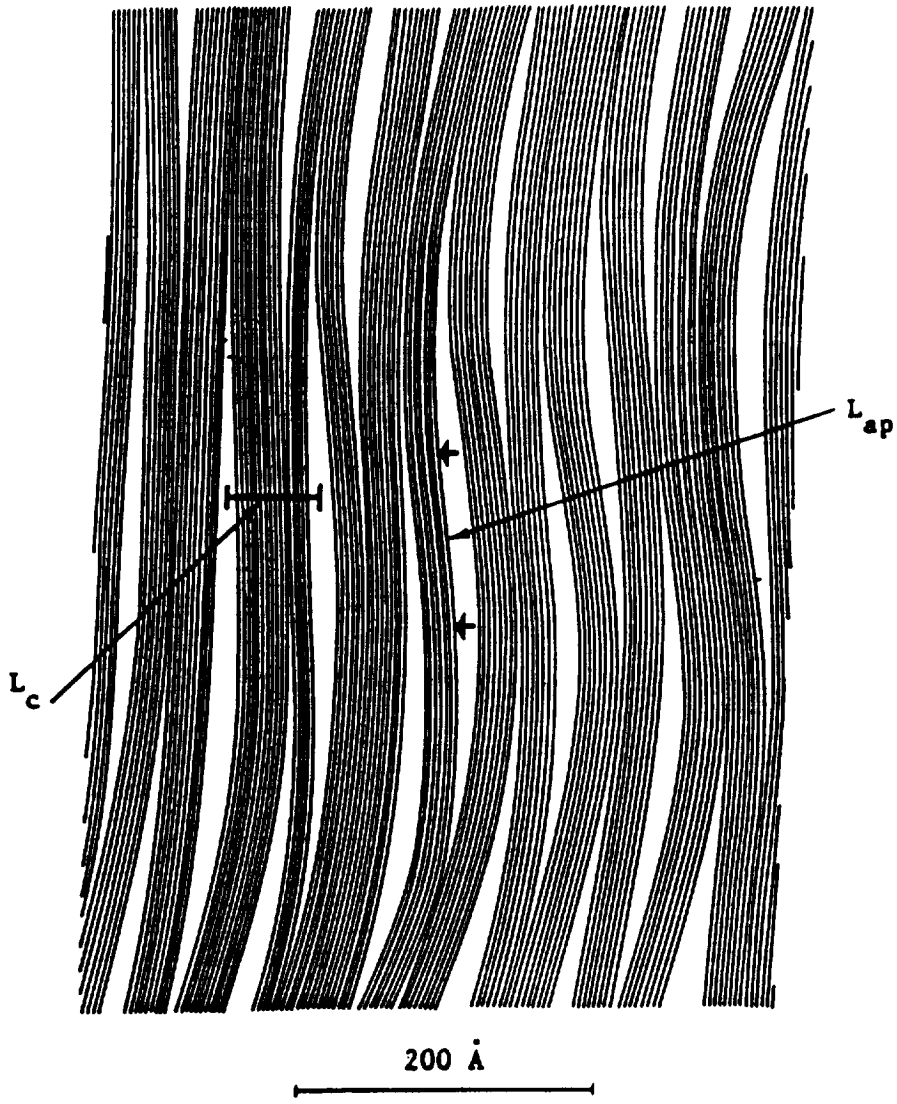

Figure 2.5 Proposed structure of PAN based carbon fibers showing layers undulating in and out of crystalline regions. L_c is the width of the turbostratic crystals. L_{ap} is the length of the crystal. (ref. 34)

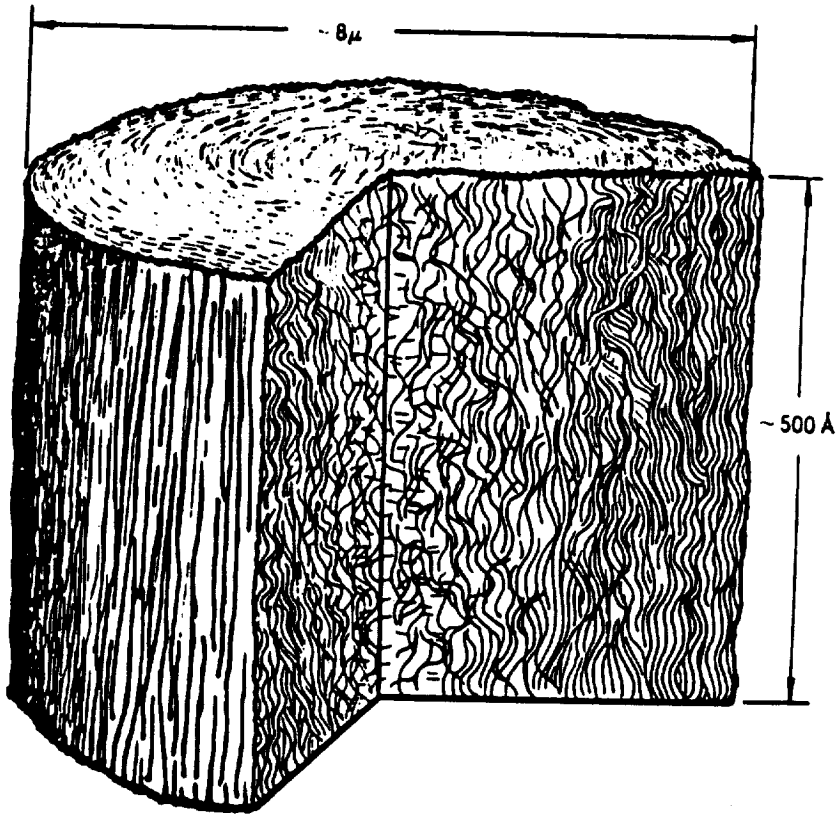

Figure 2.6 Proposed structure of carbon fiber morphology showing higher order at the fiber surface. Outer layers have basal planes oriented normal to the fiber surface (ref. 36)

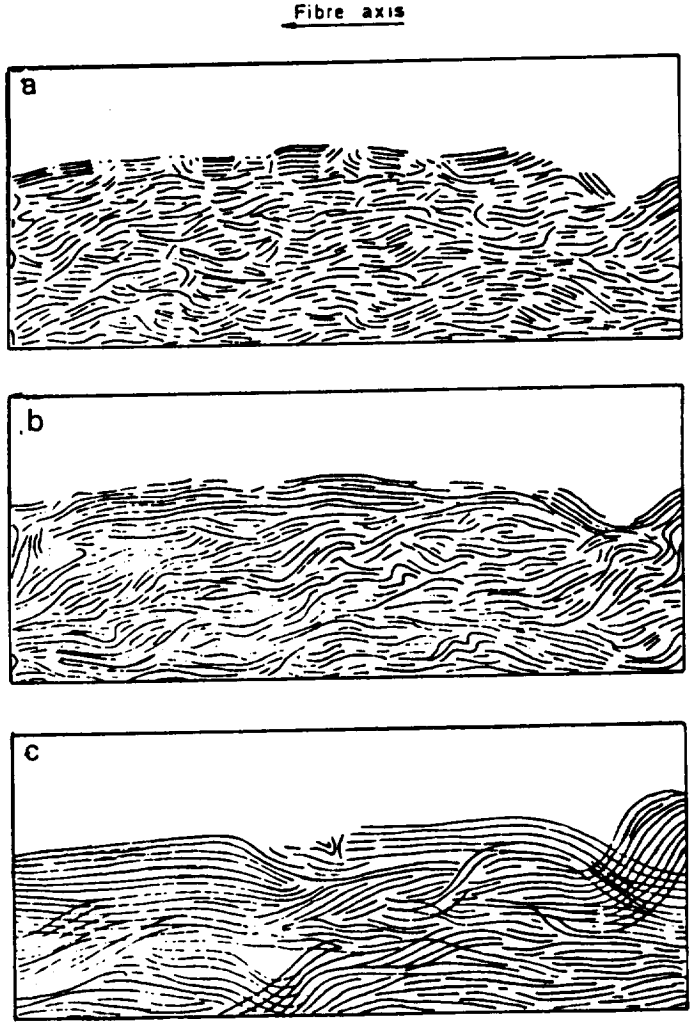

Figure 2.7 Sketches of TEM images of carbon fiber surface after carbonization at a) 1000° C, b) 1500° C, c) 2500° C. The crystalline order increases with carbonization temperature. (ref. 38)

2.2.3 Tensile Breaking Strength and Modulus of Carbon Fibers

The tensile modulus (E) and strength (σ_B) of carbon fibers are shown as a function of carbonization temperature in Figure 2.8 (28). The carbon fiber modulus increases with increasing carbonization temperature. This increase in modulus is caused by increased graphitization of the carbon at higher temperatures, since the more perfect graphite has a higher modulus than the less ordered carbon sheets.

Carbon fibers formed at higher temperatures (>2000° C) are referred to as high modulus or Type I fibers in the literature. Fibers formed at lower temperatures (1000 - 1600° C) are referred to as low modulus or Type II fibers. Recent developments in carbon fiber synthesis have resulted in carbon fibers with a tensile modulus intermediate between Type I and II but with a tensile strength similar to Type II (32). These newer fibers have been referred to as intermediate modulus. Many improvements in the processing of PAN fibers are being made. A wide range of mechanical properties is available for specific design applications.

The tensile breaking strength of a carbon fiber is dominated by flaws within the fiber and on its surface. Some of the flaws that can affect the fiber strength include

1) discontinuities in the crystal or fibrillar structure of the fiber;

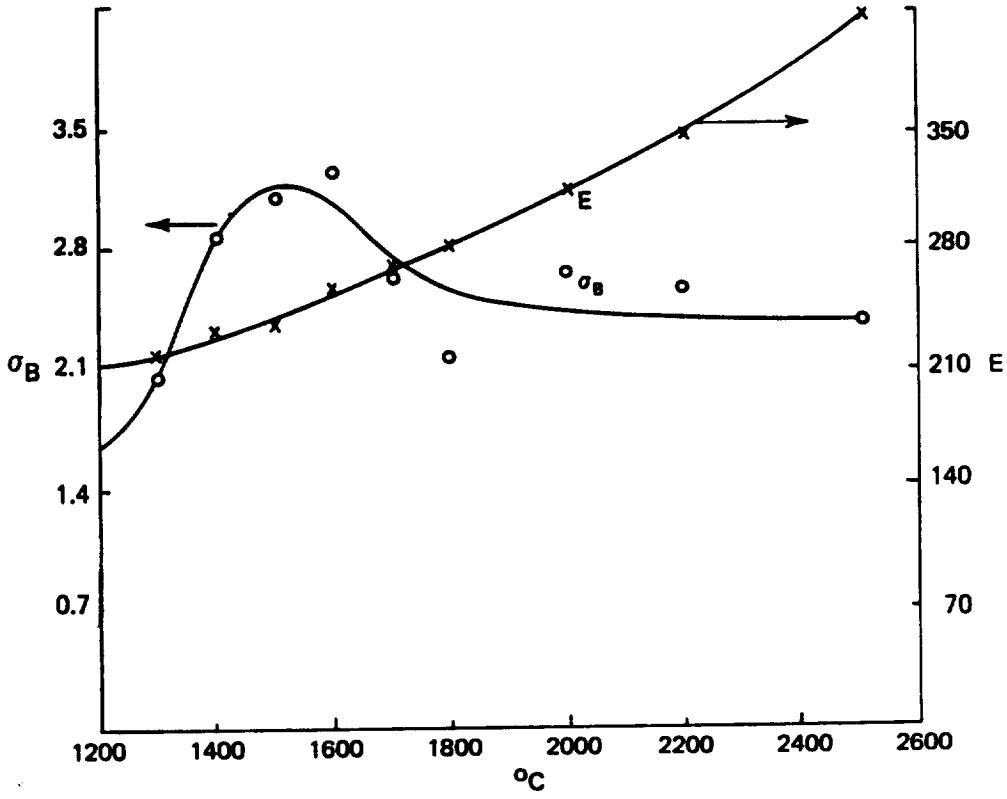

Figure 2.8 Dependence of PAN based carbon fiber tensile strength (σ_B) and modulus (E) on carbonization temperature. (ref. 28)

2) variations in the thickness of the onion skin layer;

3) variations in the overall thickness of the fiber;

4) microscopic impurities in the precursor; and

5) surface defects due to handling and processing.

Since the breaking strength of the fiber is controlled by the presence of flaws, it is expected that as the length of the fiber decreases, the breaking strength will increase. The strength versus length dependence is expected since there is a lower probability of encountering a defect in the shorter length fiber.

Surface treatment has been observed to change the breaking strength of carbon fibers. Bahl, et al. (40) and Fitzer, et al. (41) have observed that treatment of carbon fibers in HNO_3 initially increases the fiber tensile strength. Continued anodization results in a loss in strength caused by fiber damage. This initial increase in strength can be explained by removal of defects, that can initiate fracture, from the fiber surface.

2.2.4 Carbon Fiber Surface Treatment

After the carbon fibers come out of the carbonization furnace, they are surface treated. This surface treatment serves several purposes: (i) to remove the outer layer of

the carbon fiber surface which is believed to be disordered carbon and of low shear strength, (ii) to oxidize the fiber surface thus fixing functional groups on the fiber surface which will promote adhesion to the polymer matrix used for making composites, and (iii) to modify the structure of the carbon fiber surface.

Possible surface treatment mechanisms include anodization (42-44), plasma and flame treatment (45), solution oxidation (46,47), gas phase oxidation, and high temperature oxidation. Some of these treatments have been reviewed by Donnet and coworkers (25,48). The most practical surface treatment for commercial production of carbon fibers is anodization. This is because anodization can be performed continuously on carbon fibers. Typical anodizations have been performed in aqueous acidic or basic solutions. Electrolytes include sodium hydroxide, potassium hydroxide, sulfuric acid, nitric acid, and solutions of amine salts. Amine salts have an added advantage in that after treatment, excess electrolyte can be removed simply by heating the fiber to high temperatures (250° C).

2.2.5 Carbon Fiber Sizing

After surface treatment, the fibers are heated to remove volatile materials from the fiber surface which would

otherwise create voids in the composite during high temperature processing. The fibers are sized to protect the fiber surface from surface damage during handling and to protect the surface chemistry created by the surface treatment (49).

2.3 SURFACE ENERGY MEASUREMENT

There are many techniques for probing the chemical and physical properties of a solid surface in order to predict the bonding of organic polymers to solid surfaces. The electronic structure of solid surfaces has been studied by measuring the thermodynamic interaction of the solid surface with simple liquids of known molecular structure. Experimental techniques for measuring the thermodynamic interaction between solid and liquid include contact angle measurement, calorimetry, and gas chromatography. Some of these techniques will be discussed below. Specific techniques related to characterization of carbon fiber surfaces will also be discussed.

2.3.1 Contact Angle Measurement

When a liquid drop is placed on a solid surface, the liquid will either spread on the surface or form a drop. This drop will have an angle between itself and the solid which is indicative of the interaction between the two

materials (50). In addition, the liquid will have a vapor pressure which the solid surface will be in equilibrium with. The forces in the drop are balanced as shown in Figure 2.9 (51). These forces include the tendency of the drop to minimize its surface area by forming a sphere, and the tendency to spread on the solid surface and thus increase the interfacial contact. This balance of forces has been described by the Young equation.

$$(2.1) \qquad \gamma_{sl} - \gamma_{sv} + \gamma_{lv} \cos(\theta) = 0$$

where γ_{sl} is the surface energy between solid and liquid
γ_{sv} is the surface energy between solid and vapor
γ_{lv} is the surface energy between liquid and vapor
θ is the angle of the drop between solid and liquid

By measuring the angle between the liquid drop and the solid surface, the interaction between solid and liquid (γ_{sl}) can be estimated.

Adhesion is defined thermodynamically by the change in free energy when two materials come into contact. The work of adhesion in the contact angle experiment has been defined (50) by Equation 2.2

$$(2.2) \qquad W_a^T = \gamma_{lv} (1 + \cos(\theta))$$

where W_a^T is the total work of adhesion

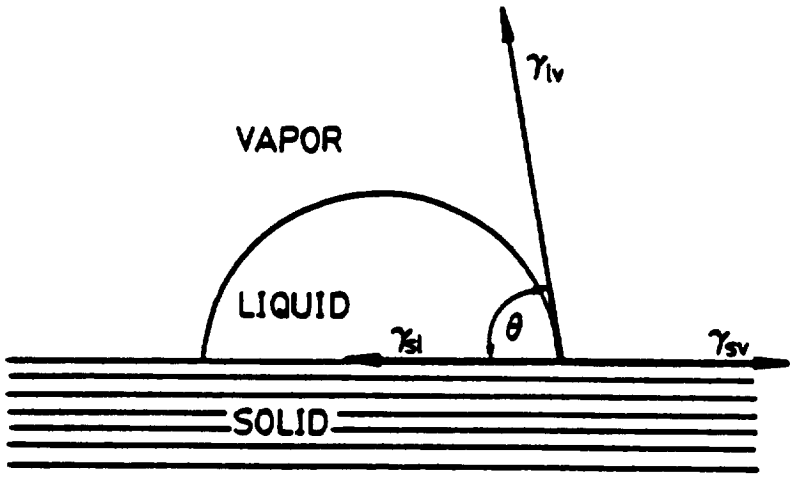

Figure 2.9 Diagram of contact angle experiment. (ref. 51)

γ_{lv} is the surface energy of liquid in vapor
γ_{sl} is the surface energy of solid-liquid interface
γ_{sv} is the surface energy of solid in vapor

Girifalco and Good (52) assumed the interaction between a solid and a liquid could be quantified by an interaction parameter (Φ) times the geometric mean of the surface tension of the solid and the liquid. Equation 2.3 results.

$$(2.3) \qquad \gamma_{sl} = \gamma_{sv} + \gamma_{lv} - 2\Phi \sqrt{\gamma_{sv}\ \gamma_{lv}}$$

Fowkes (53) later postulated that the interaction energy due to wetting of solids by liquids with dispersive force interactions only, could be described by a geometric mean equation as shown in equation 2.4.

$$(2.4) \qquad \gamma_{sl} = \gamma_{sv} + \gamma_{lv} + 2 \sqrt{\gamma^d_{sv}\ \gamma^d_{lv}}$$

where γ^d_{sv} is the dispersive surface energy of the solid

γ^d_{lv} is the dispersive surface energy of the liquid

The interaction between solid and liquid due to polar groups has been considered by Fowkes (54) to be more accurately defined by acid-base interactions. In this model, Fowkes assumes that the interaction between two materials can be described by a component due to dispersive interactions in the form of a geometric mean relationship plus a component due to acid-base interaction. The acid-base interaction indicates the ability of a polar group on one surface to

donate or accept electrons from polar groups on the other surface. The work of adhesion is then described by equation 2.5.

$$(2.5) \qquad W_a^T = W_a^d + W_a^{ab}$$

where W_a^d is the work due to dispersion forces

Kaelble et. al., (55,56) have developed a technique to determine the polar and dispersive components of the surface energy of carbon fibers and other solid surfaces. In this technique, the contact angle of the fibers in several liquids of varying polar and dispersive components is measured. The work of adhesion (W_a) is assumed to be equal to the sum of the geometric mean of the polar components of the surface energies plus a geometric mean for the dispersive surface energy components of the liquid and solid surface energies as shown in equation 2.6.

$$(2.6) \quad W_a = 2\sqrt{\gamma_{sv}^d \gamma_{lv}^d} + 2\sqrt{\gamma_{sv}^p \gamma_{lv}^p} = \gamma_{lv}(1 + \cos(\theta))$$

where γ_{sv}^p is the polar component of the solid surface energy

γ_{lv}^p is the polar component of the liquid surface energy

The polar and dispersive components of the surface energy were calculated by dividing both sides of equation 2.6 by

$2\sqrt{\gamma^d_{lv}}$ as shown in equation 2.7.

$$(2.7) \quad \gamma_{lv}\left[\frac{(1+\cos(\theta))}{2\,\gamma^d_{lv}}\right] = \sqrt{\gamma^d_{sv}} + \sqrt{\frac{\gamma^p_{lv}}{\gamma^d_{lv}}} \times \sqrt{\gamma^p_{sv}}$$

The contact angle is measured in a series of liquids with varying polar and dispersive surface energy components. The components of the fiber surface energy can be determined by plotting the left hand side of equation 2.7 as a function of $\sqrt{\gamma^p_{lv}}/\sqrt{\gamma^d_{lv}}$ of the liquid. The slope of this plot will be equal to $\sqrt{\gamma^p_{lv}}$ of the solid. The intercept will be equal to $\sqrt{\gamma^d_{lv}}$ of the solid.

If the surface energy of a polymer and a solid are both estimated using Kaelble's method, the work of adhesion between polymer and solid can be calculated using equation 2.6. However, it should again be noted that Fowkes (54) has argued that the geometric mean relationship to describe the polar group interaction between two materials may better be described by acid-base interactions.

2.3.2 Contact Angle Measurement on Small Diameter Fibers

Since carbon fibers are so small, it is very difficult to measure the contact angle of a drop on a fiber. Several techniques have been developed to measure the contact angle of a drop on a small fiber under a microscope (57). A

simpler method for contact angle determination is to measure the wetting force of the fiber when it comes into contact with a liquid (55,56,58,59). If the surface energy of the liquid is known, the contact angle of the liquid on the fiber can be calculated by the relationship shown in equation 2.8.

$$F = \pi d \gamma_{lv} \cos(\theta) \qquad (2.8)$$

where F is the wetting force
d is the fiber diameter

This equation assumes that the cross section of the fiber is circular. If the cross section is not circular, the πd term in equation 2.8 would be replaced by the actual circumference of the fiber. The circumference could be determined by measuring the wetting force of the fiber in a liquid that completely wets the fiber (ie. $\cos(\theta) = 0$) as described by Herb, et al. (60).

2.3.3 Inverse Gas Chromatography for Measurement of Solid/Vapor Interaction

The idea of putting carbon fibers in a gas chromatography column and passing probe molecules through the column to measure the fiber-liquid interaction was first used by Brooks and Scola (61). Initial investigations using this technique known as inverse gas chromatography (IGC) were inconclusive (62). However, Schultz (63) has used IGC

to show that the surface of carbon fibers obtained from Hercules Inc. were acidic in nature.

IGC measures the retention times of the probe molecules in the column. Molecules with a high adsorption enthalpy will take longer to pass through the column than molecules with a low adsorption enthalpy. If probe molecules of varying acid-base character are used, the acid-base properties of the fiber can be determined. This technique has also been used to determine the surface area of carbon fibers by using non-polar probe molecules (64).

2.3.4 Calorimetric Measurement of Solid/Liquid Interaction

The thermodynamic interaction between a liquid and a solid can be measured using calorimetry. In this technique, a solid and liquid are brought into contact with each other in a cell with a sensitive heat detector. As the liquid wets the solid, heat is generated which is detected by the heat detector. This technique has been used by Rand and Robinson (65) to measure the heats of wetting of carbon fibers in acidic and basic liquids. It was found that basic probes gave a much higher heat of wetting indicating an acidic fiber surface. Since the surface areas of carbon fibers are low, the amount of heat generated is low and precise measurement is difficult.

2.4 DETECTION OF FUNCTIONAL GROUPS AND MOLECULAR STRUCTURE OF CARBON AND POLYMER SURFACES

Some of the functional groups expected on carbon surfaces include carboxylic acids, phenols, quinones, lactones, ethers, peroxides, and esters. These groups are shown in Figure 2.10. Functional groups on carbon surfaces have been detected by such methods as polarography, titration, x-ray photo-electron spectroscopy, radioisotope labelling (44), and infrared spectroscopy. Some of these techniques are discussed below.

2.4.1 Titrimetric Methods for Carbon Fiber Surface Functionality Determination

Functional groups on carbon surfaces have been identified by reacting the material with reagents that will react with specific functional groups on the carbon surface. The amount of reagent reacted is determined by titration. Several reviews of these techniques for analysis of carbon surfaces are available (66-71). These reactions require very large surface areas or else large quantities of material for the method to be sensitive enough to detect these functional groups.

2.4.2 X-ray Photoelectron Spectroscopy (XPS) of Carbon Fiber Surfaces

X-ray photoelectron spectroscopy commonly referred to

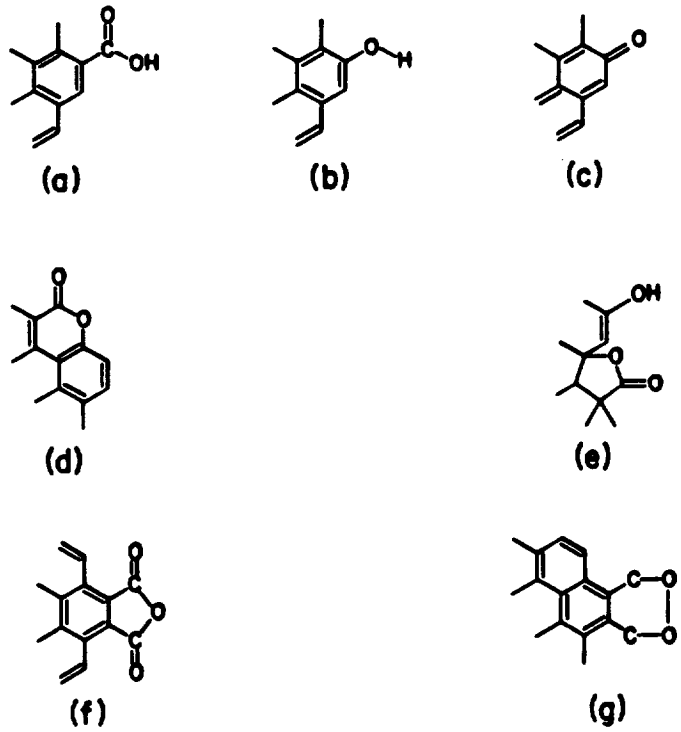

Figure 2.10 Predicted oxygen functional groups on carbon surfaces a) carboxyl group, b) phenolic hydroxyl, c) quinone, d) lactone, e) fluorescein - like lactone, f) carboxylic acid anhydride, g) cyclic peroxide (ref. 66)

as XPS or ESCA (for electron spectroscopy for chemical analysis) uses the photoelectric effect to analyze the chemistry of solid surfaces (72). In this technique shown schematically in Figure 2.11, a solid surface is exposed to nearly monochromatic x-rays. This exposure causes electrons to be ejected from the solid surface. These ejected electrons will have a spectrum of kinetic energies as they come from within the structure of the solid. At certain energies the number of ejected electrons will increase. This peak in intensity is caused by ejection of electrons from within the atomic structure of atoms on the surface of the solid.

The energy of the electrons at the peak is indicative of the element present. Since the x-rays are nearly monochromatic, the kinetic energy distribution of these electrons will be the narrow. The kinetic energy (KE) will be equal to the photon energy of the x-rays (hv) minus the binding energy of the electron in the atomic structure of the element (BE) minus a work function (Ω) as shown in equation 2.9.

$$KE = hv - BE - \Omega \tag{2.9}$$

The intensity of this photoelectron peak for element (i) is proportional to the number of atoms on the solid

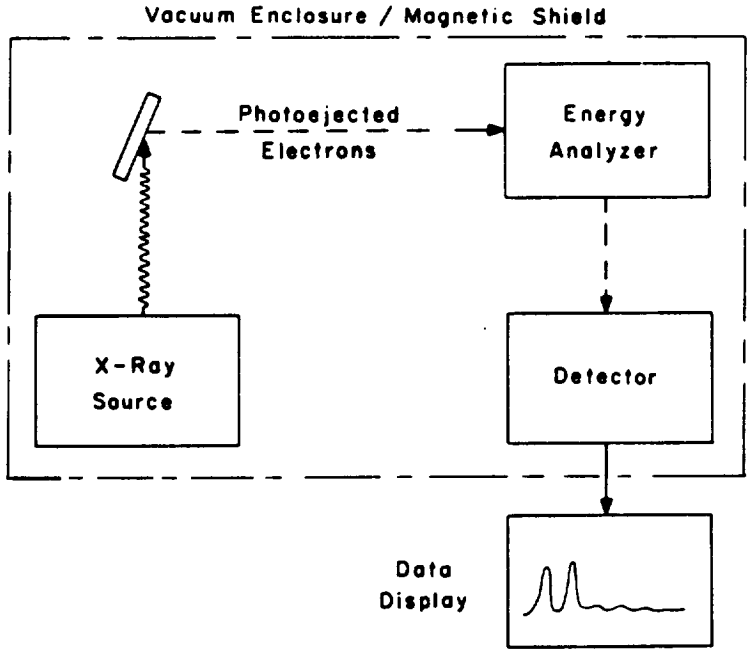

Figure 2.11 Schematic diagram of x-ray photoelectron spectroscopy experiment (ref. 72)

surface (N_i), the cross section of the atom to x-rays (μ), the mean free path (λ) of the electrons in the solid which is typically 5 nm, the x-ray energy flux (F), and the geometric arrangement of the spectrometer (73). The relationship for the photoelectron peak intensity (I_i) for element (i) is shown in equation 2.10.

$$(2.10) \qquad I_i = \int_0^\infty F\, k\, N_i(x)\, \mu \exp^{-[\, d\, /\, \lambda\,]}\, dx$$

where k is a constant specific to spectrometer
x is the perpendicular distance from the surface into the sample
d is the distance the electrons travel through the solid before exiting

This relationship allows determination of the relative percentage of a given element on a surface from the relative peak intensities. Values for the atomic cross sections have been calculated by Scofield (74). Empirical equations for calculating the electron mean free path have been developed by Cadman, et al (75). Wagner (76) has determined sensitivity factors for each element to relate peak intensities to atomic concentration.

2.4.2.1 Angular Dependent Depth Profiling

Many materials will have a variation of chemical groups present from the surface into the bulk of the material. The surface composition profile can be studied by varying the

angle at which the electrons ejected from the solid surface are detected.

The calculated escape depth for photo emitted electrons is about 5 nm. Ejected electrons measured at 90 degrees to the surface will come from 0-5 nm within the surface. Ejected electrons measured at less than 90 degrees, will come from less than 5 nm. This is shown schematically in Figure 2.12. Thus by varying the angle between the surface and analyzer, a depth profile can be obtained. The escape depth normal to the sample (x) will be equal to the electron escape depth (d) times the sine of the take-off angle (θ) as shown in Figure 2.12 and described in equation 2.11.

$$x = d\ (\sin(\theta)) \qquad (2.11)$$

By decreasing the take-off angle in the XPS experiment, a higher percentage of atoms from the top few atomic layers of a solid surface can be analyzed. The change in relative amounts of elements detected as the take-off angle is changed will give an indication of the distribution of elements from near the surface into the surface of the material.

2.4.2.2 Peak Shape Analysis

If all the elements present on a solid surface were in

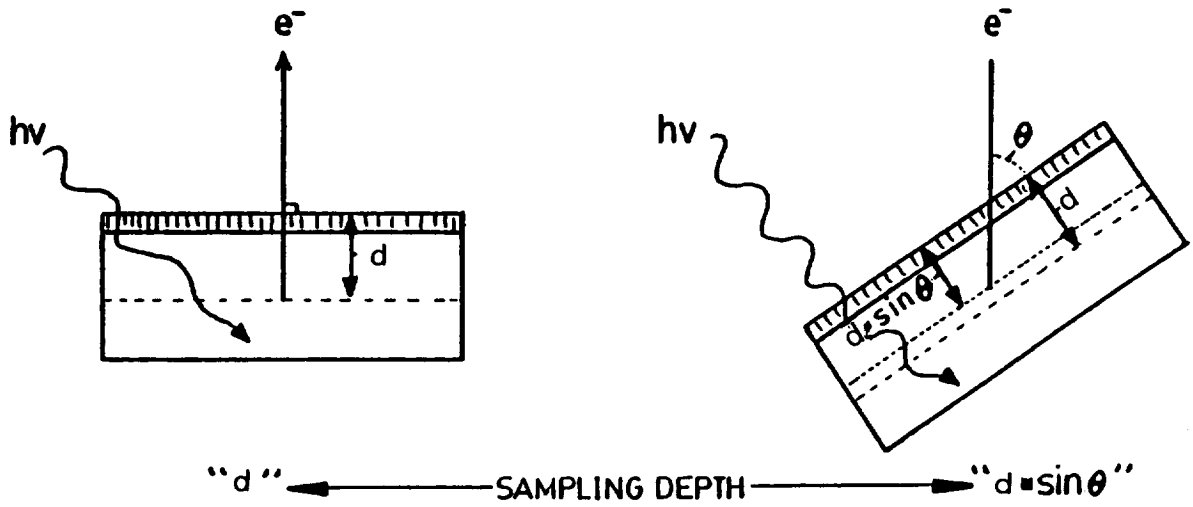

Figure 2.12 Schematic diagram for angular dependent depth profiling using XPS (ref. 51)

the same bonding environment, it would be expected that the kinetic energy of the photoelectrons emitted from the solid surface would have a very narrow distribution. However, the actual width of the peak measured on an electron spectrometer is influenced by interaction of the ejected electrons with the solid material as well as by the spectrometer itself.

The elements in most materials are not in just one binding state. The binding energy of electrons in the atom is influenced by the valence state of the atom. The functionality of a solid surface can thus often be determined by observing shifts in the XPS peaks.

XPS photopeaks are typically curve fit with gaussian shaped peaks. The peaks are assigned a width typical of the spectrometer being used and of the element being studied. The peaks are shifted in binding energy to represent the chemical environment of the element. The intensity of the curve fit peak is proportional to the amount of that functional group present.

For a particular element, the number of peaks used to fit the photopeak is equal to the number of different functionalities expected for that element. Sometimes, the expected functionalities will have similar or overlapping binding energies. In this case, either several overlapping

peaks can be used to fit the overall peak, or else the width of the curve fit peak can be increased.

For each element there has been much work done to observe the binding energy shift caused by specific binding states (77). The shifts in binding energy expected for carbon, oxygen, and nitrogen in organic materials are summarized below.

2.4.2.2.1 Carbon 1s Peak Shape Analysis

The photopeak observed from the carbon 1s atomic orbital has been widely analyzed. The peak due to C-C bonding occurs at a binding energy of 285.0 eV which is often used for instrument calibration. Many standard materials have been examined and the corresponding shift due to functional groups present observed. Clark (77) has performed many studies on XPS analysis of polymer surfaces. He has reported the carbon 1s binding energy shifts of many functional groups. Clark's results have been briefly reviewed by Briggs (78). A basic trend reported by Briggs (78) is that R-C-O type bonds will shift the carbon 1s photopeak about +1.5 eV, R-C=O bonds will cause about a +3 eV binding energy shift, and R-C$\lesssim^{O}_{O}$ bonds will cause about a + 4.5 eV binding energy shift.

Proctor and Sherwood (79) have studied the carbon 1s spectrum of carbon fiber and graphitic surfaces. They have

shown that in addition to peak shifts due to functional groups there is also a peak at about +6 eV from the main C-C peak due to interaction of ejected core electrons with plasmons from the conduction electrons in graphite. They also pointed out that certain functional groups on graphitic type surfaces may occur at different binding energies due to aromaticity of the carbon structure to which the functional group is attached.

2.4.2.2.2 Oxygen 1s Peak Shape Analysis

The binding energy shift for oxygen bound to carbon is less well defined than the shift of carbon. Most of the oxygen peaks fall in a narrow (2 eV) range centered around 533 eV. Oxygen doubly bound to carbon tends to have a lower binding energy than singly bound oxygen.

2.4.2.2.3 Nitrogen 1s Peak Shape Analysis

Most nitrogen associated with carbon also falls in a narrow region between 399-401 eV. Oxidized nitrogen shifts (6-8 eV) to higher binding energy. Clark (77) has shown for polymers that a nitrogen binding energy of about 400 eV is due to amine groups whereas a binding energy of about 401.5 eV is due to nitrogen bound to oxygen and/or nitrogen bound to carbon containing carbonyl groups.

2.4.2.3 Derivatization

Everhart and Reilley (80) have developed a systematic approach to the identification of functional groups on oxidized polymer surfaces. In their work, they have reacted polymer surfaces with a series of reagents that will react with specific functional groups. The reagents chosen also contained an element that could easily be detected with XPS. Some of the reagents used by Everhart and Reilley are described in Appendix I. Most of these reagents were fluorine containing compounds.

This technique does have several drawbacks including the specificity of the derivatizing reagent, determination of the extent of the reaction and determining how many of the actual functional groups have reacted, and the stability of the reagent to x-rays. The question of whether reactions that occur in solution can be extended to a two dimensional surface remains unanswered.

2.4.3 Secondary Ion Mass Spectrometry

In secondary ion mass spectrometry (SIMS), a solid surface is bombarded with ions causing ion fragments from the solid surface to be removed. The mass to charge ratios of the ion fragments ejected from the surface are analyzed in a mass spectrometer. By analyzing the mass to charge ratios of these fragments, the molecular and atomic

structure of the solid can be inferred. Trace elements can also be detected.

With high primary ion currents, material is removed from the solid surface rapidly and a depth profile is obtained. At low ion currents, the top few atomic layers of the surface are removed. Detailed information about the molecular structure of the solid surface is thus obtained.

This technique has been applied to the analysis of polymer surfaces by Briggs (81,82) and Brown (83). Spectra obtained at low current observation led to detailed fingerprint spectra of polymer surfaces. Specific fragments could be assigned to either aliphatic or aromatic compounds.

One problem with analyzing polymer surfaces with SIMS is static charging caused by the primary ion current. In Briggs' work (81,82), the ion current was neutralized with an electron gun. Recent developments in the analysis of polymer surfaces by mass spectrometry have included a gun that will bombard the solid surface with neutral atoms such as argon (83). This neutral atom bombardment referred to as fast atom bombardment mass spectrometry (FABMS) greatly reduces the static charging problem encountered in the normal SIMS experiment.

2.4.4 Models for Fiber Breaking Strength as a Function of Length

The mathematical models used to predict the fiber strength as a function of length considers the fiber as chain of links (84-87). When the chain is pulled in tension, it will break at the weakest link. The probability of a fiber having a specific breaking strength is equal to the probability that each link in the chain will have a breaking strength larger than the fiber breaking strength, i.e., the reliability. This is shown in equation 2.12.

$$g(\sigma) = [\, R_o\,(\sigma)\,]^n \qquad (2.12)$$

where
- σ is the stress
- $g(\sigma)$ is the probability distribution for fiber strength
- R_0 is the reliability of a link surviving to stress (σ)
- n is the number of links in the fiber

Taking the logarithm of both sides of this equation gives equation 2.13.

$$\ln [\, g(\sigma)\,] = \sum_{1}^{n} \ln [\, R_0\,(\sigma)\,] \qquad (2.13)$$

Assuming an infinite number of links the summation can be replaced with an integral over the length (L) of the fiber. The integral is shown in equation 2.14.

$$(2.14) \qquad \ln [\, g(\sigma) \,] = \int_0^L \ln [\, R_0 (\sigma) \, dx \,]$$

The reliability function has been assumed (84) to take the the form of the Weibull distribution (85) shown in equation 2.15 where α and β are shape and scale parameters, respectively.

$$(2.15) \qquad R_0 = \exp - [\, \sigma / \beta \,]^{\alpha}$$

Substituting equation 2.15 into equation 2.14, integrating and taking the exponent of the integral gives equation 2.16.

$$(2.16) \qquad g(\sigma) = \exp - \left[\, L \, [\, \sigma / \beta \,]^{\alpha} \right]$$

Equation 2.16 gives the dependence of fiber strength on fiber length. Methods for estimating the parameters α and β are given in Appendix II. The parameter α is a shape parameter and is indicative of the distribution of flaws on the surface of the fiber (86,87). A high value of α indicates a high flaw density and thus little dependence of strength on length. A low value of α indicates few flaws on the fiber surface and thus a strong dependence of strength on length.

2.5 TESTS OF ADHESION OF CARBON FIBERS TO POLYMERIC MATRICES

Tests for adhesion of polymeric matrices to carbon fibers can be classified into two general categories: single fiber tests and multiple fiber or composite tests. Single fiber tests have the advantage that they are normally easy to perform and can be done on a small quantity of fiber. Sample preparation is generally inexpensive. A disadvantage is that the single fiber test is possibly not indicative of the performance of an actual composite. Multiple fiber or composite tests on the other hand will give a very good indication of the expected composite performance. These tests have the disadvantage of expensive and time consuming sample preparation requiring large quantities of material.

2.5.1 Single Fiber Adhesion Tests

Single fiber adhesion tests are performed by embedding a single fiber in a matrix and then measuring the adhesive strength by applying a force and observing the failure of the bond. Two common single fiber tests are the fiber pull-out test and the fiber critical length test.

2.5.1.1 Fiber Pull Out

In the fiber pull-out test, a fiber is embedded in a very thin (normally about 0.5 mm) film (88) or bead (89) of

polymer. The fiber and film are placed in a tensile testing machine. The fiber is pulled out of the polymer film. The force required to remove the fiber is measured with a load cell. The adhesive strength of the joint is calculated by dividing the measured load by the area of contact of the fiber with the polymer. The area of contact is normally measured in a scanning electron microscope.

This technique is very tedious and time consuming. The small diameter of the fiber requires that the area of interfacial contact be small. If the contact area is not small, the risk of fiber breakage rather than fiber pull out will alter the data analysis.

2.5.1.2 Fiber Critical Length Experiment

In the fiber critical length (FCL) experiment, a single fiber is embedded in a polymeric matrix (90-97). A typical specimen is shown in Figure 2.13. The specimen is then pulled in tension. As the strain is increased, the fiber will break. When the fiber first breaks, the matrix will retain the fiber fragments from attaining their unstressed dimension. Stress will be transferred to the fiber by the matrix. The axial stress in the fiber at a distance from the break will increase until it reaches the original stress in the fiber before the first break. Further increase in the specimen strain will result in another break in the

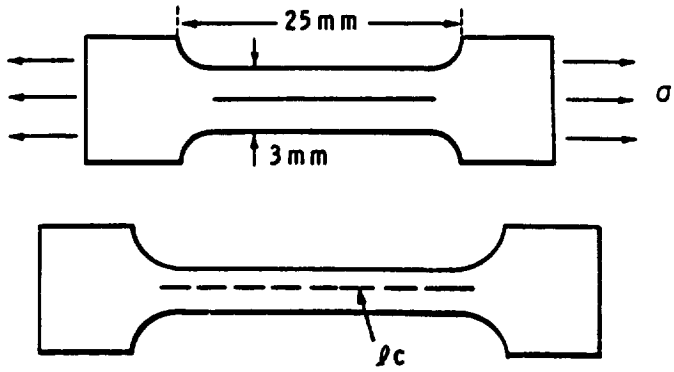

$$\tau = \frac{\sigma_c}{2}\left(\frac{d}{\ell_c}\right)$$

Figure 2.13 Diagram of fiber critical length experiment (ref. 90)

fiber. This fiber breakage will continue with increased strain until the fiber fragments become so small that the matrix can no longer transfer stress over a long enough distance to break the fiber. The length of the broken fiber fragments is referred to as the fiber critical length (l_c). The fiber critical length is an indication of the ability of the polymeric matrix to transfer stress to the fiber.

If the stress transferred across the interface (τ) acts over a length l_c then a force balance can be obtained by setting the total force transferred across the interface equal to the breaking strength of the fiber (σ_f) times the area of the fiber as shown in equation 2.17.

$$(2.17) \qquad \int_0^{l_c} 2\pi r \tau(l)\, dl = \pi r^2 \sigma_f$$

where r is the fiber radius

The shear stress is assumed to be some function of the distance (l) along the length of the fiber. If we assume that the shear stress is a maximum at the fiber tip (τ_{max}) and decays linearly along the length of the fiber fragment (l_c) equation 2.18 results.

$$(2.18) \qquad \int_0^{l_c} 2\pi r \tau_{max} \left[1 - \frac{l}{l_c} \right] dl = \pi r^2 \sigma_f$$

Integrating and rearranging to solve for τ_{max} gives equation

2.19.

$$\tau_{max} = \frac{\sigma_f \; r}{l_c} \qquad (2.19)$$

Assuming that the average shear stress transferred is equal to one half of the maximum shear stress, an equation for the average shear stress shown in equation 2.20 results.

$$\tau_{ave} = \frac{\sigma_f \; r}{2 \; l_c} \qquad (2.20)$$

Calculation of τ_{ave} gives an indication of the ability of the matrix to transfer stress to the fiber. Since there is normally no interfacial failure between fiber and matrix, it is incorrect to call τ the interfacial shear strength. Rather, it is a measure of the stress transfer across the interface and should be referred to as the stress transfer or stress transfer coefficient.

In an actual experiment, the fiber fragments will have a range of lengths. This is due to the statistical nature of fiber fracture. The lengths of the broken fragments will range from the critical length to two times the critical length. Ohsawa, et al. (91) have used a simple average to calculate l_c from the average fiber length l_a as shown in equation 2.21.

$$(2.21) \qquad l_a = \frac{l_c + 2l_c}{2} \; ; \quad l_c = \frac{2}{3} l_a$$

A more sophisticated model by Drzal, et al. (92) uses a Weibull distribution to describe the fragment lengths.

In order to calculate the interfacial shear stress in the fiber critical length experiment, the strength of the fiber at the critical length must be known. However, the strength of the fiber depends on the flaw distribution of the fiber. Typical fragment lengths in a fiber critical length experiment for carbon fibers are about 0.5 mm. Rich and Drzal (93) have measured the strength of carbon fibers at these short lengths. This process is very tedious.

Estimates of the fiber strength at shorter lengths have been made by extrapolation using equation 2.16 and breaking strengths at longer lengths. Correlation between predicted strengths and measured strengths are not good however (86). This is due to the fact that at shorter lengths, the fiber strength will approach the ultimate strength of the material. The strength will no longer be flaw dominated which is what is being measured at the longer lengths. Use of this extrapolation then for calculating interfacial stress in the FCL experiment may lead to incorrect conclusions.

2.5.2 Photoelastic Stress Transfer Observation in the Fiber Critical Length Experiment

Additional information can be obtained by observation of the stress transferred between fiber and matrix at the broken end of a fiber fragment. The stress in the matrix at the tip of the broken fiber will rise sharply as shown in Figure 2.14 (94). Failure modes at the fiber tip have been reviewed by Mullin and co-workers (95,96). If the fiber matrix adhesion is poor, failure will occur at the interface as shown in Figure 2.15b. If the matrix is brittle, matrix cracking will occur and the specimen will fail after one fiber break as shown in Figure 2.15a. If a ductile matrix is used and the adhesion between fiber and matrix is high, the matrix will fail by shear as shown in Figure 2.15c. Observation of these failure modes can be observed under a microscope with crossed polarizers (90,92,93) to enhance the information obtained from measurement of the fiber critical length.

2.6 SURFACE PROPERTIES OF CARBON FIBERS

Carbon fiber surfaces are treated chemically in order to enhance bonding of the fiber to the resin in a composite. In so surface treating, functional groups are created on the fiber surface. Many studies have been conducted to observe the effect of functional groups on carbon fiber/epoxy matrix adhesion (97-102).

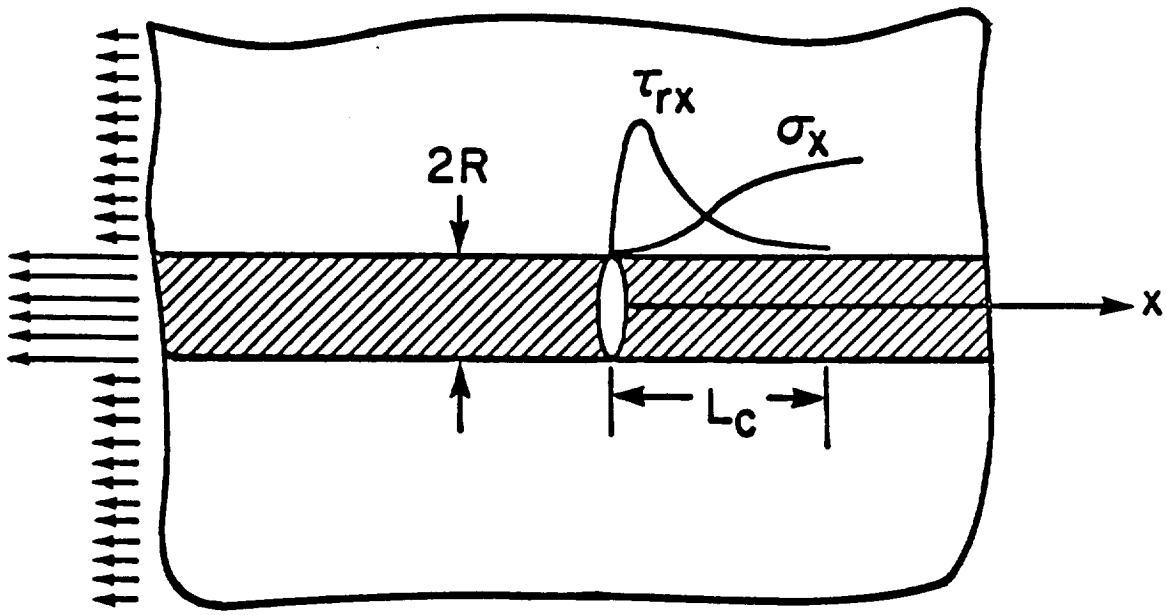

Figure 2.14 Theoretical stress distribution at the tip of a broken fiber in the fiber critical length experiment (ref. 92)

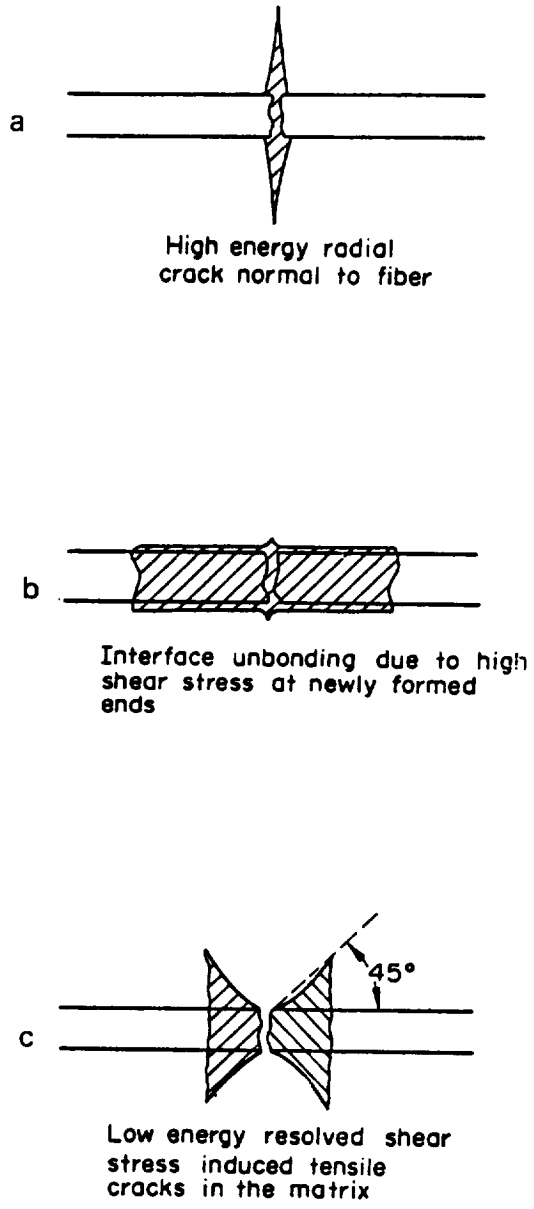

Figure 2.15 Diagram of possible failure modes in the fiber critical length experiment a) matrix cracking, b) frictional stress transfer, c) shear stress transfer (ref. 95)

2.6.1 Studies of Carbon Fiber Adhesion to Polymeric Matrices

Donnet and co-workers (97-99) have studied adhesion between epoxy resins and carbon fibers after anodization in NaOH and HNO_3. The amount of acid groups on the fiber surface was determined by titration. Mild NaOH was used to neutralize strong acidic groups such as carboxyl and phenol. $NaOC_2H_5$ was used to neutralize weaker acidic groups such as hydroxyl and carbonyl. A direct correlation was found between the number of carboxylic acid groups and the interlaminar shear strength of the composite as shown in Figure 2.16.

Fitzer, et al. (100) have studied the surface treatment of carbon fibers by boiling in nitric acid. By chemically blocking specific functional groups, they were able to determine which groups were most responsible for adhesion. Blocking of strong and weak acidic oxides resulted in significant reduction of composite shear strength. Adhesion was thus concluded to be caused by chemical bonding of the epoxy to acidic groups on the fiber surface.

In addition to functional groups being created by surface treatment, it is also possible that the surface treatment will affect the molecular and morphological structure of the carbon fiber surface. Pores may be created which can enhance mechanical bonding. This has been best

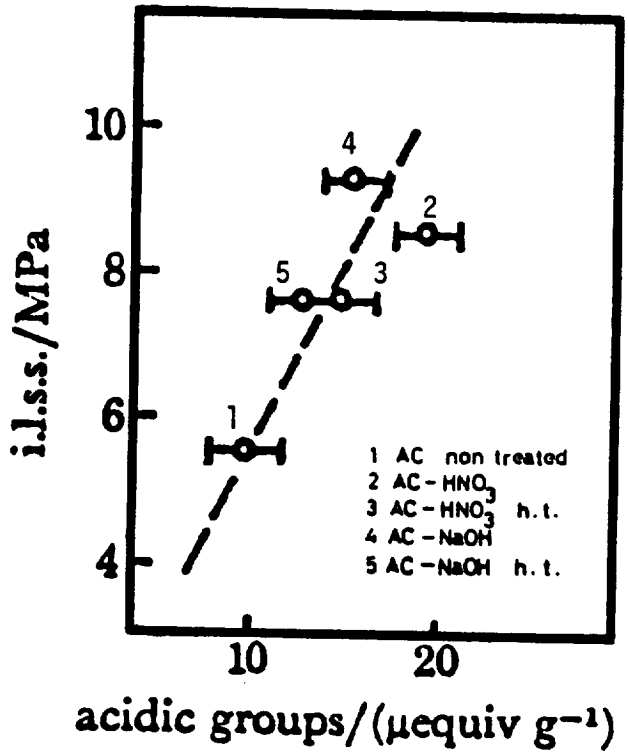

Figure 2.16 Effect of surface acidic groups on the interlaminar shear strength (i.l.s.s.) of carbon fiber composites. (ref. 97)

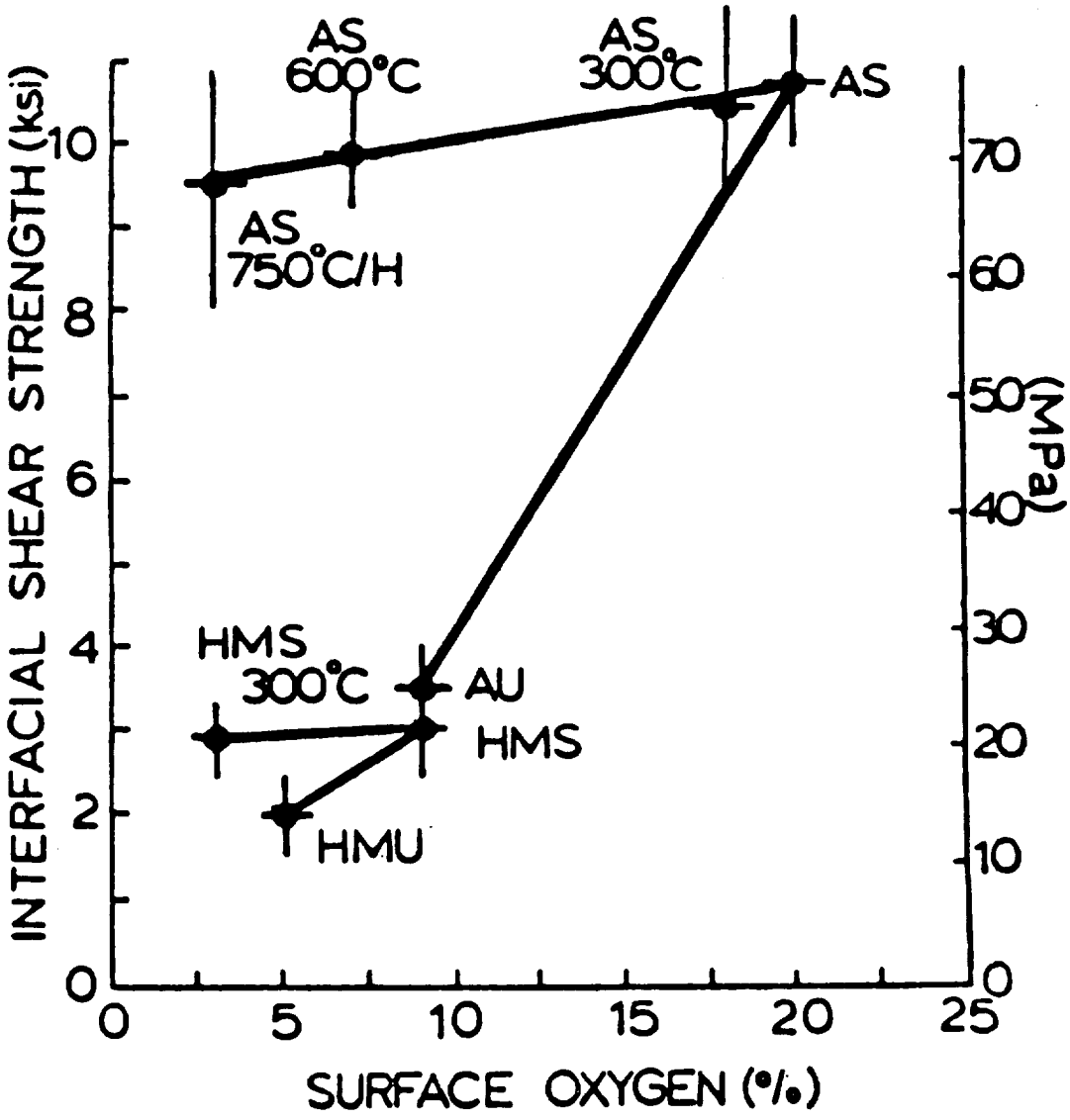

Figure 2.17 Effect of surface oxygen content on interfacial shear strength measured on single fiber. AU and HMU indicate no commercial surface treatment. AS and HMS indicate commercial surface treatment. Temperatures indicate heat treatment for removal of oxygen. (ref. 102)

demonstrated by Drzal (101,102) whose results are shown in Figure 2.17. In this figure, the interfacial shear strength of a carbon fiber/epoxy matrix bond is plotted against the surface oxygen content of the carbon fiber. The oxygen content is indicative of the amount of functional groups on the surface. The AU fiber had no surface treatment and thus a low oxygen content. The AS fiber had been surface treatedcommercially and thus had a high oxygen content. The AU fiber had a very low interfacial shear strength. The AS fiber had a high shear strength. Upon removal of the functional groups from the AS fiber, the oxygen content is greatly reduced indicating loss of functional groups. However, the interfacial shear strength remains high. This indicates that adhesion promotion is not due solely to the addition of functional groups on the fiber surface, but also to the crystal and molecular structure of the fiber surface.

The crystal structure of carbon fiber surfaces has been studied with Raman spectroscopy (103-105). The Raman spectrum of carbon fibers gives two peaks. One peak due to the graphitic nature of carbon fibers occurs at 1575 cm^{-1}. The other peak at 1355 cm^{-1} has an intensity inversely proportional to the graphite crystal size. By comparing the ratio of the 1355 cm^{-1} peak to the 1575 cm^{-1} peak, the crystal size at the surface of carbon fibers can be estimated. Tuinstra and Koenig (104) have observed that as

the 1355 cm^{-1} peak decreases, the interlaminar shear strength of the composite also decreases. This indicates that bonding is affected by the crystal structure of the carbon fiber surface. Further evidence supporting this idea has been expressed by Brelant (106) who showed an inverse correlation between the thermal conductivity of the composite and its interlaminar shear strength.

2.6.2 Effect of Surface Treatment on Carbon Fiber Surface Properties

In order to understand how these surface treatments enhance adhesion, it is necessary to understand how specific surface treatments alter the surface properties of carbon fibers. Considering the turbostratic carbon structure shown in Figure 2.4, there are three possible locations for oxidation to occur. Functional groups can be created at the crystal edges, between layers, or at the basal planes.

Unfortunately, the surface treatments used by commercial producers of carbon fibers are proprietary. Much of the work on characterization of carbon fiber surfaces has been performed on fibers with proprietary surface treatments (101,102, 107-111). Although these studies show that oxygen and nitrogen functionalities are being added to the fiber surface treatment by surface treatment, they do not give much insight into the reactions occurring during surface

treatment. Nor do these studies begin to set a standard for surface treatment.

The most extensive study of carbon fiber surface treatments has been done by Sherwood and co-workers (112-116). Some of their conclusions are outlined here. The functional groups created by anodization in H_2SO_4 and NH_4HCO_3 were dependent on the anodization potential (112). Carbonyl (R-C=O) bonds were formed at low potentials while (R-C-O) bonds were formed at higher potentials (112). Anodization in nitric acid yielded mostly C=O functionality (114). Anodization at high pH attacked primarily the edges of the graphitic planes while anodization at neutral and low pH attacked between the carbon layers creating a graphite oxide (115). Nitrogen functionality can be created on the carbon fiber surface by anodization in ammonia saturated ammonium bicarbonate solution (116).

3) METHODS AND MATERIALS

3.1 APPROACH

Carbon fibers produced by different companies are prepared under various conditions. These varying conditions will affect the surface as well as the bulk properties of the fiber. The surface treatment also varies with each company. Since the production conditions and surface treatments are proprietary information, it is difficult to determine which factors are responsible for differences in adhesion of carbon fibers to polymeric matrix materials. The approach taken in this work was to treat carbon fibers from three different companies with the same surface treatment. If the reactivity of each fiber is the same the same surface functionality will result on each fiber. Differences in fiber/matrix adhesion will thus be caused by differences in fiber surface topography and morphological structure.

First, the anodization mechanism was studied. Fibers from one producer were anodized in various electrolytes and the chemical functionality observed with XPS. The chemical and molecular structure of the fiber surface was further probed after anodization in NaOH and H_2SO_4 by angular dependent depth profiling using x-ray photoelectron spectroscopy, ultraviolet absorption spectroscopy of the

anodization bath, fast atom bombardment mass spectrometry (FABMS) of the anodized fiber surfaces, and surface free energy analysis. The effect of surface treatment on breaking strength of the fiber was studied. An optimum anodization time for maximum fiber breaking strength was determined. The bond formation between thermoplastic resin and carbon fiber was studied by observing the effect of annealing temperature on adhesion to carbon fibers.

Carbon fibers synthesized from polyacrylonitrile with about the same mechanical properties were chosen from several producers. The as received fibers were studied by STEM and XPS before and after commercial surface treatment. These fibers were then given the same surface treatment. X-ray photoelectron spectroscopy (XPS) was used to determine if the chemical functionality of each fiber surface was the same after treatment. The topography of the fiber surfaces was observed by scanning transmission electron microscopy (STEM). Fiber breaking strengths were measured before and after surface treatment. Adhesion tests were performed using a fiber critical length test on these treated fibers. The results were compared between different fibers with the same treatment, and between the same fiber with different treatments. Since these fibers had the same surface treatment, differences in adhesion should be caused by physical differences, such as surface and bulk morphology.

3.2 MATERIALS

3.2.1 Carbon Fibers

The carbon fibers used in this study and their properties are summarized in Table 3.1. The 'S' designation indicates that the fiber had undergone a proprietary surface treatment. The 'U' designation indicates that the fiber had not been surface treated. All of the fibers were received without sizing. These are all considered to be high strength - low modulus carbon fibers.

The fibers were received on spools containing 12,000 continous filaments (6,000 for the untreated Union Carbide T-300). After discarding the first ten meters of fibers on each spool, the fibers were used as-received. The Union Carbide fibers were used without discarding the first ten meters due to the limited amount available.

3.2.2 Thermoplastic Resins

The resins used for the adhesion studies and some of their mechanical properties are listed in Table 3.2. These resins are generally considered to be high toughness thermoplastics. They are all soluble in methylene chloride and do not crystallize easily. The molecular repeat units for each of these polymers are shown in Figure 3.1.

Table 3.1. Carbon fibers used for adhesion studies

Producer	Fiber	Lot number	Production Date	Tensile Modulus (GPa)	Tensile Strength (GPa)
Dexter Hysol***	XAS	XA0059E	11/85	231	3.09●●
Dexter Hysol***	XAU	XA0066	1/86	228	3.41●●
Hercules*	AS-4	193-6			3.45●●
Hercules*	AU-4	126694A			3.91●
Union Carbide**	T-300S	-----	12/83	318*	2.32*●●
Union Carbide**	T-300U	-----	12/83	345*	2.25*●●

*** obtained from RK Fibers, Philadelphia, PA.

* Obtained from Dr W.D. Bascom, Hercules Aerospace, Magna, Utah

** Obtained from Dr. D. Everhart, Union Carbide, Bound Brook, NJ

* Lot Number unknown values are average for fibers manufactured in that time period

● Fiber Lot Acceptance Data

●● Laminate Data

Table 3.2. Thermoplastic resins used for adhesion studies (reference in parenthesis)

	Poly-Sulfone	Poly-Carbonate	Poly Ether Imide
Source Catalogue No. Lot No.	SPP* #046 #8	SPP* #035 #7	GE**
Density (g/cm^3)	1.24 (118)	1.20 (118)	1.27 (119)
Tg (°C)	190 (118)	150 (118)	219 (119)
Tensile Strength (MPa)	65.5 (118)	105 (118)	
Tensile Modulus (MPa)	2482 (118)	2379 (118)	3000 (119)
Tensile Yield Strength (MPa)	70.3 (118)	62.1 (118)	105 (119)
Tensile Elongation Ultimate (%)	50-100 (118)	110 (118)	60 (119)
Shear Strength (MPa)			100 (119)
Critical Stress Intensity ($MPam^{1/2}$)	2.4 (120)	3.6 (120)	3.5 (120)
Thermal Expansion Coefficient (ppm/°C)	55.8 (118)	7.5 (118)	62 (119)

* Scientific Polymer Products
** General Electric (Ultem 1000)

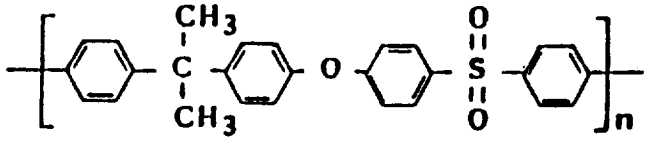

a) Polysulfone

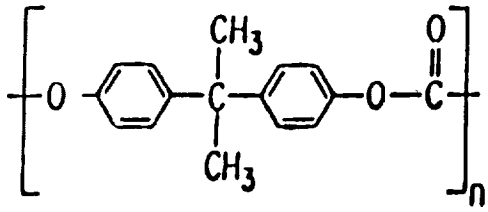

b) Polycarbonate

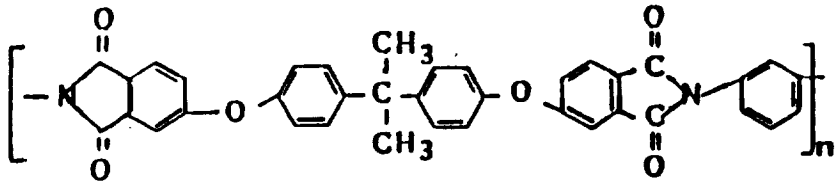

c) Polyetherimide

Figure 3.1 Chemical structure of thermoplastic resins used for adhesion studies a) polysulfone, b) polycarbonate, c) polyetherimide.

3.3) CARBON FIBER SURFACE ANALYSIS

3.3.1) X-Ray Photoelectron Spectroscopy

XPS spectra of the carbon fibers were recorded on a Perkin Elmer PHI 5300 electron spectrometer with a magnesium K_α x-ray source operated at 250 milliwatts power. Operating pressures in the spectrometer ranged from 2 X 10^{-8} to 4 X 10^{-7} torr. Approximately thirty six thousand parallel fibers 25.4 mm long were placed on the sample mounting probe. The fibers were held to the probe by painting about 3 mm of each end of the fiber bundle with silver paint. Fibers were mounted in the spectrometer such that the fibers were aligned parallel to the line from the mounting probe to the electron energy analyzer. Rotation for angular dependent studies thus occurred around an axis perpendicular to the long fiber axis.

The area (A) under each photopeak was divided by a sensitivity factor (SF) specific to each element and the time (ST) that the element was scanned for in the spectrometer. The atomic fraction of each element detected (AF) was equal to this quantity divided by the sum of this quantity for each element detected as shown in equation 3.1. On the Perkin Elmer instrument, the area is divided by the scan time by the intruments's computer. The sensitivity factors used for each element detected were the same as reported by Wagner (76) and are listed in Table 3.3.

$$(3.1) \qquad AF_i = \frac{(A_i)\ /[(SF_i)(ST_i)]}{\sum_{i=1}^{n} (A_i)\ /[(SF_i)(ST_i)]}$$

3.3.2 Elemental Labelling of Functional Groups

In order to obtain a better understanding of the functional groups on the carbon fiber surface, the Hercules AS-4 fibers before and after boiling in 70% nitric acid were reacted with a series of reagents which leave an elemental tag on various functional groups. These reagents are shown in Figure 3.2. The reagents were chosen so that they should react only with a specific functional group on the surface.

The XPS spectra for the derivatized fibers were obtained on a KRATOS XSAM 800 electron spectrometer operated in the fixed retarding ratio (FRR) mode. Operating pressures were about 2 X 10^{-7} torr. K_α radiation from a magnesium anode operating at 250 mW was used as the x-ray source.

The area under each photopeak was integrated and the percentage of each element present on the fiber surface was determined using equation 3.1. The sensitivity factors used for each element are listed in Table 3.3. The values of the sensitivity factor for the Kratos instrument are different

Table 3.3. Sensitivity factors, kinetic energies, and photoionization cross sections (74), used for quantitative analysis of XPS data.

Photopeak	Perkin Elmer Sens-itivity Factor SF	Kratos Sens-itivity Factor SF	Kinetic Energy (eV) KE	Cross Section (kilobarn) σ
Carbon 1s	0.25	389.9	966.6	22.2
Oxygen 1s	0.66	667.9	722.6	63.3
Nitrogen 1s	0.42	553.0	851.6	39.3
Fluorine 1s	1.00	654.3	567.6	94.6
Sulfur 2p	0.54	834.7	1088.1	38.6
Silicon 2p	0.27	457.9	1151.1	19.2
Sodium 1s	2.3	-----	-----	----

DERIVATIZATION SCHEME

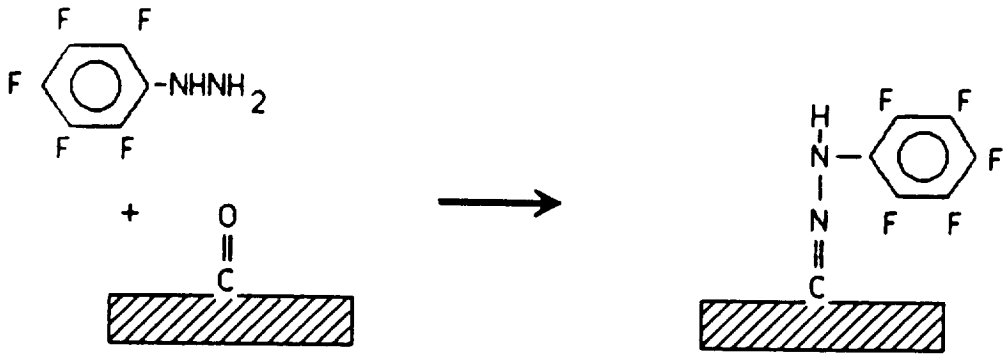

PENTAFLUOROBENZALDEHYDE (PFB)

$-NH, -NH_2 + OCHC_6F_5 \longrightarrow N=CHC_6F_5$

TRIFLUOROETHANOL (TFE)

$-COOH + CF_3CH_2OH \longrightarrow CO_2HCH_2CF_3$

TRIFLUOROACETIC ANHYRDRIDE

$-COOH$
$-COH$ $+ (CF_3CO)_2O \longrightarrow COOCOCF_3$

PENTAFLUOROPHENYLHYDRAZINE (PFPH)

$-C=O + C_6F_5NHNH_2 \longrightarrow C=NNHC_6F_5$

MERCURIC TRIFLUOROACETATE (HgTFA)

C
$\|$ $+ Hg(CF_3CO_2)_2$ $\longrightarrow$ $C-Hg(CF_3CO_2)$
C $+ CCl_3CH_2OH$ $C-OCH_2CCl_3$

Figure 3.2 Schematic diagram of derivatization scheme and reagents

than for the Perkin Elmer instrument. This difference is due to the fact that the Perkin Elmer instrument is operated in the fixed analyzer transmission (FAT) mode while the Kratos instrument is operated in the FRR mode. The sensitivity factors (SF) for the Kratos instrument were calculated by substituting the factors listed in Table 3.3 into equation 3.2.

$$(3.2) \qquad SF = (KE)\,(\sigma)\,\left[\,0.105\,(KE)^{0.75}\,\right]$$

where KE is the kinetic energy of the photoelectron
σ is the photoionization cross section of the atom

The term in brackets represents the mean free path of the ejected photoelectrons in angstroms (75).

3.3.3 Scanning Transmission Electron Microscopy

STEM photomicrographs were obtained on a Philips 420 scanning transmission electron microscope. The fibers were mounted in a double sided copper grid. Approximately twelve thousand fibers were cut to about 1 mm length with scissors and allowed to fall onto the open grid. The grid was then closed thereby sandwiching the fibers. It was not necessary to coat the fibers before SEM examination since the carbon fibers are electrically conductive.

3.3.4 Surface Energy Analysis

The polar and dispersive components of the fiber surface energies were determined using Kaelble's method described in section 2.3.1. The wetting force of the fiber surface in a series of liquids of varying polar and dispersive surface energy was measured. The apparatus used for wetting force measurement is shown schematically in Figure 3.3. Several pieces of nichrome wire about 2.5 cm long were bent so that there was a hook on one end and a loop on the other end. Fibers were glued to the end of the wire containing the loop with a cyanoacrylate adhesive. The wire hook and fibers were placed in an oven at 110° C for 4 hours. The hooks were removed individually from the oven and mounted on a Perkin Elmer TGA-2 thermogravimetric balance. A small cup containing the liquid was raised up to the fiber and the wetting force measured. After the wetting force of two fibers was measured, the cup was overflowed with more of the wetting liquid to create a clean liquid surface. The fibers were removed from the hook and mounted on a microscope slide. The diameters of the fibers were measured on a microscope equipped with a filar eyepiece at 600X magnification.

The liquids used and there surface energy properties are listed in Table 3.4. The contact angle was calculated using equation 2.8. The polar and dispersive components of

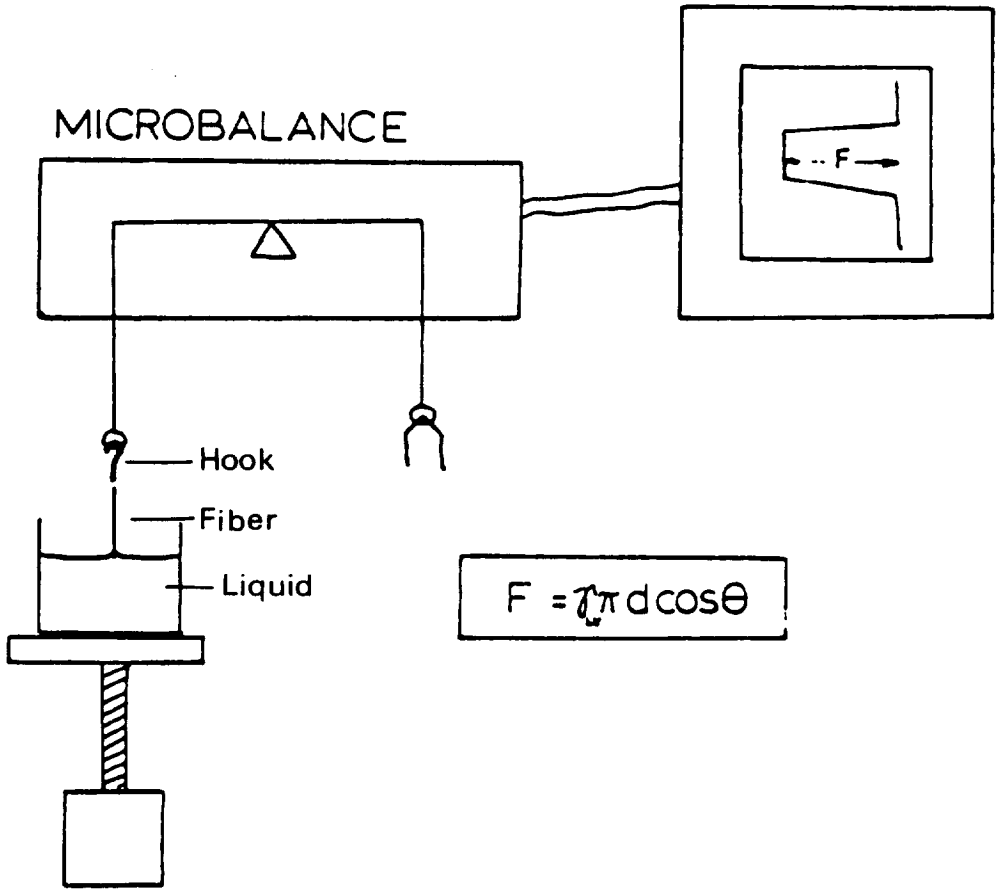

Figure 3.3 Schematic diagram of apparatus used for wetting force measurement

Table 3.4. Liquids used for surface energy determination and their surface energy components

Liquid	Total Surface Energy (ergs/cm²)	Polar Component (ergs/cm²)	Dispersive Component (ergs/cm²)
Water	72.8	51.0	21.8
Ethylene Glycol	48.3	19.0	29.3
Formamide	8.3	26.0	32.3
Methylene Iodide	50.8	48.4	2.4
Bromo-naphthalene	44.6	44.6	0.0

the fiber surface energy were calculated by fitting the data to equation 2.7 by linear regression using the computer program listed in Appendix VIII.

3.3.5 Breaking Strength Measurement

The breaking strengths of the fibers were measured at three lengths. The breaking strengths of thirty fibers were measured at each length. Single fibers were mounted across a hole (diameter equal to the chosen gage length) in a paper tab with a cyanoacrylate adhesive. The tabs were mounted in a Table Model Instron with a 50 gram load cell. Alligator clips were used as the test clamps. The paper was burned away with a nichrome wire attached to a variable resistance power supply (approx. 10 V ac). The fiber was then tested in tension. The breaking strengths were fitted to a Weibull distribution using maximum likelihood estimations as outlined in Appendix II. The computer program used to calculate the Weibull distribution parameters is listed in Appendix IX.

3.4 ADHESION OF THERMOPLASTIC RESINS TO CARBON FIBERS

Adhesion of the thermoplastic matrices to the carbon fibers was measured using the fiber critical length test as described in section 2.5.1.2. It was found easier to prepare samples and perform the fiber critical length test on an aluminum coupon (as shown in Figure 3.4) than to embed the

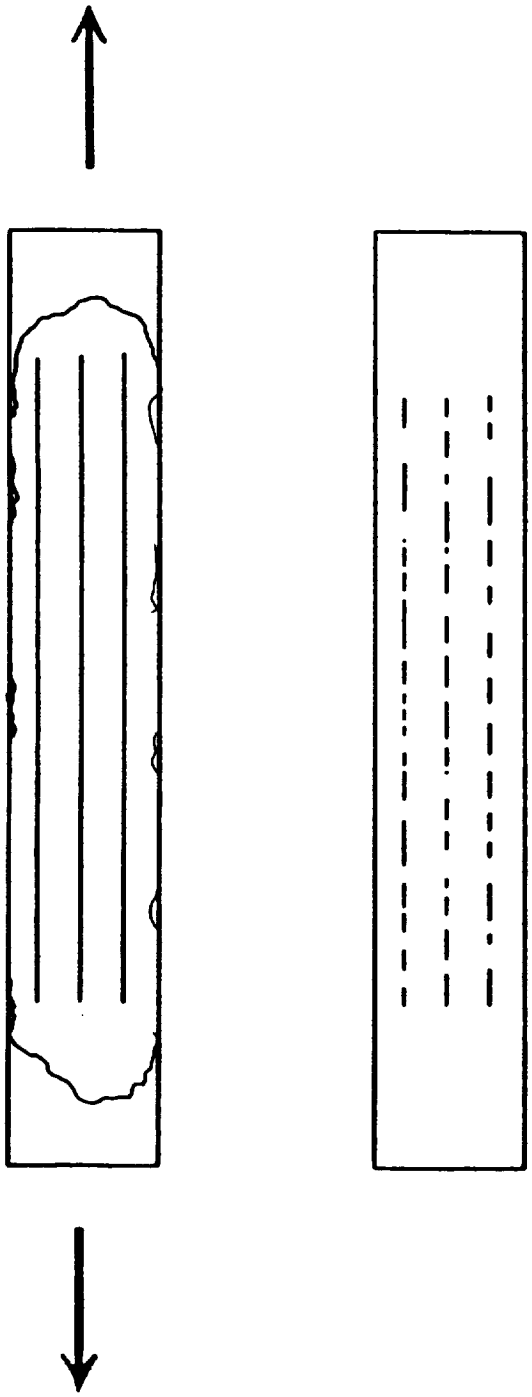

Figure 3.4 Schematic diagram of fiber critical length experiment using an aluminum substrate

fibers in a solid dogbone sample. The aluminum coupon fiber critical length test as described by Wadsworth, et al. (121) was used as a method for obtaining data quickly and is described in section 3.4.1. The results obtained from the fiber critical length test were compared with the photoelastic stress transfer measurement which will be described in section 3.4.2.

3.4.1 Fiber Critical Length Experiment

Sheets of A1100 aluminum 0.16 cm thick were annealed at 316° C for 30 minutes and slowly cooled. Coupons 2.5 X 15.2 cm. in size were cut from the annealed aluminum sheets. The surfaces of the aluminum were prepared by wet sanding with 400 grit sandpaper, rinsing with deionized water and oven drying at 100° C for 24 hours. The coupons were coated with about 3 ml of a solution of polymer dissolved in methylene chloride (5g/100 ml). The solvent was allowed to evaporate from the polymer film at room conditions for 24 hours. The dry film thickness was about 40 μm. Single fibers (about 4 per coupon) were carefully teased from the fiber bundle and placed on the polymer film parallel to the long axis of the coupon. The fibers were coated with another 3 ml of polymer solution. The solvent was allowed to evaporate at room conditions for 24 hours. The samples were then heated to 70° C under vacuum for 8 hours to remove excess solvent. The

coupons were annealed at about +10 °C and -10°C from the T_g of the polymer and also at 265 °C for 8 hours. After cooling, the coupons were cooled by placing them on a laboratory table top.

After cooling, the coupons were placed in an Instron testing machine and pulled in tension to 30 % strain (at 25 % per minute strain rate). This straining caused the fibers to be broken into their critical length. The fiber breakage was normally complete after about 5-10% strain. The coupon was strained to 30% to make the fiber breaks more visible. The lengths were measured on a microscope equipped with a micrometer stage. Typically, the length of 50 fiber fragments was measured. Cumulative frequency plots of fiber lengths were obtained using the computer program listed in Appendix X.

3.4.2 Photoelastic Stress Transfer Observation

Stress transfer between fiber and matrix was observed by stretching a dogbone shaped polymer sample containing a single fiber embedded along its length under a polarizing light microscope. At the fiber breaks, a stress pattern caused by birefringence in the stressed polymer could be observed. The dogbone was prepared as described below.

A silicone mold containing 0.8 mm thick by 38 mm long dogbone impressions was prepared from Dow Corning 3120 RTV

silicone rubber. A 0.4 mm step in the mold was made at the end of each dogbone impression to support the fiber. Regular size paper clips were bent into a U shape with a span of about 6.5 cm. A single fiber was teased from a tow and glued across the U shaped paper clip with a cyanoacrylate adhesive. The adhesive was allowed to dry overnight. Polymer films were compression molded to 0.017 inch thickness. Dogbone shapes identical in shape to the dogbones used for making the mold were cut from these films. The dogbones were soaked and wiped with methanol then dried in an oven at 130° C for 24 hours. A 0.4 mm thick polymer dogbone was placed in the bottom of the dogbone shaped silicone mold. The fiber (glued to the paper clip) was placed across the dogbone in the mold. Another 0.04 mm. thick polymer dogbone was placed on top of the fiber. Each silicone mold was loaded with 3-5 specimens. The mold, dogbone, fiber assembly was placed in an oven at 130° C for 1.5 hrs. The oven temperature was then raised to the appropriate temperature for each polymer (190° C for polycarbonate, 245° C for polysulfone, and 295° C for polyetherimide). All samples were annealed for 1.5 hrs. The molds were removed from the oven and the samples removed from the mold in the molten state. The dogbones were rapidly cooled by placing them on a laboratory table top.

The dogbone specimens were then placed in a small hand-screw driven tensile stage and pulled in tension. The

tensile stage was placed under a Zeiss polarizing light microscope with crossed polarizers. The stress pattern created at fiber breaks was photographed with a Minolta X700 35 mm camera (equipped with an automatic shutter control) which was attached to the microscope. Kodak PX-125 film was used in the camera. A 6 volt light source operating at 2.4 amperes was used for illumination.

3.5 CARBON FIBER SURFACE TREATMENT

3.5.1 Anodization Apparatus

The anodization apparatus is shown in Figure 3.5. The fibers were anodized by wrapping bundle fibers around a glass frame (8.3 X 8.3 X 3.8 cm.). The glass frame had copper foil on its top surface to allow electrical contact. The fibers were painted to the copper foil with silver paint. The copper foil was attached to the positive output of a Hewlett Packard HP6284A power supply. The negative output of the power supply was attached to a stainless steel wire screen. The frame and wire screen were placed in a 1500 ml beaker containing about 800 ml of electrolyte solution. The screen did not touch the copper foil or the fibers and the copper foil was not in contact with the electrolyte solution. After treatment, the fibers were rinsed with deionized water and dried in an oven at 120° C for 12 hours.

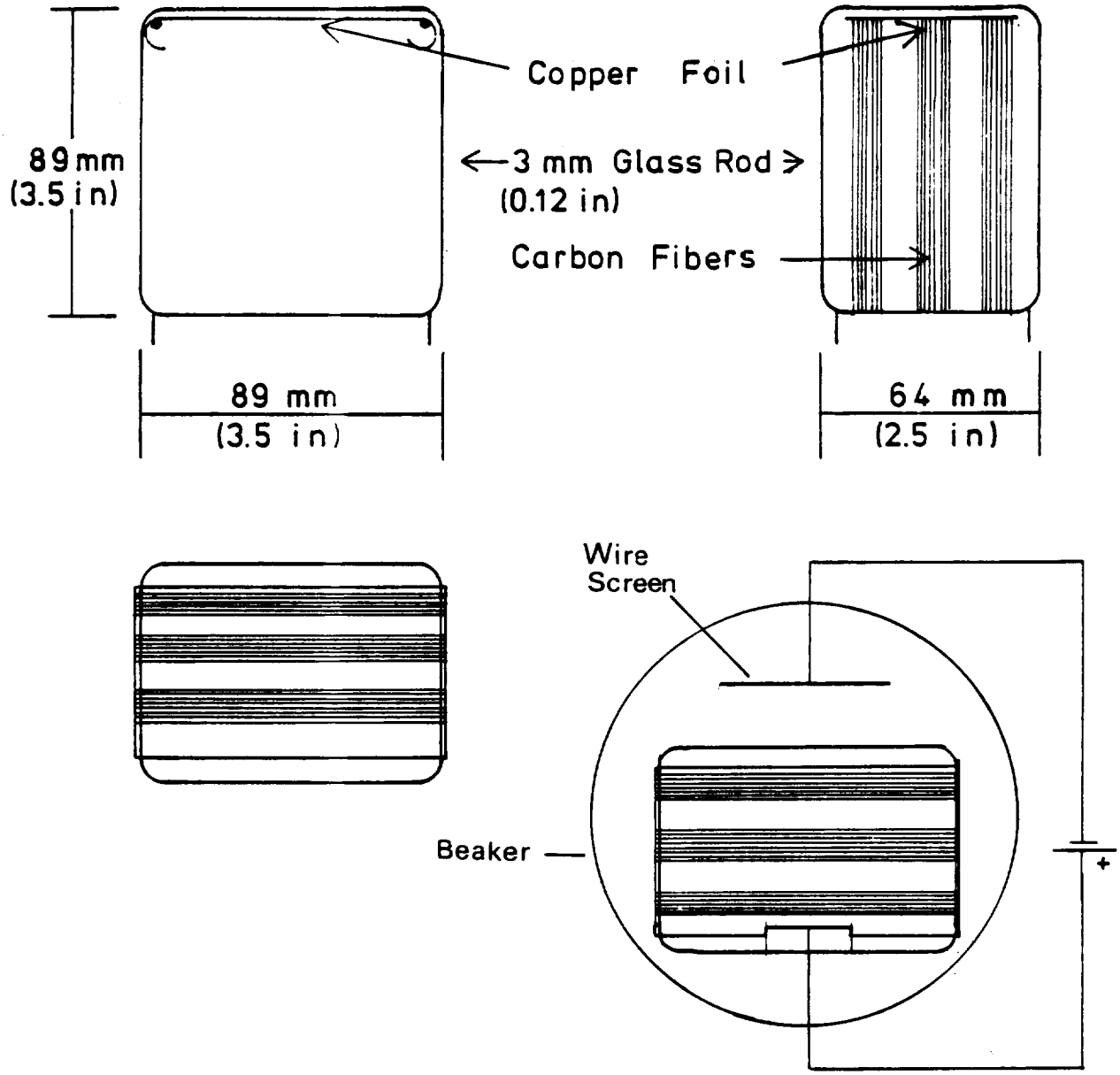

Figure 3.5 Schematic diagram of anodization apparatus

Table 3.5. Anodization conditions in various electrolyte solutions

Electrolyte	Concentration	Voltage (volts)	Current Density (amp/m^2)	Time (minutes)
NaOH	0.50 M	6.0	11.6	2
H_2SO_4	0.50 M	6.0	14.5	2
NH_4HCO_3	5 %	2.4	0.48	30
$(NH_4)_2SO_4$	5 %	4.0	3.86	30
H_2O		4.0	0.48	30

3.5.2 Anodization in Various Electrolyte Solutions

As an initial study of the surface chemistry of the carbon fiber anodization process, Hercules AU-4 fibers were anodized in various electrolyte solutions. The anodization conditions are listed in Table 3.5. In addition, Hercules AS-4 fibers were boiled in nitric acid for 3 hours. These fibers were then analyzed by XPS to determine their surface chemistry.

3.5.3 Anodization at Different Electrolyte Solution Concentrations

During the anodization, it was noticed that the electrolyte solution turned brown. Further studies of this discoloration process were conducted on the sulfuric acid and sodium hydroxide electrolytes. Fibers were anodized in these electrolyte solutions under the conditions listed in Table 3.6. The anodization baths from these treatments were then analyzed by ultraviolet/visible absorption spectroscopy in a Perkin Elmer 3300 UV/Vis spectrometer. The sodium hydroxide solution had to be diluted 10:1 before spectroscopic analysis. The sulfuric acid solution was not diluted. The solutions before anodization were used in the reference cell.

Table 3.6. Anodization conditions for ultraviolet-visible absorption spectroscopy of anodization bath

Electrolyte	Concentration (M)	Fiber	Voltage (volts)	Current Density (amp/m^2)	Time (min)
NaOH	0.05	AU-4	4.0	1.45	30
	0.10	AU-4	4.0	1.93	30
	0.25	AU-4	4.0	2.90	30
	0.50	AU-4	4.0	4.83	30
	1.00	AU-4	4.0	7.74	30
H_2SO_4	0.05	AU-4	4.0	2.90	30
	0.10	AU-4	4.0	3.87	30
	0.25	AU-4	4.0	7.74	30
	0.50	AU-4	4.0	11.1	30
	1.00	AU-4	4.0	10.6	30

3.5.4 Anodization as a Function of Time

To study the effect of anodization on tensile strength of the fiber, the AU-4 fiber was treated in 0.5 M H_2SO_4 and 0.5 M NaOH for varying lengths of time as listed in Table 3.7. The tensile strengths of these fibers after treatment were measured at 6 mm gauge length.

3.5.5 Anodization of Fibers From Various Producers

To compare differences in adhesion between fibers from different companies, sodium hydroxide and sulfuric acid were chosen as the electrolytes for anodizing all fibers. It was found from the previous experiment that 15 seconds was the optimum time for the anodization of AU-4 fiber at 6 volts and 0.5 M concentration. For the final treatment, all of the untreated fibers were anodized at these conditions. The actual anodization conditions are listed in Table 3.8.

Table 3.7. Anodization conditions of AU-4 fibers as a function of time

Electrolyte	Concentration (M)	Voltage (volts)	Current Density (amp/m^2)	Time (seconds)
NaOH	0.5	6.0	11.6	8
	0.5	6.0	11.6	15
	0.5	6.0	11.6	30
	0.5	6.0	11.6	60
	0.5	6.0	11.6	120
H_2SO_4	0.5	6.0	14.5	8
	0.5	6.0	14.5	15
	0.5	6.0	14.5	30
	0.5	6.0	14.5	60
	0.5	6.0	14.5	120

Table 3.8. Anodization conditions for treatment of various commercial fibers

Electrolyte	Concentration (M)	Fiber	Voltage (volts)	Current Density (amp/m^2)	Time (seconds)
NaOH	0.5 M	AU-4	6.0	20.3	15
	0.5 M	XAU	6.0	17.4	15
	0.5 M	T-300U	6.0	17.4	15
H_2SO_4	0.5 M	AU-4	6.0	13.1	15
	0.5 M	XAU	6.0	13.1	15
	0.5 M	T-300U	6.0	17.4	15

4) RESULTS AND DISCUSSION

4.1) ANALYSIS OF EFFECT OF SURFACE TREATMENT ON SURFACE CHEMISTRY OF CARBON FIBERS

Anodization of carbon fibers will affect the functional groups of the fiber surface as well as the structure of the fiber. The results presented in this section are aimed at understanding the nature and location of surface functional groups on the fiber surface as well as the mechanism of attack of the anodization on the carbon fiber.

The potentials used for anodizations in this study were high compared to the potentials used by Sherwood, et al (114-118). In the past, low potentials have been applied to graphite surfaces in order to probe their surface structure (62). The potentials applied here were used for the purpose of creating functional groups and altering the morphology of the fiber surface. It is felt that on an industrial scale surface treatment will have to be performed at higher potentials in order to increase production.

4.1.1 Analysis of X-ray Photoelectron Spectroscopy Data

The binding energies of the carbon peaks were calibrated relative to gold with a binding energy of 83.8 eV. The binding energy of carbon in graphite powder was 284.4 eV. The binding energy of carbon in Hercules AS-4 fibers was 284.6 eV. All peaks were shifted so that the

main carbon 1s peak was located at 285 eV as a reference.

The carbon, oxygen, and nitrogen XPS signals were curve fit using the data massage program equipped with the Perkin Elmer 5300 electron spectrometer (version 0.8). Curve-fits of graphite powder and polysulfone indicated that the full width at half maximum (FWHM) of the carbon 1s signals was about 1.33 to 1.36 eV. Peaks of this width were initially fit to each carbon 1s signal. The peaks were made wider to improve the quality of the curve fit. Wider curve-fit peaks indicate a spectrum of functional groups rather than just one group, and/or variation of the molecular structure of the carbon fiber. The FWHM for the oxygen signal of polysulfone was about 1.6 eV. The curve-fit oxygen peaks were originally set at 1.6 eV and widened to improve the quality of the curve-fit. No standard was used as a guide for setting the FWHM of the nitrogen peaks. The curve-fit peaks were originally set at 1.6 eV and widened to improve the quality of the fit.

The carbon 1s signals were fit with five peaks. The first peak (C1) was set at 285 eV and assigned to carbon-carbon bonding. The second peak (C2) occurred at about +1.5 eV from the 285 eV peak and is assigned to R-C-O and/or R-C-N type bonds. The third peak (C3) occurred at about +2.5 eV from the 285 eV peak and is assigned to carbonyl (R-C=O) type bonds. The fourth peak (C4) occurred at about +4.0 eV

from the 285 eV peak and is assigned to carbon bound to more than one oxygen i.e. carboxylic functionality. These assignments are in accordance with Clark's work (77) on polymers of known functionality. The fifth carbon 1s peak (C5) was a tail at about +6eV on the high binding energy side due to plasmon excitation as described by Sherwood, et al. (79). Carbon 1s photo peaks were analysed by reporting the percentage of the C-C type bonding relative to the overall peak and the ratio of the intensity of the secondary peaks (C2-C5) to the intensity of the C1 peak.

The oxygen 1s signals were typically fit with 3 peaks. The oxygen peak assignments were not as definitive as the assignments for the carbon peaks. The first peak occurred at about 530 eV and is thought to be due to R-C=O bonding. The second peak occurred at about +1.4 eV from the first and is thought to be due to R-C-O bonding. The third peak occurred at higher binding energy and is possibly due to oxygen associated with inorganic contaminants or water.

The nitrogen 1s signals were fit with 2 peaks. A peak at about 400 eV was assigned to R-C-N bonding. The second peak occurred at about 401.5 eV and is assigned to nitrogen bonded to carbon which is in turn bonded to oxygen (R-O-C-N). There was also occasionally a third nitrogen peak at about 399 eV probably due to nitrogen associated with aromatic structures in the carbon fiber. The data obtained

from the curve fitting program on the Perkin Elmer system for all the fibers reported in this study are listed in Appendix III. The tables list the binding energy (BE) of the lowest binding energy peak in the spectrum, the shift of each subsequent peak in eV, the FWHM of the peak, and the relative percentage of the peak within the overall peak for that element (%).

4.1.2 XPS Analysis of the Effect of Anodization of Carbon Fibers in Various Electrolyte Solutions on Surface Functionality

The percentage of elements detected by XPS, and their binding energies for the Hercules AU-4 fibers anodized in various electrolytes under the conditions listed in Table 3.5 are shown in Table 4.1. The binding energies listed are for the point of maximum signal intensity. The XPS results for the commercially treated AS-4 fibers are also included for comparison. The anodizations in NH_4HCO_3, NaOH, and H_2SO_4 were performed under a range of varying conditions. The variation atomic percentages was about ±3% for carbon, ±2% for oxygen, and ±1% for nitrogen. A representative spectrum is presented here. The anodizations in $(NH_3)_2SO_4$ and distilled H_2O were performed only once. However, the results reported here for anodization in $(NH_3)_2SO_4$ are similar to the results reported by King and Gynn (44). The curve fit carbon, oxygen, and nitrogen peaks for the surface

Table 4.1 Atomic percentages (%), binding energies (BE) of elements, oxygen to carbon (O/C), and nitrogen to carbon (N/C) ratios detected by XPS on the surface of carbon fibers after anodization.

Fiber	Carbon	Oxygen		Nitrogen		Other		O/C	N/C
	%	%	BE (eV)	%	BE (eV)	%	Element		
AU-4	96	1.8	532.9	2.0	401.6			0.02	0.02
AS-4	84	9.9	532.0	5.0	399.8	0.8	Na	0.12	0.06
AU-4 NH_4HCO_3	76	17	532.0	6.4	400.2			0.23	0.08
AU-4 $(NH_4)_2SO_4$	68	26	532.1	3.0	400.1	2.6	Si	0.38	0.04
AS-4 HNO_3 Boil	75	12	532.5	6.7	399.8			0.16	0.09
AU-4 NaOH	76	13	532.0	1.6	401.4	8.9	Na	0.17	0.02
AU-4 H_2SO_4	73	23	533.8	2.4	400.4	1.3	S	0.32	0.03
AU-4 H_2O	64	29	532.9	4.1	400.5	2.6	S	0.46	0.06

treated fibers are shown in Figure 4.1. A summary of results obtained by curve fitting the carbon 1s peak for the anodized fibers is given in Table 4.2.

The commercially treated AS-4 fiber had a total oxygen and nitrogen content of 15% (see Table 4.1). The oxygen and nitrogen content is larger than the untreated fiber. Both oxygen and nitrogen are shifted to lower binding energy with surface treatment. It is concluded that oxygen as well as nitrogen functionality is being added to the fiber surface with the commercial surface treatment. The surfaces of commercially treated fibers will be discussed in greater detail in section 4.3.

XPS spectra of the AU-4 fibers anodized in NH_4HCO_3 are shown in Figure 4.1c. These fibers had a total oxygen and nitrogen content of about 23 %. Both the oxygen and nitrogen content increased with treatment. The oxygen and nitrogen peaks both shifted to lower binding energy upon surface treatment. The increase in nitrogen from 2 to 6 % and the binding energy shift indicate that nitrogen functionality may also be added to the fiber surface during NH_4HCO_3 anodization. The carbon peak consisted mostly of 3 peaks as seen in Table 4.2. Besides the C1 peak due to C-C bonding (285 eV) there are C2 and C4 peaks due to R-C-O and/or R-C-N, and R-C$\lesssim^{O}_{O}$ bonding, respectively. The plasmon C5 peak was only slightly increased after anodization.

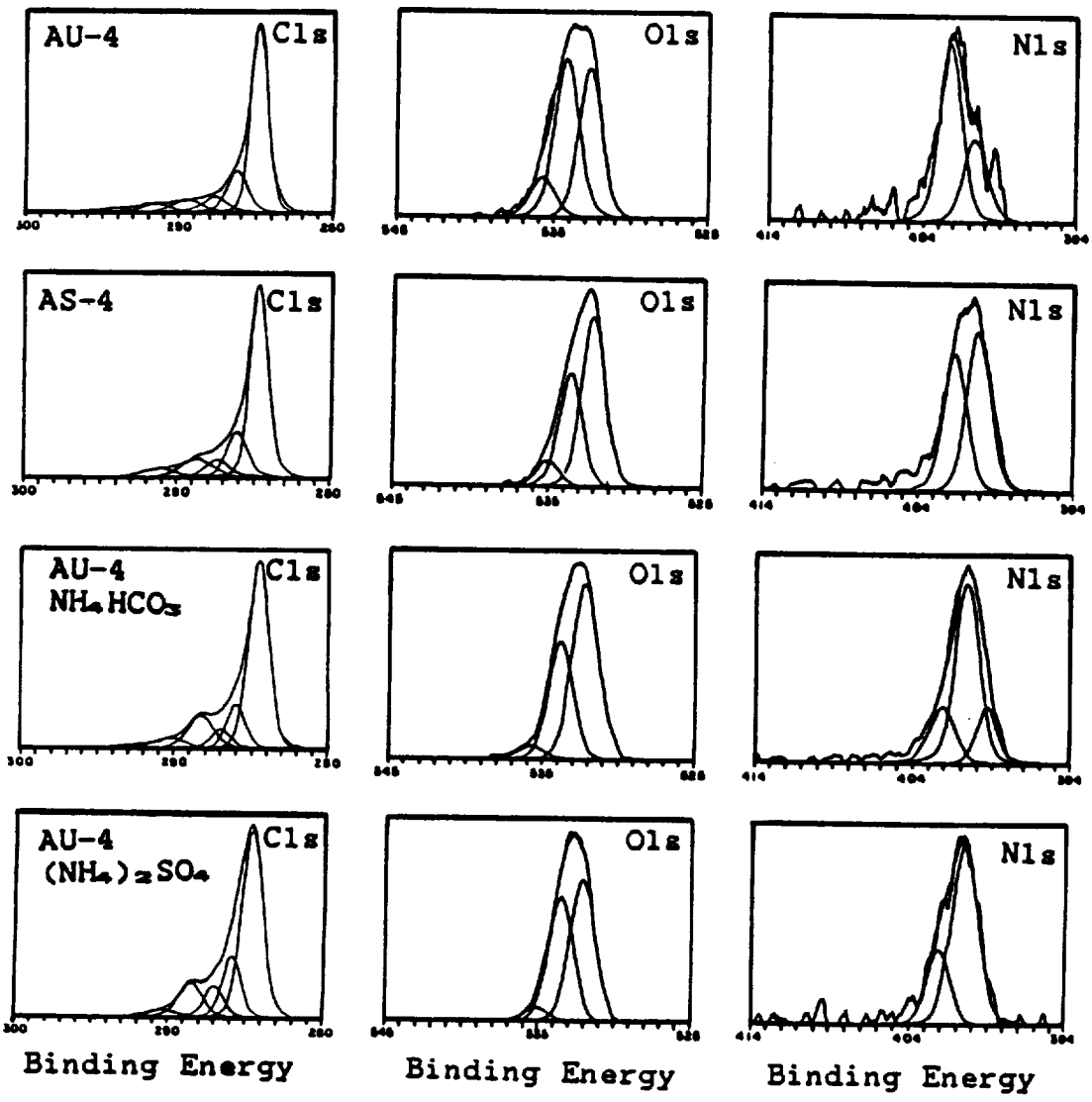

Figure 4.1 Curve fit XPS photopeaks obtained on Hercules AU-4 fibers anodized in various electrolytes. a) untreated fiber, b) commercially treated fiber, c) anodized in NH_4HCO_3, d) anodized in $(NH_4)_2SO_4$. Anodization conditions are listed in Table 3.5.

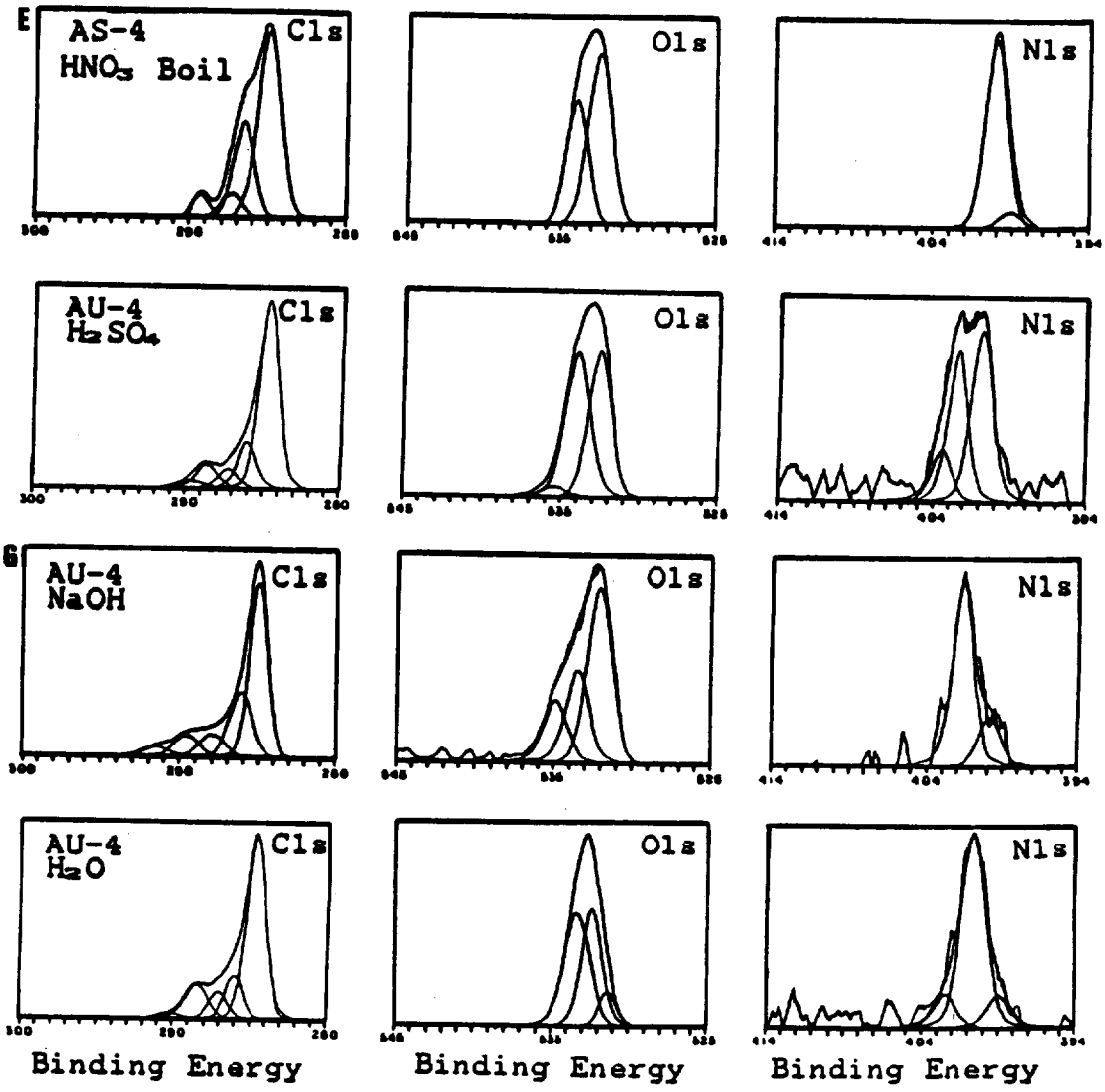

Figure 4.1 (cont.) Curve fit XPS photopeaks obtained on Hercules AU-4 fibers anodized in various electrolytes e) commercially treated fiber (AS-4) boiled in HNO_3, f) anodized in H_2SO_4, g) anodized in NaOH, h) anodized in H_2O. Anodization conditions are listed in Table 3.5.

Table 4.2 Summary of results obtained by curve fitting XPS carbon 1s peaks of Hercules A fibers anodized in various electrolytes

Fiber	C_1 (%)	$\frac{C_2}{C_1}$ X100	$\frac{C_3}{C_1}$ X100	$\frac{C_4}{C_1}$ X100	$\frac{C_5}{C_1}$ X100
AU-4	67	25	10	9	5
AS-4	65	25	10	14	5
AU-4 NH_4HCO_3	64	21	9	21	6
AU-4 $(NH_4)_2SO_4$	60	29	14	20	3
AS-4 HNO_3 Boil	59	47	12	10	0
AU-4 NaOH	54	44	17	17	7
AU-4 H_2SO_4	67	24	9	13	3
AU-4 H_2O	61	23	14	22	3

The XPS spectra of the fibers anodized in $(NH_4)_2SO_4$ are shown in Figure 4.1d. These fibers had a total oxygen and nitrogen content of 29 %. The nitrogen content of the fiber surface increased only slightly from 2 to 3 %. However, the binding energy of the nitrogen decreased by about 1.5 eV. The decrease in binding energy indicates that the nitrogen functionality may have been changed by anodization. The carbon peak was similar in appearance to that of the NH_4HCO_3 anodized fibers. Table 4.2 shows that it had peaks due to all three functionalities as well as a plasmon peak. The plasmon peak intensity was decreased by surface treatment. The oxygen signal was a narrow peak under which two peaks could be assigned.

The XPS spectra of the AS-4 fibers boiled in nitric acid for 3 hours are shown in Figure 4.1e. These fibers had a total oxygen and nitrogen content of about 19%. The carbon peak in this spectrum had a large shoulder due to R-C-O and/or R-C-N species. There was no plasmon peak visible in the carbon signal. The absence of a plasmon peak indicates that the HNO_3 treatment may be disrupting the conduction band and hence the graphitic structure of the carbon fiber surface. The oxygen signal consisted of two peaks. The largest peak occurred at 532.5 eV and was assigned R-C=O type bonding. A second oxygen peak was observed at +1.5 eV and was assigned to R-C-O bonding. The

nitrogen signal was a narrow peak centered at 399.8 eV.

The XPS spectra of the H_2SO_4 anodized fibers are shown in Figure 4.1f. These fibers had a total oxygen and nitrogen content of about 25%. The carbon 1s signal had three main peaks. The peaks were due to C-C, R-C-O, and/or R-C-N, and R-C$\lesssim^{O}_{O}$ bonding. The plasmon peak decreased in intensity indicating that the conduction band and hence the graphitic structure of the carbon fiber had been disrupted by this treatment. The oxygen signal showed two major peaks of almost equal intensity giving the peak a broad symmetric appearance. The strongest peak was located at 533.8 eV and is assigned to R-C-O bonding. The less intense oxygen peak was located at lower binding energy and is possibly due to R-C=O bonding. The nitrogen peak was very broad with three peaks fitting under it. The main peak was centered at 400.4 eV. A second peak was located at +1.6 eV from the main peak. The third peak was small and at +2.6 eV from the first peak.

The XPS spectra for the fibers anodized in NaOH are shown in Figure 4.1g. These fibers had a total oxygen and nitrogen content of about 15%. The plasmon peak increases in intensity for this fiber. This increase in the plasmon peak intensity with anodization in NaOH could be due to removal of amorphous carbon from the fiber surface that would otherwise not contribute to the plasmon peak

intensity.

The XPS spectra for the fibers anodized in distilled deionized H_2O are shown in Figure 4.1.h. These fibers had a total oxygen and nitrogen content of about 33%. The carbon 1s signal had a peak due to R-C-O and/or R-C-N species and a peak due to R-C=O species. The oxygen signal for these fibers was narrow with two closely spaced peaks fitting under it. The main oxygen peak was centered at 532.9 eV. The second peak was located at +1.1 eV from the main peak. The nitrogen content increased upon H_2O anodization. The nitrogen peak was narrow and centered at 401.5 eV. This higher nitrogen binding energy is probably due to nitrogen in higher oxidation states ie. R-N=O.

To summarize the effect of electrolyte on the anodization of carbon fibers as studied by XPS, it appears that anodization in amine salts can create oxygen as well as nitrogen functionality. Anodization in amine salts decreased the binding energy and increased the atomic percentage of nitrogen on the fiber surface, indicating that nitrogen functionality is being added to the fiber surface. The nitrogen increase was more pronounced for NH_4HCO_3 anodization than for $(NH_4)_2SO_4$ anodization. Anodization in H_2SO_4 and H_2O showed a larger increase in surface oxygen than anodization in NaOH. Treatment in acidic environments reduced the plasmon peak intensity indicating disruption of

the graphite layers. Anodization in NaOH increased the plasmon peak indicating that the conduction band of the graphite structure of the carbon fiber surface is being enhanced, or that amorphous regions are being removed during NaOH anodization thus exposing more of the graphite structure.

4.1.3 Derivatization

Differences in molecular and morphological structure of the fiber surface may cause binding energy shifts of the functional groups. It is therefore possible that carbon 1s peak shifts can occur simply by altering the carbon fiber structure. Assignment of functional groups based on XPS peak shape analysis may lead to inaccurate conclusions. Apparent formation of new functional groups could in reality be binding energy shifts caused by structural changes in the fiber. In addition, functional groups that normally occur at a certain binding energy in a polymer or other known molecule may be shifted to higher or lower binding energy by the molecular structure of the fiber.

Specific functional groups can sometimes be observed by labelling them with an elemental tag. Derivatization reactions were performed on the surfaces of Hercules AS-4 fibers before and after boiling in 70% nitric acid for 3 hours. The derivatization reactions are outlined in

outlined in Appendix I.

The results from the derivatization experiments on the Hercules AS-4 fibers are listed in Table 4.3. The significant feature here is the amount of each elemental tag which has been detected by XPS. In most cases, the element of interest is fluorine. It can be seen that the reaction with pentafluorobenzaldehyde (PFB) showed a large increase in fluorine as detected by XPS. Since this reagent reacts with amine groups, the presence of this group on the fiber surface is expected. This finding supports the XPS results which indicated an increase in nitrogen content and a shift in nitrogen binding energy with commercial surface treatment. Further evidence for the presence of amine groups on the surface of Hercules AS-4 fibers has been presented by Drzal (36) who studied the thermal desorption of compounds from the surface of Hercules AS-4 fibers using mass spectrometry. Drzal found a large amount of NH_3 being desorbed from the AS-4 fiber at about 200° C.

The presence of amine groups on the fiber surface makes the possibility of chemical bonding between fiber and an epoxy matrix likely since these groups can react with epichlorohydrin which is present in most epoxy formulations.

The results from the derivatization experiments on the Hercules AS-4 fibers boiled in nitric acid for 3 hours are shown in Table 4.4. The most significant increase in

fluorine signal occurs after reaction with pentafluorophenylhydrazine indicative of carbonyl type functionality.

The reagent used in the derivatization reactions have either three or five fluorine atoms per molecule. The percentage of fluorine should be divided by three or five to obtain the percentage of each functional group on the fiber surface. When this division is carried out, the percentage of each functional group is less than 1%. The XPS results indicate that the total oxygen and nitrogen content is about 15% for the AS-4 fiber and about 19% for the nitric acid boiled fibers. Therefore, the derivatization reactions account for only a small percentage of the total oxygen and nitrogen functionality. Possible explanations for the difference between the oxygen content and the functional groups detected by derivatization are; inaccessibility of the functional group to the derivatization reagent, oxygen functionality other than those that the reagents react with, incomplete derivatization reaction, and degradation of the fluorine signal under the x-ray source.

Table 4.3 Percentage of elements detected on the surface of Hercules AS-4 fibers after derivatization reactions.

Reagent	Functional Group	C	O	N	F	Hg
Control		85	11	4.1	---	
PFB	NH, NH_2	78	14	3.3	5.2	
TFE	C-OH	87	8.4	3.8	1.3	
TFAA	C-OH, COOH	86	9.4	3.4	1.4	
PFPH	C=O	83	12	4.4	---	
Hg(TFA)	C=C	81	15	2.9	---	1.8

--- None detected (< 0.1 %)

Table 4.4 Percentage of elements detected by XPS after derivatization on the surface of Hercules AS-4 fibers boiled in nitric acid for 3 hours.

Reagent	Functional Group	C	O	N	F	Hg
Control		75	18	6.7	---	
PFB	NH, NH_2	72	24	1.9	2.2	
TFE	C-OH	73	24	1.9	1.6	
TFAA	C-OH, COOH	74	23	2.1	0.5	
PFPH	C=O	71	24	2.6	2.4	
Hg(TFA)	C=C	74	23	0.3	---	---

--- None detected (< 0.1 %)

4.2) EFFECT OF ANODIZATION IN SULFURIC ACID AND SODIUM HYDROXIDE ON THE PHYSICAL PROPERTIES OF CARBON FIBERS

During graphite anodization, oxidation can conceivably occur at three locations within the graphite structure namely, at the crystal edges, between the graphitic layers, or at the basal planes. Oxidation can also occur in the amorphous regions of carbon fibers. It is expected that the mode of attack of an anodizing reagent will have an effect on the fiber/matrix adhesion. Observation of changes in the plasmon peak intensity have already been made in Section 4.1.2. It was therefore concluded that the mode of attack differs depending on the electrolyte used. The approach thus taken here was to study the surface of carbon fibers after anodization in more detail. Aqueous solutions of sulfuric acid and sodium hydroxide were chosen as electrolytes because of the large difference in pH, and because the possibility of nitrogen functionality being created is reduced with these electrolyte solutions.

4.2.1 Scanning Transmission Electron Microscopy

A STEM photomicrograph of the Hercules AU-4 fiber after anodization in 0.05 M NaOH for 30 minutes is shown in Figure 4.2a. This treatment caused large etch pits on the fiber surface. The treatment appears to have attacked particular areas on the fiber surface preferentially over other areas. The AU-4 fiber after anodization in 0.5 M NaOH is shown in

a) 0.05M NaOH 4V 30 min

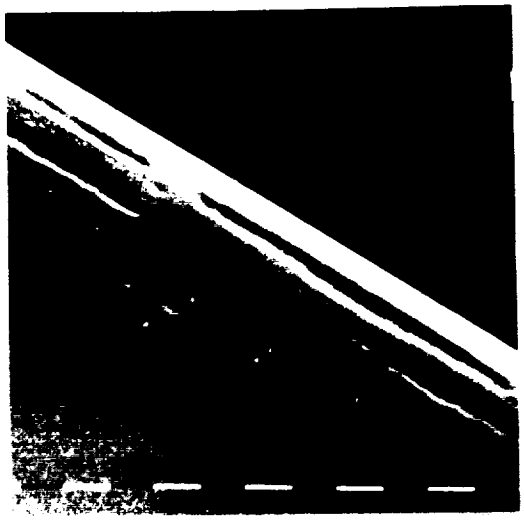

b) 0.5M NaOH 4V 30 min

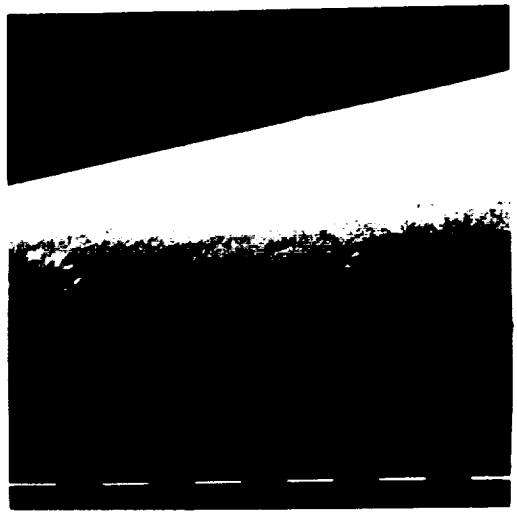

c) 0.05M H_2SO_4 4V 30 min

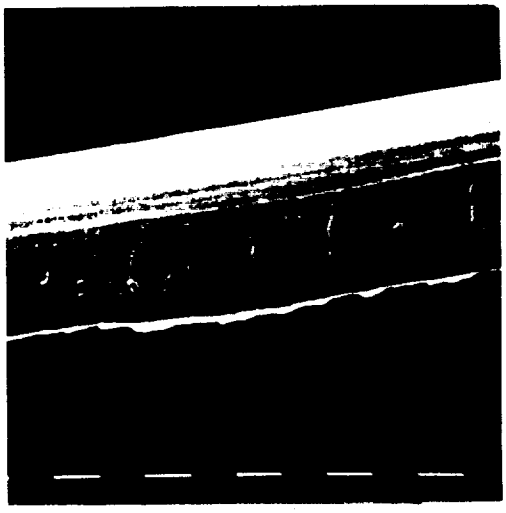

d) 0.25M H_2SO_4 4V 30 min

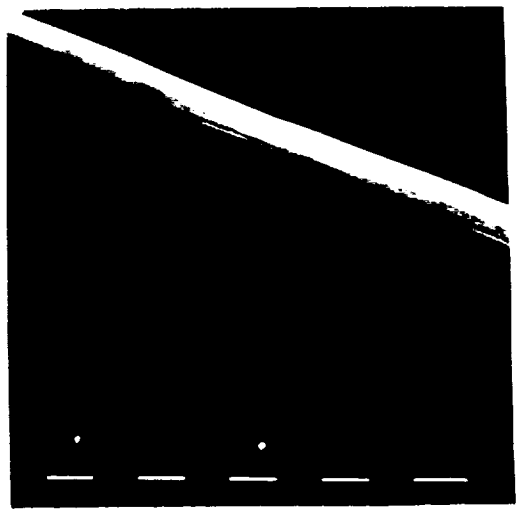

Figure 4.2 STEM photomicrographs of Hercules AU-4 fibers anodized at 4V for 30 min in a) 0.05M NaOH, b) 0.5M NaOH, c) 0.05M H_2SO_4, and d) 0.5M H_2SO_4, (12,500 X).

Figure 4.2b. The surface is smooth with some areas giving a mottled appearance. The anodization at this higher electrolyte concentration appears to attack the surface more uniformly than the 0.05 M solution.

A possible explanation for pit formation during anodization in dilute NaOH is that at the lower electrolyte concentration, the activation energy for anodization is very high. Oxidation thus occurs at the sites of minimum potential energy possibly at edge sites of the graphitic structure. The result is that the surface treatment is very non-uniform. At the higher electrolyte concentration, the activation energy for anodization is lowered. Oxidation is less site specific, and occurs almost uniformly over the fiber surface.

An STEM photomicrograph of the AU-4 fiber after anodization in 0.05 M H_2SO_4 is shown Figure 4.2c. This electrolyte apparently attacks the surface by removing layers from the fiber surface. The AU-4 fiber after anodization in 0.25 M H_2SO_4 is shown in Figure 4.2d. Again, at the higher electrolyte concentration, the surface treatment appears to be more uniform.

4.2.2 Depth Profiling of Sulfuric Acid and Sodium Hydroxide Anodized Fibers using Angular Dependent XPS

The surfaces of the AU-4 fibers were analyzed using

angular dependent XPS after anodization in H_2SO_4 and NaOH. The atomic percentage (%) and binding energies (BE) of elements detected on the surface of the anodized fibers at several take-off angles are shown in Table 4.5 along with the oxygen to carbon (O/C) and nitrogen to carbon (N/C) ratios. The O/C ratios versus the sine of the take-off angles are plotted in Figure 4.3. The O/C ratios decrease with decreasing sine of the take-off angle for the H_2SO_4 anodized fiber while the O/C ratio increases with decreasing sine of the take-off angle for the NaOH anodized fibers.

If oxygen was concentrated in the topmost layers of the fiber surface, it is expected that the O/C ratio would increase with decreasing sine (θ) as seen for the NaOH anodized fibers. On the other hand, if carbon were on the top of the fiber surface, the O/C ratio would decrease with decreasing sine (θ) as seen for the H_2SO_4 anodized fibers. It is therefore concluded that oxygen is predominant on the top layer of the NaOH anodized fibers and that carbon is predominant on the top layer of the H_2SO_4 anodized fibers.

A summary of results obtained by curve fitting the carbon 1s peaks for the anodized fibers at several take-off angles is shown in Table 4.6. There is a large increase in the C_2 peak with decreasing take-off angle for the NaOH anodized fibers. The plasmon peak for the H_2SO_4 anodized fibers is not affected by take-off angle. The plasmon peak

Table 4.5 Atomic percentages (%), binding energy (BE) of elements, oxygen to carbon (O/C), and nitrogen to carbon (N/C) ratios detected by XPS at 90°, 30°, and 10° take off angles on the surface of Hercules AU-4 fibers anodized in 0.5 M NaOH and 0.5 M H_2SO_4 at 6 V for 2 minutes.

Fiber	Carbon	Oxygen		Nitrogen		Other		O/C	N/C
	%	%	BE (eV)	%	BE (eV)	%	Element		
AU-4 H_2SO_4									
90°	66	32	532.7	1.9	400.7	*	S	0.48	0.03
30°	70	28	532.9	1.6	400.5	*	S	0.40	0.02
10°	74	25	533.1	1.0	400.7	*	S	0.34	0.01
AU-4 NaOH									
90°	71	15	531.8	2.1	401.1	12	Na	0.21	0.03
30°	70	17	531.9	1.4	400.9	12	Na	0.24	0.02
10°	72	18	531.9	1.6	400.5	8	Na	0.25	0.02

* Sulfur detected in survey spectra but was not scanned

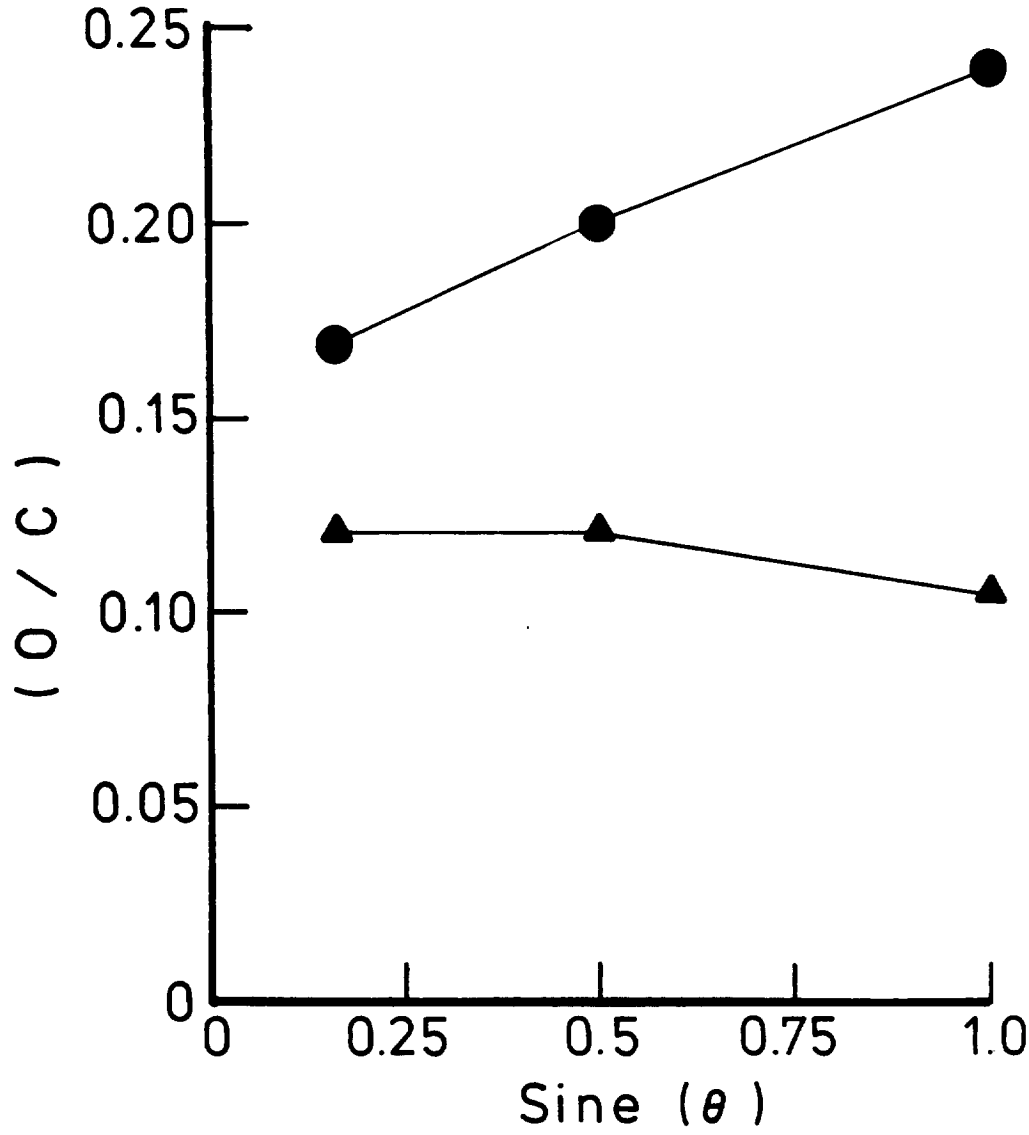

Figure 4.3 Oxygen to carbon ratios as detected by XPS versus sine of the take-off angle for Hercules fibers anodized in (▲) 0.5M NaOH, and (●) 0.5M H_2SO_4.

Table 4.6 Summary of results obtained by curve fitting XPS carbon 1s photopeaks obtained at 90°, 30°, and 10° take-off angles of Hercules AU-4 fibers anodized in 0.5 M NaOH and 0.5 M H_2SO_4 at 6V for 2 minutes.

Fiber	C_1 (%)	$\frac{C_2}{C_1}$ X100	$\frac{C_3}{C_1}$ X100	$\frac{C_4}{C_1}$ X100	$\frac{C_5}{C_1}$ X100
AU-4 H_2SO_4					
90°	56	28	16	30	6
30°	56	27	17	28	5
10°	50	36	31	25	6
AU-4 NaOH					
90°	59	31	14	14	10
30°	53	39	17	17	15
10°	42	67	27	25	18

for the NaOH anodized fibers increases with decreasing take-off angle.

4.2.3 Ultraviolet Absorption Spectra of Anodization Bath

It was noticed during the anodization of the carbon fibers in NaOH and H_2SO_4 that the anodization bath turned brown during the anodization. It was further noticed that the color was different depending on the electrolyte used for anodization. The NaOH anodization bath turned a dark brown color while the H_2SO_4 bath turned a yellowish brown. This phenomena has also been observed by King and Gynn (44) and by Kozlowski and Sherwood (115).

It is possible that the chemical groups responsible for the color change in the bath may be similar to the molecular species being formed on the fiber surface during anodization. It is also possible that these species are being preferentially removed from the fiber surface. The species remaining on the fiber surface thus may be completely different from the species in the anodization bath.

The ultraviolet absorption spectra of the anodization baths are shown in Figure 4.4. Figure 4.4a shows the spectra of the NaOH anodization bath. The spectra have an absorption tail into the visible range. This tail indicates that there are aromatic species present in the solution.

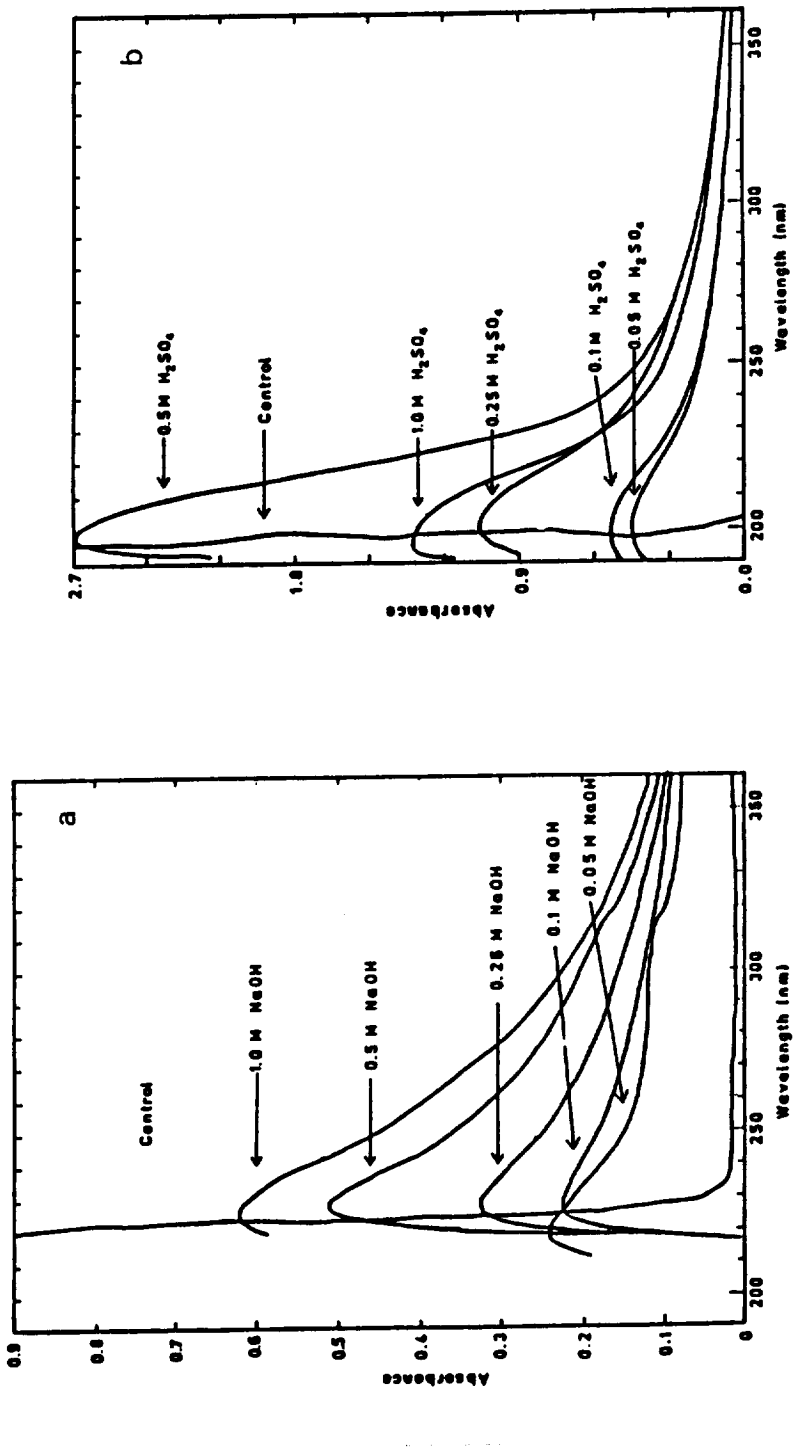

Figure 4.4 Ultraviolet absorption spectra of a) NaOH and b) H_2SO_4 anodization baths after anodization of Hercules AU-4 fibers at 4V

Figure 4.4b shows the spectra of the H_2SO_4 anodization bath. These spectra have a high absorbance at short wavelengths and then drops abruptly at about 230 nm. This lack of absorption into the visible range is indicative of non-aromatic species. It should also be mentioned that the NaOH anodization bath had to be diluted 10:1 before the spectra were recorded. The H_2SO_4 anodization bath did not have to be diluted. The amount of molecular species present in the NaOH anodization bath was thus much greater than in the H_2SO_4 anodization bath.

The results from UV absorption spectroscopy of the anodization bath suggest that large amounts of aromatic material are being removed from the fiber surface during NaOH anodization. Smaller amounts of less aromatic compounds are being removed from the fiber surface during H_2SO_4 anodization.

4.2.4 Fast Atom Bombardment Mass Spectra

In order to obtain a better understanding of the molecular structure of the carbon fiber surfaces, they were examined by fast atom bombardment mass spectrometry (FABMS) after anodization in 0.5 M NaOH and 0.5 M H_2SO_4 at 6 V for 2 minutes. The spectra of positive ions ejected from the H_2SO_4 anodized fibers after argon atom bombardment are shown in Figure 4.5. The spectrum in the range 0-100 atomic mass

units shows major peaks spaced 12 AMU apart. This pattern is typical of aliphatic compounds. The 12 AMU spacing is due to the loss of a carbon atom from the fragment.

The +FABMS spectra for the NaOH anodized fibers are shown in Figure 4.6. Again, the spectrum also has a mass fragment pattern typical of aliphatic compounds as well as a peak at 23 AMU due to sodium from the anodization.

The spectra from 100-200 AMU for the two fibers appear to be similar. There are peaks at 104, 115, 128, 132, 149, and 165 AMU due to aromatic type compounds. A summary of peak assignments for the significant peaks above 90 atomic mass units is shown in Table 4.7. The only difference in these spectra is that the spectrum for the H_2SO_4 anodized fibers is 10 times more intense than the spectrum for the NaOH anodized fibers. This may indicate that there are more aromatic species present on the surface of the H_2SO_4 anodized fibers.

It is expected that the intensity for the higher AMU fragments would be lower for more ordered carbon since atom bombardment would have to degrade the morphological structure of the carbon before molecular fragments are ejected from the carbon surface. For amorphous carbon it is expected that only slight atom bombardment would be required to cause ejection of a molecular fragment. If the amorphous regions within the carbon fiber are being removed by

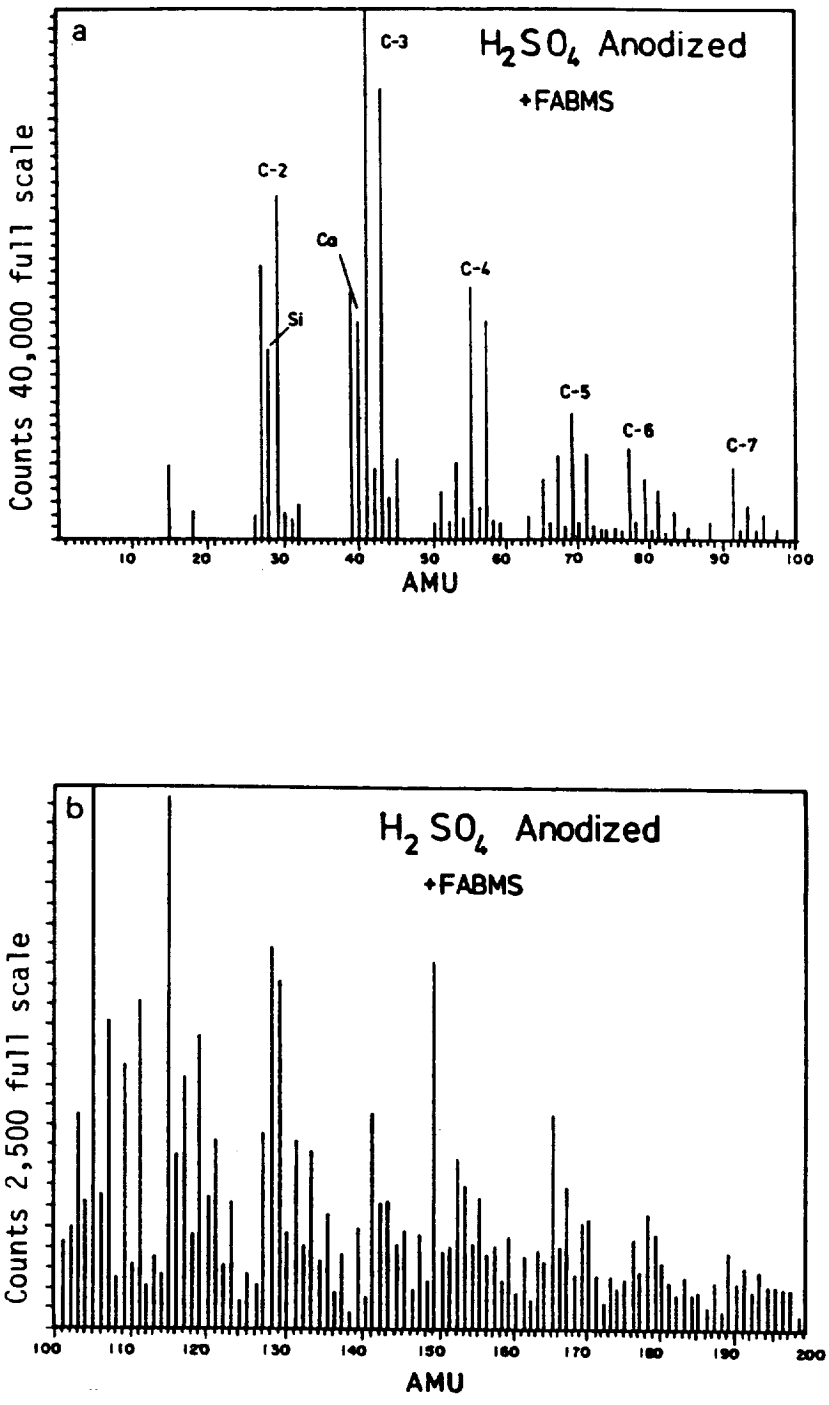

Figure 4.5 Positive fast atom bombardment mass spectra of Hercules AU-4 fibers anodized in 0.5 M H_2SO_4 at 6V for 2 minutes. a) 0 - 100 atomic mass units (AMU) b) 100 -200 AMU

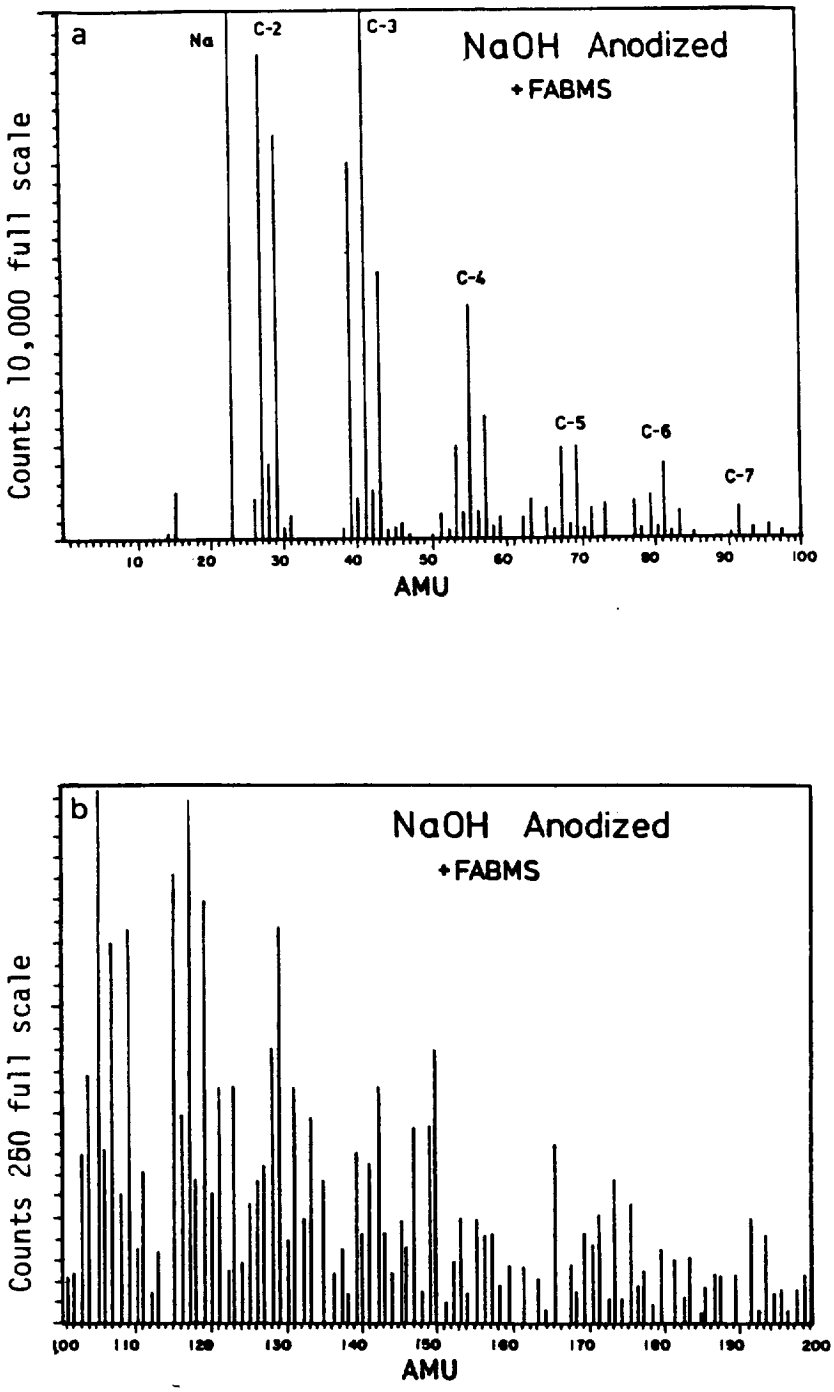

Figure 4.6 Positive fast atom bombardment mass spectra of Hercules AU-4 fibers anodized in 0.5 M NaOH at 6V for 2 minutes. a) 0 -100 atomic mass units (AMU) b) 100 -200 AMU

Table 4.7 Summary of organic mass fragments ejected from fiber surfaces during fast atom bombardment

Fragment Atomic Mass Unit	Possible Chemical Structure
+ 77	
+ 91	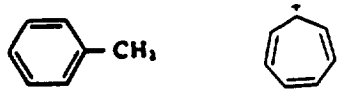
+ 104	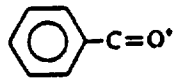
+ 115	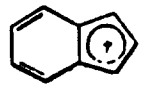
+ 128	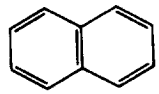
+ 132	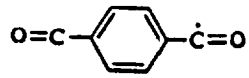
+ 149	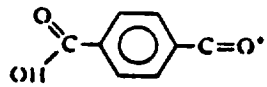
+ 165	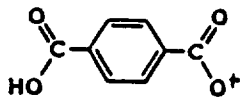
- 93	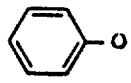

anodization in NaOH leaving only more ordered carbon on the fiber surface, the lower signal intensity would be expected.

The spectra of negative ions ejected from the surface of the NaOH and H_2SO_4 anodized fibers during argon atom bombardment are shown in Figures 4.7 a and b respectively. The negative ion spectrum of the NaOH anodized fibers has peaks at 12, 13, 16, 17, 24, and 35/37 due to C^-, CH^-, O^-, OH^-, $C2^-$, and Cl^- respectively. The negative ion spectrum of the H_2SO_4 anodized fibers has peaks at 16, 17, 80, and 97 due to O^-, OH^-, SO_3^-, and SO_4H^- respectively. The sulfur containing ions being residual material from the anodization.

4.2.5 Surface Energy Analysis of Treated Fibers

The surfaces of the Hercules AU-4 fibers anodized in NaOH and H_2SO_4 were analyzed to determine the polar and dispersive components of their surface energy. The polar and dispersive components of the anodized fibers are listed in Table 4.8. The linear regression plots of equation 2.7 used to obtain the polar and dispersive surface energy components of the anodized fibers are shown in Figure 4.8 The vertical lines represent plus or minus one standard deviation (obtained from measurement on six fibers) in the calculated parameter for the Y axis.

The NaOH anodized fibers have a dispersive component 6

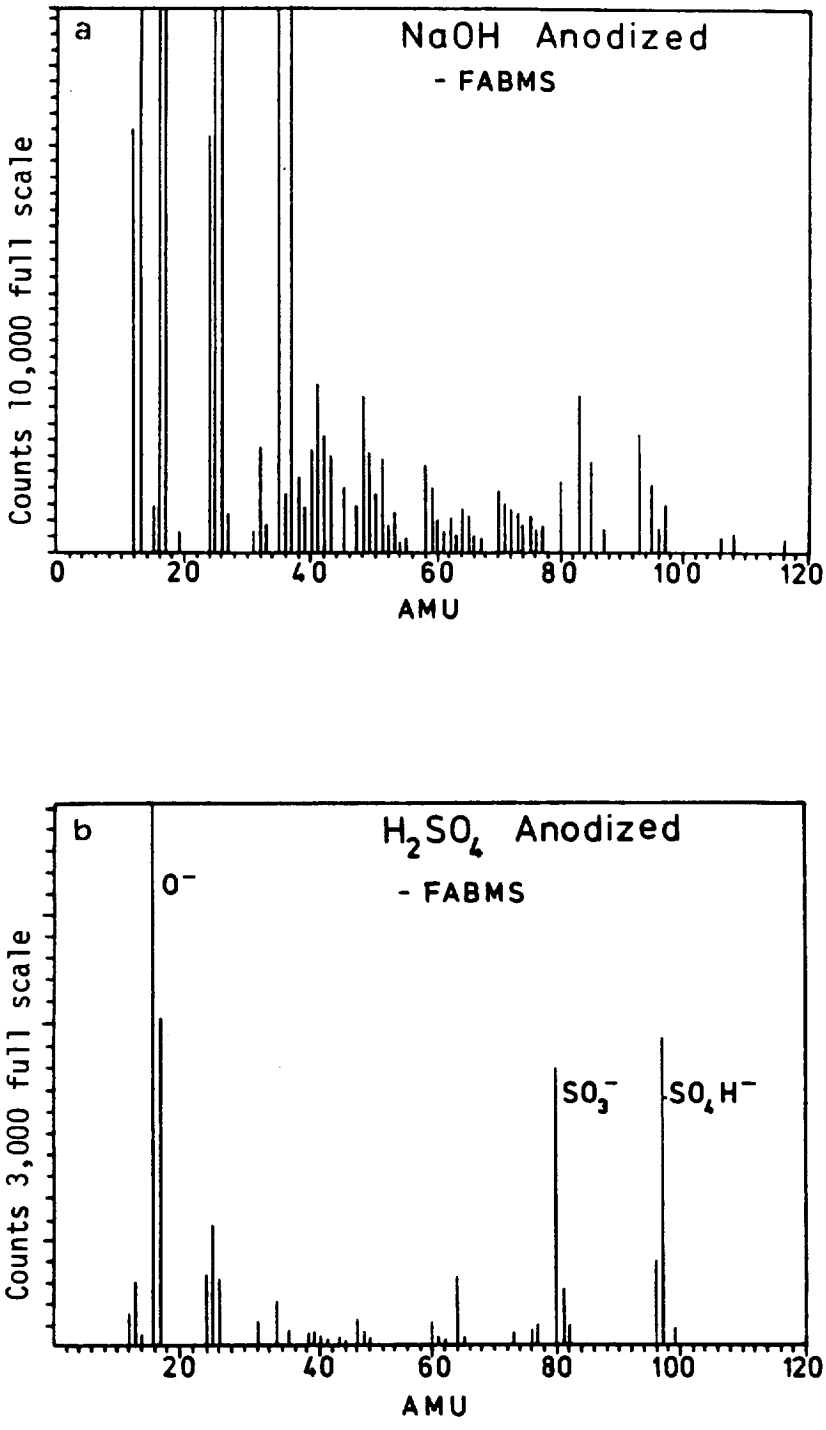

Figure 4.7 Negative fast atom bombardment mass spectra of Hercules AU-4 fibers anodized in a) 0.5 M H_2SO_4 and b) 0.5 M NaOH at 6V for 2 minutes

Table 4.8 Surface energies of Hercules AU-4 fibers anodized in 0.5 M NaOH and 0.5 M H_2SO_4 at 6V for 2 minutes.

Fiber	Treatment	γ^p_{sv} (erg/cm²)	γ^d_{sv} (erg/cm²)	γ^t_{sv} (erg/cm²)
AU-4	0.5M H_2SO_4 6V 2 m	21	28	50
AU-4	0.5M NaOH 6V 2 m	22	34	56

γ^p_{sv} is the polar component of solid surface energy

γ^d_{sv} is the dispersive component of solid surface energy

γ^t_{sv} is the total solid surface energy

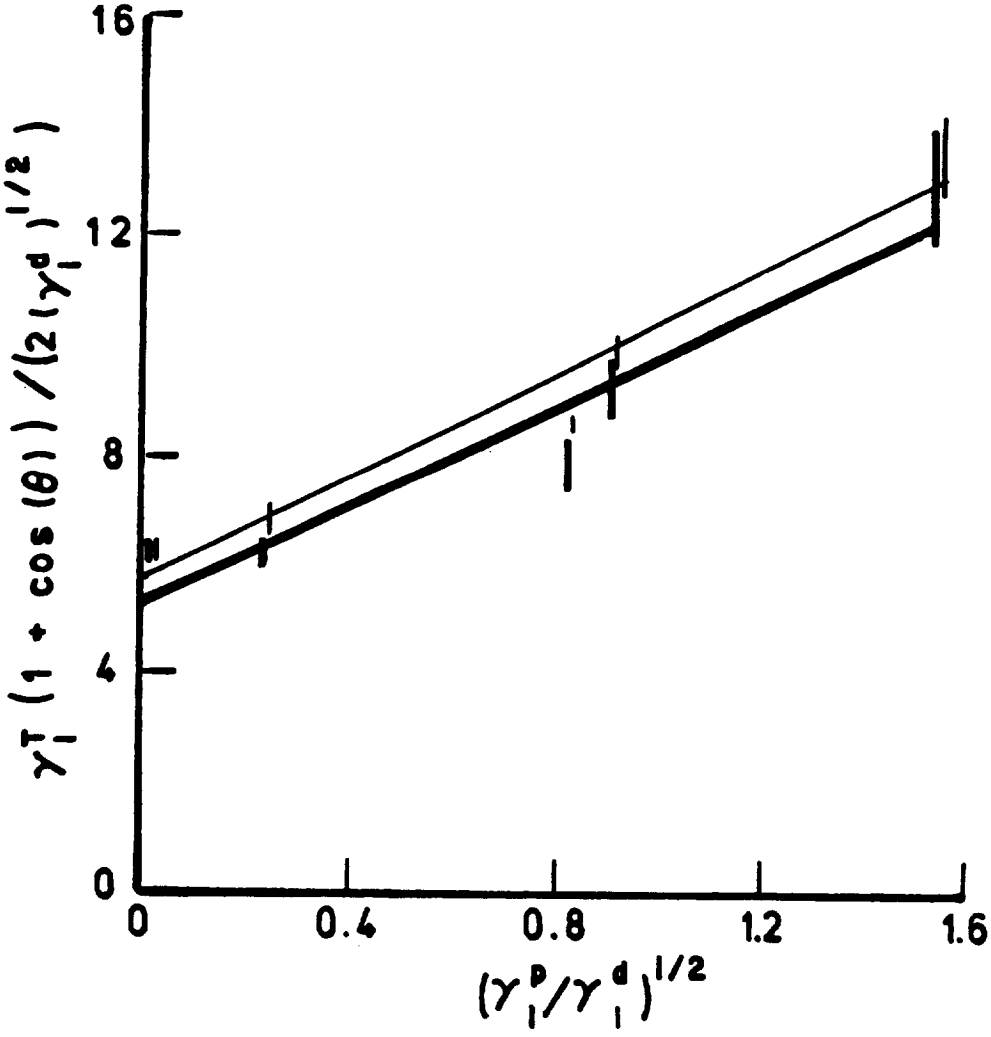

Figure 4.8 Linear regression plot for determination of polar and dispersive components of surface energy of Hercules AU-4 fibers anodized in (▬) H_2SO_4, and (——) NaOH. Vertical lines indicate standard deviation in calculated parameter.

ergs/cm^2 higher than the H_2SO_4 anodized fibers. A more graphitic structure would have more conduction electrons and thus more polarizable electrons to contribute to the dispersive force interaction. This supports the XPS findings that the graphite structure is enhanced by the NaOH anodization.

4.2.6 Breaking Strength as a Function of Anodization Time

The STEM photomicrographs in Figure 4.2 show that anodization can create defects on the fiber surface. These defects will cause sites on the fiber surface where fracture can occur thus decreasing the fiber strength. It is also possible that the fiber already has many surface flaws as it comes out of the carbonization furnace. The surface treatment may remove these defects and thus increase the breaking strength of the fiber.

The effect of surface treatment on the breaking strength of carbon fibers is shown in Table 4.9. This table lists the breaking strength of Hercules AU-4 fibers after 0 to 2 minutes anodization in 0.5 M NaOH and 0.5 M H_2SO_4 at 6 volts. The average, standard deviation, and the shape and scale parameters of the Weibull distribution, α and β (see Appendix II), are listed in Table 4.9. The breaking strength increases after up to 15 seconds of anodization and then begins to decrease rapidly. In both electrolytes, the

Table 4.9 Breaking strengths of carbon fibers after anodization in 0.5M NaOH at 0.5M H_2SO_4 at 6 volts for various lengths of time.

	Average (GPa)	Standard Deviation (GPa)	Beta (GPa)	Alpha
AU-4 0.5M H_2SO_4 6V				
0 sec	3.00	0.580	3.24	5.82
8 sec.	3.23	0.712	3.51	4.95
15 sec.	3.26	0.570	3.50	6.62
30 sec	3.00	0.764	3.28	4.95
60 sec.	2.30	0.731	3.60	3.60
120 sec.	2.55	1.140	2.89	2.66
AU-4 0.5M NaOH 6V				
0 sec.	3.00	0.580	3.24	5.82
8 sec.	3.17	0.892	3.49	4.59
15 sec.	3.45	0.852	3.77	4.91
30 sec.	2.52	0.941	2.82	2.97
60 sec.	1.81	0.661	2.03	3.06
120 sec.	2.22	0.905	2.50	2.78

optimum treatment time was 15 seconds.

It should be mentioned that this breaking strength versus anodization time study was only done at 0.5 M electrolyte concentration and 6 V. It is expected that the optimum anodization time will change with electrolyte concentration and applied voltage. Further, the optimum treatment condition for Hercules fibers may not be the same as for fibers from other companies. In later studies however, this treatment i.e., 0.5 M/6 V/15 seconds was chosen for treatment of fibers from the other producers.

4.2.7 Summary of Effect of Anodization on Surface Properties of Carbon Fibers

STEM photomicrographs indicate that at lower electrolyte concentrations, pitting of the fiber surface occurs during NaOH anodization, and exfoliation of graphitic layers occurs during H_2SO_4 anodization. At higher electrolyte concentrations, the surface treatment appears more uniform. Angular dependent XPS analysis indicated that at lower take-off angles, the oxygen to carbon ratio increases for the NaOH anodized fibers and decreases for the H_2SO_4 anodized fibers. The plasmon peak increases with decreasing take-off angle for the NaOH anodized fibers but remains the same for the H_2SO_4 anodized fibers. UV absorption spectra of the anodization baths show that the

NaOH bath contains many aromatic species while the H_2SO_4 bath contains a few less aromatic species. The FABMS signal from the NaOH anodized fibers is much less intense than from the H_2SO_4 anodized fibers. The NaOH anodized fibers have a much higher dispersive force surface energy contribution than the H_2SO_4 anodized fibers.

The results summarized in the preceding paragraph indicate that anodization in H_2SO_4 results in oxidation occurring between the carbon layers. Anodization in NaOH results in removal of amorphous carbon from the fiber surface leaving behind more ordered graphitic carbon with functional groups on the crystal edges.

4.3) SURFACE ANALYSIS OF COMMERCIAL CARBON FIBERS

4.3.1 Scanning Transmission Electron Microscopy

STEM photomicrographs of the untreated fibers as received are shown in Figure 4.9. All micrographs were taken at 12,500X magnification. The Hercules AU-4 fiber has small ridges about 0.05 μm wide parallel to the fiber axis. The Dexter Hysol and Union Carbide fibers have ridges about 0.1 μm wide parallel to the fiber axis.

STEM photomicrographs of the fibers with a commercial treatment are shown in Figure 4.10. There is little difference in appearance between the treated and the

Hercules AU - 4 Dexter Hysol XAU Union Carbide T - 300U

Figure 4.9 STEM photomicrographs of untreated commercial fibers as received (12,500 X)

Hercules AS-4 Dexter Hysol XAS Union Carbide T-300S

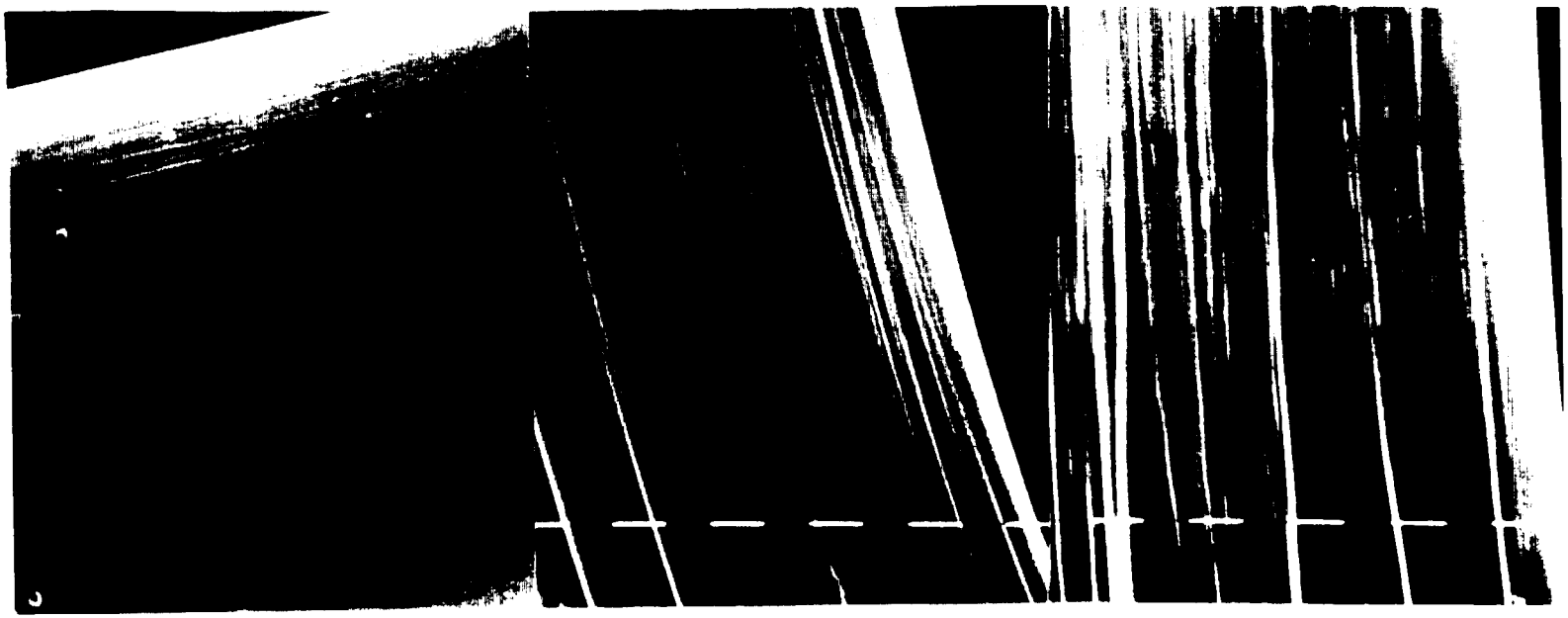

Figure 4.10 STEM photomicrographs of commercially treated fibers as received (12,500 X)

untreated fibers. The features on the treated fibers are perhaps slightly more distinct than on the untreated fibers.

Observation of the fiber surfaces at higher magnification revealed that the untreated Dexter Hysol XA fiber had a textured surface as shown in Figure 4.11a. The commercially surface treated XA fiber shown in Figure 4.11b did not have this textured surface. Observation of the fibers from Hercules and Union Carbide at higher magnification revealed no further structure.

4.3.2 X-ray Photoelectron Spectroscopy

The elements detected by x-ray photoelectron spectroscopy (XPS), their atomic percentages and binding energies for the fibers as received from the producer are listed in Table 4.10. At least two XPS spectra were obtained on fibers from each producer. The results listed are for a representative spectrum.

In general, the oxygen content increases upon commercial surface treatment. The binding energy of the oxygen increases after surface treatment. The nitrogen content variation upon surface treatment is different for each producer.

The carbon, oxygen, and nitrogen XPS signals were curve-fit as described in section 4.1.1. The curve fit carbon, oxygen, and nitrogen XPS spectra for the untreated

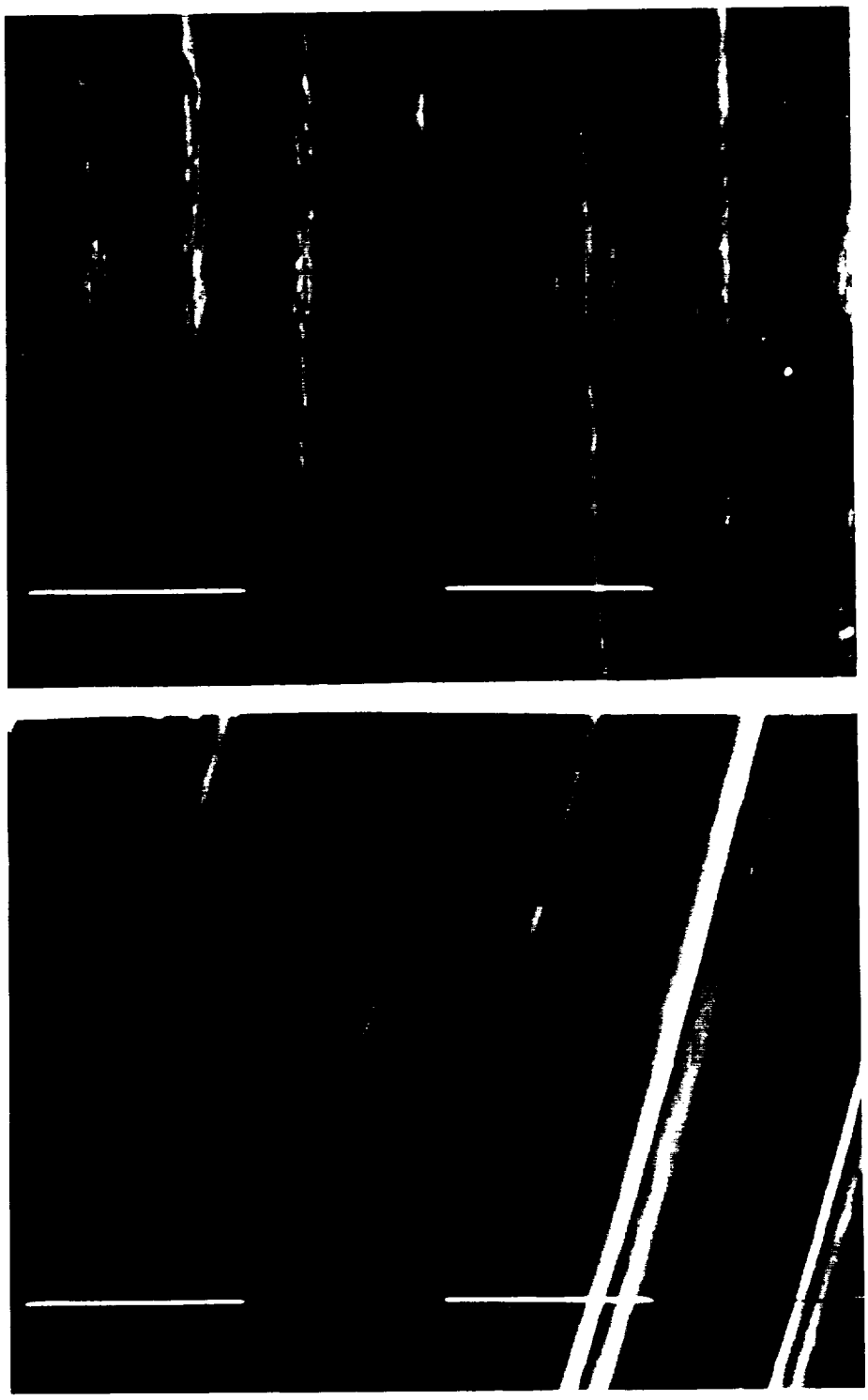

Figure 4.11 STEM photomicrograph of Dexter Hysol XA fibers a) before and b) after commercial surface treatment (50,000 X).

Table 4.10 Atomic percentages (%), binding energies (BE) of elements, oxygen to carbon (O/C) and nitrogen to carbon (N/C) ratios detected by XPS on the surface of carbon fibers as received.

	Carbon	Oxygen		Nitrogen		Other		O/C	N/C
Fiber	%	%	BE (eV)	%	BE (eV)	%	Element		
AU-4	96	1.8	532.9	2.0	401.6			0.02	0.02
AS-4	84	9.9	532.0	5.0	399.8	0.8	Na	0.12	0.06
XAU	81	9.7	532.7	9.8	399.7			0.12	0.12
XAS	77	17	534.1	5.5	400.6			0.22	0.07
T-300U	96	2.0	532.9	2.1	401.5			0.02	0.02
T-300S	81	17	532.9	2.2	400.3			0.21	0.03

fibers are shown in Figure 4.12. The curve fit carbon, oxygen, and nitrogen XPS spectra for the commercially treated fibers are shown in Figure 4.13. The actual results obtained by curve fitting these peaks are listed in Appendix III. A summary of results obtained by curve fitting the carbon 1s peaks for the as received fibers is listed in Table 4.11.

For the Hercules fiber, the shape of the carbon 1s peak is essentially the same before and after treatment. There is a small increase in the peak due to carboxylic acid type functionalities. The plasmon peak is not affected by surface treatment. The oxygen peak increases in intensity, becomes narrower and, shifts to lower binding energy with surface treatment. The nitrogen content increases and the nitrogen binding energy decreases with surface treatment indicating the presence of nitrogen functionality.

For the Dexter Hysol fiber, the carbon 1s peak becomes much broader with surface treatment. There is a significant increase in contribution from R-C-O and R-C=O type bonding. The plasmon peak is enhanced by surface treatment. The oxygen binding energy increases and the peak becomes wider with surface treatment. The nitrogen content decreases and the nitrogen binding energy decreases with surface treatment.

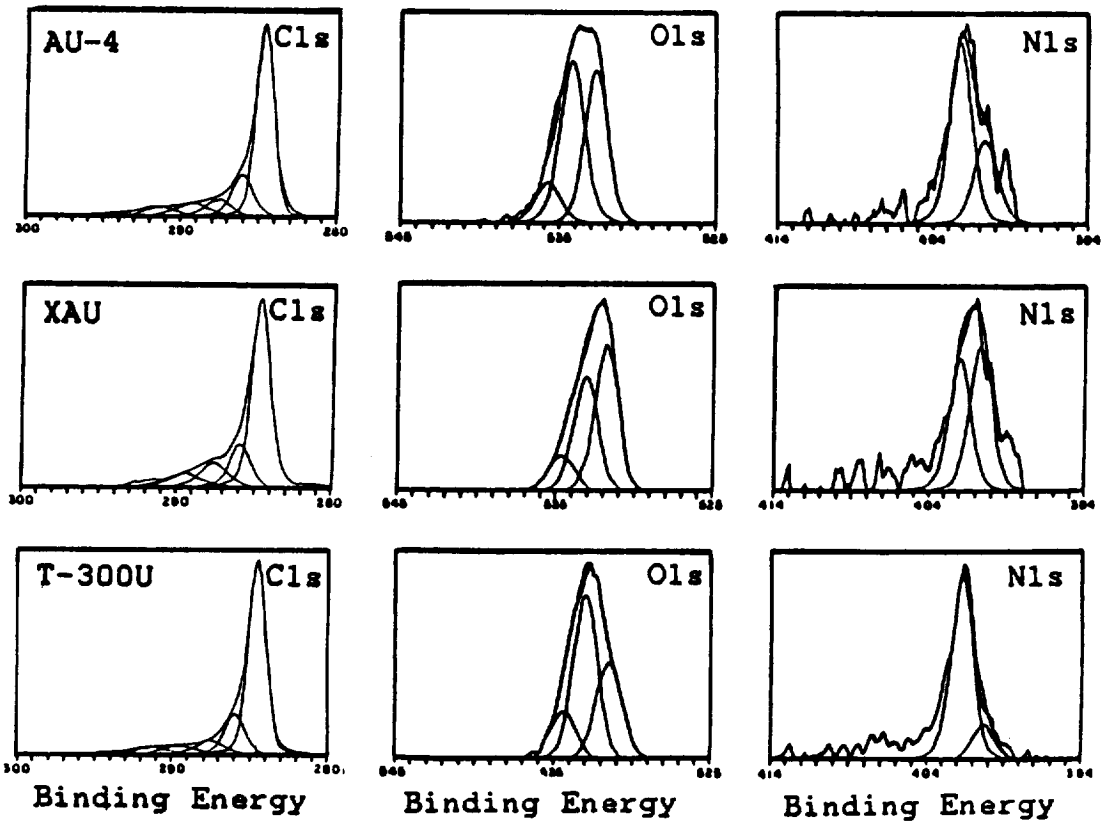

Figure 4.12 Curve fit XPS photopeaks for untreated commercial fibers as received.

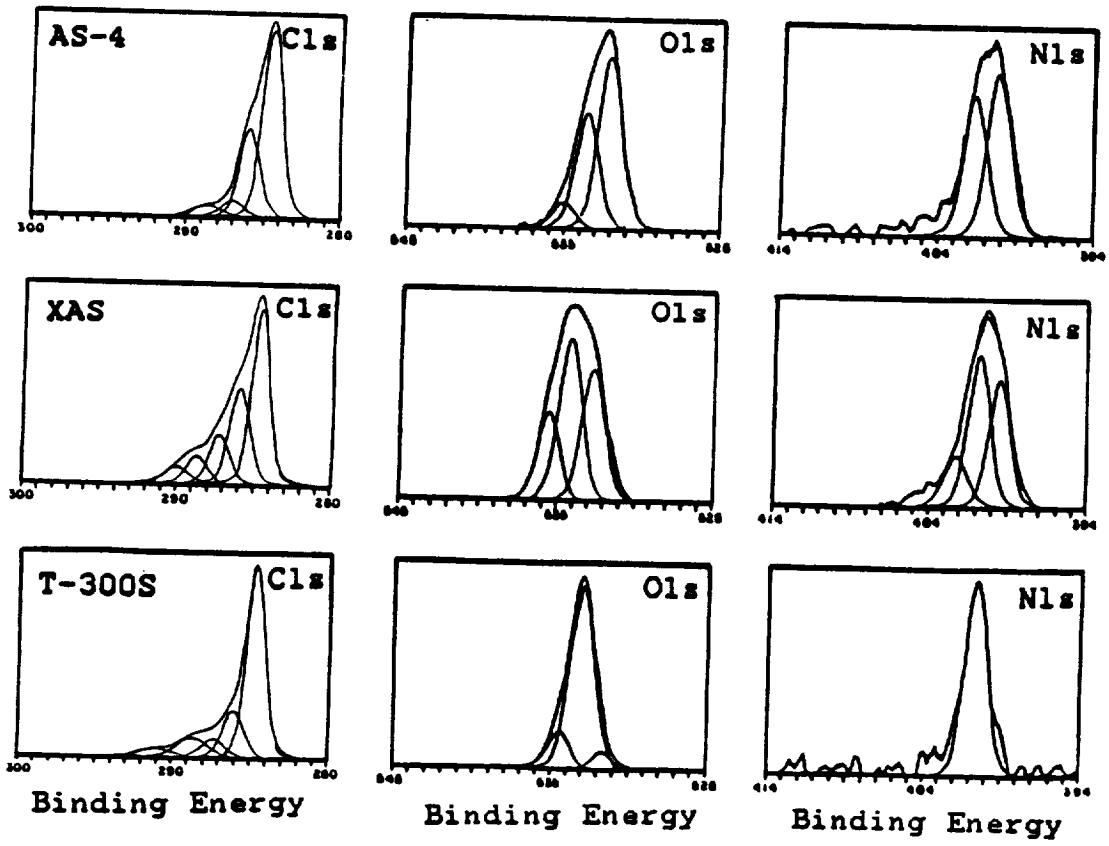

Figure 4.13 Curve fit XPS photopeaks for commercially treated fibers as received.

Table 4.11 Summary of results obtained by curve fitting XPS carbon 1s peaks of fibers before and after commercial surface treatment

Fiber	C_1 (%)	$\frac{C_2}{C_1}$ X100	$\frac{C_3}{C_1}$ X100	$\frac{C_4}{C_1}$ X100	$\frac{C_5}{C_1}$ X100
AU-4	67	25	10	9	5
AS-4	65	25	10	14	5
XAU	61	32	15	10	5.4
XAS	46	59	29	16	11
T-300U	72	22	8.6	5.1	4.3
T-300S	63	46	7.6	6.4	

For the Union Carbide fiber, the carbon 1s peak increases in width with surface treatment. The most significant increase is in the peak due to R-C-O type bonding. The plasmon peak is almost nonexistent after surface treatment. The oxygen binding energy stays the same. However, the oxygen peak becomes narrower due to a decrease in the lower binding energy side of the peak. The nitrogen content decreases with surface treatment. The nitrogen binding energy decreases slightly and the peak becomes narrower.

The oxygen to carbon ratios as a function of the sine of the take-off angle for the fibers before and after commercial surface treatment are shown in Figure 4.14. For the Hercules AS-4 and Dexter Hysol XAS fibers, the spectra were recorded more than once to check the reproducibility of the results. The two spectra for the Hercules AS-4 fiber showed a O/C ratio that differed by about 20%. The AU-4 fiber also showed much variability. Initial spectra obtained on AU-4 indicated an O/C ratio greater than 0.3. However, it was suspected that this oxygen might be due to contamination. After removal of about 20 meters of fiber from the spool, the variability was reduced to about 20%. The variability of the O/C and N/C ratios for the Dexter Hysol fibers was about 8% for the surface treated fibers and 20% for the untreated fibers.

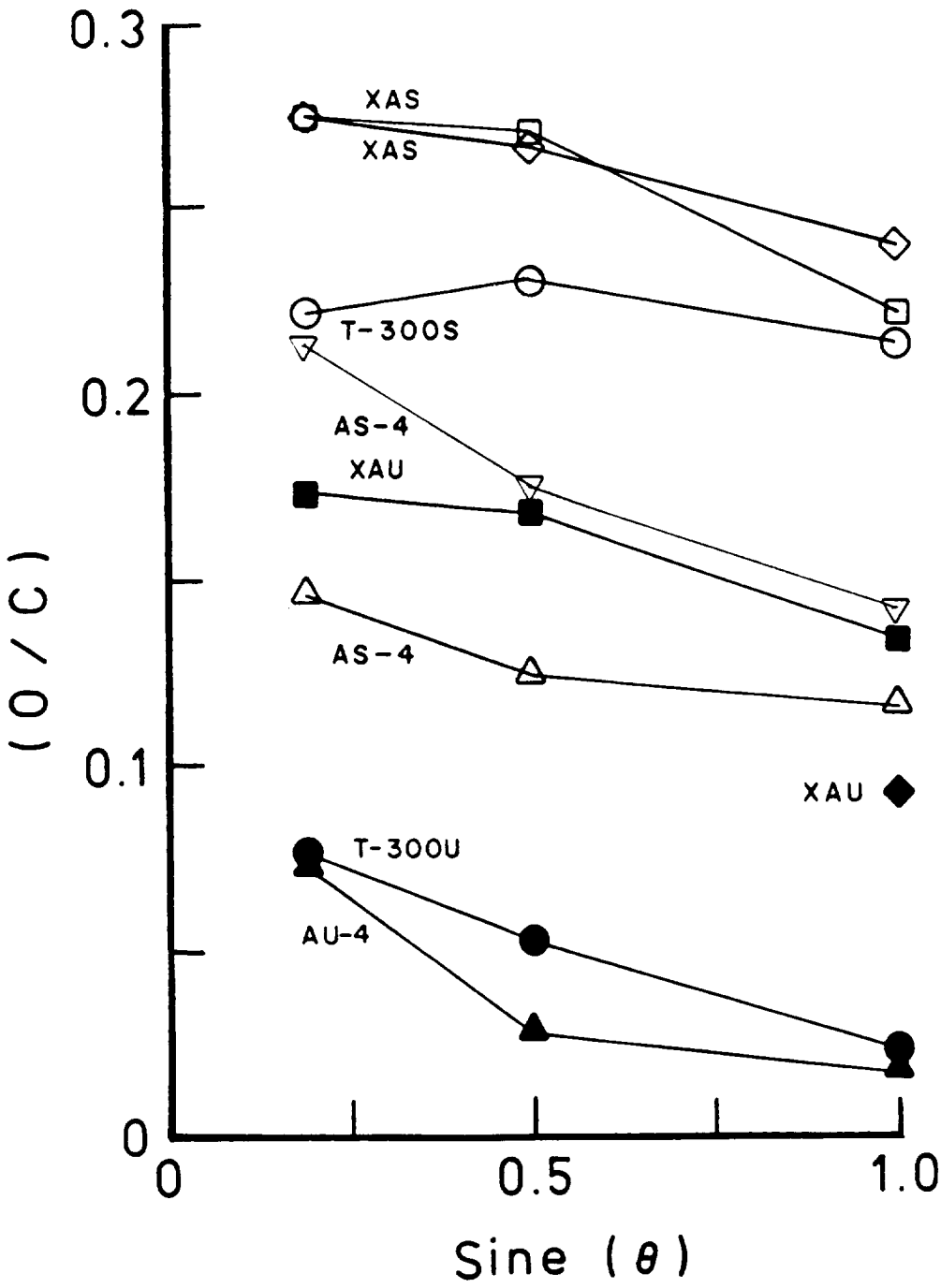

Figure 4.14 Oxygen to carbon ratios as detected by XPS versus sine take-off angle (θ) for commercial fibers before and after commercial surface treatment

It is informative to observe the effect of sine take-off angle on the O/C and N/C ratios for the surface treated fibers. For the Hercules AS-4 and the Dexter Hysol XAS fibers, the O/C ratio increases with decreasing sine take-off angle. For the Union Carbide T-300 fiber, the O/C ratio decreases with decreasing sine take-off angle. This result for the Union Carbide fiber coupled with the fact that the plasmon peak decreases with surface treatment indicates that the oxygen is probably being added between the graphitic layers in a manner similar to the H_2SO_4 anodization discussed in section 4.2.

The nitrogen to carbon ratios versus sine of the take-off angle for the fibers before and after commercial surface treatment are shown in Figure 4.15. The N/C ratio increases with decreasing sine take-off angle for the Hercules AS-4 fibers indicating that nitrogen functionality may be present on the fiber surface. The N/C ratio decreases with decreasing sine take-off angle for the Union Carbide T-300S and Dexter Hysol XAS fibers indicating that nitrogen is probably not predominant on the fiber surface.

To summarize, the Hercules AS-4 and Dexter Hysol XAS fibers have nitrogen as well as oxygen functionality. The Union Carbide fibers have predominantly oxygen functionality. The oxygen on the AS-4 and XAS fibers was seen by angular dependent XPS studies to be present on

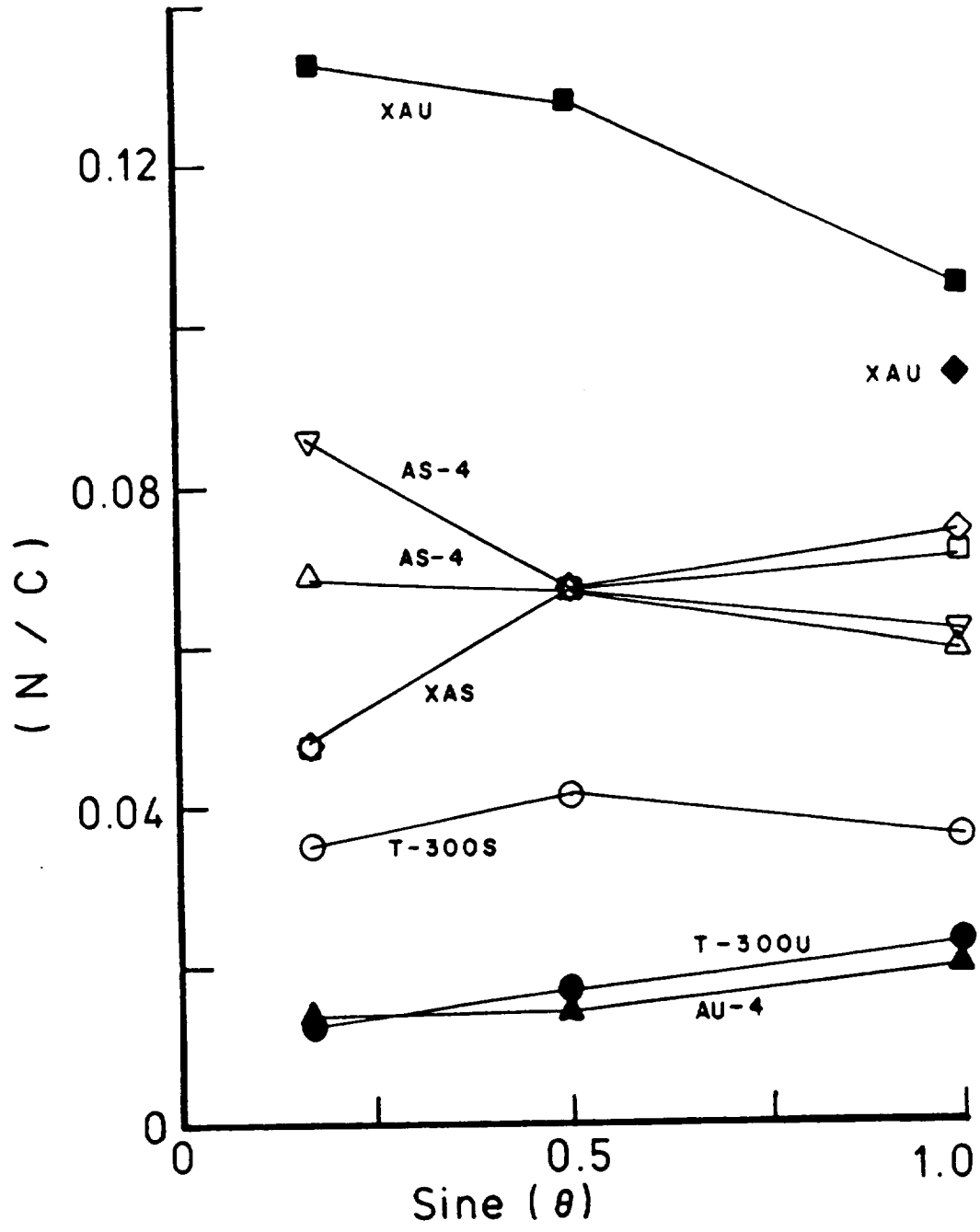

Figure 4.15 Nitrogen to carbon ratios as detected by XPS versus sine take-off angle (θ) for commercial fibers before and after commercial surface treatment

the top layer of the fiber surface. The oxygen on the T-300 fiber was possibly present between the graphitic layers of the carbon fiber.

4.4) SURFACE ANALYSIS OF FIBERS FROM VARIOUS PRODUCERS WITH THE SAME SURFACE TREATMENT

In this study, fibers from various producers were treated with the same surface treatment in order to obtain the same functional groups on the surface of each fiber. It was assumed that the fibers would have similar reactivity to the anodization reactions. The differences in surface properties of the fibers after they have undergone the same treatment were examined by STEM, XPS, surface energy analysis, and breaking strength measurement at several gauge lengths.

4.4.1 Scanning Transmission Electron Microscopy

STEM photomicrographs of the fibers used in this study before and after surface treatment are shown in Figures 4.15 to 4.18. All micrographs were taken at 12,500X magnification. The white markers indicate 0.5 μm. Examination of these micrographs show no change in surface topography upon surface treatment. Observation at higher magnification also showed no significant difference in surface topography for the AS-4 and T-300 fibers. The

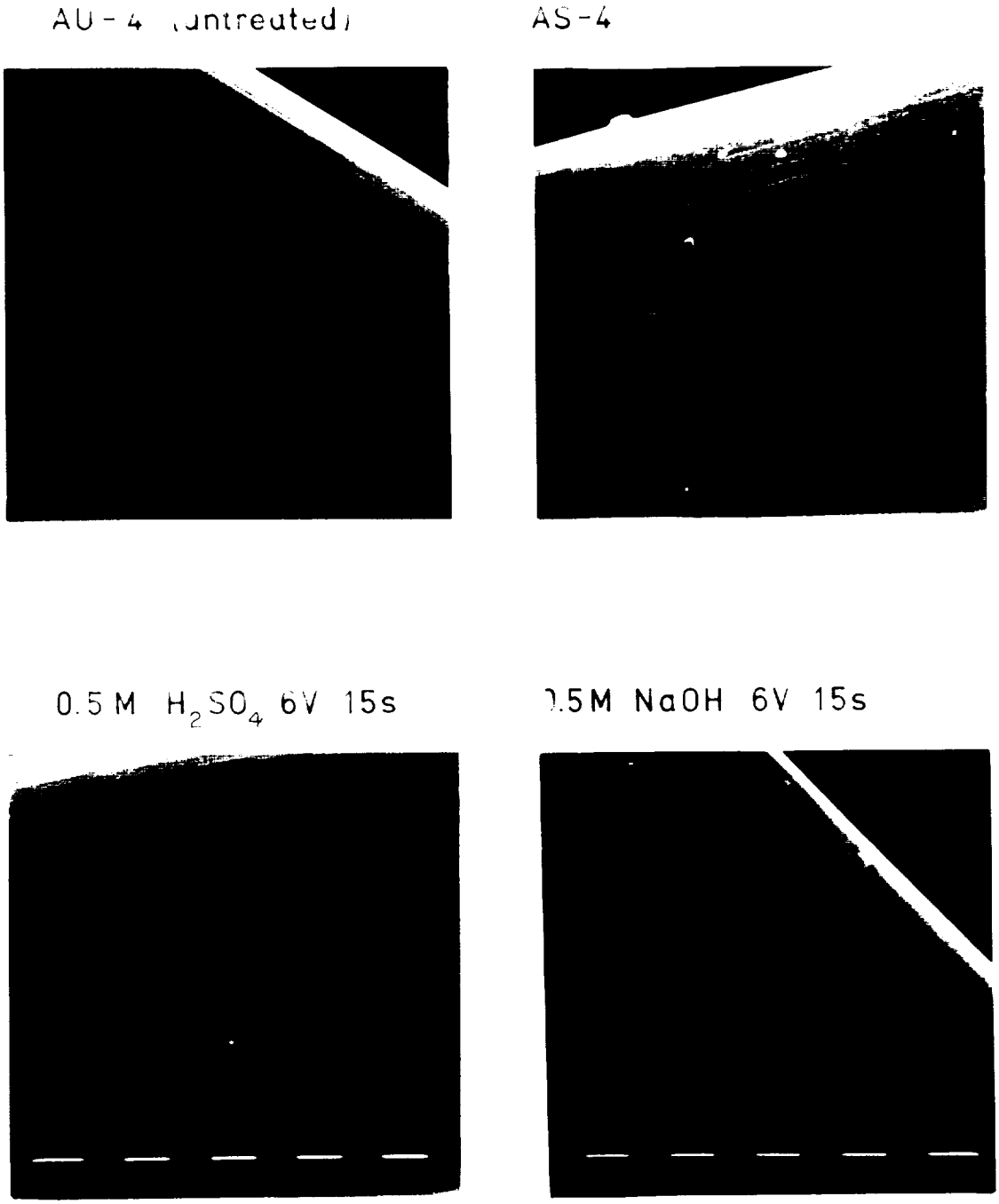

Figure 4.16 STEM photomicrographs of Hercules A fibers before and after surface treatment (12,500 X).

XAU (untreated)

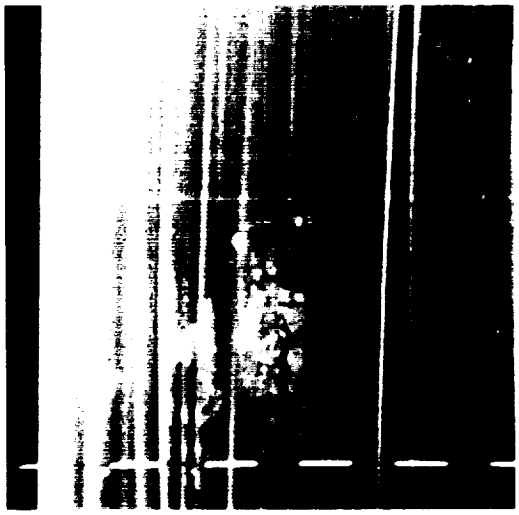

XAS

0.5 M H_2SO_4 6V 15s

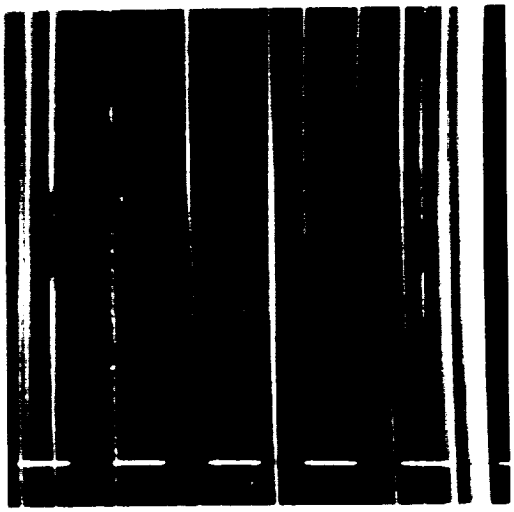

0.5 M NaOH 6V 15s

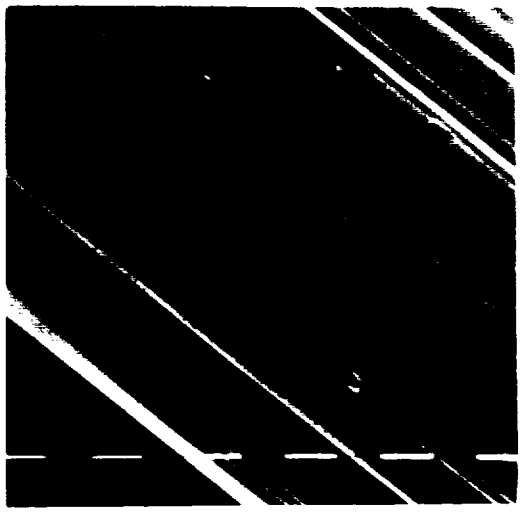

Figure 4.17 STEM photomicrographs of Dexter Hysol XA fibers before and after surface treatment (12,500 X).

T-300 U (untreated)

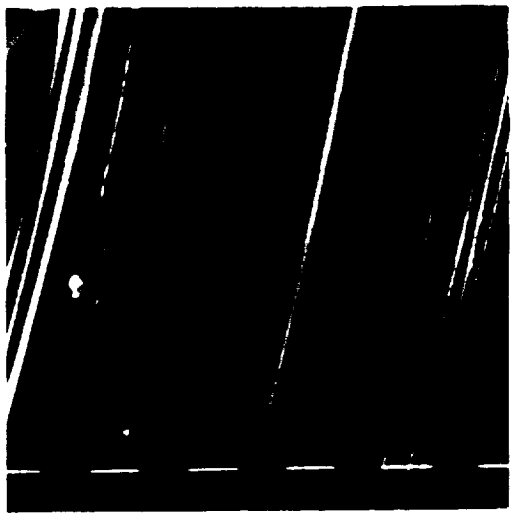

T-300 S

0.5 M H_2SO_4 6V 15s

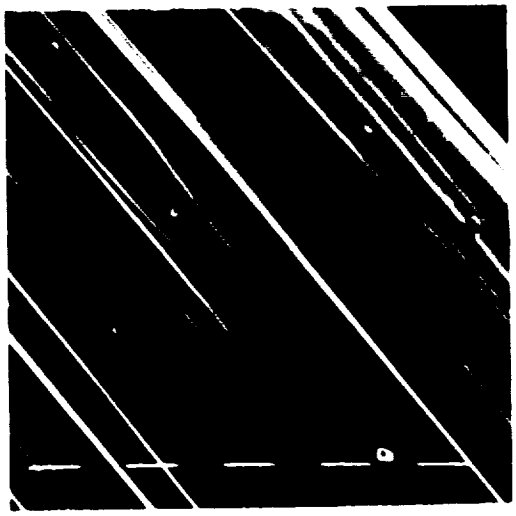

0.5 M NaOH 6V 15s

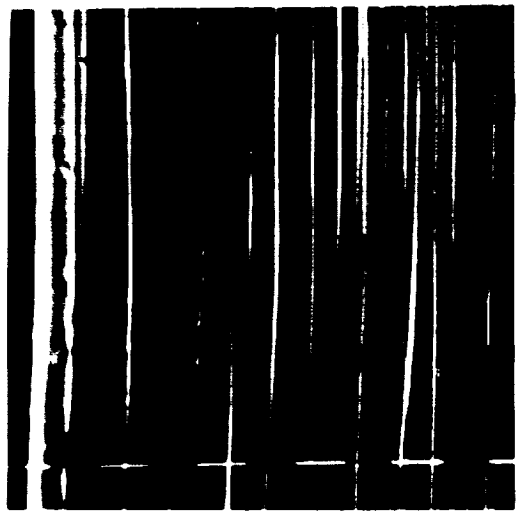

Figure 4.18 STEM photomicrographs of Union Carbide T-300 fibers before and after surface treatment (12,500 X).

untreated Dexter Hysol showed the porous structure as reported in section 4.3.1. This porous structure was also seen on the laboratory treated fibers but not on the commercially treated fiber.

The fact that no differences were seen, does not lead to the conclusion that there are no sub-microscopic differences in surface topography. It is most likely that these surface treatments are altering the fiber surface structure in the way suggested in section 4.2, i.e. pit formation by NaOH anodization, and exfoliation by H_2SO_4 anodization. The scanning transmission electron microscope is just not capable of detecting these changes.

4.4.2 X-Ray Photoelectron Spectroscopy

The XPS results for the commercial fibers after anodization in NaOH and H_2SO_4 are listed in Table 4.12. It can be seen that H_2SO_4 anodization resulted in about 26% oxygen on the fiber surface. The binding energy of the most intense oxygen peak was at a high binding energy. This is due to oxygen strongly bound to other elements, possibly sulfur. The amount of nitrogen on the fiber surface was reduced by anodization in both H_2SO_4 and NaOH.

The amount of oxygen added to the fiber surfaces was lower on the T-300 fiber than on the fibers from the other companies for both anodization conditions. This indicates

Table 4.12 Atomic percentages (%), binding energies (BE) of elements, oxygen to carbon (O/C), and nitrogen to carbon (N/C) ratios detected by XPS of on the surface carbon fibers after laboratory surface treatment.

Fiber	Carbon	Oxygen		Nitrogen		Other		O/C	N/C
	%	%	BE (eV)	%	BE (eV)	%	Element		
AU-4 H_2SO_4	72	26	533.6	1.9	400.2	0.1	S	0.36	0.03
XAU H_2SO_4	72	26	535.1	1.9	400.7	0.1	S	0.36	0.03
T-300U H_2SO_4	75	23	534.7	1.7	400.7	0.2	S	0.31	0.02
AU-4 NaOH	72	15	534.0	1.8	401.9	5.6	Na	0.21	0.03
XAU NaOH	78	14	531.7	0.9	400.4	6.8	Na	0.18	0.01
T-300U NaOH	92	6.4	532.9	0.9	401.5	0.6	Na	0.07	0.01

that either the morphological or chemical structure of the surface of this fiber is different than the AS or XAS fibers. The oxygen content on the surface treated AU-4 and XAU fibers was close indicating that the reactions occurring on these fibers during anodization may be similar.

The curve fit carbon, oxygen, and nitrogen signals for the commercial fibers after anodization in 0.5 M H_2SO_4 at 6 V for 15 seconds are shown in Figure 4.19. The curve fit carbon, oxygen, and nitrogen signals for the commercial fibers after anodization in 0.5 M NaOH at 6 V for 15 seconds are shown in Figure 4.20.

A summary of results obtained by curve fitting the carbon 1s peaks of the surface treated fibers is shown in Table 4.13. The Dexter Hysol XA fiber anodized in H_2SO_4 has a C_2 peak much larger than the other fibers. This may indicate that the functionality on the XA fiber is different than on the other two fibers, or that the chemical structure of the surface of this fiber is causing a binding energy shift in the carbon 1s signal.

4.4.3 Surface Energy Analysis

The polar and dispersive and surface energy components of the commercial fibers before and after surface treatment were calculated. The surface energies of the carbon fibers are listed in Table 4.14. The table lists the polar

Table 4.13 Summary of results obtained by curve fitting XPS carbon 1s peaks of fibers before and after laboratory surface treatment

Fiber		C_1 (%)	$\frac{C_2}{C_1}$ X100	$\frac{C_3}{C_1}$ X100	$\frac{C_4}{C_1}$ X100	$\frac{C_5}{C_1}$ X100
AU-4	H_2SO_4	62	23	13	20	4.4
XAU	H_2SO_4	44	75	24	26	1.4
T-300U	H_2SO_4	59	32	13	19	6.7
AU-4	NaOH	63	30	15	8.7	4.6
XAU	NaOH	64	31	8.4	12	5.7
T-300	NaOH	70	24	7.4	6.7	3.6

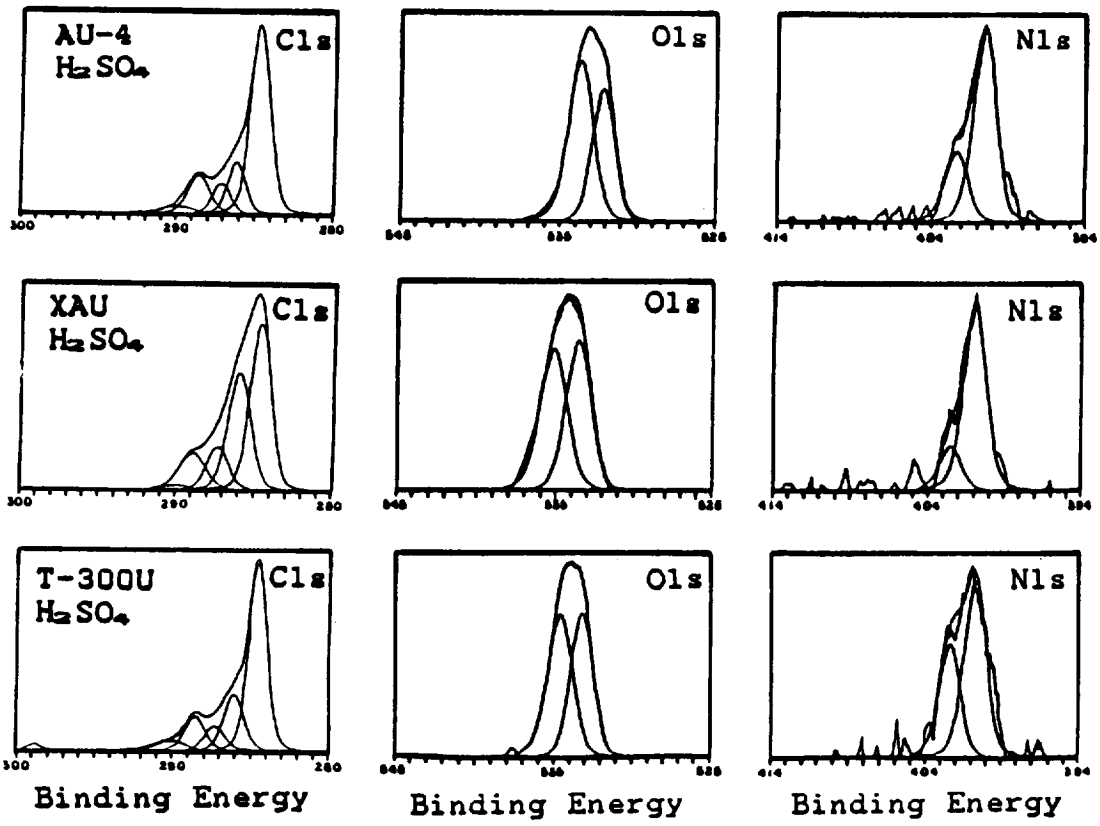

Figure 4.19 Curve fit XPS photopeaks for commercial fibers anodized in H_2SO_4. Anodization conditions are listed in Table 3.8

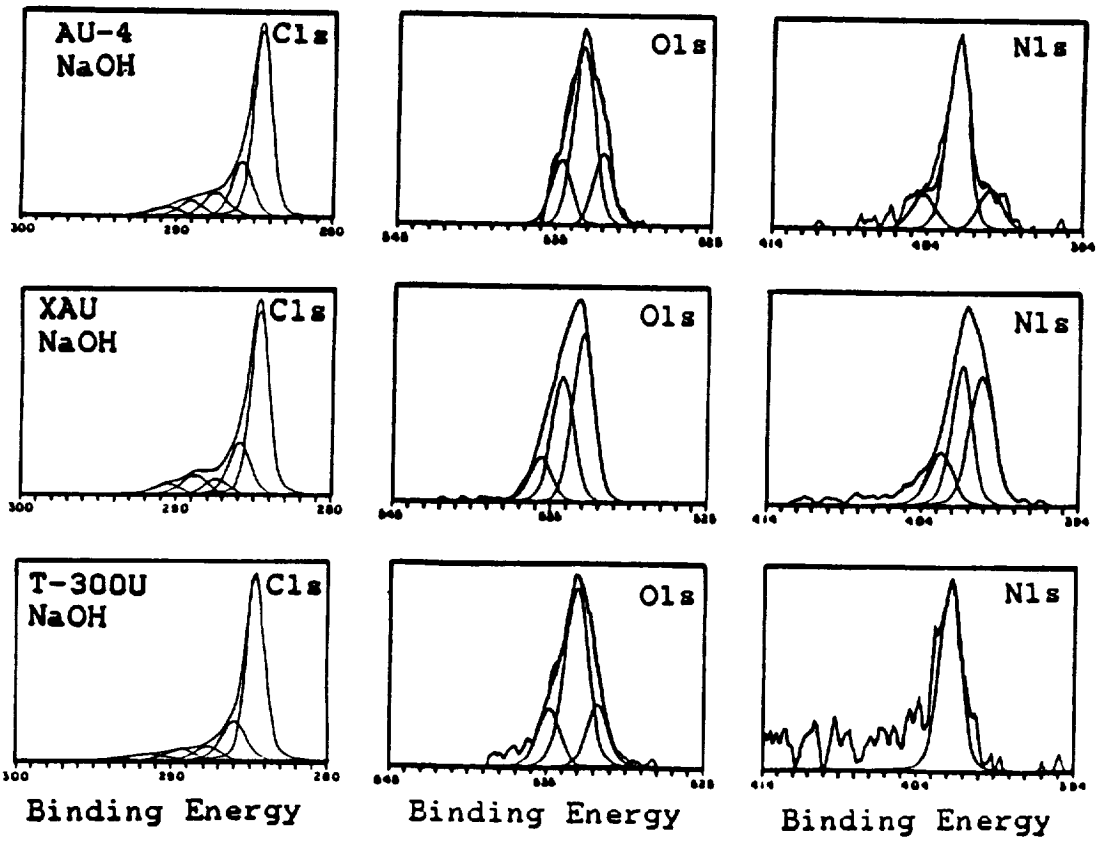

Figure 4.20 Curve fit XPS photopeaks for commercial fibers anodized in NaOH. Anodization conditions are listed in Table 3.8

Table 4.14 Surface energies of carbon fibers before and after surface treatment.

Fiber	Treatment	γ^p_{sv} (erg/cm²)	γ^d_{sv} (erg/cm²)	γ^t_{sv} (erg/cm²)
AU-4		18	28	46
AS-4		22	29	51
AU-4	0.5M H_2SO_4 6V 15s	20	36	56
AU-4	0.5M NaOH 6V 15s	17	36	53
XAU		23	33	56
XAS		28	31	59
XAU	0.5M H_2SO_4 6V 15s	14	39	53
XAU	0.5M NaOH 6V 15s	25	33	57
T-300U		10	33	43
T-300S		11	36	47
T-300U	0.5M H_2SO_4 6V 15s	12	35	47
T-300U	0.5M NaOH 6V 15s	24	33	57

γ^p_{sv} is the polar component of solid surface energy

γ^d_{sv} is the dispersive component of solid surface energy

γ^t_{sv} is the total solid surface energy

component, the dispersive component, and the total surface energy.

It should be pointed out that these surface energies were calculated by assuming that the cross section of the fibers was circular. STEM observation shows that these fibers have a textured surface. Since these fibers differ in surface topography, it is doubtful that differences in surface energy of fibers from one company can be compared to that of another company. However, it is expected that comparisons in surface energy between the same fiber with different surface treatments can be made.

In general, the total surface energy of the laboratory treated fibers was higher than for the as received fibers. The surface energy of the commercially treated fiber was higher than the untreated fiber. The dispersive component of the surface energy was higher for the H_2SO_4 anodized fibers than for the NaOH anodized fibers. The polar component of the surface energy was higher for the NaOH anodized fibers than for the H_2SO_4 anodized fibers. This is consistent with attack of the edge planes by NaOH anodization leaving functional groups on the surface of the graphitic carbon. Whereas the H_2SO_4 anodization is likely to attack between the carbon layers leaving functional groups below the fiber surface. The polar component for the T-300 fiber was doubled by anodization in NaOH.

The polar component of the surface energy is thought to be caused by the presence of specific functional groups on the fiber surface. It is assumed that these functional groups are in the form of carbon oxygen bonds. Hammer and Drzal (58) reported a relationship between the polar surface energy of Hercules AS-4 fibers and the O/C ratio as detected by XPS. A plot of the polar surface energy versus the oxygen to carbon ratio for the fibers anodized under the conditions listed in Table 3.8 is shown in Figure 4.21. There is no observable correlation between the two parameters. A possible explanation for the discrepancy between the results presented here and Drzal's results are that in Drzal's work, the functional groups on the fiber surfaces being examined were essentially the same. The amount of functional groups was changed by thermal desorption. In this case, the polar component will be a simple indication of the amount of functional groups remaining on the fiber surface. In the present work, the fibers have been treated under varying conditions. The surface treatments affect the functional groups as well as the fiber surface morphology. The polar surface energy component in this work is thus being measured on fibers with large dif-ferences in surface functionality and morphology. Therefore, it is not surprising that there was little correlation between the polar surface energy and the oxygen to carbon ratios.

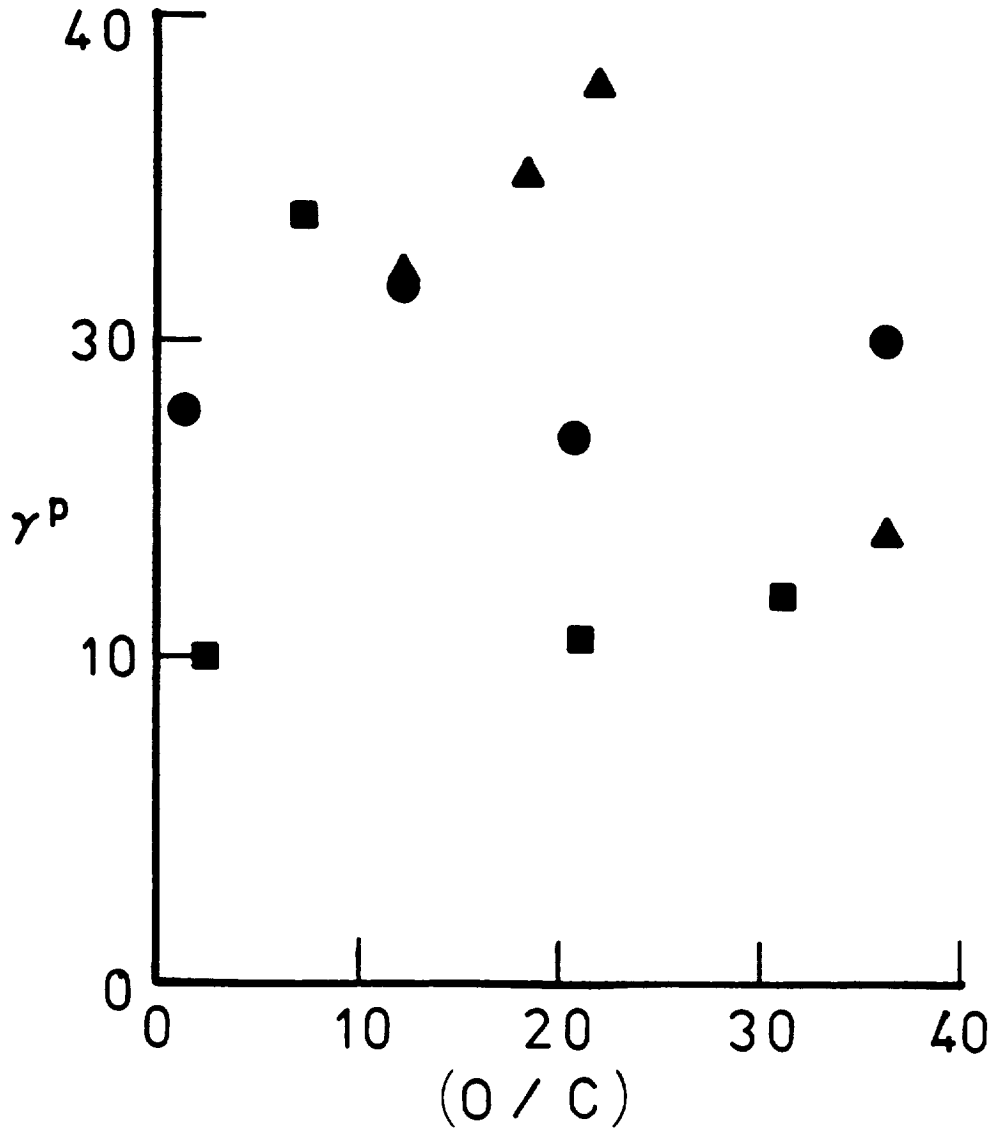

Figure 4.21 Plot of polar component of surface energy versus oxygen to carbon ratio as detected by XPS for carbon fibers before and after surface treatment (●), Hercules fibers (▲), Dexter Hysol fibers, (■), Union Carbide fibers

4.4.4 Breaking Strengths

The average breaking strengths, standard deviations, and the shape and scale parameters (α and β) of the Weibull distribution (Appendix II) for the commercially available fibers are listed in Table 4.15. Histograms of breaking strengths are shown in Appendix V. The fibers listed in order of increasing breaking strength are Hercules > Dexter Hysol > Union Carbide.

The breaking strengths of the fibers after anodization are listed in Table 4.16. The surface treated fibers were stronger than the untreated fibers. The strength of the fiber increases with decreasing length.

The breaking strengths as a function of length are plotted in Figures 4.22-4.24. The parameters in equation 2.16 which describe the length dependence of strength are listed in Table 4.17. These parameters were obtained by the method described in Appendix II. The Hercules fiber showed the sharpest increase in strength with decreasing length followed by the Union Carbide fiber then the Dexter Hysol fiber. The strength of the Dexter Hysol fiber was almost independent of length at the gauge lengths tested.

After surface treatment, the Hercules fibers increased even more in strength with decreasing length. The strength of the Dexter Hysol fibers after anodization increased more with decreasing length than the untreated or commercially

Table 4.15 Breaking strengths at different lengths of commercial carbon fibers as received.

Fiber	Average (GPa)	Standard Deviation (GPa)	Beta (GPa)	Alpha
AU-4				
2.5 cm.	2.48	0.725	2.73	4.14
1.3 cm.	2.84	0.541	3.06	6.00
0.6 cm.	3.00	0.580	3.24	5.82
AS-4				
2.5 cm.	2.98	0.799	3.27	4.34
1.3 cm.	3.08	0.580	3.32	5.68
0.6 cm.	3.76	0.584	4.00	8.13
XAU				
2.5 cm.	2.33	0.425	2.50	6.67
1.3 cm.	2.50	0.512	2.70	6.35
0.6 cm.	2.51	0.627	2.74	4.53
XAS				
2.5 cm.	2.12	0.430	2.29	5.54
1.3 cm.	2.34	0.317	2.48	8.35
0.6 cm.	2.26	0.517	2.46	4.99
T-300U				
2.5 cm.	2.10	0.376	2.25	7.40
1.3 cm.	2.01	0.499	2.20	4.59
0.6 cm.	2.53	0.446	2.71	6.40
T-300S				
2.5 cm.	2.19	0.605	2.40	4.31
1.3 cm.	2.32	0.584	2.54	4.79
0.6 cm.	2.60	0.618	2.83	5.67

Table 4.16 Breaking strengths at different lengths of carbon fibers after laboratory surface treatment.

Fiber	Average (GPa)	Standard Deviation (GPa)	Beta (GPa)	Alpha
AU-4 H_2SO_4				
1.9 cm.	2.68	0.629	2.92	5.43
1.3 cm.	3.15	0.609	3.38	6.86
0.6 cm.	3.26	0.570	3.50	6.62
AU-4 NaOH				
1.9 cm.	2.93	0.897	3.24	4.04
1.3 cm.	3.32	0.724	3.60	5.41
0.6 cm.	3.45	0.852	3.77	4.91
XAU H_2SO_4				
1.9 cm.	2.85	0.566	3.07	6.11
1.3 cm.	2.87	0.576	3.09	6.08
0.6 cm.	3.09	0.605	3.33	6.01
XAS NaOH				
1.9 cm.	2.46	0.484	2.65	6.18
1.3 cm.	2.76	0.584	3.00	4.55
0.6 cm.	2.65	0.538	2.86	5.75
T-300U H_2SO_4				
1.9 cm.	2.43	0.525	2.64	5.44
1.3 cm.	2.58	0.530	2.79	5.88
0.6 cm.	2.46	0.689	2.71	4.19
T-300S NaOH				
1.9 cm.	2.74	0.575	2.97	5.70
1.3 cm.	2.62	0.620	2.86	5.05
0.6 cm.	2.83	0.830	3.14	3.95

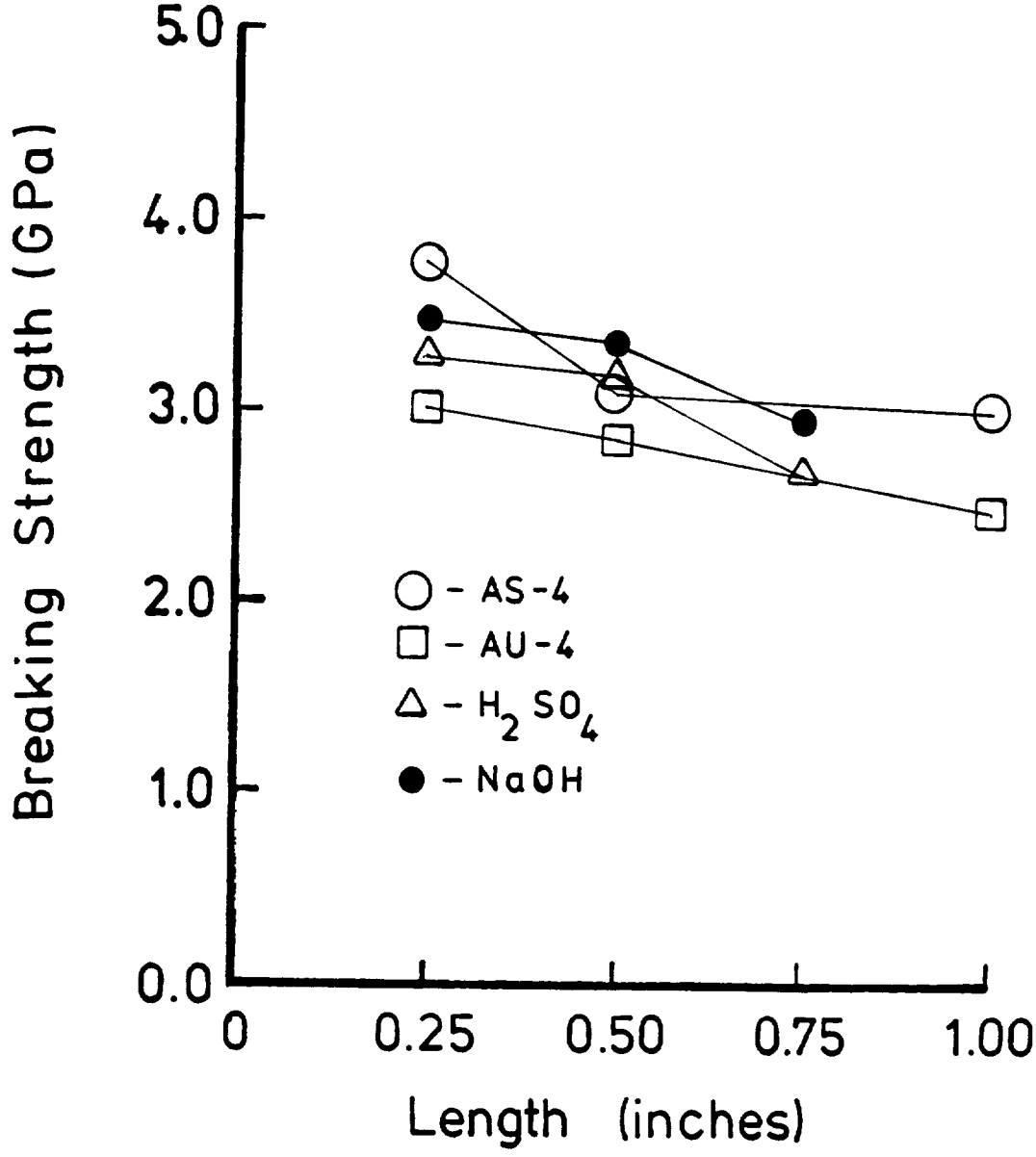

Figure 4.22 Breaking strength of Hercules A fibers at three gauge lengths before and after surface treatment

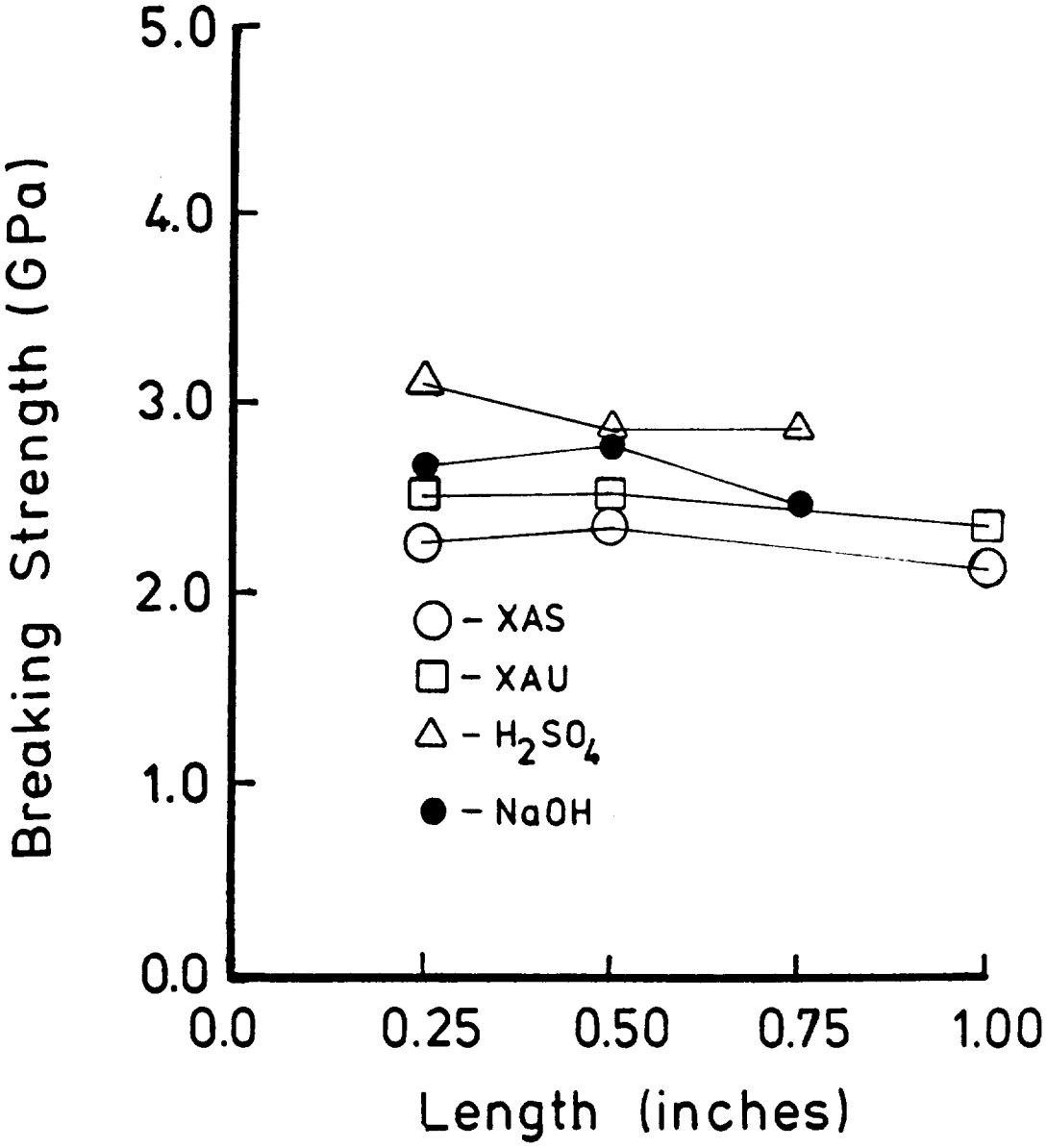

Figure 4.23 Breaking strength of Dexter Hysol XA fibers at three gauge lengths before and after sunburn treatment

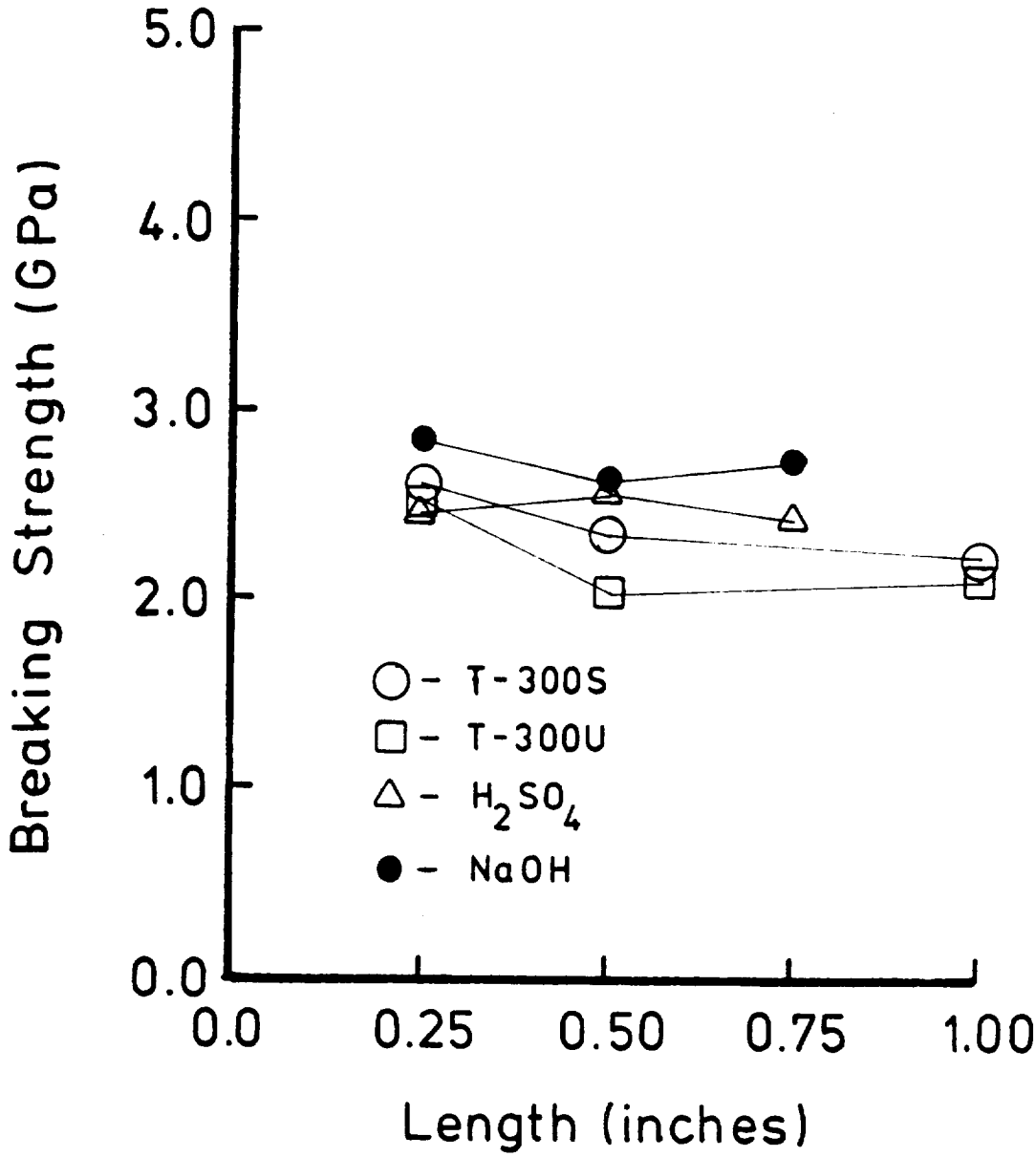

Figure 4.24 Breaking strength of Union Carbide T-300 fibers at three gauge lengths before and after surface treatment

Table 4.17 Slope and intercept of logarithm breaking strength vs. logarithm length for carbon fibers before and after laboratory surface treatment.

Fiber	Treatment	Slope	Intercept	x	β
AU-4		0.14	1.87	7.28	6.49
AS-4		0.17	2.22	5.96	9.20
AU-4	0.5M H_2SO_4 6V 15s	0.16	2.11	6.09	8.26
AU-4	0.5M NaOH 6V 15s	0.14	2.02	7.21	7.54
XAU		0.05	1.23	18.6	3.41
XAS		0.05	1.11	20.8	2.92
XAU	0.5M H_2SO_4 6V 15s	0.08	1.55	13.0	4.71
XAU	0.5M NaOH 6V 15s	0.05	1.29	18.5	3.63
T-300U		0.13	1.62	7.44	5.13
T-300S		0.12	1.63	8.06	5.11
T-300U	0.5M H_2SO_4 6V 15s	0.002	0.93	384.6	2.53
T-300U	0.5M NaOH 6V 15s	0.04	1.24	12.5	3.48

treated fibers. The strength of the anodized Union Carbide fibers was less dependent on length than the untreated or commercially treated fibers indicating creation of many flaws this fiber's surface upon surface treatment.

4.4.5 Summary of Effects of Surface Treatment on the Surface Properties of Commercially Available Fibers

STEM observation of the carbon fibers before and after surface treatment showed no change in surface topography upon surface treatment. XPS analysis of the oxygen content showed that the Hercules AS-4 and Dexter Hysol XAS fibers reacted similarly to anodization. The Union Carbide T-300 surface fiber had a much lower increase in oxygen after anodization than the AS-4 or XAS fibers. The AS-4 and T-300 fibers showed a dependence of breaking strength on length. The breaking strength of the XAS fiber was only slightly dependent on length. This breaking strength dependence on length indicates that the XAS fiber has many flaws distributed along its length. The breaking strength dependence on length was increased by anodization for the AS-4 and XAS fibers indicating removal of surface defects by anodization. The breaking strength dependence on length was decreased by anodization of the T-300 fibers indicating increased flaw density by surface treatment.

4.5) ADHESION TO THERMOPLASTIC MATRICES

In order to study the adhesion of carbon fibers to polymeric matrices, a fiber critical length test was used. The fiber critical length test was compared against observation of stress transfer between fiber and matrix with a polarizing light microscope. The work of adhesion was estimated and compared to actual adhesion results using the fiber critical length test.

4.5.1 Effect of Annealing Temperature on Adhesion

It is necessary to remove all the solvent from the polymer in order to obtain meaningful adhesion information from the fiber critical length test. In order to remove all of the solvent from the polymer, the sample should be heated above the glass transition temperature (T_g) of the polymer. When this is done, the mobility of the polymer chains is increased to the point where solvent molecules can diffuse out of the system. When the polymer cools down from above the glass transition temperature, it will shrink. In a single fiber test, this shrinkage will create a force normal to the fiber surface. Adhesion will thus be a result of thermal shrinkage plus the actual fiber/matrix adhesion. In a multiple fiber composite, the effect of thermal shrinkage is not well understood since the shrinkage is occurring on adjacent fibers also. Therefore, the adhesion measured in a

single fiber test may not be indicative of the stress transfer that will occur in a multiple fiber composite. Because of these considerations (solvent removal and thermal shrinkage), it was thought necessary to study the effect of annealing temperature of the single fiber specimen on the fiber/matrix adhesion.

Cumulative frequency plots for Hercules AS-4 fibers embedded in polysulfone and annealed at various temperatures are shown in Figure 4.25. The slope of the length-frequency plots increases with increased annealing temperature. The plots are also shifted to shorter fiber length with increased annealing temperature. The cumulative frequency plots of the fiber critical lengths for the AS-4 and XAS fibers embedded in polysulfone, polycarbonate, and polyetherimide and annealed at various temperatures are shown in Appendix VI. The fiber critical length of Hercules AS-4 and Dexter Hysol XAS fibers embedded in polysulfone, polycarbonate, and polyetherimide and annealed at various temperatures for 8 hours are listed in Table 4.18.

The interfacial stress transfer coefficient (ISTC) is plotted as a function of annealing temperature for each polymer in Figures 4.26 - 4.28. The dashed vertical line drawn in these figures indicates the glass transition temperature for the polymer used. The ISTC increases with increasing annealing temperature. The ISTC also increases

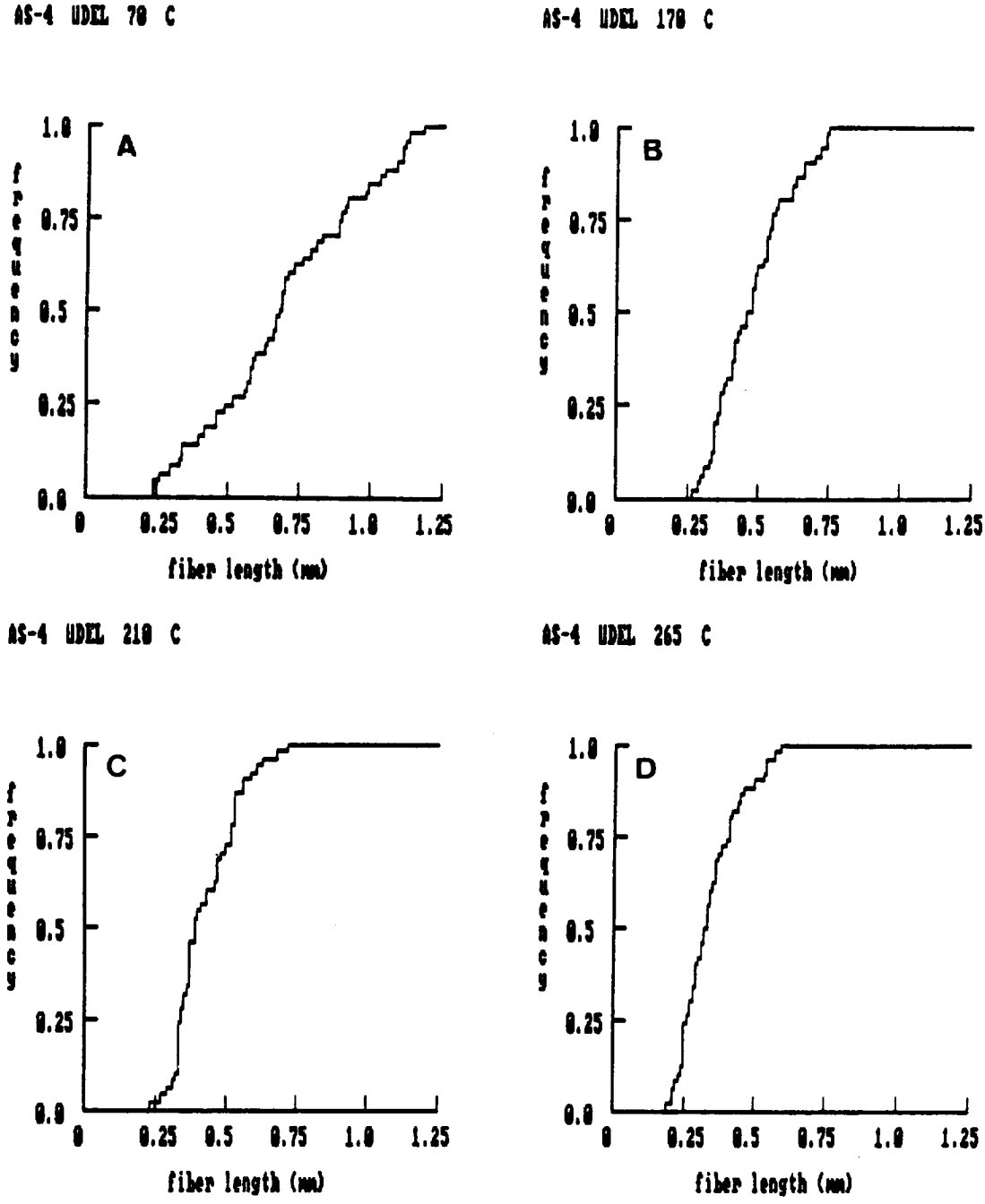

Figure 4.25 Cumulative frequency plots of fragment lengths in fiber critical length test of Hercules AS-4 fibers in polysulfone a) 70 °, b) 170°, c) 210°, and d) 265° C annealing temperature.

Table 4.18 Fiber critical lengths (FCL) of Hercules AS-4 and Dexter Hysol XAS fibers embedded in polysulfone (PS), polycarbonate (PC), and polyetherimide (PEI) and annealed at various temperatures for 8 hours.

Polymer	Temperature (°C)	Fiber			
		AS-4		XAS	
		FCL (mm)	SD (mm)	FCL (mm)	SD (mm)
PS	70	0.70	0.26	0.52	0.17
	170	0.48	0.13	0.46	0.14
	210	0.43	0.11	0.33	0.10
	265	0.34	0.10	0.29	0.08
PC	70	0.70	0.19	0.53	0.17
	140	0.78	0.20	0.33	0.07
	170	0.49	0.11	0.34	0.11
	265	0.27	0.08	0.22	0.07
PEI	70	0.77	0.22	0.47	0.18
	140	0.61	0.19	0.40	0.16
	210	0.61	0.16	0.21	0.07
	260	0.25	0.06	0.19	0.07

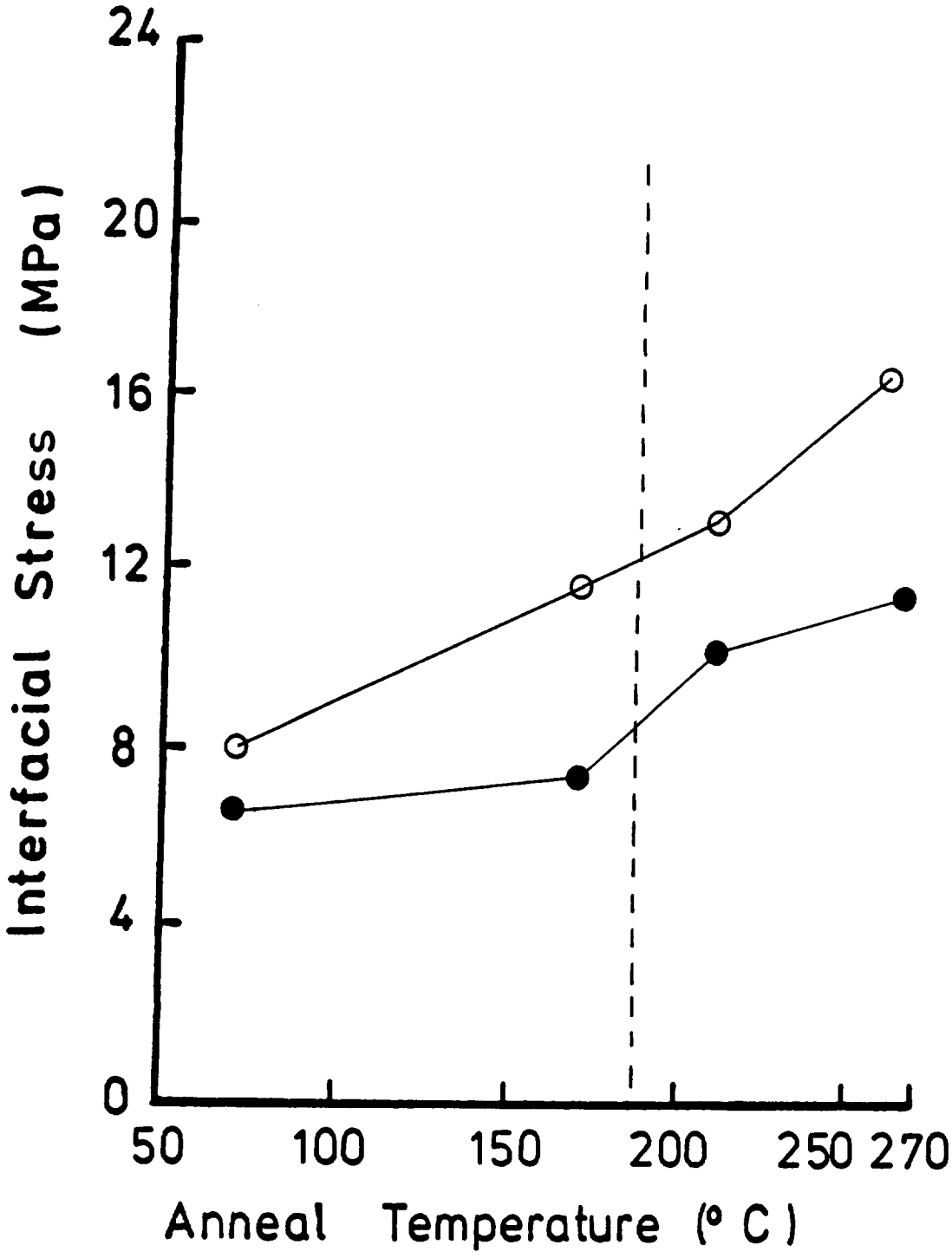

Figure 4.26 Interfacial shear stress transfer coefficient across fiber/polysulfone interface as a function of annealing temperature (○) Hercules AS-4, (●) Dexter Hysol XAS

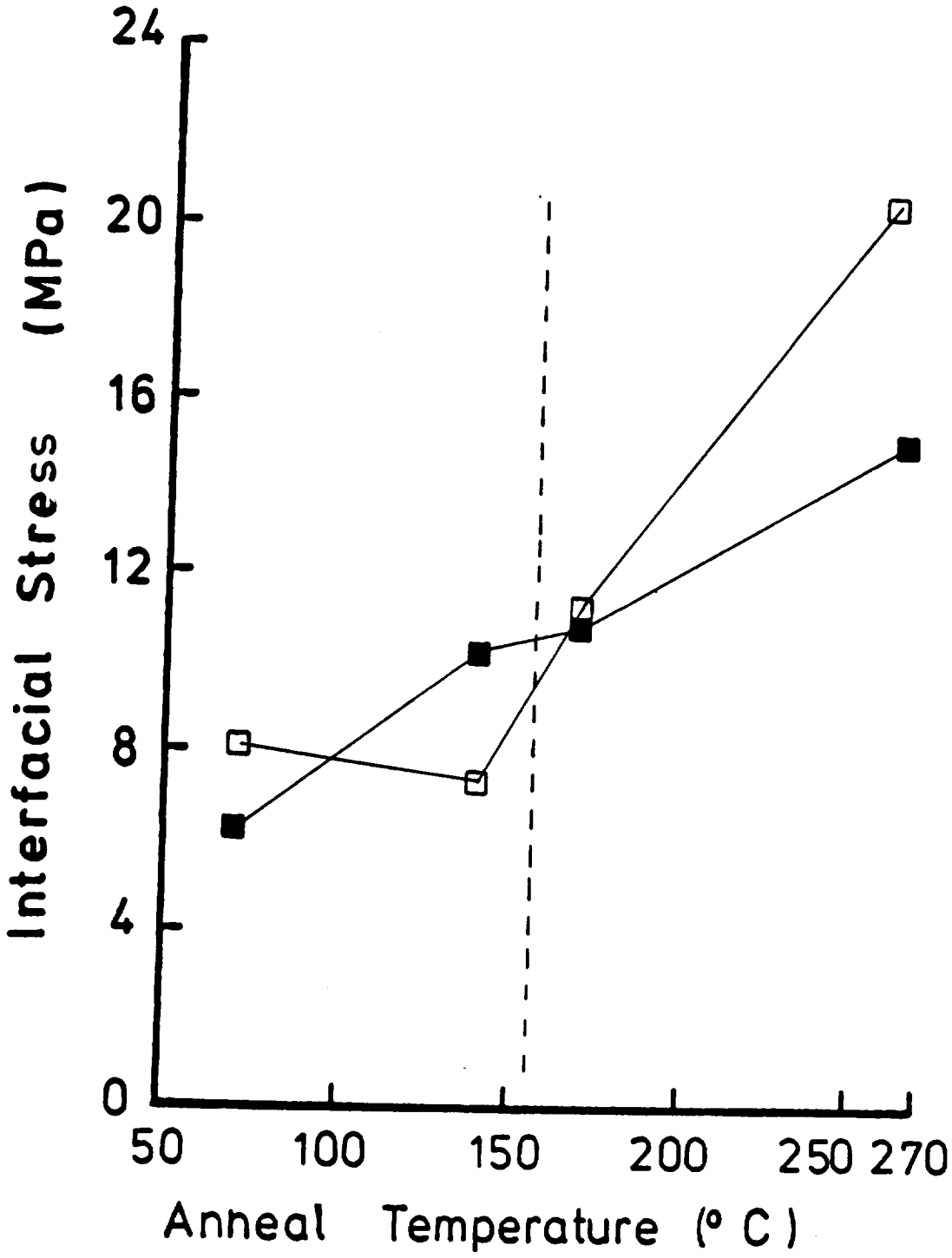

Figure 4.27 Interfacial shear stress transfer coefficient across fiber/polycarbonate interface as a function of annealing temperature (□) Hercules AS-4, (■) Dexter Hysol XAS

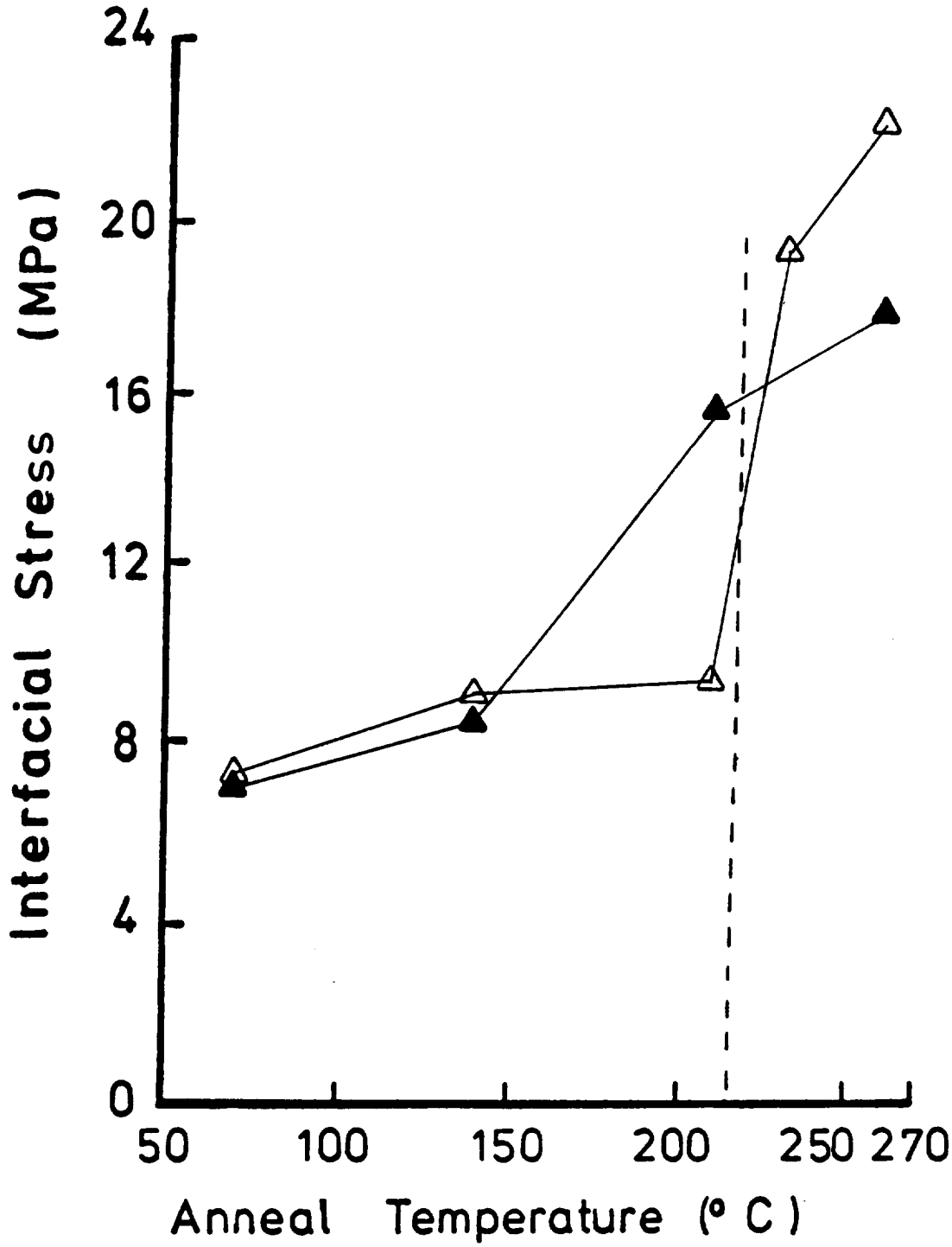

Figure 4.28 Interfacial shear stress transfer coefficient across fiber/polyetherimide interface as a function of annealing temperature (△) Hercules AS-4, (▲) Dexter Hysol XAS

with annealing above the glass transition temperature. This increase in ISTC above the glass transition is thought to be caused by improved contact between the polymer and the fiber. Better contact between fiber and matrix is thus occurring with increased annealing temperature.

4.5.2 Adhesion to Surface Treated Fibers

Cumulative frequency plots of fiber lengths in the fiber critical length test are shown in Figure 4.29. The plots are shown for the Hercules fiber before and after surface treatment and embedded in polysulfone. The fragment are much shorter in length for the laboratory anodized fibers. The commercially treated fibers have slightly shorter lengths than the untreated fiber. Similar plots for all three commercial fibers embedded in polysulfone, polycarbonate, and polyetherimide are shown in Appendix VII.

The average fiber lengths and standard deviation for the surface treated carbon fibers embedded in polysulfone, polycarbonate, and polyetherimide before and after treatment are listed in Table 4.19. The interfacial shear transfer coefficients (ISTC) between fiber and matrix are listed in Table 4.20.

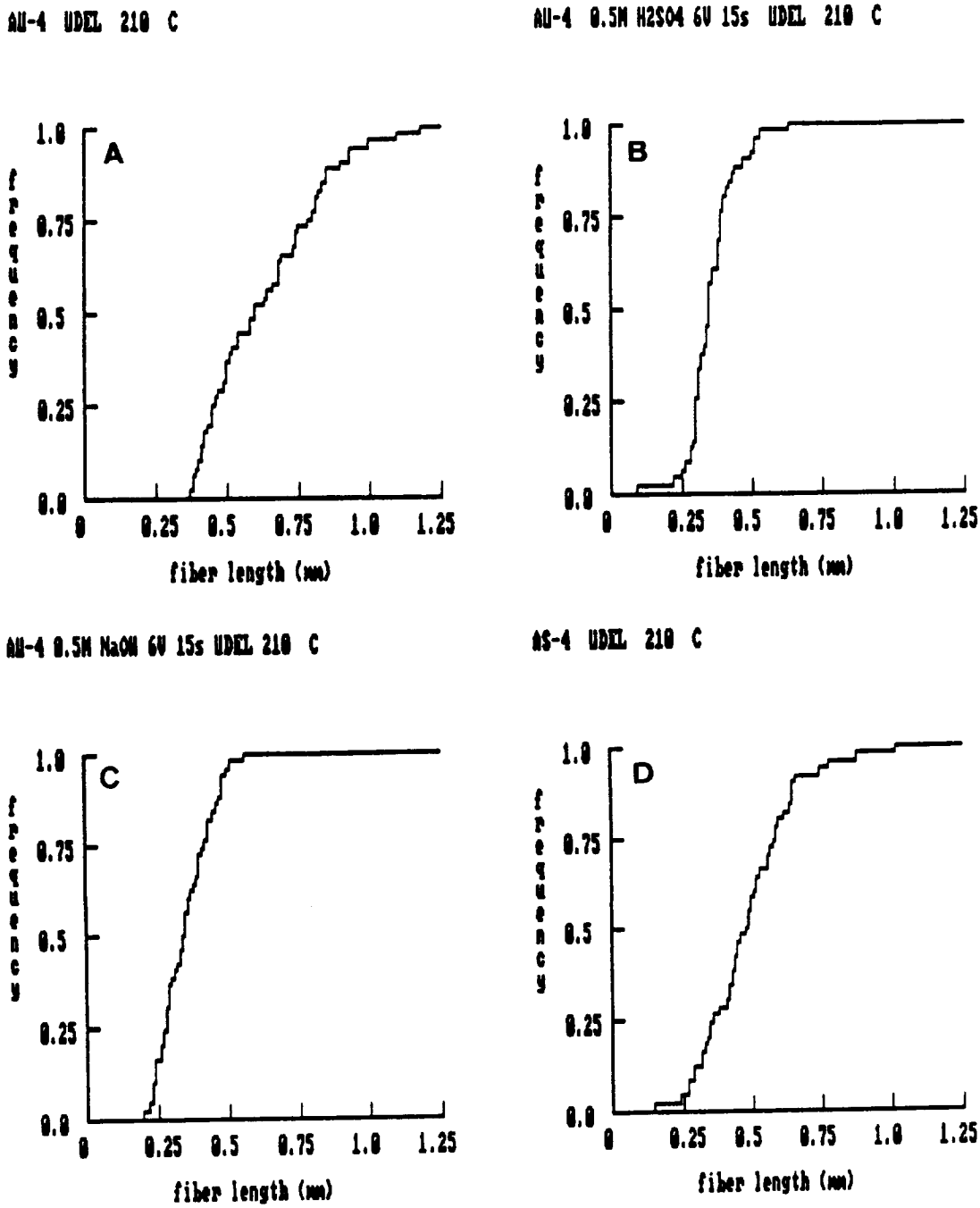

Figure 4.29 Cumulative frequency plots of fragment lengths in fiber critical length test of surface treated Hercules AU-4 fibers in polysulfone a) untreated fiber, b) H_2SO_4 anodized fiber, c) NaOH anodized fiber, and d) commercially treated fiber.

Table 4.19 Fiber critical lengths (FCL) of surface treated fibers embedded in polysulfone (PS), polycarbonate (PC), and polyetherimide (PEI).

Fiber	Polymer					
	PS		PC		PEI	
	FCL (mm)	SD (mm)	FCL (mm)	SD (mm)	FCL (mm)	SD (mm)
AU-4	0.63	0.20	0.71	0.22	0.68	0.18
AS-4	0.49	0.17	0.63	0.18	0.28	0.07
AU-4 H_2SO_4	0.36	0.09	0.36	0.09	0.18	0.04
AU-4 NaOH	0.35	0.09	0.40	0.11	0.26	0.07
XAU	0.39	0.11	0.39	0.13	0.24	0.06
XAS	0.38	0.10	0.29	0.07	0.25	0.08
XAU H_2SO_4	0.36	0.10	0.37	0.10	0.24	0.07
XAU NaOH	0.42	0.12	0.35	0.10	0.23	0.08
T-300U	0.58	0.16	0.64	0.18	0.70	0.20
T-300S	0.33	0.09	0.33	0.08	0.22	0.07
T-300U H_2SO_4	0.37	0.10	0.40	0.10	0.26	0.06
T-300U NaOH	0.61	0.20	0.47	0.27	0.34	0.17

NaOH - 0.5M NaOH / 6V / 15s
H_2SO_4 - 0.5M H_2SO_4 / 6V / 15s

Table 4.20 Interfacial stress transfer coefficients (ISTC) for fibers embedded in polysulfone (PS), polycarbonate (PC), and polyetherimide (PEI)

Fiber	Treatment	ISTC		
		PS (MPa)	PC (MPa)	PEI (MPa)
AU-4		7.1	6.4	5.4
AS-4		11.5	9.1	19.6
AU-4	0.5M H_2SO_4 6V 15s	13.7	13.7	27.1
AU-4	0.5M NaOH 6V 15s	14.8	13.9	19.6
XAU		9.6	9.7	15.4
XAS		8.9	11.9	13.6
XAU	0.5M H_2SO_4 6V 15s	13.0	12.7	19.7
XAU	0.5M NaOH 6V 15s	9.5	11.4	17.3
T-300U		6.6	5.9	5.4
T-300S		12.0	11.9	17.4
T-300U	0.5M H_2SO_4 6V 15s	9.9	9.3	14.2
T-300U	0.5M NaOH 6V 15s	6.9	9.1	12.5

In general, the untreated fiber gives a very low value for the ISTC. The H_2SO_4 anodized fiber gives a higher ISTC than the NaOH anodized fiber. The commercially treated fibers have a lower ISTC than the laboratory treated fibers for both the Hercules and Dexter Hysol fibers. The commercially treated Union Carbide fibers gives a higher ISTC than the laboratory treated fibers. The low ISTC for the laboratory treated Union Carbide fibers was expected since a low oxygen content was observed by XPS on the surface of these fibers after treatment.

4.5.3 Photoelastic Stress Transfer Observation

One of the problems with the fiber critical length adhesion test is that the breaking strength of the fiber is used to calculate the interfacial stress transfer. This calculation assumes the fiber strength at the length of the broken fragment. Typical fragment lengths are about 0.5 mm. Measurement of fiber breaking strength at these short lengths is very tedious. Therefore, the strength of the fiber at some reasonable length (in this case 6 mm) has been used for the interfacial stress transfer calculation. The exact breaking strength at the shorter lengths may be much different than at 6 mm. Rich and Drzal (92) have actually measured the breaking strengths at these short lengths. However, this measurement is tedious and requires special

equipment. Therefore, a better test for fiber matrix adhesion is needed.

It is also possible to qualitatively observe the stress transfer by observing breaks in a fiber embedded in a polymeric dogbone under stress. The fibers breaks must be observed under a microscope equipped with crossed polarizers. As stress is transferred from the tip of the broken fiber to the matrix, a birefringence pattern can be observed. The shape of the pattern will be indicative of the stress being transferred. Birefringence patterns were thus observed to verify the calculated stress transfer coefficients.

Photographs of the stress birefringence occurring at a fiber break in the dogbone shaped single fiber specimen are shown in Figures 4.30-4.33. There are three modes of stress transfer between fiber and matrix which can be observed in these figures. These modes which are shown schematically in Figure 2.15 are shear stress transfer, frictional forces, and fiber matrix debonding.

A summary of the stress transfer modes between fiber and matrix are shown in Table 4.21. The surface treated fibers have more failure by shear stress transfer. The untreated fibers have more failure by debonding. Better control of sample strain is needed to obtain more conclusive information from this test.

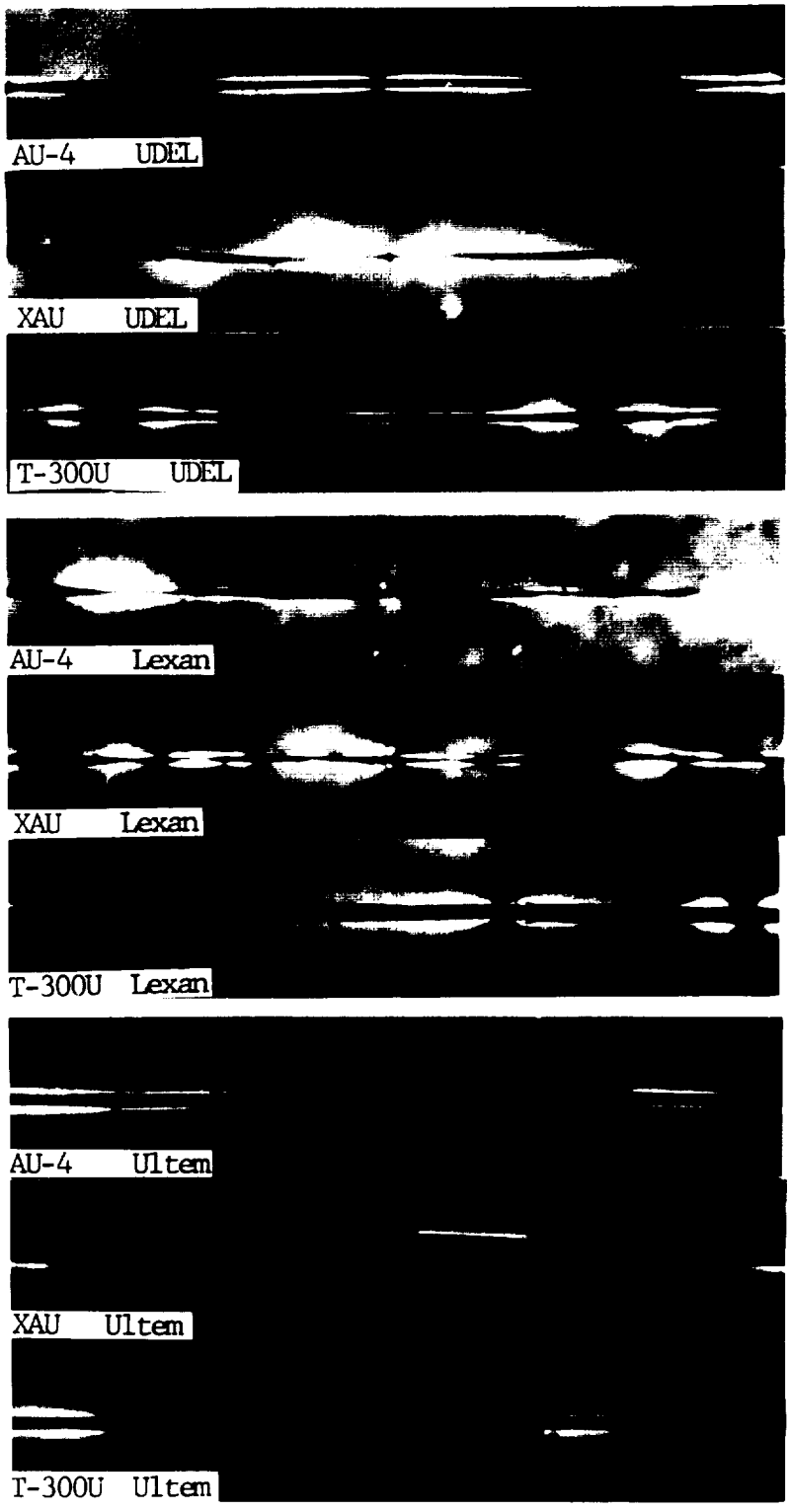

Figure 4.30 Optical photomicrographs of fiber break obtained from a single fiber embedded in a thermoplastic and pulled in tension for untreated fibers.

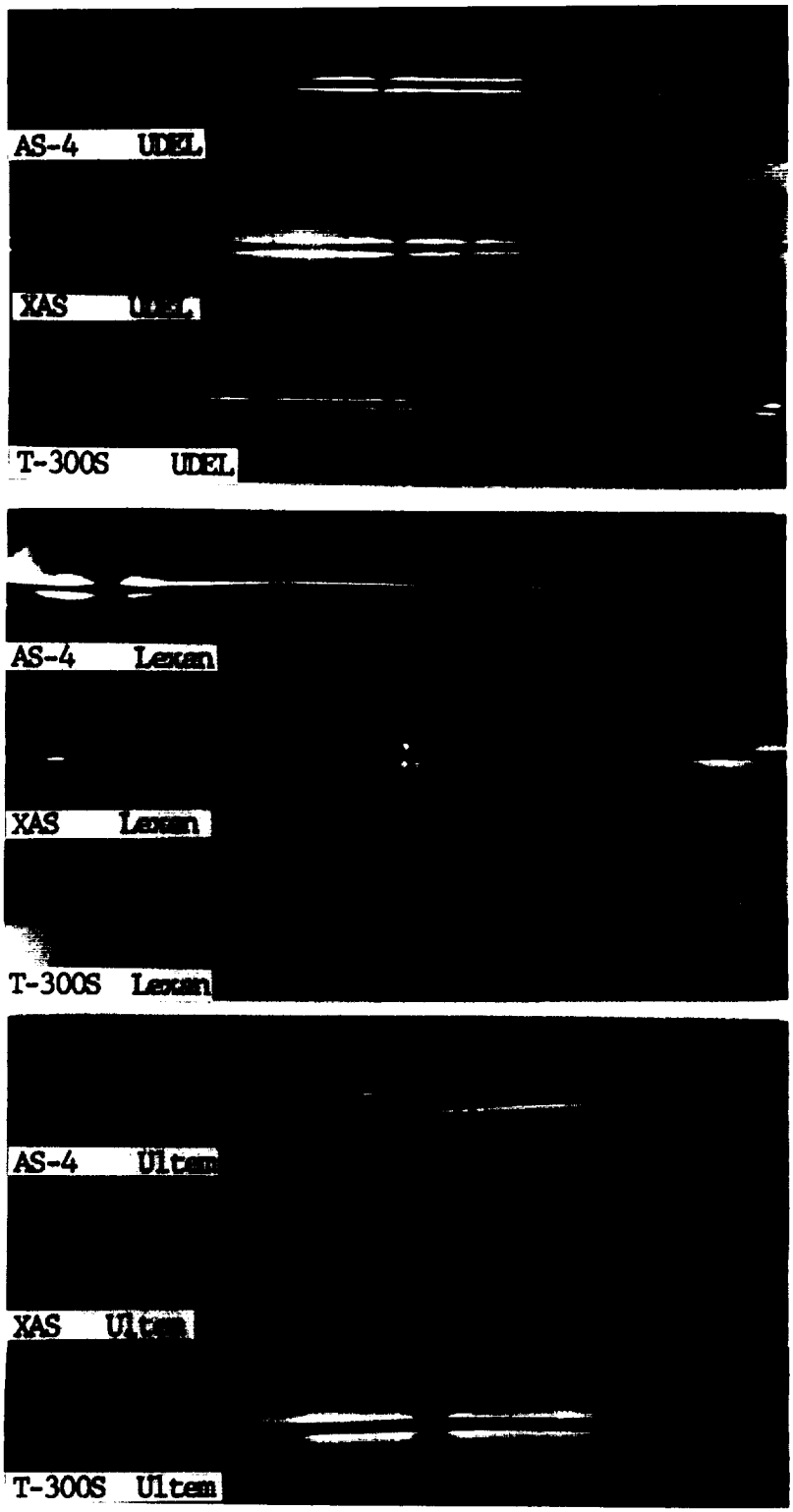

Figure 4.31 Optical photomicrographs of fiber break obtained from a single fiber embedded in a thermoplastic and pulled in tension for commercially treated fibers.

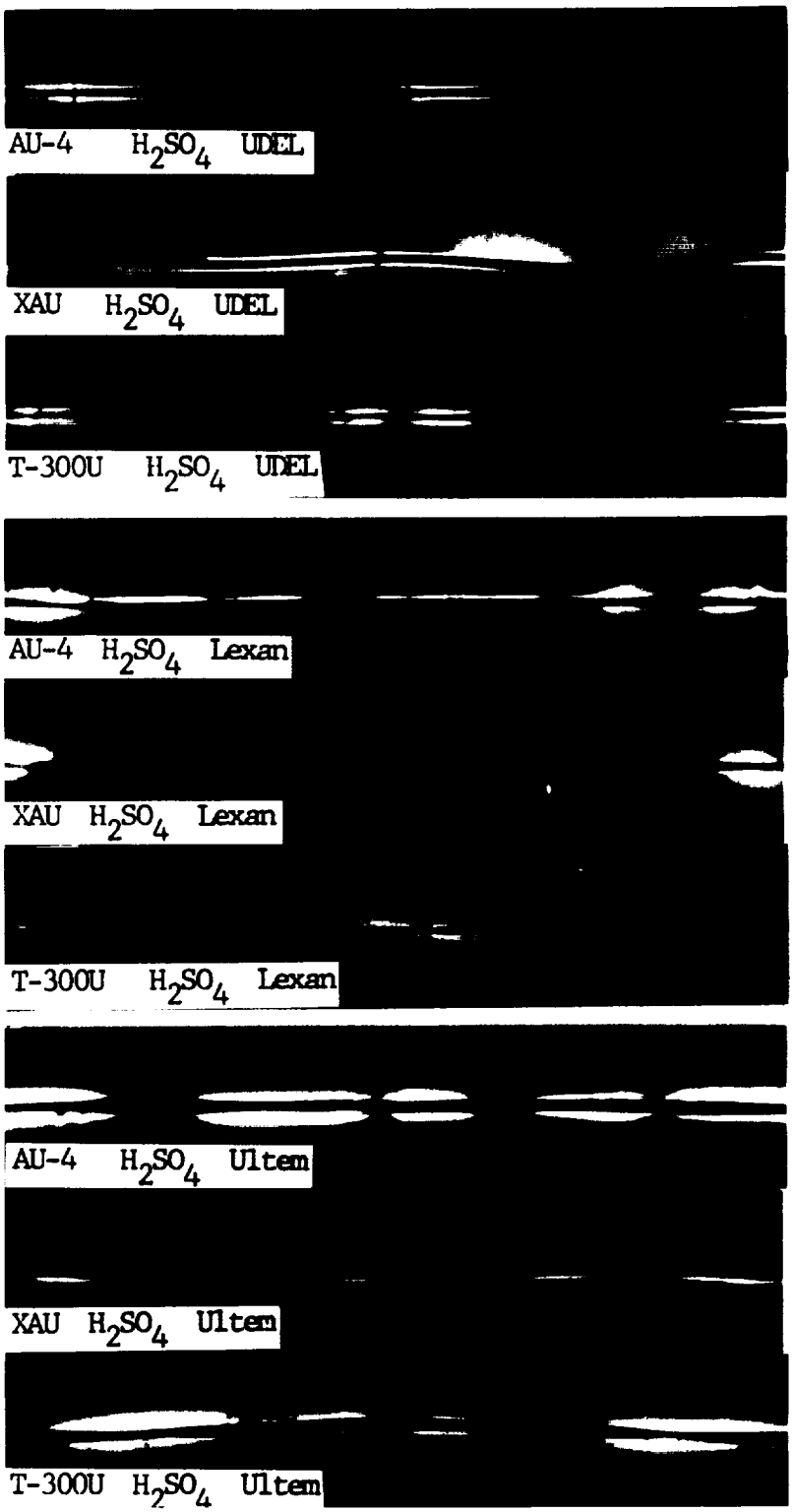

Figure 4.32 Optical photomicrographs of fiber break obtained from a single fiber embedded in a thermoplastic and pulled in tension for H_2SO_4 anodized fibers.

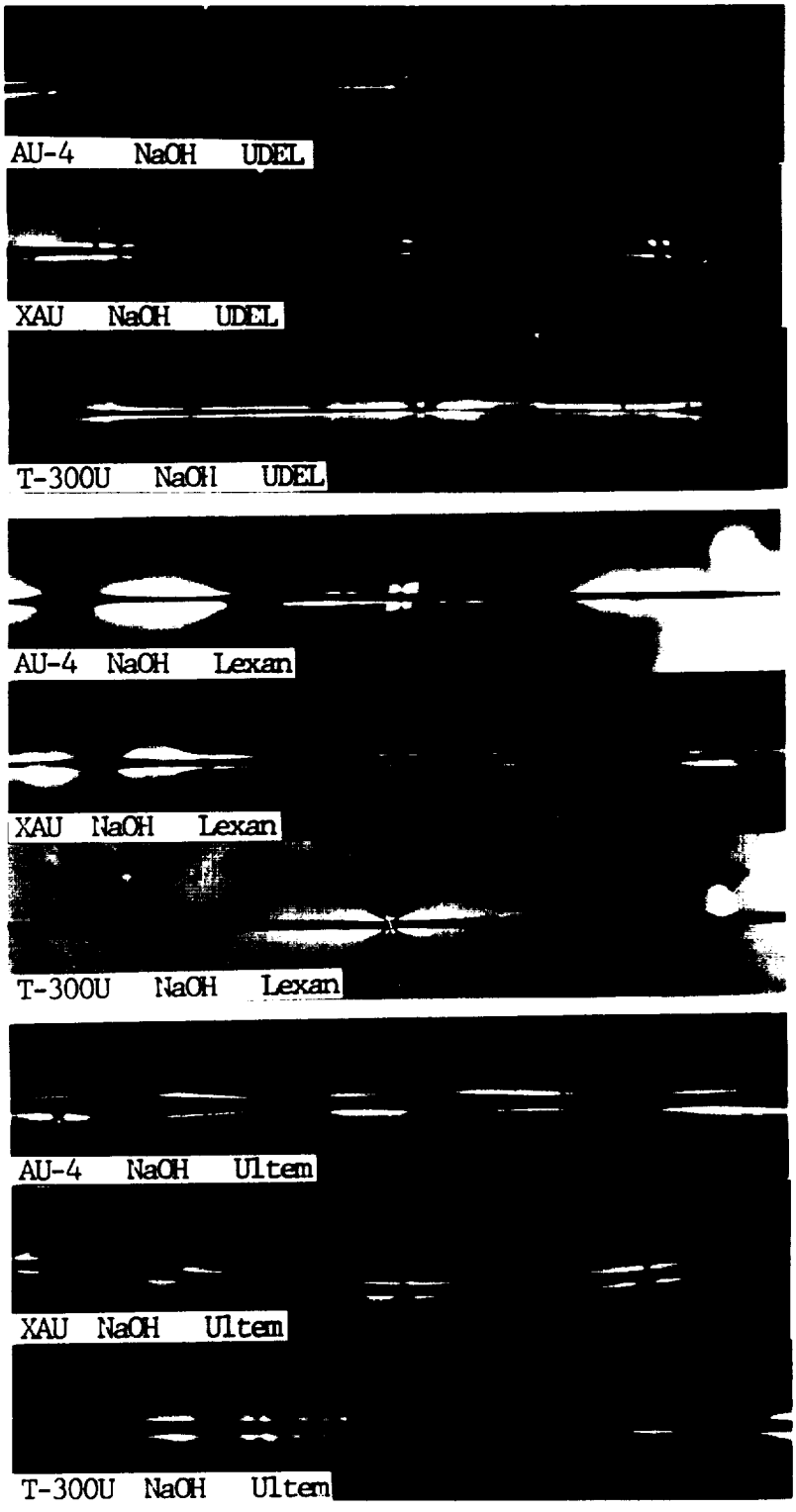

Figure 4.33 Optical photomicrographs of fiber break obtained from a single fiber embedded in a thermoplastic and pulled in tension for NaOH anodized fibers.

Table 4.21 Modes of failure of fiber/matrix interface as observed under crossed polarizers in the fiber critical length experiment.

Fiber	Treatment	Stress Transfer Mode		
		Poly-sulfone	Poly-carbonate	Poly-ether imide
AU-4		F	D	D
AS-4		F	F	F
AU-4	0.5M H_2SO_4 6V 15s	S,F	M	S,F
AU-4	0.5M NaOH 6V 15s	F	M	F
XAU		S,F	S,F	F
XAS		S	M	D,F
XAU	0.5M H_2SO_4 6V 15s	S,F	D	F,D
XAU	0.5M NaOH 6V 15s	S,F	F,D	F,D
T-300U		D,F	S	D
T-300S		F	F,S	F,D
T-300U	0.5M H_2SO_4 6V 15s	F	S	F,D
T-300U	0.5M NaOH 6V 15s	F,S	S	D,F

S - shear bands indicating good adhesion.
F - frictional stress transfer indicating weak interfacial bonding.
D - fiber matrix interfacial debonding
M - mixed mode failure (combination of all three modes)

4.5.4 Work of Adhesion

The work of adhesion between fiber and matrix was determined using equation 2.6. The polar and dispersive component for the fiber surface energies listed in Table 4.14 were used. For polysulfone, the polar and dispersive components were estimated to be 3.6 ergs/cm^2 and 26.1 ergs/cm^2 respectively (51). For polycarbonate, the polar and dispersive components were estimated to be 2.6 ergs/cm^2 and 38.7 ergs/cm^2 respectively (119).

The work of adhesion between the surface treated fibers and polysulfone is listed in Table 4.22. This table lists the work due to dispersive forces, polar forces, and the total work of adhesion (sum of polar and dispersive). The percentage of the total work due to polar force contribution is also listed in the last column. The work of adhesion between the surface treated fibers and polycarbonate is listed in Table 4.23.

The work of adhesion due to polar groups for both polymers was only 12-26% of the total work of adhesion. The remaining work was due to dispersive force interactions. This is due to the fact that the thermoplastic polymers used in this study were of low polarity.

Table 4.22 Work of adhesion for surface treated fibers in polysulfone

Fiber	Treatment	W_a^P (erg/cm²)	W_a^d (erg/cm²)	W_a^T (erg/cm²)	percent polar
AU-4		27.1	8.1	35.2	23.0
AS-4		27.7	8.9	36.6	24.3
AU-4	0.5M H_2SO_4 6V 15s	30.5	8.4	38.9	21.7
AU-4	0.5M NaOH 6V 15s	30.8	7.7	38.5	20.1
XAU		29.5	9.1	38.6	23.7
XAS		28.5	10.0	38.5	25.9
XAU	0.5M H_2SO_4 6V 15s	31.7	7.1	38.8	18.3
XAU	0.5M NaOH 6V 15s	29.3	9.4	38.7	24.3
T-300U		29.4	5.8	35.2	16.6
T-300S		30.6	6.3	36.9	17.1
T-300U	0.5M H_2SO_4 6V 15s	30.2	6.6	36.8	17.9
T-300U	0.5M NaOH 6V 15s	29.3	9.3	38.6	24.2

Table 4.23 Work of adhesion for surface treated fibers in polycarbonate

Fiber	Treatment	W_a^p (erg/cm²)	W_a^d (erg/cm²)	W_a^T (erg/cm²)	per-cent polar
AU-4		32.9	6.9	39.8	17.3
AS-4		33.7	7.5	41.2	18.3
AU-4	0.5M H_2SO_4 6V 15s	37.0	7.2	44.2	16.2
AU-4	0.5M NaOH 6V 15s	37.5	6.6	44.1	14.9
XAU		35.8	7.8	43.6	17.8
XAS		34.7	8.5	43.2	19.6
XAU	0.5M H_2SO_4 6V 15s	38.7	6.0	44.7	13.5
XAU	0.5M NaOH 6V 15s	35.7	8.0	43.7	18.3
T-300U		36.0	4.7	40.7	11.5
T-300S		37.2	5.4	42.6	12.6
T-300U	0.5M H_2SO_4 6V 15s	36.8	5.6	42.4	13.2
T-300U	0.5M NaOH 6V 15s	35.7	7.9	43.6	18.2

C-3

The work of adhesion is plotted against the interfacial stress transfer coefficient (ISTC) in Figure 4.34. This figure includes 9 plots. The Hercules fibers are shown in Figures 4.34 a-c; the Dexter Hysol fibers are shown in Figures 4.34 d-f; the Union Carbide fibers are shown in Figures 4.34 g-i. The open symbols indicate the values for UDEL. The closed symbols indicate the values for Lexan. The first figure in each series shows the dependence of the ISTC on the dispersive forces. The second figure shows the dependence of the ISTC on the polar forces. The third figure in each series show the dependence of ISTC on the total work of adhesion.

With the exception of the Hercules fibers, there is no correlation between the total work of adhesion and the interfacial stress. There is even less correlation between the polar force contribution and the interfacial stress. However, there does appear to be a correlation between the dispersive force contribution to the work of adhesion and the interfacial stress.

It is expected that the dispersive component contribution to the surface energy of the fiber is dependent on conduction electrons in the graphitic carbon on the fiber surface. Therefore, a dependence of the fiber-matrix adhesion on the graphitic structure of the fiber surface is reasonable.

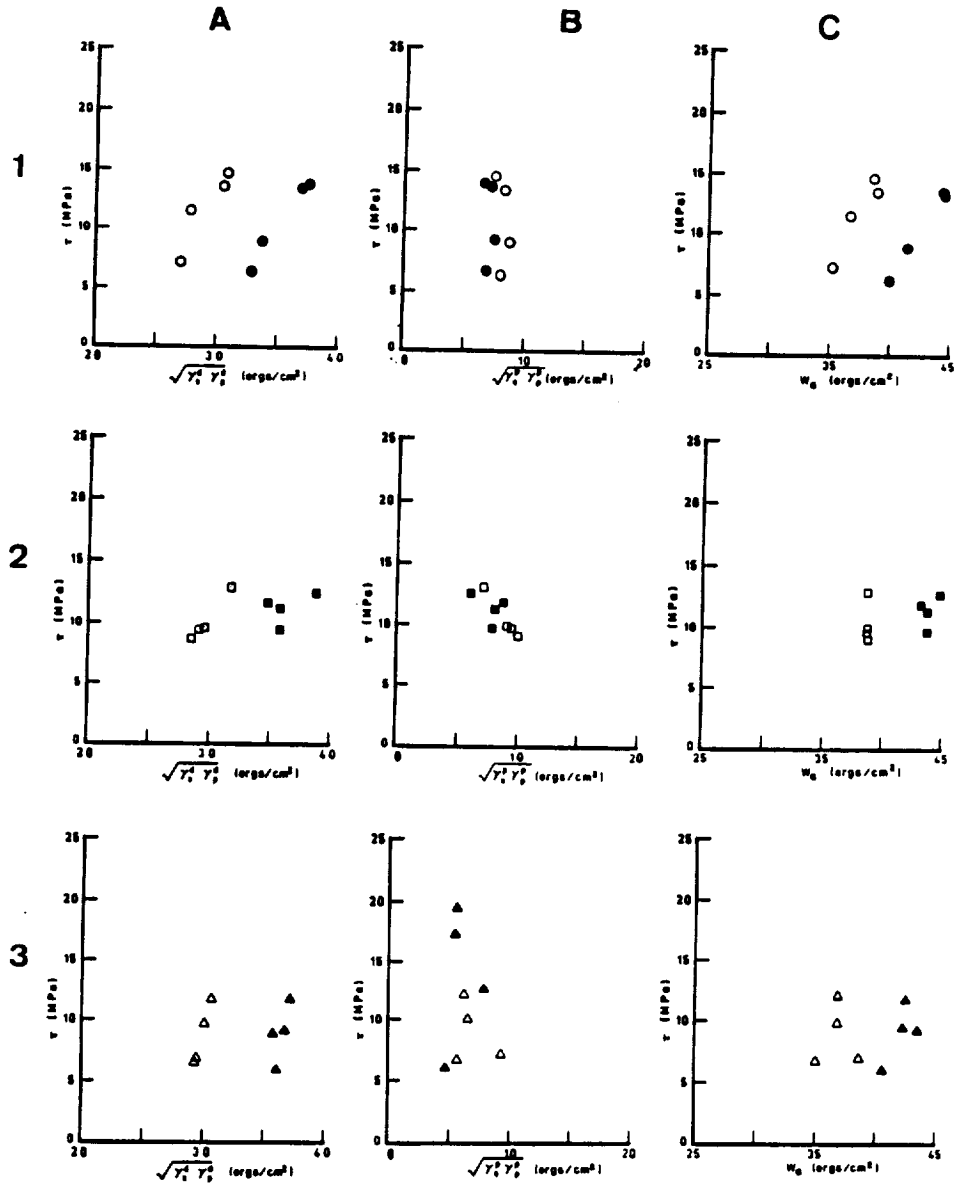

Figure 4.34 Work of adhesion due to a) dispersion forces, b) polar groups, and c) total surface energy versus interfacial stress transfer coefficient for 1) Hercules A fibers, 2) Dexter Hysol XA fibers, and 3) Union Carbide T-300 fibers
○□△ polysulfone
●■▲ polycarbonate

5) SUMMARY

This study set out to observe the effect of surface treatment on the physical properties of carbon fiber surfaces and the adhesion of thermoplastic polymers to surface treated carbon fibers. It was intended that once we understood how the surfaces of carbon fibers can be altered, then it might be possible to improve or control interfacial interactions of carbon fibers with polymeric matrices.

Hercules AS-4 carbon fibers were surface treated by anodization in acidic and basic solutions as well as in aqueous solutions of amine salts. Anodization in amine salts created oxygen as well as nitrogen functionality. Anodization in acidic and basic environments yielded mostly oxygen functionality. The carbon 1s plasmon peak intensity observed by x-ray photoelectron spectroscopy (XPS) is reduced after H_2SO_4 anodization and boiling in nitric acid. This indicates that anodization in acid environments disrupts the graphitic structure of the carbon fiber. Anodization in basic solutions enhanced the plasmon peak. This enhancement is most likely due to removal of amorphous carbon from the carbon fiber during anodization. Further evidence for the removal of amorphous carbon during anodization in basic solutions came from observation of the anodization bath with ultraviolet absorption spectroscopy,

and the low intensity of ejected ions during fast atom bombardment of the NaOH anodized fiber surface.

The surfaces of commercial fibers from several producers were examined by scanning transmission electron microscopy (STEM), XPS, surface energy measurement, and breaking strength, before and after commercial surface treatment. Hercules AS-4, Dexter Hysol XAS, and Union Carbide T-300 fibers were examined. Nitrogen as well as oxygen functionality was seen to be present on the surface of the AS-4 and XAS fibers. Examination of the AS-4 surface by derivatization indicates that the nitrogen functionality may be in the form of amine groups. Oxygen appeared to be the predominant functionality present on the T-300S carbon fiber surfaces. Angular dependent XPS studies indicate that the oxygen present on the AS-4 and XAS fibers is predominant on the fiber surface. The oxygen on the T-300 fiber appeared to be present below the fiber surface, possibly between the graphitic layers. Observation of the carbon 1s plasmon peak intensity for the fibers from the three producers before and after commercial surface treatment indicates that the Hercules surface treatment does not affect the structure of the AS-4 fiber. The Dexter Hysol surface treatment enhances the plasmon peak intensity. The Union Carbide surface treatment almost completely disrupts the plasmon excitation.

An attempt was made to create similar chemistry on the surfaces of the carbon fibers from several producers. Untreated fibers from Hercules, Dexter Hysol, and Union Carbide were anodized in 0.5 M H_2SO_4 and 0.5 M NaOH at 6 V for 15 seconds. STEM observation of the fiber surfaces before and after treatment indicated no change in surface topography. XPS examination indicated that the Hercules AS-4 and Dexter Hysol XAS had the same oxygen and nitrogen content after surface treatment. However, the carbon 1s peak for the XAS fiber differed in appearance from the Union Carbide or the Hercules fibers. The Union Carbide T-300 fiber reacted much differently to the surface treatment. The oxygen content on the T-300 fiber surface was much lower than the AS-4 or XAS fiber surfaces after treatment. Surface energy analysis of the fiber surfaces before and after treatment did not lead to conclusive evidence about the carbon fiber structure.

Measurement of the fiber breaking strength at several gauge lengths before and after surface treatment was performed. The strength of the T-300 and AS-4 fibers was dependent on length. The strength of the XAS fiber was almost independent of length. The length dependence of the breaking strengths of the AS-4 and XAS fibers was increased by anodization in H_2SO_4 and NaOH indicating that surface flaws were removed by anodization. The length dependence of

the breaking strengths of the T-300 fibers was greatly reduced by anodization, indicating that many flaws were created on the fiber surface during anodization.

Adhesion of the carbon fibers before and after surface treatment to the thermoplastic matrices polysulfone, polycarbonate, and polyetherimide was studied using the fiber critical length test. The interfacial stress transfer between fiber and matrix was dependent on the temperature at which the bond was formed. This temperature dependence indicates that molecular rearrangement is occurring during bond formation. The untreated fibers had poorer adhesion to thermoplastic than the surface treated fibers. For the Hercules AS-4 and Dexter Hysol XAS fibers, laboratory anodization yielded a higher interfacial stress transfer coefficient (ISTC) than the commercially treated fibers. The commercially treated Union Carbide T-300 fibers had a higher ISTC than the laboratory anodized fibers.

The work of adhesion was calculated from measured values of the polar and dispersive components of the surface energy of the fibers using a geometric mean relationship. There was little correlation between the total work of adhesion and the ISTC. However, there appeared to be a correlation between the work of adhesion due to dispersion forces and the ISTC.

6) REFERENCES

1. Reisch M.S. "High-Performance Fibers Find Expanding Military, Industrial Uses" Chem. Eng. News. Feb. 2, (1987), pp. 9-14

2. Delmonte J. Technology of Carbon and Graphite Fiber Composites New York: Van Nostrand (1981)

3. Diamont J. and Moulton R.J. "Developement of Resins for Damage Tolerant Composites-A Systematic Approach" SAMPE Quat. Oct. (1984), pp. 13-21

4. DiSalvo G.D.M. and Lee S.M. "Fracture Tough Composites-The Effect of Toughened Matrices on the Mechanical Performance of Carbon Fiber Reinforced Laminates" SAMPE Quat. Jan. (1983), pp. 14-17

5. Brandt J. and Warnecke J. "Influence of Material Parameters on the Impact Performance of Carbon Fibre Reinforced Polymers" in High Tech-the Way into the Nineties edited by Brunsch K., Gölden, and Herkert C.M.: Amsterdam: Elsevier (1986), pp. 251-260

6. Yee A.F. and Pearson R.A. "Toughening Mechanisms in Elastomer-Modified Epoxies Part 1: Mechanical Studies" J. Mat. Sci. Vol. 21 (1986), pp. 2462-2474

7. Yee A.F. and Pearson R.A. "Toughening Mechanisms in Elastomer-Modified Epoxies Part 2: Microscopy Studies" J. Mat. Sci., Vol. 21 (1986), pp. 2475-2488

8. Willats D.J. "Advances in the Use of High Performance Continuous Fibre Reinforced Thermoplastics" SAMPE J. Sept./Oct. (1984), pp. 6-10

9. Kardos J.L. "Regulating the Interface in Graphite/Thermoplastic Composites" J. Adhesion, Vol. 5 (1973), pp. 119-138

10. Johnson T.W. and Ryan C.L. "Crystallization in Polyphenylene Sulfide-Carbon Fiber Composites" Int. SAMPE Symp. Exhib., Vol. 31 (1986), pp. 1537-1548

11. Hunston D.L. "Composite Interlaminar Fracture: Effects of Matrix Fracture Energy" Comp. Tech. Rev., Vol. 6 Winter (1984), pp. 176-180

12. Williams J.H. and Kousiounelos P.N., "Thermoplastic Fibre Coatings Enhance Composite Strength and Toughness" Fibre Sci. Tech., Vol. 11 (1978), pp. 83-88

13. Subramanian R.V., Sundram V., and Patel A.K. "Electrodeposition of Polymers on Graphite Fibers: Effects on Composite Properties" In Proc. 33rd. Annual Tech. Conf. SPI Reinforced plast./Comp. Inst. 20F (1978), pp. 1-8

14. Subramanian R.V., Jakubowski J.J., and Williams F.D. "Interfacial Aspects of Polymer Coating by Electropolymerization" J. Adhesion, Vol. 9 (1978), pp. 185-195

15. Ying L. "Role of Fiber/Matrix Interphase in Carbon Fiber-Epoxy Composite Impact Toughness" SAMPE Quat. April (1983), pp. 26-33

16. Lehmann S., Megerdigian C., and Papalia R. "Carbon Fiber Resin Matrix Interphase: Effect of Carbon Fiber Surface Treatment on Composite Performance" SAMPE Quat. April (1985), pp. 7-13

17. Robinson R., Lehmann S., Askew G., Wilford D., Megerdigian C., and Papalia R. "A Preliminary Assessment of the Role of Fibre Surface Properties in Controlling Composite Performance" in High Tech-the Way into the Nineties edited by Brunsch K., Gölden H.D., and Herkert C.M., Amsterdam: Elsevier (1986), pp. 299-310

18. Sharpe L.H., "The Theory of Adhesion", The Adhesion Society, short course notes Feb. 23, (1985)

19. Huntsberger J.R. "The Mechanisms of Adhesion" In Treatise on Adhesion and Adhesives Volume 1 edited by R.L Patrick, New York, (1967), pp. 119-149

20. Huntsberger J.R., "Mechanisms of Adhesion", J. Paint Tech., Vol. 39 No. 507 (1967), pp. 199-211

21. Kittel C. Introduction to Solid State Physics 5th ed. Wiley, New York (1976)

22. Good R.J. "Intermolecular and Interatomic Forces" in Treatise on Adhesion and Adhesives Vol. 1 edited by R.L. Patrick, New York: Marcel Dekker (1967), pp. 9-68

23. Atkins P.W. Physical Chemistry 3rd. ed. Freeman, New York (1986)

24. Wake W.C. Adhesion and the Formulation of Adhesives 2nd. Edition London: Applied Sciences (1982)

25. Donnet J.B. and Bansal R.C. Carbons Fibers. New York: Marcel Dekker 1984

26. Diefendorf R.J., Stevens W.C., and Chen S.H. "Carbon Fibers" Fiber Producer Dec. (1979), pp. 16-

27. Diefendorf R.J. and Tokarsky E. "High-Performance Carbon Fibers" Polym. Eng. and Sci., Vol. 15(1975), pp. 150-159

28. Watt W. "Chemistry and Physics of the Conversion of Polyacrylonitrile Fibres into High-Modulus Carbon Fibres" in Strong Fibers edited by Watt W. and Perov B.V., Elsevier, Amsterdam, (1985), pp.

29. Goodhew P.J., Clarke A.J., and Bailey J.E. "A Review of the Fabrication and Properties of Carbon Fibers" Mat. Sci. Eng., Vol. 17 (1975), pp. 3-30

30. Coleman M.M. and Sivy G.T. "Fourier Transform IR Studies of the Degradation of Polyacrylonitrile Copolymers-I" Carbon, Vol. 19 (1981), pp. 123-126

31. Coleman M.M. and Petcavich R.J. "Fourier Transform Infrared Studies on the Thermal Degradation of Polyacrylonitrile" J. Polym. Sci. Polym. Phys. Ed., Vol. 16 (1978), pp. 821-832

32. Bacon R. "Newer Carbon Fibers and Their Properties" In Tough Composite Materials edited by Vosteen L.F., Johnston N.J., and Teichman L.A. NASA CP-2334 (1983)

33. Bokros J.C. "Deposition, Structure, and Properties of Pyrolytic Carbon" in Chemistry and Physics of Carbon Vol. 5 edited by Walker P.L., Marcel Dekker, New York (1969), pp. 1-118

34. Perret R. and Ruland W. "The Microstructure of PAN Based Carbon Fibres" J. Appl. Cryst., Vol. 3 (1970), pp. 525-532

35. Guigon M., Oberlin A., and Desarmot G. "Microtexture and Structure of Some High Tensile Strength, PAN Base

Carbon Fibers" Fibre Sci. Tech., Vol. 20 (1984), pp. 55-72

36. Drzal L.T. "Surface Composition and Energetics of Type A Graphite Fibers" Carbon, Vol. 15 (1977), pp. 129-138

37. Johnson W. "The Structure of PAN Based Carbon Fibres and Their Relationship to Physical Properties" in Strong Fibers edited by Watt W. and Perov B.V., Elsevier, Amsterdam (1985), pp. 389-443

38. Bennet S.C. Strength Structure Relationships in Carbon Fibres, PhD. Thesis, University of Leeds (1976), reported by reference (37)

39. Diefendorf R.J. "The Chemical Nature of the Fiber/Resin Interface in Composite Materials" In Tough Composite Materials edited by Vosteen L.F., Johnston N.J., and Teichman L.A. NASA CP-2334 (1983), pp. 209-225

40. Bahl O.P., Mathur R.B., and Dhami T.L. "Effects of Surface Treatment on the Mechanical Properties of Carbon Fibers" Polym. Eng. Sci., Vol. 24 (1984), pp. 455-459

41. Fitzer E. and Weiss R. "Influence of Various Polar Surface Oxides on the Reinforcement Behaviour of C-Fibres in C-Fibre Reinforced Epoxy Composites" In Extended Abstacts and Program 16th Biennial Conf. Carbon July 18-22 (1983), pp. 473-475

42. Paul J.T. "Electrolytic Treatment of Graphite Fibers" British Patent Specification 1,433,712 (1976)

43. Saito K., Ogawa H., and Shigei T. "Surface Treatment of Carbon Fiber" United States Patent 4,401,533 (1983)

44. Gynn G., King R.N., Chappell S.F., and Deviney M.L. "Improved Graphite Fiber Adhesion" AFWAL-TR-81-4096

45. Pinchin D.J. and Woodhams R.T. "Pyrolytic Surface Treatment of Graphite Fibres" J. Mat. Sci., Vol. 9 (1974), pp. 300-306

46. Brewis D.M., Comyn J., Fowler J.R., Briggs D., and Gibson V.A. "Surface Treatments of Carbon Fibres Studied by X-Ray Photoelectron Spectroscopy" Fibre Sci. Tech, Vol. 12 (1979), pp. 41-52

47. Goan J.C., Joo L.A., and Sharpe G.E. "Surface Treatment for Graphite Fibers" 27th Ann. Tech. Conf. RP/Comp. Ind. SPI 21E (1972), pp. 1-6

48. Ehrburger P. and Donnet J.B. "Surface Treatment of Carbon Fibres for Resin Matrices" in Strong Fibers edited by Watt W. and Perov B.V., Elsevier, Amsterdam, (1985), pp. 577-603

49. Drzal L.T., Rich M.J., Koenig M.F., and Lloyd P.F., "Adhesion of Graphite Fibers to Epoxy Matrices: II. The Effect of Fiber Finish" J. Adhesion, Vol. 16 (1983), pp. 133-152

50. Bateup B.O. "Surface Chemistry and Adhesion" Int. J. Adhesion and Adhesives (1981), pp. 233-239

51. Webster H.F. Characterization of Thin Silicone Films Formed by Migration Across Defined Polymer Substrates M.S. Thesis, Virginia Tech, Blacksburg, Va. (1985)

52. Girifalco L.A. and Good R.J. "A Theory for the Estimation of Surface and Interfacial Energies I. Derivation and Application" J. Phys. Chem., Vol. 61 (1957), pp. 904-909

53. Fowkes F.M. "Attractive Forces at Interfaces" Ind. Eng. Chem., Vol. 56 (1964), pp. 40-52

54. Fowkes F.M. "Acid Base Interactions in Polymer Adhesion" in Physicochemical Aspects of Polymer Surfaces Vol. 2 edited by K.L. Mittal. New York: Plenum (1983), pp. 583-603

55. Kaelble D.H., Dynes P.J., and Cirlin E.H. "Interfacial Bonding and Environmental Stability of Polymer Matrix Composites" J. Adhesion, Vol. 6 (1974), pp. 23-48

56. Kaelble D.H., Dynes P.J., and Maus L. "Surface Energy Analysis of Treated Graphite Fibers" J. Adhesion, Vol. 6 (1974), pp. 239-258

57. Jones W.C. and Porter M.C. "A Method for Measuring Contact Angles on Fibers" J. Colloid Interface Sci., Vol. 24 (1967), pp. 1-3

58. Hammer G.E. and Drzal L.T. "Graphite Fiber Surface Analysis by X-Ray Photoelectron Spectrocopy and Polar-

Dispersive Free Energy Analysis" Appl. Surf. Sci., Vol. 4 (1980), pp. 340-355

59. Schultz J., Cazeneuve C., Shanahan M.E.R., and Donnet J.B. "Fibre Surface Energy Characterization" J. Adhesion, Vol. 12 (1981), pp. 221-231

60. Herb C.A., Buckner J.L., and Overton J.R. "The Effect of Cross-Sectional Geometry on the Accuracy of the Fiber Wetting Balance" J. Colloid Interface Sci., Vol. 94 (1983), pp. 14-24

61. Brooks C.S. and Scola D.A. "An Examination of the Surface Reactivity of Graphite Fibers by Gas Solid Chromatography", J. Colloid Interface Sci., Vol. 32 (1970), pp. 561-569

62. Larsen J.V., Smith T.G., and Erickson P.W. "Carbon Fiber Surface Treatments" NOLTR 71-165 (1971)

63. Schultz J., Lavielle L., and Simon H. "Surface and Adhesion Properties of Carbon Fibres", Int. Symp. Sci. and New Appl. Carbon Fibers, Toyohashi Univ. Japan (1984), pp. 125-139

64. Gozdz A.S. and Weigmann H. D. "Surface Characterization of Intact Fibers by Inverse Gas Chromatography", J. Appl. Polym. Sci., Vol. 29 (1984), pp. 3965-3979

65. Rand B. and Robinson R. "A Preliminary Investigation of PAN Based Carbon Fibre Surfaces by Flow Microcalorimetry" Carbon, Vol. 15 (1977), pp. 311-315

66. Randin J.P. "Carbon" in Encyclopedia of Electrochemistry of the Elements edited by Bard A.J.: New York, Marcel Dekker (1976), pp. 1-291

67. Donnet J.B. "The Chemical Reactivity of Carbons" Carbon, Vol. 6 (1968) 161-176

68. Boehm H.P. "Functional Groups on the Surfaces of Solids" Angewandte Chemie, Vol. 5 (1966), pp. 533-544

69. Rivin D. "Surface Properties of Carbon" Rubber Chem. Tech., Vol. 44 (1971), pp. 307-343

70. Rivin D. "Use of Lithium Aluminum Hydride in the Study of Surface Chemistry of Carbon Black" Rubber Chem. Tech., Vol. 36 (1963), pp. 729-739

71. McKee D.W. and Mimeault V.J. "Surface Properties of Carbon Fibers" In Chemistry and Physics of Carbon Vol. 8, p. 151, edited by P.L. Walker and P.A. Thrower New York Marcel Dekker (1973), pp. 151-245

72. Riggs W.M. and Parker M.J. "Surface Analysis by X-Ray Photoelectron Spectroscopy" in Methods of Surface Analysis edited by Wolsky S.P. and Czanderna A.W., Elsevier, Amsterdam (1975), pp. 103-158

73. Fadley C.S. "Solid State and Surface Analysis by Means of Angular Dependent X-ray Photoelectron Spectroscopy" Prog. Solid State Chem., Vol. 11 (1976), pp. 265-343

74. Scofield J.H. "Hartree Slater Subshell Photoionization Cross-Sections at 1254 and 1487 eV" J. Electr. Spec. Related Phen., Vol. 8 (1976), pp. 129-137

75. Cadman P., Gossedge G., and Scott J.D. "The Determination of the Photoelectron Escape Depths in Polymers and Other Materials" J. Electron Spectroscopy Related Phen., Vol. 13 (1978), pp. 1-6

76. Wagner C.D. "Sensitivity Factors for XPS Analysis of Surface Atoms" J. Elect. Spect. Related Phen., Vol. 32 (1983), pp. 99-102

77. Clark D.T. and Harrison A. "ESCA Applied to Polymers. XXXI. A Theoretical Investigation of Molecular Core Binding and Relaxation Energies in a Series of Prototype Systems for Nitrogen and Oxygen Functionalities in Polymers" J. Polym. Sci. Polym. Sci. Ed., Vol. 19 (1981), pp. 1945-1955, (and previous articles)

78. Briggs D. and Seah M.P., Practical Surface Analysis, Wiley, New York, (1983)

79. Proctor A. and Sherwood P.M.A. "X-Ray Photoelectron Spectroscopic Studies of Carbon Fibre Surfaces. I. Carbon Fibre Spectra and the Effects of Heat Treatment" J. Electron Spect. and Related Phen., Vol. 27 (1982), pp. 39-56

80. Everhart D.S. and Reilley C.N. "Chemical Derivatization in Electron Spectroscopy for Chemical Analysis of Surface Functional Groups Introduced on Low Density

Polyethylene Film" Anal. Chem., Vol. 53 (1981), pp. 665-676

81. Briggs D. "Analysis of Polymer Surfaces by SIMS 2- Fingerprint Spectra from Simple Polymer Films" Surf. Interface Anal., Vol. 4 (1982), pp. 151-155

82. Briggs D. "SIMS for the Study of Polymer Surfaces: A Review" Surf. Interface Anal., Vol. 9 (1986), pp. 391-404

83. Brown A. and Vickerman J.C. "A Comparison of Positive and Negative Ion Static SIMS Spectra of Polymer Surfaces" Surf. Interface Anal., Vol. 8 (1986), pp. 75-81

84. Tsai S.W. and Hahn H.T. "Introduction to Composite Materials" Chap. 9., Westport, Conn.: Technomic (1980)

85. Weibull W. "A Statistical Distribution Function of Wide Applicability" J. Appl. Mech., Vol. 18 (1951), pp. 293-297

86. Hitchon J.W. and Phillips D.C. "The Dependence of the Strength of Carbon Fibres on Length" Fibre Sci. Tech., Vol. 12 (1979), pp. 217-233

87. Manders P.W. and Chou T.W. "Variability of Carbon and Glass Fibers, and the Strength of Aligned Composites" J. Reinforced Plastics and Composites", Vol. 2 (1983), pp. 43-59

88. Penn L., Bystry F., Karp W., and Lee S. "Aramid Epoxy vs. Graphite Epoxy: Origin of the Difference in Strength at the Interface" In Molecular Characterization of Composite Interfaces edited by H. Ishida and G. Kumar. New York: Plenum (1985), pp. 93-109

89. Miller B. and Tallent M.A. "Application of the Microbond Method to Studies of Adhesive Bonding in Fiber/Resin Systems" paper presented at the Ninth Annual Meeting of the Adhesion Society, Feb. 9-12, Hilton Head, S.C.

90. Bascom W.D. and Jensen R.M. "Stress Transfer in Single Fiber Resin Tensile Tests" J. Adhesion, Vol. 19 (1986), pp. 219-239

91. Ohsawa T., Nakayama A., Miwa M, and Hasegawa A. "Temperature Dependence of Critical Fiber Length for Glass Fiber Reinforced Thermosetting Resins" J. Appl. Polym. Sci., Vol. 22 (1978), pp. 3203-3212

92. Drzal L.T., Rich M.J., Camping J.D., and Park W.J. "Interfacial Shear Strength and Failure Mechanisms in Graphite Fiber Composites" In Proc. 35th Ann. Tech Conf. Reinf. Plastics/Composites Inst. SPI 20-C (1980), pp. 1-7

93. Rich M.J. and Drzal L.T. "Interfacial Properties of Some High Strain Carbon Fibers in an Epoxy Matrix" In Proc. 41st. Ann. Tech Conf. Reinf. Plastics/Composites Inst. SPI 2-F (1986), pp. 1-5

94. Whitney J.M. and Drzal L.T. "Three Dimensional Stress Distribution Around an Isolated Fiber Fragment" proc. ASTM conf. Tough Composites, in ASTM STP, submitted (1985)

95. Mullin J.V. and Mazzio V.F. "The Effects of Matrix and Interface Modification on Local Fractures of Carbon Fibers in Epoxy" J. Mech. Phys. Solids, Vol. 20 (1972), pp. 391-400

96. Mullin J., Berry J.M., and Gatti A. "Some Fundamental Fracture Mechanisms Applicable to Advanced Filament Reinforced Composites" J. Comp. Mat., Vol. 2 (1968), pp. 82-103

97. Ehrburger P. and Donnet J.B. "Interface in Composite Materials" Phil. Trans. R. Soc. Lond. A295 (1980), pp. 495-

98. Ehrburger P., Herque J.J., and Donnet J.B. "Interface Properties of Carbon Fiber Composites" In Proc. London Int. Carbon Graphite Conf. 5th meeting Soc. Chem. Ind., pp. London (1978), pp. 398-404

99. Lahaye J., Herque J.J., and Donnet J.B. "Electrochemical Treatment of Carbon and Graphite Fibers" In Lond. Int. Conf. Carbon Graphite 4th Meeting Soc Chem. Ind. London (1976), pp. 201-208

100. Fitzer E., Geigl K-H, HÜttner W. "Chemical Interactions Between the Carbon Fibre Surface and Epoxy Resins" Carbon, Vol. 18 (1980), pp. 389-393

101. Drzal L.T. "Composite Interphase Characterization" SAMPE J. Sept/Oct. (1983), pp. 7-13

102. Drzal L.T., Rich M.J., and Lloyd P.F. "Adhesion of Graphite Fibers to Epoxy Matrices: I. Role of Fiber Surface Treatment" J. Adhesion, Vol. 16 (1982), pp. 1-30

103. Tuinstra F. and Koenig J.L. "Raman Spectrum of Graphite", J. Chem. Phys., Vol. 53 3 (1970), pp. 1126-1130

104. Tuinstra F. and Koenig J.L. "Characterization of Graphite Fiber Surfaces with Raman Spectroscopy" J. Comp. Mat., Vol. 4 (1970), pp. 492-499

105. Ishitani A., Ishida H., Katagiri G., and Tomita S. "New Techniques for Characterization of Surfaces and Interfaces of Carbon Fibers" In Composite Interfaces edited by Ishida H. and Koenig J.L.. New York: North Holland (1986), pp. 195-202

106. Brelant S. "The Interaction of Carbonaceous Fibers with Organic Matter" SAMPE jou. Sept./Oct. (1985), pp. 6-9

107. Hopfgarten F. "Surface Study of Carbon Fibres with ESCA and Auger Electron Spectroscopy" Fibre Sci. Tech., Vol. 11 (1978), pp. 67-79

108. Hopfgarten F. "ESCA Studies of Carbon and Oxygen in Carbon Fibres" Fibre Sci. Tech., Vol. 12 (1979), pp. 283-294

109. Ishitani A. "Application of X-Ray Photoelectron Spectroscopy to Surface Analysis of Carbon Fiber" Carbon, Vol. 19 (1981), pp. 269-275

110. Takahagi T. and Ishitani A. "XPS Studies of the Digital Difference Spectrum Technique of Functional Groups on the Surface of Carbon Fiber" Carbon, Vol. 22 (1984), pp. 43-46

111. Waltersson K. "ESCA Studies of Carbon Fibres: Part I. The Chemical Composition of a Carbon Fibre Subsurface" Fibre Sci. Tech., Vol. 17 (1982), pp. 289-302

112. Proctor A. and Sherwood P.M.A. "X-Ray Photoelectron Spectroscopic Studies of Carbon Fibre Surfaces II. The

Effect of Electrochemical Treatment" Carbon, Vol. 21 (1983), pp. 53-59

113. Proctor A. and Sherwood P.M.A. "X-Ray Photoelectron Spectroscopic Studies of Carbon Fibre Surfaces III. Industrially Treated Fibres and the Effect of Heat and Exposure to Oxygen" Surf. Interface Anal., Vol. 4 (1982), pp. 212-219

114. Proctor A. and Sherwood P.M.A. "X-Ray Photoelectron Spectroscopic Studies of Carbon Fibre Surfaces IV. The Effect of Electrochemical Treatment in Nitric Acid" J. Chem. Soc., Faraday Trans. I., Vol. 80 (1984), pp. 2099-2107

115. Kozlowski C. and Sherwood P.M.A. "X-Ray Photoelectron Spectroscopic Studies of Carbon Fibre Surfaces V. The Effect of pH on Surface Oxidation" J. Chem. Soc. Faraday Trans. I., Vol. 8 (1984), pp. 2745-2756

116. Kozlowski C. and Sherwood P.M.A. "X-Ray Photoelectron Spectroscopic Studies of Carbon Fibre Surfaces VII. Electrochemical Treatment in Ammonium Salt Electrolytes" Carbon, Vol. 24 (1986), pp. 357-363

117. Cherry B.W. and Evely P.B. "The Interaction Parameter and the Strength of Adhesive Joints" Paper presented at symposium, 1987 International Meeting the Adhesion Society", Williamsburg, VA, USA, Feb. (1987)

118. Modern Plastics Encyclopedia 57 New York: McGraw-Hill (1980)

119. General Electric Co. "Product Identification-Ultem

120. Hinkley J.A. "Small Compact Tension Specimens for Polymer Toughness Screening" J. Appl. Polym. Sci., Vol. 32 (1986), pp. 5653-5655

121. Wadsworth N.J. and Spilling I. "Load Transfer from Broken Fibers in Composite Materials" Brit. J. Appl. Phys. (J. Phys. D) ser. 2,, Vol. 1 (1968), pp. 1049-1058

122. Bury K.V. Statistical Models in Applied Science New York: Wiley (1975)

APPENDIX I

I. DERIVATIZATION REACTIONS

1) Pentafluorobenzaldehyde (PFB)
To a solution containing 300 μL of PFB (0.1M) in 15 mL of pentane in a 25 mL erlenmeyer flask, an 8 cm. by 12,000 filament tow of carbon fibers was reacted for 2h at 35 - 40 °C. The sample was washed with pentane and Soxhlet extracted with pentane for 12 hours. The temperature was controlled by placing the flask in a water bath.

2) Trifluoroethanol (TFE)
To a solution containing 500 μL of TFE, 1 mL pyridine, and 200 mg of dicyclohexylcarbodiimide in 15 mL of CH_2Cl_2, an 8cm. by 12,000 filament tow of carbon fibers was reacted for 15 hours at 25 °C. The sample was then washed with anhydrous ethyl ether and Soxhlet extracted for 12 h with ethyl ether.

3) Trifluoroacetic Anhydride (TFAA)
To a solution containing 1mL of TFAA and 1mL of pyridine in 15 mL of benzene, an 8 cm. by 12,000 filament tow of carbon fibers was reacted for 1.5 h at 25 °C. The sample was washed with benzene and Soxhlet extracted for 12 h with ethyl ether.

4) Pentafluorophenyl hydrazine (PFPH)
To a solution containing 150 mg of of PFPH (ca. 0.1 M) and 1 drop of concentrated HCl in 15 mL of 95% ethanol, an 8 cm. by 12,000 filament tow of carbon fibers was reacted for 2 h at 25 °C. The sample was then washed with 100% ethanol and Soxhlet extracted for 12 h in ethyl ether.

5) Mercuric Trifluoroacetate (HgTFA)
To a solution containing 400 mg of $Hg(TFA)_2$ (0.06 M) and 500 μL of Trichloroethanol in 15 mL of benzene, an 8 cm by 12,000 filament tow of carbon fibers was reacted for 2 h at 25 °C. The sample was then washed with benzene and Soxhlet extracted for 12 h with pentane.

APPENDIX II

MAXIMUM LIKELIHOOD ESTIMATION OF PARAMETERS OF THE WEIBULL DISTRIBUTION

The probability distribution function for the Weibull distribution is shown in equation II.1 where α and β are shape and scale parameters respectively.

$$g(\sigma_i) = \frac{\alpha}{\beta}\left[\frac{\sigma_i}{\beta}\right]^{\alpha-1} \exp - [\sigma_i/\beta]^{\alpha} \qquad \text{(II.1)}$$

In order to estimate the parameters in this equation we use the maximum likelihood estimate (122) of the Weibull distributon shown in equation II.2. Where σ_i represents the individual stress values.

$$L(\alpha,\beta) = \prod_{i=1}^{n}\left[\frac{\alpha}{\beta}\left[\frac{\sigma_i}{\beta}\right]^{\alpha-1} \exp - [\sigma_i/\beta]^{\alpha}\right] \qquad \text{(II.2)}$$

Equation II.2 can be rearranged to equation II.3

$$L(\alpha,\beta) = \frac{\alpha^n}{\beta^{n\alpha}} \prod_{i=1}^{n} \sigma_i^{\alpha-1} \exp\left[-\beta^{-\alpha}\sum_{i=1}^{n}\sigma_i^{\alpha}\right] \qquad \text{(II.3)}$$

The parameters are best found by maximizing the derivatives of the logarithm of the likelihood function with respect to each of the parameters. The logarithm of the

likelihood function is shown in equation II.4.

(II.4)

$$\ln (L) = n \ln (\sigma) - n \ln \alpha - n(\beta-1) \ln \alpha + (\beta - 1) \left(\sum_{i=1}^{n} \ln \sigma_i \right) - \frac{1}{\beta^{\alpha}} - \frac{1}{\beta^{\alpha}} \sum_{i=1}^{n} \alpha_i^{\beta}$$

The partial derivatives of the logarithm of the likelihood function with respect to α and β are shown in equations II.5 and II.6 respectively.

(II.5)

$$\frac{d \ln (L)}{d \alpha} = \frac{n}{\alpha} - n \ln \beta + \left(\sum_{i=1}^{n} \ln \sigma_i \right) + \beta^{-\alpha} \sum_{i=1}^{n} \sigma_i^{\alpha} \ln \sigma_i - \left(\sum_{i=1}^{n} \sigma_i^{\alpha} \right) (\beta^{-\alpha} \ln \beta)$$

(II.6)

$$\frac{d \ln (L)}{d\beta} = - n \alpha + \alpha \beta^{-\alpha} \sum_{i=1}^{n} \sigma_i^{\alpha}$$

Equation II.4 will be maximized when each of equations II.5 and II.6 equal zero. Equation II.5 and II.6 can be solved simultaneously using an iterative technique to determine α and β. However, it is easier to solve the maximum likelihood of the extreme value distribution to obtain α and then substitute α into equation II.6 to obtain β. Equation II.6 can be rearranged to obtain an equation

that gives β in terms of α as shown in equation II.7.

(II.7)

$$\beta = \left[\frac{\sum_{i=1}^{n} \sigma_i^{\alpha}}{n} \right]^{1/\alpha}$$

Thus α can be found from the maximum likelihood of the extreme value distribution (described below) using an iterative procedure and substituted into equation II.7 to find β. The probability distribution function for the extreme value distribution is shown in equation II.8. This distribution is equaivalent to the weibull distribution in that if a set of data fit the weibull distribution, the logarithm of the data will fit the extreme value distribution. In this equation "a" is equivalent to 1/α in the weibull equation.

(II.8)

$$G(\sigma) = \frac{1}{a} \exp\left[-\left[\frac{\sigma_i - \beta}{a} \right] - \exp\left[-\left[\frac{\sigma_i - \beta}{a} \right] \right] \right]$$

The likelihood function of the extreme value distribution is shown in equation II.9.

(II.9)

$$L(\sigma:a,\beta) = \frac{1}{a^n} \exp\left[-\sum_{i=1}^{n}\left[\frac{\sigma - \beta}{a}\right] - \sum_{i=1}^{n} \exp\left[-\left[\frac{\sigma_i - \beta}{a}\right]\right]\right]$$

The parameters in equation II.9 can be obtained by setting the partial derivatives with respect to a and β equal to zero and solving simultaneously. The partial derivatives of L with respect to a and β are shown in equation II.10 and II.11 respectively.

(II.10)

$$\frac{dL}{da} = a + \beta + \frac{1}{n}\sum_{i=1}^{n}\sigma_i \exp\left[-\left[\frac{\sigma_i-\beta}{a}\right]\right] - \frac{\beta}{n}\sum_{i=1}^{n}\left[\exp -\left[\frac{\sigma_i-\beta}{a}\right]\right] - \bar{\sigma}$$

(II.11)

$$\frac{dL}{d\beta} = \frac{1}{n}\sum_{i=1}^{n} \exp\left[-\left[\frac{\sigma_i - \beta}{a}\right]\right] - 1 = 0$$

Substituting equation II.11 into equation II.10 leads to equation II.12.

(II.12)

$$g(a) = -a - \bar{\sigma} + \frac{\sum_{i=1}^{n}\sigma_i \exp^{-\left[\frac{\sigma_i}{a}\right]}}{\sum_{i=1}^{n}\exp^{-\left[\frac{\sigma_i}{a}\right]}}$$

The parameter a can be obtained by setting this equation equal to zero. The derivative of equation II.12 is shown in equation II.13.

(II.13)

$$g'(a) = -1 + \frac{\left[\sum_{i=1}^{n} \sigma \exp -\left[\frac{\sigma_i}{a}\right]\right]^2 - \sum_{i=1}^{n} \exp\left[\frac{\sigma_i}{a}\right] \sum_{i=1}^{n} \sigma_i^2 \exp\left[\frac{\sigma_i}{a}\right]}{a^2\left[\sum_{i=1}^{n} \exp -\left[\frac{\sigma_i}{a}\right]\right]^2}$$

To find the value of a which will cause equation II.12 to equal zero can be accomplished using an iterative technique (in this case Newton's method). This is done by first assuming a value for a. The value of a is then substituted into equation II.12 and II.13 and a new value of a determined by equation II.14. This procedure is repeated until $a_{j+1} - a_j$ is less than some small value. The final value of a is assumed to be a fair representation of the actual value of a.

(II.14)

$$a_{j+1} = a_j + \frac{g(a)}{g'(a)}$$

Initial estimates of "a" can be obtained using the cumulative extreme value distribution shown in equation II.15.

$$S(\sigma) = \exp\left[\exp\left[-\left[\frac{\sigma - \beta}{a}\right]\right]\right] \quad \text{(II.15)}$$

Taking the logarithm of minus the logarithm of equation II.15 leads to equation II.17.

$$\ln S(\sigma_i) = -\exp\left[-\left[\frac{\sigma - \beta}{a}\right]\right] \quad \text{(II.16)}$$

$$\ln(-\ln S(\sigma_i)) = \left[\frac{\sigma_i - \beta}{a}\right] \quad \text{(II.17)}$$

Thus plotting σ_i versus $\ln(-\ln S(\sigma))$ will give a straight line with slope $1/a$ and intercept $-\beta/a$. The values of S are determined by ordering the measured values of σ in numerical order and assigning S equal to the numerical order of the measured value and dividing by the total number of measurements.

The computer program used to perform these calculations is presented in Appendix IX.

DETERMINATION OF PARAMETERS FOR BREAKING STRENGTH AS A FUNCTION OF LENGTH EQUATION

The equation which describes the strength-length

dependence of fibers is shown in equation II.18. Where α and β are shape and scale parameters. The parameters of this equation can be obtained by taking the logarithm of minus the logarithm of $P(\sigma)$. The logarithm of $P(\sigma)$ is shown in equation II.19. The logarithm of minus the logarithm of $P(\sigma)$ is shown in equation II.20.

(II.18)

$$P(\sigma) = \exp\left[- L \left[\sigma / \beta \right]^{\alpha} \right]$$

(II.19)

$$\ln (P(\sigma)) = \left[- L \left(\sigma / \beta \right)^{\alpha} \right]$$

(II.20)

$$\ln (-\ln (P(\sigma))) = \left[\ln (L) + \alpha \ln (\sigma / \beta) \right]$$

The mean value of breaking strength will have a cumulative frequency of 0.5. Thus, plotting ln(L) against $\ln(\sigma_{avg})$ will give a straight line with slope $-1/\alpha$ and intercept $\ln(\beta) + \ln(-\ln(0.5)/\alpha$

(II.21)

$$\ln (\bar{\sigma}) = \frac{\ln (-\ln (0.5))}{\alpha} + \ln (\beta) - \frac{\ln (L)}{\alpha}$$

APPENDIX III

RESULTS OBTAINED BY CURVE FITTING X-RAY PHOTOELECTRON SPECTRA OF CARBON FIBERS

The tables list the lowest binding energy (BE) peak in the spectra, the shift of each subsequent peak in eV, the width of the peak at one half height (FWHM), and the relative percentage of the peak within the overall peak for that element (%).

1) Resutls from curve fitting XPS peaks of surface treated fibers

AU-4 NH_4HCO_3

	BE	%	FWHM
C1s			
	285.00	64.0	1.60
	+1.46	13.2	1.40
	+2.43	5.4	1.39
	+3.77	13.3	1.89
	+5.73	4.1	2.13
O1s			
	531.97	58.8	2.08
	+1.61	37.0	1.91
	+3.54	4.2	1.81
N1s			
	398.93	16.7	1.50
	+1.30	62.1	1.80
	+2.80	21.2	2.80

AS-4 HNO_3 Boil

	BE	%	FWHM
C1s			
	285.00	59.2	1.72
	+1.58	28.0	1.60
	+2.31	7.1	1.61
	+4.29	5.7	1.30
O1s			
	532.49	60.2	1.91
	+1.46	39.8	1.73
N1s			
	398.84	8.3	1.80
	+0.96	91.7	1.63

AU-4 H_2SO_4

	BE	%	FWHM
C1s			
	285.00	67.2	1.51
	+1.42	16.0	1.44
	+2.58	6.1	1.40
	+4.01	8.5	1.58
	+5.05	2.2	1.63
O1s			
	532.34	44.7	1.77
	+1.42	51.8	1.91
	+3.00	3.6	1.77
N1s			
	400.40	46.6	1.68
	+1.59	39.9	1.63
	+2.60	13.5	1.60

AU-4 $(NH_4)_2SO_4$

	BE	%	FWHM
C1s			
	285.00	60.1	1.64
	+1.30	17.4	1.42
	+2.43	8.6	1.39
	+3.94	12.0	1.75
	+5.65	2.0	1.63
O1s			
	532.06	51.4	1.99
	+1.41	44.5	1.97
	+2.99	4.1	1.71
N1s			
	400.13	74.1	2.00
	+1.64	25.9	1.70

AU-4 H_2O

	BE	%	FWHM
C1s			
	285.00	61.5	1.54
	+1.34	13.8	1.40
	+2.39	8.8	1.40
	+3.85	13.8	1.72
	+5.59	2.1	1.73
O1s			
	531.32	9.4	1.27
	+1.09	42.4	1.65
	+2.08	48.3	1.99
N1s			
	398.78	11.1	1.70
	+1.70	77.2	1.90
	+3.50	11.7	1.70

AU-4 NaOH

	BE	%	FWHM
C1s			
	285.00	53.8	1.37
	+1.12	23.8	1.72
	+2.93	9.2	1.90
	+4.61	9.2	1.90
	+6.54	4.0	1.78
O1s			
	531.95	52.7	1.89
	+1.41	28.2	1.79
	+2.80	19.1	1.80
N1s			
	399.50	20.8	1.70
	+1.85	79.2	1.70

2) Results from curve fitting XPS peaks of commercial fibers

AU-4

	BE	%	FWHM
C1s			
	285.00	67.3	1.37
	+1.41	16.5	1.53
	+2.94	6.6	1.70
	+4.68	6.0	2.05
	+6.77	3.5	1.93
O1s			
	531.59	21.2	1.46
	+1.26	58.2	1.62
	+2.64	20.7	1.59
N1s			
	399.35	16.0	1.80
	+2.20	69.5	1.60
	+4.40	14.6	1.80

XAU

	BE	%	FWHM
C1s			
	285.00	68.0	1.48
	+1.38	14.4	1.44
	+3.05	10.9	1.80
	+4.89	6.8	2.20
O1s			
	532.67	48.4	1.61
	+1.27	38.1	1.69
	+2.63	13.5	1.70
N1s			
	399.72	43.0	1.93
	+1.29	39.9	1.66
	+2.60	17.1	1.90

T-300U

	BE	%	FWHM
C1s			
	285.00	71.5	1.36
	+1.41	15.6	1.46
	+3.28	5.5	1.81
	+4.93	3.6	1.74
	+6.95	3.1	1.96
O1s			
	531.43	18.9	1.61
	+1.42	62.3	1.86
	+3.11	18.7	1.70
N1s			
	401.53	100.0	1.70

AS-4

	BE	%	FWHM
C1s			
	285.00	65.0	1.44
	+1.43	16.5	1.52
	+2.72	6.4	1.60
	+4.08	9.1	2.15
	+6.44	3.1	1.90
O1s			
	531.98	54.5	1.76
	+1.42	37.7	1.82
	+2.89	7.8	1.64
N1s			
	399.79	53.8	1.80
	+1.50	46.2	1.80
	+2.70	17.6	1.90

XAS

	BE	%	FWHM
C1s			
	285.00	46.4	1.36
	+1.31	27.2	1.57
	+2.62	13.6	1.56
	+4.09	7.4	1.54
	+5.36	5.3	1.68
O1s			
	532.61	34.8	1.81
	+1.50	43.1	1.83
	+2.84	22.1	1.70
N1s			
	399.26	37.2	1.63
	+1.29	45.2	1.66

T-300S

	BE	%	FWHM
C1s			
	285.00	62.5	1.56
	+1.43	28.7	1.56
	+2.55	4.8	1.56
	+4.18	4.0	1.90
O1s			
	531.96	6.5	1.51
	+1.33	78.5	1.33
	+2.77	15.0	2.77
N1s			
	400.33	100.0	1.70

3) Results from curve fitting XPS peaks from surface treated commercial fibers

AU-4 NaOH

	BE	%	FWHM
C1s			
	285.00	63.1	1.40
	+1.30	19.2	1.52
	+2.98	9.2	1.77
	+4.60	5.5	1.64
	+6.15	2.9	1.66
O1s			
	532.55	40.7	1.80
	+1.52	47.3	1.88
	+3.07	12.0	1.95
N1s			
	400.31	33.1	1.80
	+1.62	66.9	1.70

AU-4 H_2SO_4

	BE	%	FWHM
C1s			
	285.00	62.3	1.53
	+1.47	14.2	1.30
	+2.45	8.0	1.30
	+3.93	12.7	1.61
	+5.36	2.7	1.96
O1s			
	532.07	41.6	1.80
	+1.51	58.4	2.00
N1s			
	400.23	73.0	1.80
	+1.82	27.0	1.80

XAU NaOH

	BE	%	FWHM
C1s			
	285.00	63.9	1.40
	+1.25	19.5	1.64
	+2.82	5.4	1.57
	+4.21	7.6	1.75
	+5.96	3.7	1.68
O1s			
	531.65	47.6	1.79
	+1.33	39.2	1.88
	+2.80	13.2	1.95
N1s			
	400.40	52.1	1.70
	+1.32	47.9	1.70

XAU H_2SO_4

	BE	%	FWHM
C1s			
	285.00	44.3	1.59
	+1.34	33.0	1.74
	+2.72	10.8	1.55
	+4.30	11.4	1.93
	+5.58	0.6	1.30
O1s			
	533.54	49.3	2.00
	+1.59	50.7	2.10
N1s			
	400.67	81.1	1.80
	+1.59	18.9	1.70

T-300U NaOH

	BE	%	FWHM
C1s			
	285.00	70.4	1.39
	+1.40	17.2	1.73
	+3.07	5.2	1.67
	+4.87	4.7	1.85
	+6.78	2.5	1.94
O1s			
	531.39	32.3	1.99
	+1.54	51.7	1.88
	+2.92	16.0	1.95
N1s			
	400.11	16.7	1.70
	+1.42	83.3	1.70

T-300U H_2SO_4

	BE	%	FWHM
C1s			
	285.00	58.8	1.42
	+1.51	18.5	1.51
	+2.70	7.7	1.45
	+4.00	11.1	1.46
	+5.58	4.0	1.98
O1s			
	533.25	47.3	1.85
	+1.42	52.7	1.98
N1s			
	400.51	61.9	1.80
	+1.65	38.1	1.70

APPENDIX IV

LINEAR REGRESSION PLOTS OF EQUATION 2.7 USED TO OBTAIN POLAR AND DISPERSIVE COMPONENTS OF SURFACE ENERGY OF CARBON FIBERS

(vertical lines indicate one standard deviation in the calculated parameter)

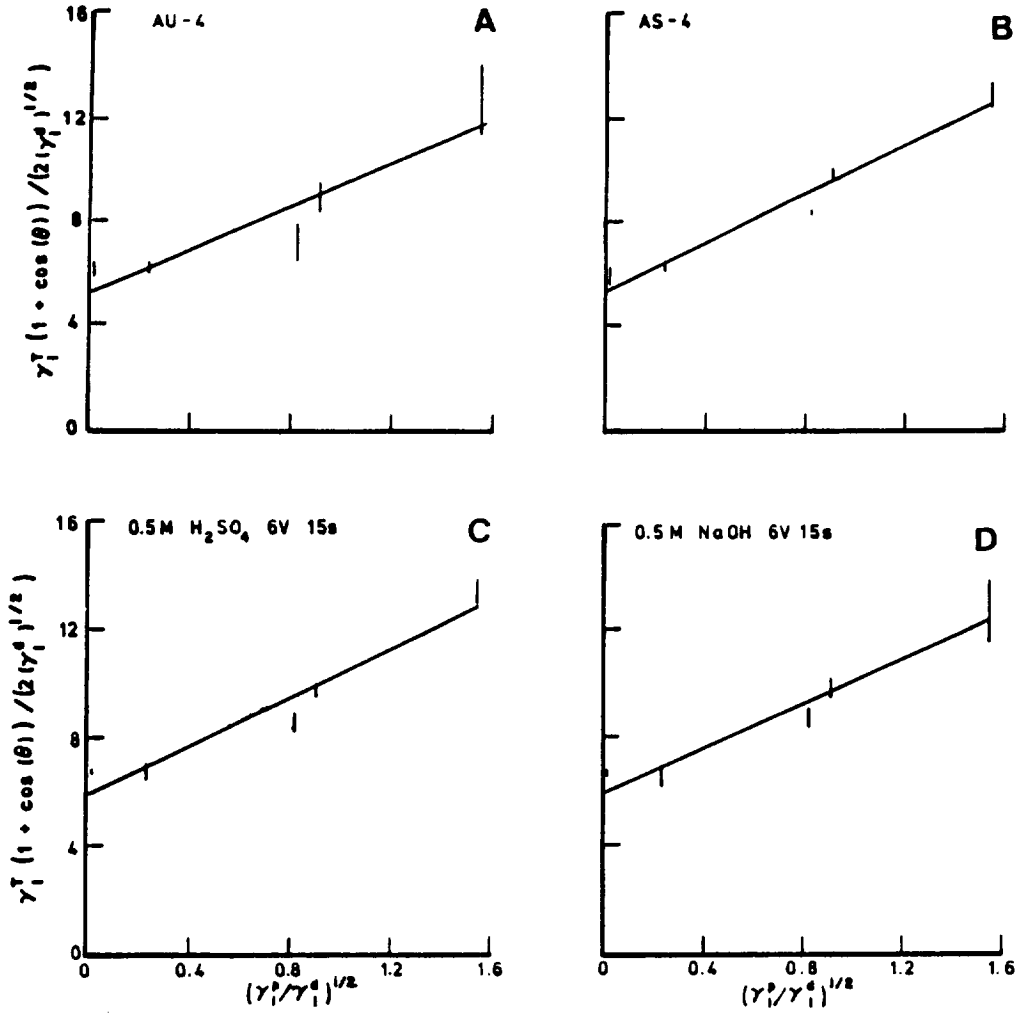

Figure IV.1 Linear regression plots used to obtain polar and dispersive components of surface energy of Hercules fibers before and after surface treatment
A) untreated fiber
B) commercially treated fiber
C) H_2SO_4 anodized fiber
D) NaOH anodized fiber
Anodization conditions are listed in table 3.8

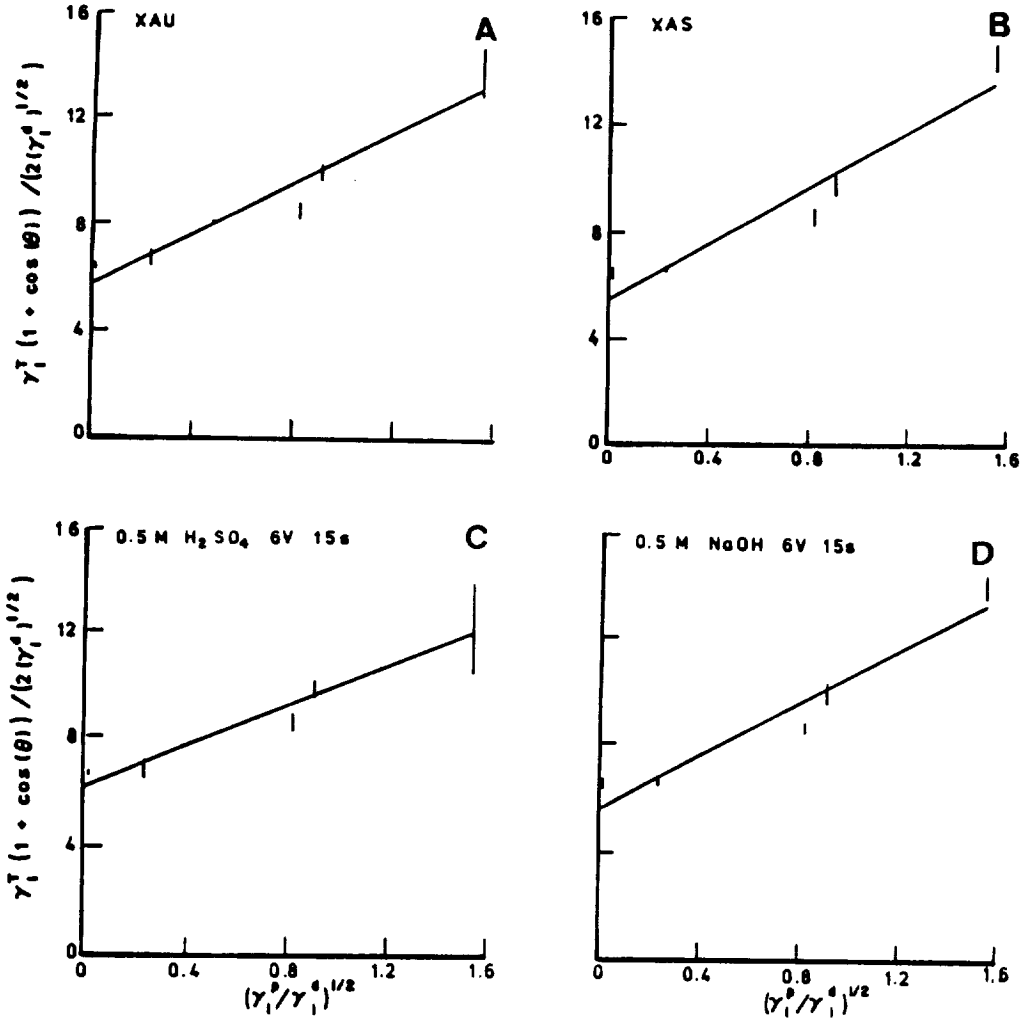

Figure IV.2 Linear regression plots used to obtain polar and dispersive components of surface energy of Dexter Hysol fibers before and after surface treatment
A) untreated fiber
B) commercially treated fiber
C) H_2SO_4 anodized fiber
D) NaOH anodized fiber
Anodization conditions are listed in table 3.8

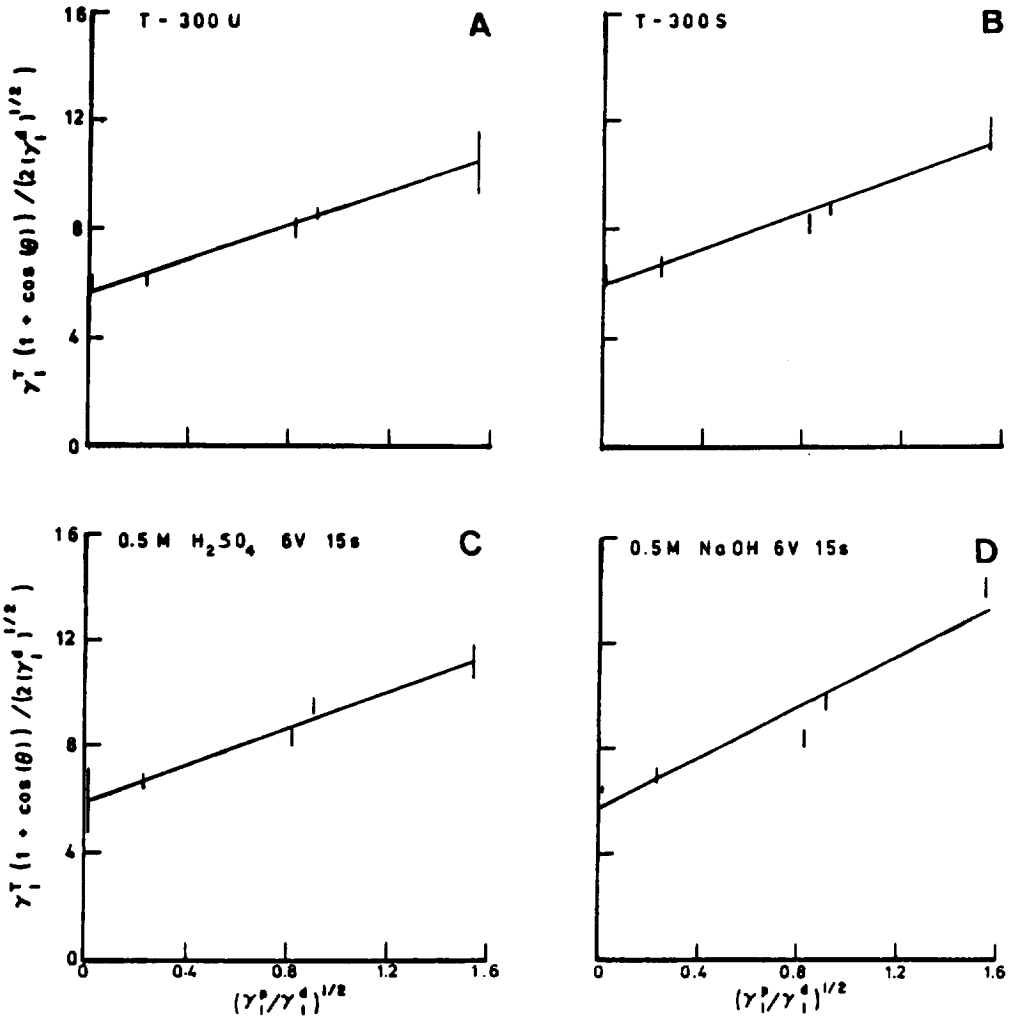

Figure IV.3 Linear regression plots used to obtain polar and dispersive components of surface energy of Union Carbide fibers before and after surface treatment
A) untreated fiber
B) commercially treated fiber
C) H_2SO_4 anodized fiber
D) NaOH anodized fiber
Anodization conditions are listed in table 3.8

APPENDIX V

HISTOGRAMS OF CARBON FIBER BREAKING STRENGTHS BEFORE AND AFTER SURFACE TREATMENT

Histograms of the breaking strengths of carbon fibers before and after surface treatment at several gauge lengths are shown in FIgures VI.1- VI.3. The continuous probability is overlayed. The continuous curve was obtained from the Weibull distribution. The parameters for the Weibull distribution were obtained by the method described in Appendix II. Surface treatment conditions are listed in table 3.8.

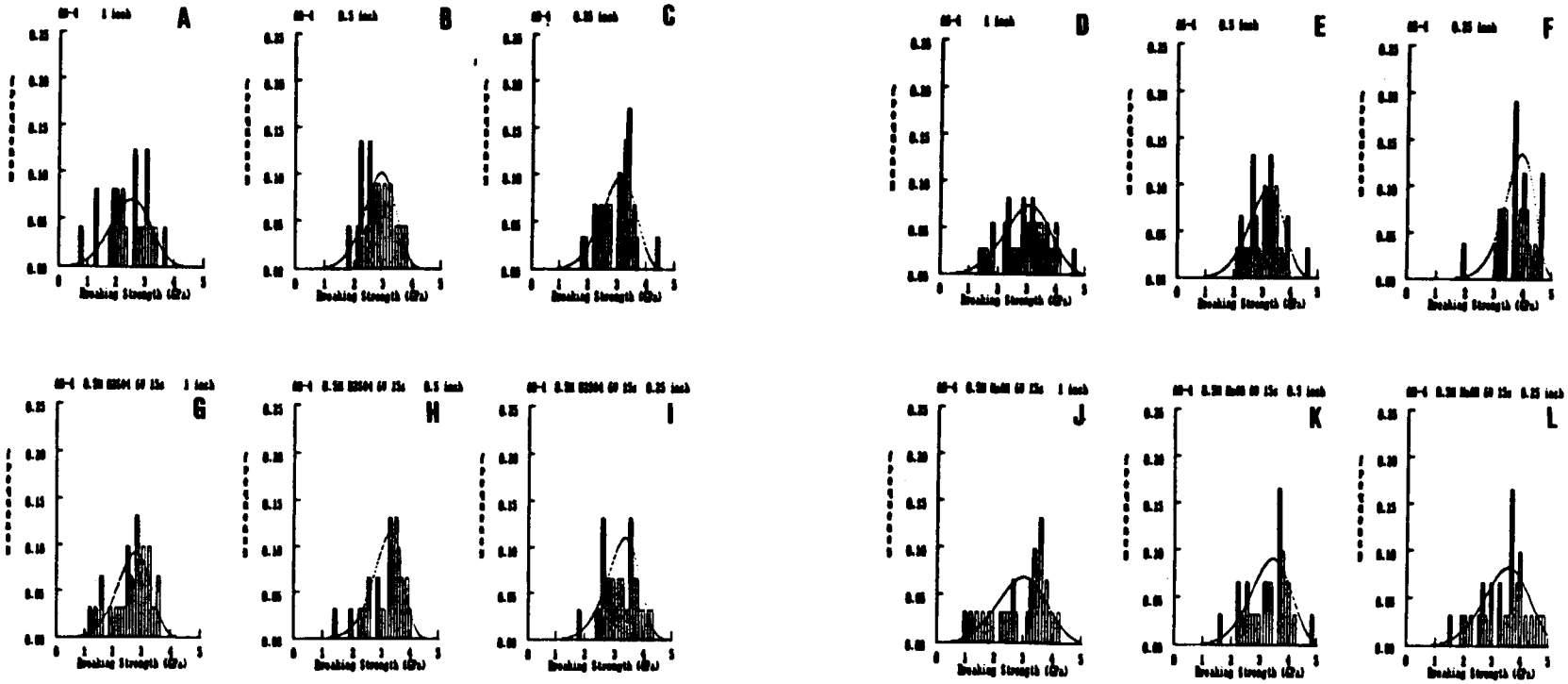

Figure V.1 Histograms of Hercules fiber breaking strengths before and after surface treatment.

A - C) untreated fiber (2.5, 1.3, 0.6 cm gage length)
D - F) commercially treated fiber (2.5, 1.3, 0.6 cm gage length)
G - I) H_2SO_4 anodized fiber (1.9, 1.3, 0.6 cm gage length)
J - L) NaOH anodized fiber (1.9, 1.3, 0.6 cm gage length)

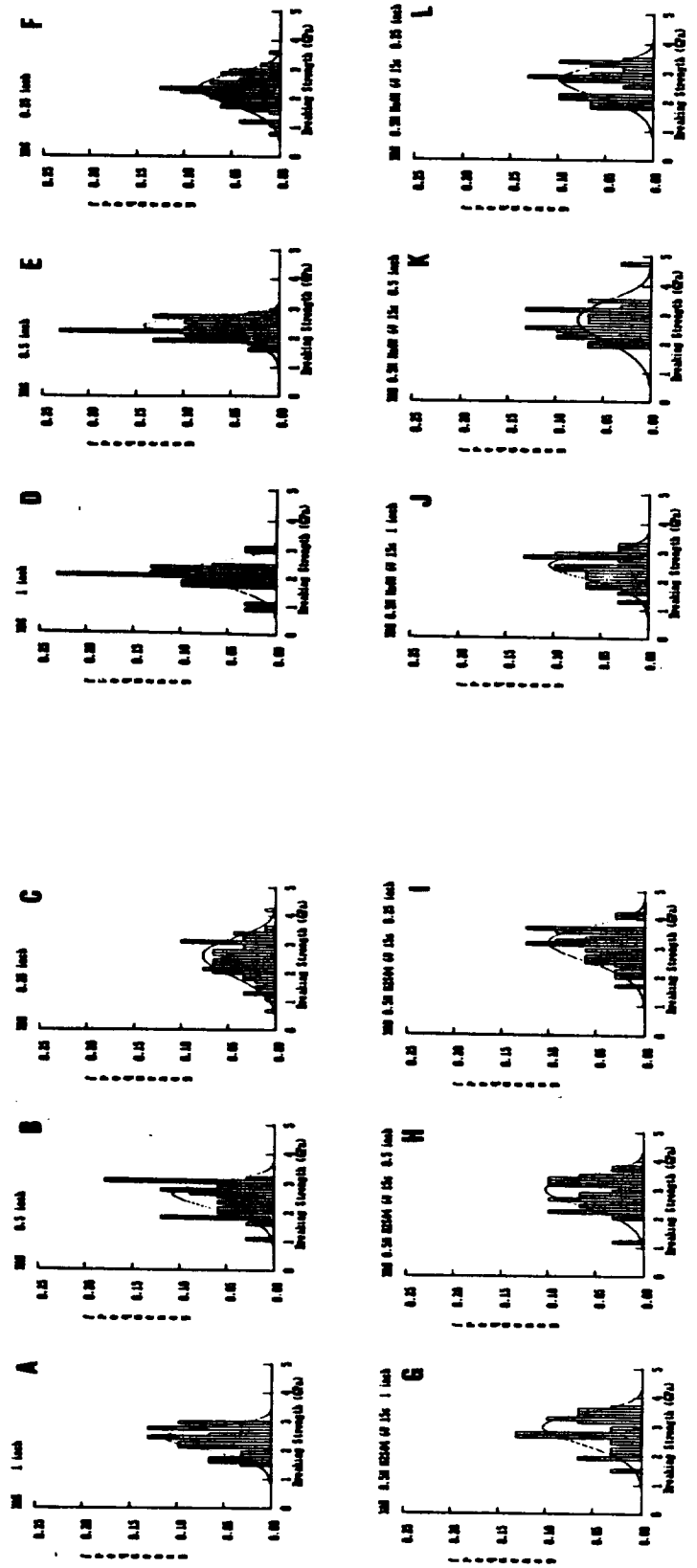

Figure V.2 Histograms of Dexter Hysol fiber breaking strengths before and after surface treatment.
A - C) untreated fiber (2.5, 1.3, 0.6 cm gage length)
D - F) commercially treated fiber (2.5, 1.3, 0.6 cm gage length)
G - I) H_2SO_4 anodized fiber (1.9, 1.3, 0.6 cm gage length)
J - L) NaOH anodized fiber (1.9, 1.3, 0.6 cm gage length)

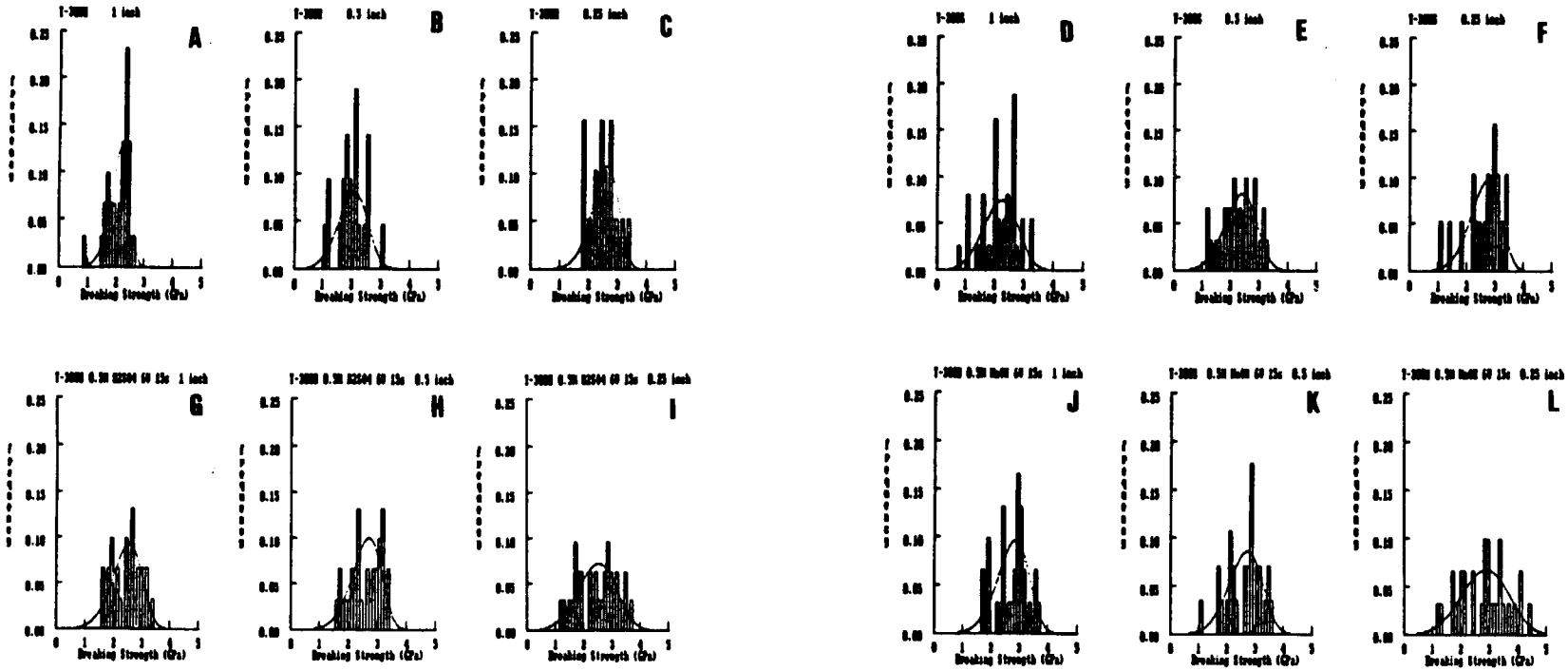

Figure V.3 Histograms of Union Carbide fiber breaking strengths before and after surface treatment.

A - C) untreated fiber (2.5, 1.3, 0.6 cm gage length)
D - F) commercially treated fiber (2.5, 1.3, 0.6 cm gage length)
G - I) H_2SO_4 anodized fiber (1.9, 1.3, 0.6 cm gage length)
J - L) NaOH anodized fiber (1.9, 1.3, 0.6 cm gage length)

APPENDIX VI

CUMULATIVE FREQUENCY PLOTS OF FIBER CRITICAL LENGTHS OF CARBON FIBERS EMBEDDED IN THERMOPLASTIC RESINS AND ANNEALED AT DIFFERENT TEMPERATURES FOR 8 HOURS

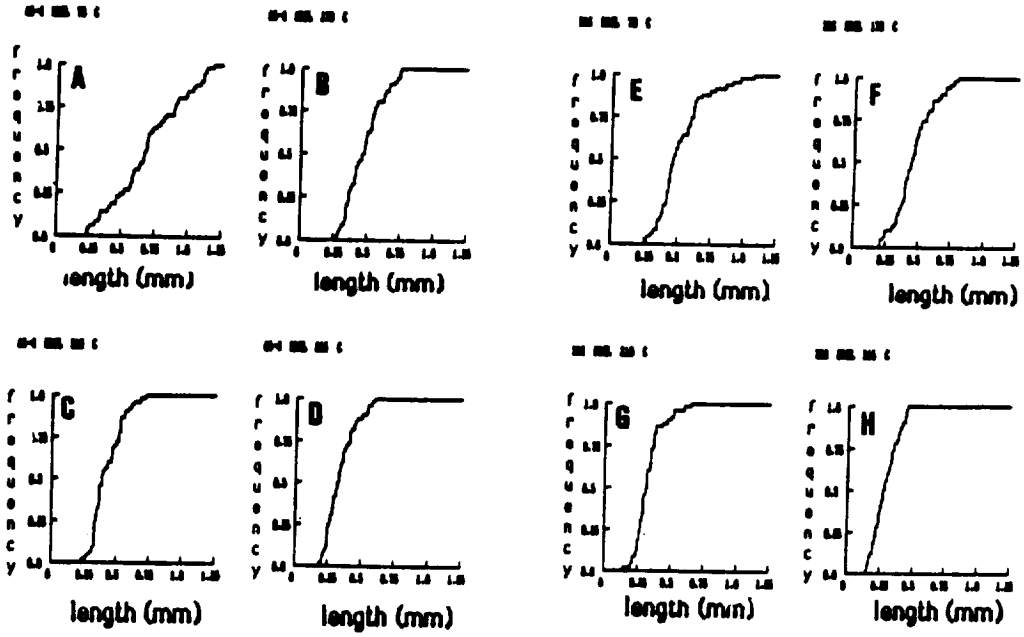

Figure VI.1 Cumulative frequency plots of fiber critical lengths of
A-D) Hercules AS-4 fibers embedded in polysulfone and annealed at 70, 170, 210, and 265° C for 8 hours.
E-H) Dexter Hysol XAS fibers embedded in polysulfone and annealed at 70, 170, 210, and 265° C for 8 hours.

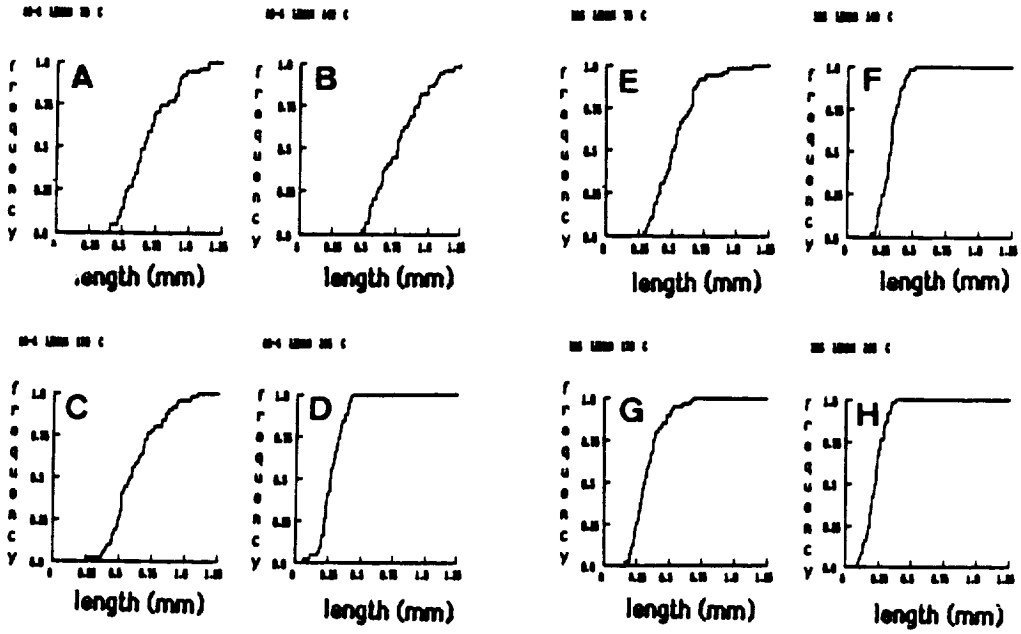

Figure VI.2 Cumulative frequency plots of fiber critical lengths of
A-D) Hercules AS-4 fibers embedded in polycarbonate and annealed at 70, 170, 210, and 265° C for 8 hours.
E-H) Dexter Hysol XAS fibers embedded in polycarbonate and annealed at 70, 170, 210, and 265° C for 8 hours.

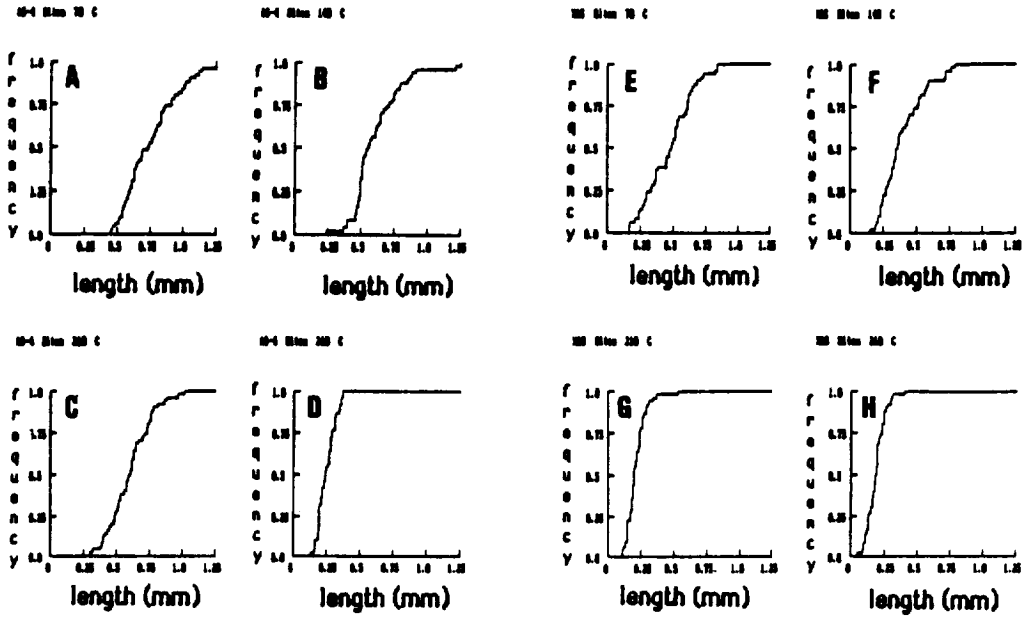

Figure VI.3 Cumulative frequency plots of fiber critical lengths of
A-D) Hercules AS-4 fibers embedded in polyetherimide and annealed at 70, 170, 210, and 265° C for 8 hours.
E-H) Dexter Hysol XAS fibers embedded in polyetherimide and annealed at 70, 170, 210, and 265° C for 8 hours.

APPENDIX VII

CUMULATIVE FREQUENCY PLOTS OF FIBER CRITICAL LENGTHS FOR SURFACE TREATED CARBON FIBERS EMBEDDED IN THERMOPLASTIC RESINS

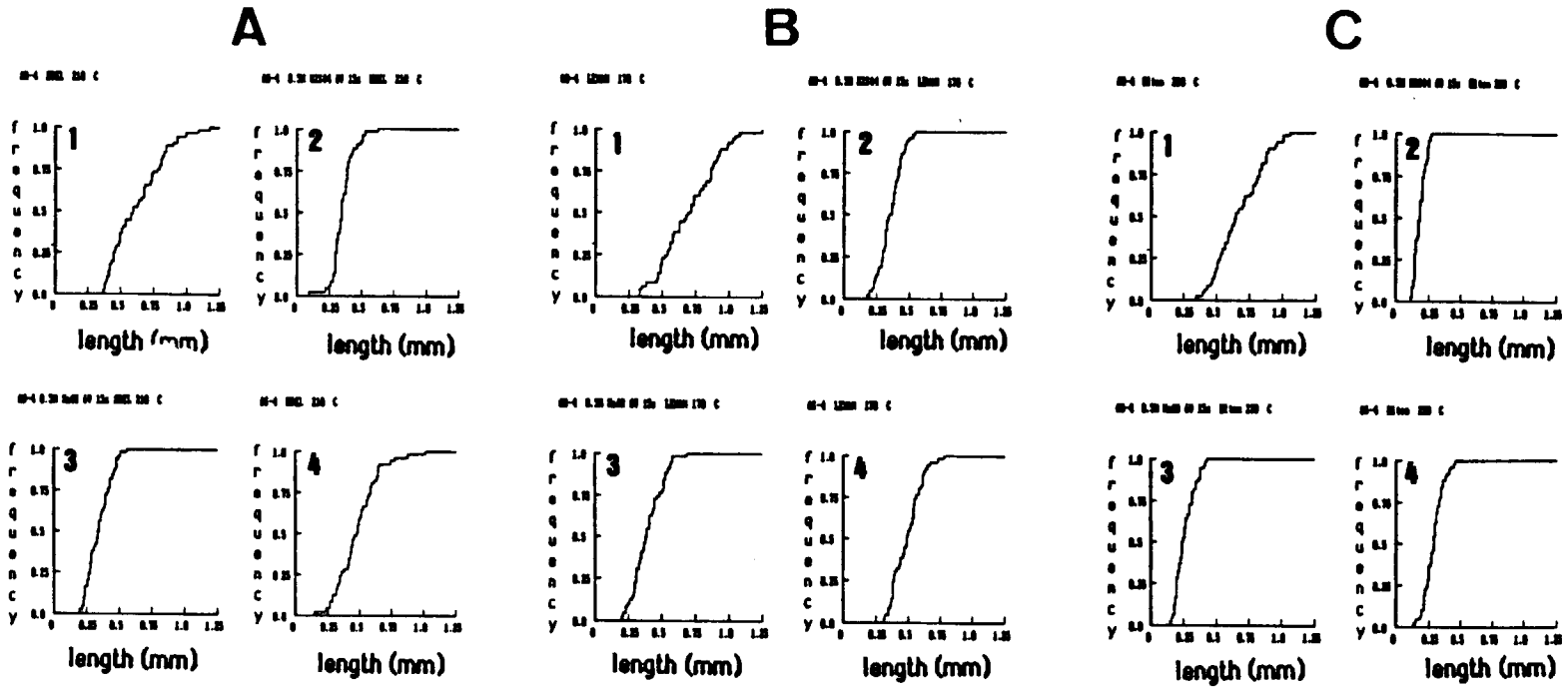

Figure VII.1 Cumulative frequency plots of fiber critical lengths of Hercules A type fibers before and after surface treatment; embedded in

A) polysulfone B) polycarbonate C) polyetherimide

1) untreated fiber
2) H_2SO_4 anodized fiber
3) NaOH anodized fiber
4) commercially treated fiber

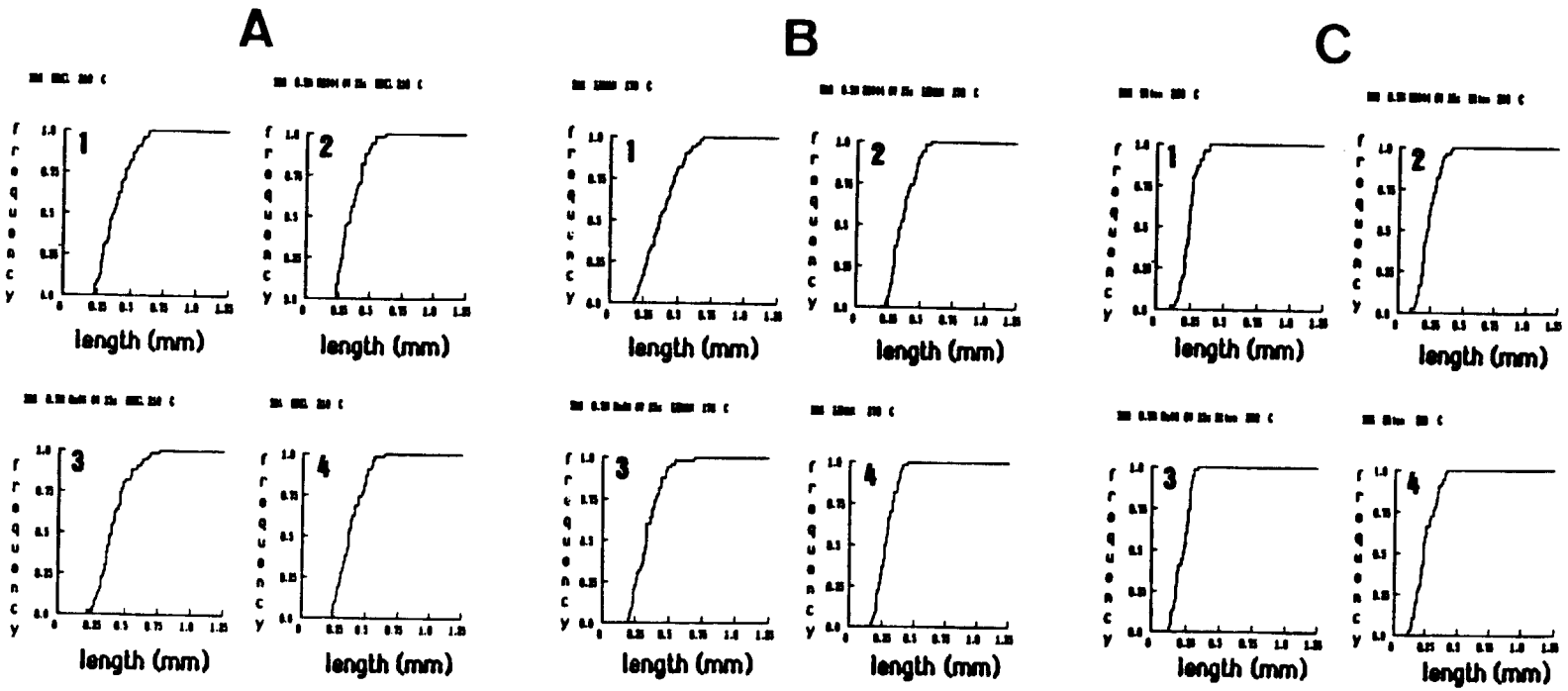

Figure VII.2 Cumulative frequency plots of fiber critical lengths of Dexter Hysol XA type fibers before and after surface treatment; embedded in

A) polysulfone B) polycarbonate C) polyetherimide

1) untreated fiber
2) H_2SO_4 anodized fiber
3) NaOH anodized fiber
4) commercially treated fiber

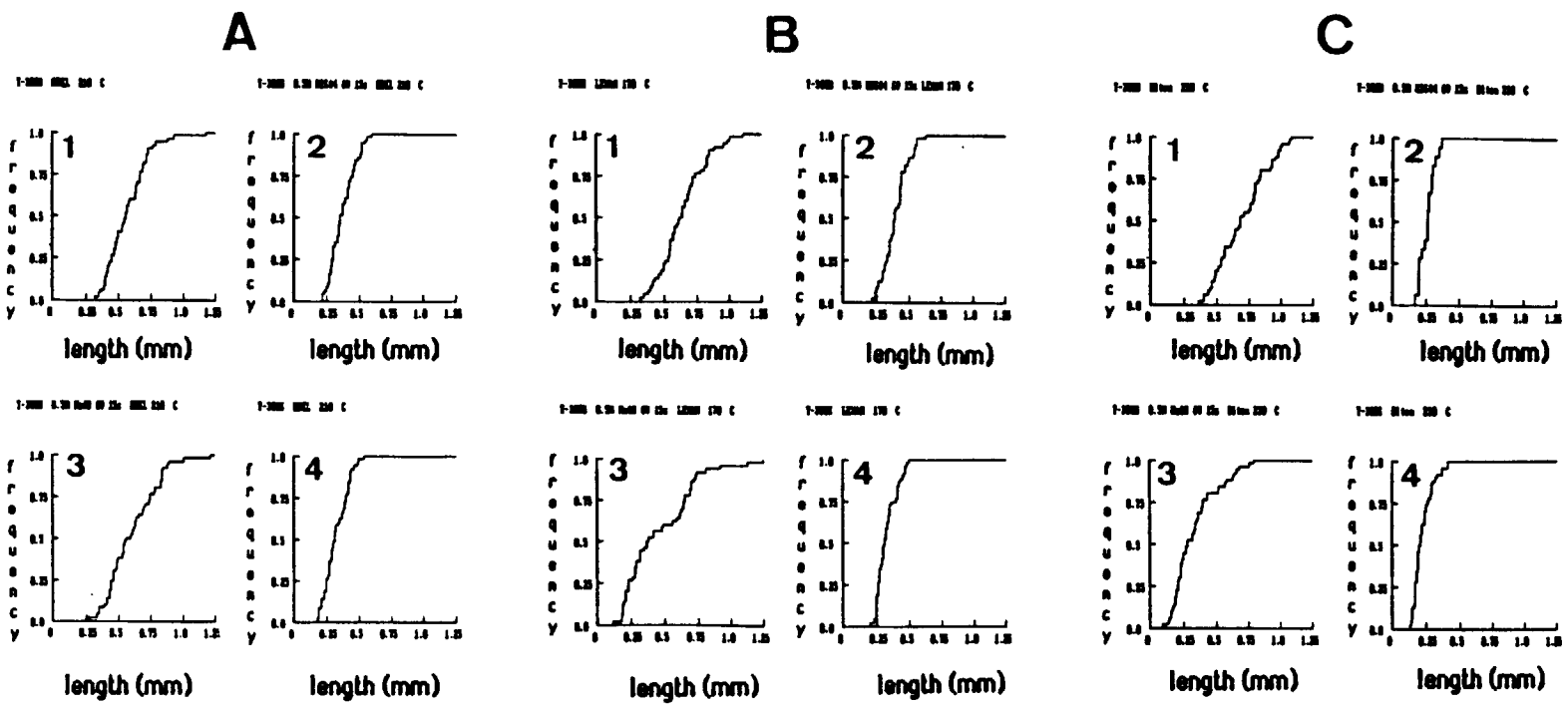

Figure VII.3 Cumulative frequency plots of fiber critical lengths of Union Carbide T-300 fibers before and after surface treatment; embedded in

A) polysulfone B) polycarbonate C) polyetherimide

1) untreated fiber
2) H_2SO_4 anodized fiber
3) NaOH anodized fiber
4) commercially treated fiber

APPENDIX VIII

COMPUTER PROGRAM USED TO CALCULATE POLAR AND DISPERSIVE COMPONENTS OF SURFACE ENERGY OF CARBON FIBERS FROM WETTING FORCE MEASUREMENT

(written on Borland's Turbo Pascal compiler version 3.0)

```
program  angle;
type
  liquids    =    (h2o,eg,form,mi,bn);

   component    =      record
       gaml,
       gamld,
       gamlp,
       gampd        :    array[liquids] of real;
       nam          :    array[liquids] of string[20];
   end;

     datas     =     record
         num         :    array[liquids] of integer ;
         wet         :    array[liquids] of array[1..6] of real;
         dia         :    array[liquids] of array[1..6] of real;
      end;
  calculations    =    record
       thet,
       coss        :    array[liquids] of array[1..6] of real;
       meant,
       meanc,
       thetsd,
       cossd       :    array[liquids] of real;
 end;
work  =  record
    mean,
    sdplus,
    sdminus    :    array[liquids] of real
  end;

  sums       =      record                  {regression sums}
      sumx,
      sumxx,
      sumy,
      sumxy     :    real
  end;
var
  datstr                :                 string[8];
  enter                 :                 string[1];
  i,j,k,l               :                 integer;
  prod                  :                 real;
  x,xx,y,yy             :                 real;
  liq                   :                 liquids;
  comp                  :                 component;
  dat                   :                 datas;
  data                  :                 file of datas;
  calc                  :                 calculations;
  sum                   :                 sums     ;
  a,b,gammap,gammad     :                 real;
  wrk                   :                 work;


procedure enterdata;
begin
for liq := h2o to bn do
  begin

    writeln('enter number of fibers for - ',comp.nam[liq]);
    readln(dat.num[liq]);
    for i := 1 to dat.num[liq] do
     begin
       writeln('enter weting force for ',comp.nam[liq],' fiber # ',i);
       readln(dat.wet[liq,i]) ;
       writeln('microscope meas. (600X) for ',comp.nam[liq],' fiber # ');
       readln(dat.dia[liq,i]);

     end;
end;
       writeln('enter data structure name')     ;
       readln(datstr)        ;
       assign(data,datstr);
       rewrite(data);
       write(data,dat);
       close(data)
end;
```

```
  procedure initialize;
  begin
      comp.nam[h2o]    :=   'Water';
      comp.nam[eg]     :=   'Ethylene Glycol';
      comp.nam[form]   :=   'Formamide';
      comp.nam[bn]     :=   'Bromonaphthalene';
      comp.nam[mi]     :=   'Methylene Iodide';
  with comp do
    begin
      gaml[h2o]    :=   72.8;
      gaml[eg]     :=   48.3;
      gaml[form]   :=   58.3;
      gaml[mi]     :=   50.8;
      gaml[bn]     :=   44.6;
      gamld[h2o]   :=   21.8;
      gamld[eg]    :=   29.3;
      gamld[form]  :=   32.3;
      gamld[mi]    :=   48.4;
      gamld[bn]    :=   44.6;
      gamlp[h2o]   :=   51.0;
      gamlp[eg]    :=   19.0;
      gamlp[form]  :=   26.0;
      gamlp[mi]    :=    2.4;
      gamlp[bn]    :=    0.0;
  end;
  end;

  procedure retreive;
    begin
                  writeln('enter name of fibers to be analyzed')  ;
          readln(datstr);
          assign(data,datstr);
          reset(data);
          read(data,dat);
    end;


  procedure calculate;
  begin
  for liq := h2o to bn do
    begin
     prod   :=   comp.gamlp[liq] / comp.gamld[liq];
      como.gampd[liq] := sqrt(prod);
      for j:= 1 to dat.num[liq] do
       begin
        calc.coss[liq,j] := (dat.wet[liq,j]*60)/(comp.gaml[liq]*
              dat.dia[liq,j]*2.54 * pi);
         if calc.coss[liq,j] > 1.0  then calc.coss[liq,j] := 1;
        xx:=calc.coss[liq,j]  ;
        x := sqrt(1-sqr(xx))/xx  ;
        calc.thet[liq,j] :=  arctan(x);
        calc.thet[liq,j] := (calc.thet[liq,j] * 180) /( pi )
       end;
    end;
  end;

procedure sdev;
begin
for liq := h2o to bn do
  begin
    x := 0;
    xx := 0;
    y := 0;
    yy := 0;
    calc.meant[liq] := 0 ;
    calc.meanc[liq] := 0 ;
    for k := 1 to dat.num[liq] do
      begin

        x := x + calc.thet[liq,k];
        xx := xx + sqr(calc.thet[liq,k]);
        y := y + calc.coss[liq,k];
        yy := yy + sqr(calc.coss[liq,k]);

      end;
```

```
      calc.meant[liq] := x / dat.num[liq];
      calc.thetsd[liq] := ((dat.num[liq] * xx) - sqr(x))/
      (dat.num[liq] * (dat.num[liq]-1));
      calc.thetsd[liq] := sqrt(calc.thetsd[liq]);
      calc.meanc[liq] := y/ dat.num[liq];
      calc.cossd[liq] :=((dat.num[liq] * yy) - sqr(y))/(dat.num[liq] *
      (dat.num[liq] - 1));
      calc.cossd[liq] := sqrt(calc.cossd[liq]);
      wrk.mean[liq] := (comp.gaml[liq] * (1 + calc.meanc[liq]))/
                (2*sqrt(comp.gamld[liq]));
      wrk.sdplus[liq] := (comp.gaml[liq]*(1+ calc.meanc[liq]+calc.cossd[liq]
      (2*sqrt(comp.gamld[liq]));
      wrk.sdminus[liq] := (comp.gaml[liq]*(1+ calc.meanc[liq]-calc.cossd[liq]
      (2*sqrt(comp.gamld[liq]));

end;
  end;
procedure print;
begin

writeln(
'                water       ethylene     formamide  methylene    bromo-    ')
writeln(
'                             glycol                  iodide    naphthalene')
writeln;
writeln(
'cosine  ',calc.meanc[h2o]:12:3,calc.meanc[eg]:12:3,calc.meanc[form]:12:3
calc.meanc[mi]:12:3,calc.meanc[bn]:12:3);
writeln(
's. dev. ', calc.cossd[h2o]:12:3,calc.cossd[eg]:12:3,calc.cossd[form]:12:3
calc.cossd[mi]:12:3,calc.cossd[bn]:12:3);
writeln(
'theta   ',calc.meant[h2o]:12:3,calc.meant[eg]:12:3,calc.meant[form]:12:3
calc.meant[mi]:12:3,calc.meant[bn]:12:3);
writeln(
's. dev. ',calc.thetsd[h2o]:12:3,calc.thetsd[eg]:12:3,calc.thetsd[form]:12
calc.thetsd[mi]:12:3,calc.thetsd[bn]:12:3);
writeln('') ;
writeln('gammap = ',gammap,'   gammad = ',gammad);
end;

procedure graph ;
var x1,x2,y1,y2 : integer;
begin
graphmode;
draw(80,166,248,166,1);
draw(80,166,80,6,1);
x1 := 122;
y1 := 126;
repeat
   draw(x1,166,x1,160,1);
   draw(80,y1,86,y1,1);
   x1 := x1 + 42;
   y1 := y1 - 40
   until x1 >249;

for liq := h2o to bn do
begin
   x1 := TRUNC(81.5 + ((comp.gampd[liq]/1.6) * 168));
   y1 := TRUNC(166.5 - ((wrk.sdplus[liq]/16) * 160));
   y2 := TRUNC(166.5 - ((wrk.sdminus[liq]/16) * 160));
   draw(x1,y1,x1,y2,1);
end;
  x1 := 81;
  y1 := TRUNC(166.5 - ((a/16)*160));
  x2 := TRUNC(81.5 + ((comp.gampd[h2o]/1.6) * 168));
  y2 := TRUNC(166.5 -((a + (b*comp.gampd[h2o]))/16) * 160);

  DRAW(x1,y1,x2,y2,1);
end;
begin

initialize;
       writeln('enter data?  Y/N')  ;
       readln(enter)  ;
       if enter = 'Y' then enterdata ;
retreive;
calculate;
sdev;
linreg;
print;
repeat until keypressed;
graph;
(repeat until keypressed;)
end.
```

APPENDIX IX

COMPUTER PROGRAM USED TO FIT CARBON FIBER BREAKING STRENGTHS TO THE WEIBULL AND PLOT HISTOGRAMS OF FIBER BREAKING STRENGTHS

(Written on Borland's Turbo Pascal compiler version 3.0)

Procedures sortSIR, LinReg, and Stats were obtained from Turbo Pascal Program Library by Rugg T. and Feldman P., Que Publ., Indianapolis (1984)

Procedure gamma was obtained from Pascal Programs for Scientists and Engineers by Miller A, Sybrex Inc. (1981)

```
program bs;

const
   ColSize   =  3;
   RowSize   =  100;
   ArraySize =  100;
   max       =  0.2;

type
   Array2Type  =  array[1..RowSize,1..ColSize] of real;
   arraytype   =  array[1..rowsize] of real;
   array1type  =  array[1..3] of real;
   array3type  =  array[1..3] of integer;
   names       =  string[14];
data =   record
            nl            :  integer;
            length        :  array1type;
            nf            :  array3type;
            break         :  array2type;
            dia           :  real;
         end;

var
  dat                                          :  data;
  breakprob                                    :  Array2Type;
  intercept, slope, corrcoef                   :  real;
  mean, median, StanDev, MinValue, MaxValue    :  real;
  i,j,k                                        :  integer;
  name                                         :  names;
  A                                            :  char;
  quit                                         :  boolean;
  alpha, beta                                  :  real;

procedure enter(var  dat  :  data);

var
   i,j      :  integer;

begin
   write('enter number of lengths '); readln(dat.nl);
   write('enter diameter in meters '); readln(dat.dia);
   for i := 1 to dat.nl do
      begin
         write('enter length number ', i); readln(dat.length[i]);
         write('enter number of ',dat.length[i], ' inch fibers');
         readln(dat.nf[i]);
         for j := 1 to dat.nf[i] do
            begin
               write('enter strength of ',dat.length[i], 'inch fiber no ')
               readln(dat.break[j,i]);
            end;
      end;
end;

procedure savedata(dat  :  data);

var
   datafile  :  text;
   name      :  names;
   i,j       :  integer;


begin
   write('enter new filename '); readln(name);
   assign(datafile,name);
   rewrite(datafile);
   writeln(datafile,dat.nl);
   writeln(datafile,dat.dia);
   for i := 1 to dat.nl do
      begin
         writeln(datafile,dat.length[i]);
         writeln(datafile,dat.nf[i]);
         for j := 1 to dat.nf[i] do
            writeln(datafile,dat.break[j,i]);
      end;
   close(datafile);
end;
```

```
procedure getdata(var dat   :  data;
                  var name  :  names);

var  datafile  :  text;
     i,j       :  integer;
begin
   write('enter filename '); readln(name);
   assign(datafile,name);
   reset(datafile);
   readln(datafile,dat.nl);
   readln(datafile,dat.dia);
   for i := 1 to dat.nl do
      begin
         readln(datafile,dat.length[i]);
         readln(datafile,dat.nf[i]);
         for j := 1 to dat.nf[i] do
            readln(datafile,dat.break[j,i]);
      end;
   close(datafile);

end;

procedure writedata(dat  :  data);

var
   i,j     :  integer;

begin
writeln(dat.dia);
   for i  :=  1 to dat.nl do
      begin
         writeln(dat.nf[i]);
         writeln(dat.length[i]);
            for j := 1 to dat.nf[i] do
               writeln(dat.break[j,i]);
      end;
end;

{$I b:plott.pas}
{$I b:SortSIR.PAS}
{$I b:LinReg.PAS}
{$I b:Stats.pas}
{$I b:gamma.pas}


procedure recurs(arrays   :   arraytype;
                 nf       :   integer;
                 slope    :   real;
           var   beta     :   real;
           var   alpha    :   real;
           var   ir       :   integer);

var
   sx, sexb, sxexb, sxxexb      :   real;
   xb, exb, xexb, xxexb, b      :   real;
   gb, gbp, gbgbp, agbgbp       :   real;
   i, j, k                  :   integer;
   tb, stb, stbn                :   real;

begin
   ir  :=  0;
   b   :=  1/slope;
   repeat
      sx      :=  0.0;
      sexb    :=  0.0;
      sxexb   :=  0.0;
      sxxexb  :=  0.0;
      for i := 1 to nf do
         begin
            xb      :=  ln(arrays[i]) / b;
            exb     :=  exp(xb);
            xexb    :=  ln(arrays[i]) * exb;
            xxexb   :=  ln(arrays[i]) * xexb;
            sx      :=  sx     +  ln(arrays[i]);
            sexb    :=  sexb   +  exb;
            sxexb   :=  sxexb  +  xexb;
            sxxexb  :=  sxxexb +  xxexb;
         end;
```

```
      gb      :=  -b - sx/nf + sxexb/sexb;
      gbp     :=  -1 + (sqr(sxexb) - sexb * sxexb)/(sqr(b*sexb));
      gbgbp   :=  gb / gbp;
      b       :=  b - gbgbp;
      agbgbp  :=  abs(gbgbp);
      ir      :=  ir +1;
   until agbgbp < 0.0000001;
   writeln(ir, ' recursions');
beta  :=  1/b;
stb   :=  0.0;
for i  := 1 to nf do
   begin
      tb   :=  exp(ln(arrays[i]) * beta);
      stb  :=  stb + tb
   end;
stbn  :=  stb/nf;
alpha :=  exp(b * ln(stbn));
end;

procedure analyze(dat        :  data;
                  name       :  names);

var
   i,j,k                                                  :   integer;
   intercept, w, corrcoeff                                :   real;
   L, sig0, dia                                           :   real;
   breakprob                                              :   array[1..2, 1..48] of real;
   arrays                                                 :   arraytype;
   mean, median, StanDev, MinValue, MaxValue              :   real;
   gmean, gsdev                                           :   real;
   anote                                                  :   string[60];
   b, c, d, ir                                            :   integer;
   point                                                  :   array[1..48] of real;
   sig                                                    :   real;

begin
   for i := 1 to dat.nl do
      begin
         for j := 1 to dat.nf[i] do
            arrays[j] := (dat.break[j,i] * 9.80665/(pi * sqr(dat.dia/2)))/
         SortSIR(arrays, dat.nf[i]);
         for j := 1 to dat.nf[i] do
            begin
               Breakprob[j,1] := ln(arrays[j]);
               breakprob[j,2] := ln(-ln(1-((j-0.5)/dat.nf[i])));
            end;

   LinReg(breakprob, dat.nf[i], intercept, w, corrcoeff);
   stats(arrays, dat.nf[i], mean, median, standev, minvalue, maxvalue);
   recurs(arrays, dat.nf[i], w, beta, alpha, ir);
   sig0   :=  exp((ln((dat.length[i] *2.54)/100) - intercept)/w);
   gsdev  :=  sqrt(gamma(1+2/w)/sqr(gamma(1 + 1/w))-1);
   gmean  :=  sig0 * (exp(-1/w * ln(dat.length[i])) * gamma(1+1/w));
   writeln(dat.length[i]:8,' inch fiber ', name);
   write('enter graph annotation ');  readln(anote);
      for j := 1 to 48 do
         point[j] := 0.0;
         for j := 1 to dat.nf[i] do
         begin
            b := round((arrays[j]/5.0e9)*240);
            if b > 240 then b := 240;
            for k := 1 to 48 do
               begin
                  c := k * 5;
                  d := c - 5;
                  if b > d then if b <= c then
                     point[k]  := point[k] + 1/dat.nf[i];
               end;
         end;
```

```
            plott;                                          {set up axis}
            gotoxy(19,1)  ; write(anote);
            gotoxy(59,2)  ; write('mean      = ',mean:9);
            gotoxy(59,4)  ; write('sdev      = ',standev:9);
            gotoxy(59,6)  ; write('beta      = ',beta:9);
            gotoxy(59,8)  ; write('alpha     = ',alpha:9);
            gotoxy(59,10) ; write('sigma 0   = ',sig0:9);
            gotoxy(59,12) ; write('gamean    = ',gmean:9);
            gotoxy(59,14) ; write('gamsdev   = ',gsdev:9);
            gotoxy(59,16) ; write('slope     = ',w:9);
            gotoxy(59,18) ; write('intercept = ',intercept:9);
            gotoxy(59,20) ; write('recurrs   = ',ir);
         for j := 1 to 48 do
            begin
               c  := 161 - round((point[j]/0.25) *160);
               b  :=  (j * 5) - 5;
               draw(b,161,b,c,1);
               draw(b,c,j*5,c,1);
               draw(j*5,161,j*5,c,1);
            end;
         for j := 1 to 240 do
            begin
               sig := (j/240 * 5.0e-9)**(1/alpha;
               c   := 161 - round(160 * (exp((beta-1) * ln(sig)) * beta/ln(2)
                        * exp(-exp(beta * ln(sig)))/0.25));
               plot(j,c,1);
            end;
            repeat
               readln(anote);
            until anote = 'q';
           textmode;
         end;
end;

begin
quit := false;
repeat
writeln('Enterdata, Savedata, Getdata, Writedata, Analyze, Quit');
readln(A);
case A of
'E','e'   :  enter(dat);
'S','s'   :  savedata(dat);
'G','g'   :  getdata(dat,name);
'W','w'   :  writedata(dat);
'A','a'   :  analyze(dat,name);
'Q','q'   :  quit := true
end;
until quit
end.
```

```
procedure plott;

var       i,j                 :   integer;
          S                   :   string[1];
          freq                :   string[26];

begin
   hires;
   draw(147,16,147,176,1);
   draw(146,16,146,176,1);
   draw(146,177,388,177,1);
   graphwindow(146,16,388,176);
   for j := 0 to 4 do
       draw(0,j*32,10,j*32,1);
   for j := 1 to 5 do
       draw(j*48,160,j*48,155,1);
   gotoxy(24,25);
   write('Breaking Strength (GPa)');
   for i := 0 to 5 do
      begin
         gotoxy(18 + i * 6,24);
         write(i:2);
      end;
     freq  := 'frequency';
     for i := 1 to 9 do
         begin
            gotoxy(9,6 + i);
            write(freq[i]);
         end;
      for i := 0 to 1 do
         begin
            j := i * 5;
            gotoxy(13,23-i*4);
            write('0.0',j:1);
         end;
      for i := 2 to 5 do
         begin
            j  :=  i * 5;
            gotoxy(13,23-i*4);
            write('0.',j:2);
         end;
end;



procedure sortSIR(var NumArray :  lengths;
                      Count    :  integer);

var
   J, K        :    integer;
   ThisValue   :    real;

begin
   if Count <= 1 then exit;
   writeln('Begin SortSIR');
   for J := 2 to Count do
      begin
         ThisValue  :=  NumArray[J];
         K  :=  J - 1;
         while (ThisValue < NumArray[K]) and
                (K > 0) do
            begin
               NumArray[K+1] := NumArray[K];
               K := K - 1
            end;
         NumArray[K + 1] := ThisValue
      end;
   writeln(Count, ' entries sorted')
end;
```

```
procedure Stats(NumArray : ArrayType; Count : Integer; var Mean,
                Median, StanDev, MinValue, MaxValue: real);

var
   J, K, Mid                    : integer;
   Temp                         : real;
   ValueSum, SquareSum          : real;

begin
   if Count < 1 then
      exit;
   for J := 2 to Count do
      begin
         Temp := NumArray[J];
         K    := J - 1;
         while (Temp < NumArray[K]) and (K > 0) do
            begin
               NumArray[K + 1] := NumArray[K];
               K := K - 1
            end;
         NumArray[K + 1] := Temp
      end;
   ValueSum  := 0.0;
   SquareSum := 0.0;
   for J := 1 to Count do
      begin
         ValueSum  :=  ValueSum + NumArray[J];
         SquareSum :=  SquareSum + sqr(NumArray[J])
      end;
   MinValue  :=  NumArray[1];
   MaxValue  :=  NumArray[Count];
   if odd(Count) then
      Median := NumArray[(Count + 1) div 2]
   else
      begin
         MId    :=  Count div 2;
         Median :=  (NumArray[Mid] + NumArray[Mid + 1]) / 2.0
      end;
   Mean  :=  ValueSum / Count;
   if Count = 1 then
      StanDev  := 0.0
   else
      StanDev  :=  sqrt((SquareSum - Count * Mean * Mean) /
                        (Count - 1))
end;



function gamma(x : real) : real;

var
   i,j     :  integer;
   y, gam  :  real;

begin
   if x >= 0.0 then
      begin
         y := x + 2.0;
         gam := sqrt(2*pi/y) * exp(y* ln(y) + (1 - 1/(30*y*y))/(12*y)-y);
         gamma := gam/(x*(x+1))
      end
   else
      begin
         j := 0;
         y := x;
         repeat
            j := j + 1;
            y := y + 1.0
         until y > 0.0;
         gam := gamma(y);
         for i := 0 to j-1 do
            gam := gam/(x+i);
            gamma := gam
      end;
end;
```

```
procedure LinReg(Num2Array:  Array2Type; NumDataPairs: Integer;
                 var Intercept, Slope, CorrCoeff: real);

var
   J: integer;
   SumX, SumY, SumXY, SumXSq, SumYSq, XVal, YVal, Denom: real;

begin
   if NumDataPairs < 2 then
      begin
         Slope      :=  0.0;
         Intercept  :=  0.0;
         CorrCoeff  :=  -5.0;
         exit
      end;
   SumX    :=  0.0;
   SumY    :=  0.0;
   SumXY   :=  0.0;
   SumXSq  :=  0.0;
   SumYSq  :=  0.0;
   for J := 1 to NumDataPairs do
      begin
         XVal     := Num2Array[J,1];
         YVal     := Num2Array[J,2];
         SumX     := SumX + XVal;
         SumY     := SumY + YVal;
         SumXY    := SumXY + XVal * YVal;
         SumXSq   := SumXSq + Sqr(XVal);
         SumYSq   := SumYSq + Sqr(YVal)
      end;
   Denom := SumXSq - SumX * SumX/NumDataPairs;
   if Denom = 0 then
      begin
         Slope      := 0.0;
         Intercept  := 0.0;
         CorrCoeff  := -10.0;
         exit
      end
   else
      Slope  := (SumXY - SumX * SumY/NumDataPairs)/Denom;
   Intercept := (SumY - Slope * SumX)/ NumDataPairs;
   Denom     := SumYSq - SumY * SumY / NumDataPairs;
   if Denom = 0.0 then
      CorrCoeff := 1.0
   else
      CorrCoeff := sqrt(Slope * (SumXY - SumX * SumY /
                        NumDataPairs) / Denom);
end;
```

APPENDIX X

COMPUTER PROGRAM USED TO PLOT CUMULATIVE FIBER FRAGMENT LENGTHS

(Written on Borland's Turbo Pascal compiler version 3.0)

Procedure sortSIR is listed in Appendix IX and/or can be found in Turbo Pascal Program Library by Rugg T. and Feldman P., Que Publ., Indianapolis, (1984)

```
program fc1;
type
   lengths      =    array[1..100] of real;
var
   W            :    char;
   quit         :    boolean;
   nl,i         :    integer;
   lngth       :    lengths;

procedure enterdata(var   nl       :    integer;
                    var  lngth   :    lengths);

var     i        :     integer;

begin
    writeln('enter number of lengths ');
    readln(nl);
    for i  :=  1 to nl do
       begin
          writeln('enter length number ',i);
          readln(lngth[i]);
       end;
end;

procedure savedata(var nl     :    integer;
                   var lngth :    lengths);

var      name         :   string[14];
         lengthfile   :   text;
         i            :   integer;

begin
   writeln('enter filename ');
   readln(name);
   assign(lengthfile,name);
   rewrite(lengthfile);
   writeln(lengthfile,nl);
   for i  :=  1 to nl do
      writeln(lengthfile,lngth[i]);
   close(lengthfile);

end;

procedure calculate(nl           :    integer;
                    lngth       :    lengths);

var  sl,sll       :    real;
     mean, sdev   :    real;
     i            :    integer;

begin
sl  :=  0;
sll :=  0;
   for i  :=  1 to nl do
      begin
          sl  :=  sl + lngth[i];
          sll :=  sll + sqr(lngth[i]);
       end;
mean  :=  sl/nl;
sdev  :=  sqrt((sll - sqr(sl)/nl)/(nl-1));

writeln('mean = ',mean);
writeln('standard deviation = ',sdev);
end;
{$I b:SortSIR.PAS}
```

```
procedure getdata(var  nl        :    integer;
                  var lngth      :    lengths);

var  name          :    string[14];
     i             :    integer;
     lengthfile    :    text;

begin
   writeln('enterfilename ');
   readln(name);
   assign(lengthfile,name);
   reset(lengthfile);
   readln(lengthfile,nl);
   for i :=  1 to nl do
     readln(lengthfile,lngth[i]);
   close(lengthfile);
end;

procedure graph(nl           :   integer;
                lngth        :   lengths);

var      i,x,y,n         :    integer;
         y1, y2          :    integer;
         x1, x2          :    integer;
         annote          :    string[255];
         cumx, cumy      :    real;

begin
sortSIR(lngth,nl);
write('enter graph annotation');


readln(annote);
hires;
x1 := 120;
y1 := 170;
cumx := 0;
cumy := 0;
for i := 1 to nl do
begin
   if lngth[i] > 1.25 then lngth[i] := 1.25;
   x2 := trunc(lngth[i]/1.25 * 300 + 120);
   y2 := trunc(170-(i/nl *128));
   draw(x1,y1,x2,y1,1);
   draw(x2,y1,x2,y2,1);
   x1 := x2;
   y1 := y2
end;
draw(x2,y1,420,y1,1);
write(annote);
draw(119,42,119,170,1);
draw(120,42,120,170,1);
draw(120,170,420,170,1);
i  :=  138;
repeat
draw(120,i,130,i,1);
i  :=  i - 32;
until  i  <  42
;
i  :=   180;
repeat
draw(i,170,i,165,1);
i  :=  i  +  60;
until i >  420;
annote  :=  'frequency';
x  :=  8;
for y := 8 to 16 do
begin
   gotoxy(x,y);
   write(annote[y-7]);
end;
x  :=  11;
y  :=  6;
```

```
gotoxy(x,y);
write('1.0');
gotoxy(x,y+4);
write('0.75');
gotoxy(x,y+8);
write('0.5');
gotoxy(x,y+12);
write('0.25');
gotoxy(x,y + 16);
write('0.0');
gotoxy(25,25);
write('fiber length (mm)');
gotoxy(15,23);
write('0');
gotoxy(22,23);
write('0.25');
gotoxy(29,23);
write('0.5');
gotoxy(36,23);


write('0.75');
gotoxy(44,23);
write('1.0');
gotoxy(51,23);
write('1.25');
repeat until keypressed;
textmode;

end;

begin
   quit := false;
      repeat
         writeln('Enterdata, Savedata, Calculate, Getdata, Write, Plot, Quit')
         readln(w);
            case W of
               'E','e'  :  enterdata(nl,lngth);
               'S','s'  :  savedata(nl,lngth);
               'C','c'  :  calculate(nl,lngth);
               'P','p'  :  graph(nl,lngth);
               'G','g'  :  getdata(nl,lngth);
               'W','w'  :  begin
                              writeln(nl);
                              for i := 1 to nl do
                              writeln(lngth[i]);
                           end;
               'Q','q'  :  quit := true;
            end;
      until quit;
end.
```